Development of a novel *Escherichia coli* production platform with uncoupled stringent response

Von der Fakultät Energie-, Verfahrens- und Biotechnik
der Universität Stuttgart zur Erlangung der Würde eines
Doktors der Naturwissenschaften (Dr. rer. nat.)
genehmigte Abhandlung

vorgelegt von
Annette Margarete Kahlig
geb. Michalowski

aus Neiße / Polen

Hauptberichter: Prof. Dr.-Ing. Ralf Takors
Mitberichter: Prof. Dr. rer.nat. Georg Sprenger

Tag der mündlichen Prüfung: 10.11.2020

Institut für Bioverfahrenstechnik
Universität Stuttgart

2021

Declaration of academic honesty

I hereby declare, that this submitted work was performed and completed by me without further help. To the best of my knowledge and belief, all references, literal and logical ideas, contributions and achievements of others as well as applied images were appropriately acknowledged at the corresponding sites in the work.

Selected results of this present work were already published in the article '*Escherichia coli* HGT: Engineered for high glucose throughput even under slowly growing or resting conditions' (Michalowski et al. 2017). In addition, several parts were subject to an announcement of the invention with the title 'Bacterial strain and method for high throughput of sugar in the microbial conversion into biosynthetic products' (Michalowski et al. 2016).

Hiermit erkläre ich, dass ich die vorliegende Arbeit selbständig und lediglich unter Verwendung der angegebenen Quellen und Hilfsmittel angefertigt habe. Wörtliche oder sinngemäße Zitate, Leistungen anderer Beteiligter sowie verwendete Abbildungen wurden als solche ordnungsgemäß kenntlich gemacht.

Die vorliegende Arbeit wurde teilweise im Artikel '*Escherichia coli* HGT: Engineered for high glucose throughput even under slowly growing or resting conditions' (Michalowski et al. 2017) veröffentlicht. Ebenso sind Teile dieser Arbeit inhaltlicher Bestandteil der Erfindungsmeldung mit dem Titel 'Bacterial strain and method for high throughput of sugar in the microbial conversion into biosynthetic products' (Michalowski et al. 2016).

Kißlegg (Germany), June 23, 2021 *Annette Margarete Kahlig*

Geradeaus kann man nicht sehr weit kommen.
Antoine de Saint-Exupéry

Für meine Familie.

Contents

List of Tables

List of Figures

Acknowledgments

During the period of accomplishing this thesis at the Institute of Biochemical Engineering at the University of Stuttgart and far beyond, many people contributed to the progress of this scientific journey. I am grateful for their support, encouragement, guidance and their endless motivation.

In the first place, I want to thank Prof. Dr.-Ing. Ralf Takors for giving me the opportunity to perform my PhD thesis on this fascinating topic. His supervision, support and his strong dedication to the project guided me through all the facets of microbial stress regulation and biochemical engineering. Furthermore, I want to thank apl. Prof. Dr. habil. Martin Siemann-Herzberg for his interest in this work, his academic assistance and for many hours of scientific discussions and advice. I am grateful to Prof. Dr. Georg Sprenger for agreeing to referee this thesis. Additional thanks are addressed to Prof. Dr. Bernhard Hauer, head of the thesis committee and to the co-referees Prof. Dr. Ingrid Weiss, apl. Prof. Dr. Dieter Jendrossek and apl. Prof. Dr. Günter Tovar.

I thank the European Commission FP7 for the financial support of this work within the 'ST-FLOW' project with the Grant Agreement number 289326. Also, I am indebted to Prof. Dr. Víctor de Lorenzo and all the members of his institute at the CNB–CSIC from the Autonomous University of Madrid. Thanks for your collaboration and the warm-hearted atmosphere in the lab during my research stay in Madrid.

Further gratitude is granted to the technical assistant Jasmin Kalmbach as well as the technical engineers Andreas Freund and Salaheddine Laghrami for their contribution to this work with laboratory support and their great efforts with the technical equipment. Andreas and Salah, you have always been true helpers, supporters and advisers in terms of scientific and personal questions. Above all, Ulrike Hillemann was undoubtedly my greatest source of inspiration, companionship and motivation during the time of my thesis. Without her unceasing support in the lab, the completion of this thesis would not have been possible. Thanks Ulrike for spending

endless hours at my side preparing, running and sampling the bioreactors and always keeping a smile on your face at the same time. It has been a pleasure to work along your side and I am truly honored to still call you one of my dearest friends.

I would like to thank Attila, Jurek and Michael for all the funny and philosophical moments and for growing probably the largest passion fruit plant in Stuttgart in our office. Especially, I like to thank Michael Kraml for always offering his help and introducing me to exotic fruits from all over the world that sometimes kept a flavorful secret, in a pleasant or other way. I am likewise indebted to my past coworkers at the IBVT - Jenny, Eugenia, Gerhard, Lisa, Max, Maria, Michi, Alex and Andrea - for the wonderful atmosphere, the delightful activities apart from the lab and their friendship.

Finally, I am happy to express my deeply-felt thanks to my parents and my parents-in-law for their everlasting encouragement and motivation. Most of all, I want to thank my loving husband Alex. I am more than happy to have you in my life. Thanks for your superhuman efforts to stay supportive, tolerant and patient throughout all these years. I love you.

DANKE

Nomenclature

Greek Letters

α	alpha
β	beta
Δ	Delta, deletion of nucleotides
λ	lambda; lambda phage
μ	mu, specific growth rate [h^{-1}]
μ_{max}	mu, maximum growth rate [h^{-1}]
Φ	Phi
σ	sigma, σ-factor for initiation of transcription

Units

x g	[m s^{-2}]	gravity, measurement of centrifugal force
h	[h]	hour
M	[mol L^{-1}]	molar, mol per liter
µg	[µg]	microgram
µL	[µL]	microliter
mg	[mg]	milligram
mL	[mL]	milliliter
µM	[µmol L^{-1}]	micromolar, micromol per liter
mM	[mmol L^{-1}]	molar, millimol per liter
mm	[mm]	millimeter
min	[min]	minute
L	[L]	liter
rpm	[min^{-1}]	rounds per minute
sec	[sec]	second
U $µL^{-1}$	[U $µL^{-1}$]	Units per microliter
V	[kg · m^2 sec^{-3} · A^{-1}]	voltage (V) or electric potential
v v^{-1}	[%]	volume per volume percent
w v^{-1}	[%]	weight per volume percent

Abbreviations

°C	degree Celsius
3’	3-prime
5’	5-prime
A	adenine (purine derivative)
aa	amino acid
ABC	ATP-binding cassette
abs	absolute
CyaA	Adenylate Cyclase
ACC	acetyl-CoA carboxylase
AckA	Acetate Kinase
ACP	acyl carrier protein
ACT	Aspartokinase, Chorismate Mutase and TyrA
ADP	Adenosine diphosphate
AEC	adenylate energy charge
AMP	Adenosine monophosphate
ANOVA	analysis of variance
AspP	ADP-sugar Pyrophosphatase
ATP	Adenosine triphosphate
atpFH	(F_1F_0) H^+-ATP Synthase Complex
BglG	transcriptional antiterminator
BHI	Brain Heart Infusion
bisP	bisphosphate
c	concentration of a compound
C	cytosine (pyrimidine derivative)
c_P	product concentration [g L^{-1}]
c_S	substrate concentration [g L^{-1}]
c_X	biomass concentration [g L^{-1}]
C	Cysteine, Cys
CC	conserved Cysteine

cAMP	cyclic-AMP
cGMP	cyclic-GMP
$CaCl_2$	Calcium chloride
Cam	chloramphenicol
CDS	coding DNA sequence
CDW	cell dry weight [g L^{-1}]
CER	carbon dioxide emission rate [mol L^{-1} h^{-1}]
cf	correlation factor
CGSC	Coli Genetic Stock Center
CO_2	carbon dioxide
$CoCl_2$	Cobalt(II) chloride
Cra	catabolite repressor/activator
CRISPR	Clustered Regularly Interspaced Short Palindromic Repeats
CRP	cAMP receptor protein also called CAP (Catabolite Activator Protein)
CsrA	Carbon Storage Regulator
CTD	C-terminal domain of a protein
$CuSO_4$	Copper(II) sulfate
D	Aspartate, Asp
DAD	diode array detector
dATP	Deoxyadenosine triphosphate
dCTP	Deoxycytidine triphosphates
dGTP	Deoxyguanosine triphosphates
DMSO	Dimethyl sulfoxide
DNA	Deoxyribonucleic acid
dNTP	Deoxyribonucleotide triphosphates
DO	dissolved oxygen at atmospheric pressure
ds	double stranded
DSMZ	German Collection of Microorganisms and Cell Cultures '*Deutsche Sammlung von Mikroorganismen und Zellkulturen*'
DTT	1,4-Dithiothreitol
dTTP	Deoxythymidine triphosphates
E	Glutamate, Glu

E. coli	*Escherichia coli*
ED	Entner-Doudoroff pathway
EDTA	Ethylenediamine tetraacetic acid
EF-G	translation elongation factor G, encoded by the *fusA* gene
EF-Tu	translation elongation factor Tu, encoded by the *tufAB* genes
e.g.	*exempli gratia*, for example
EMP	Embden-Meyerhof-Parnas pathway (Glycolysis)
F	Phenylalanine, Phe
FAD	flavin adenine dinucleotide
$FADH_2$	flavin adenine dinucleotide (reduced)
$FeCl_3$	Iron(III) chloride hexahydrate
FeS	Iron(II) sulfide or ferrous sulfide
FRT	flippase recognition target
fwd	forward
G	Glycine, Gly
G	guanine (purine derivative)
G-6-P	Glucose-6-Phosphate
GalP	Galactose Permease
GDH	Glutamate Dehydrogenase
GDP	Guanosine diphosphate
GEC	guanylate energy charge
GFP	Green Fluorescent Protein
Glc	glucose
GlgA	Glycogen Synthase
GlgB	Glycogen Branching Enzyme
GlgC	Glucose-1-P Adenylyltransferase
GlgP	Glycogen Phosphorylase
GlgS	Surface Composition Regulator
Glk	Glucose Kinase
GlpK	Glycerol Kinase
Glu	Glutamate
GMP	Guanosine monophosphate
GOGAT	Glutamate Synthase

GOI	gene of interest
GPL	General Public License
GS	Glutamine Synthase
GTP	Guanosine triphosphate
H	Histidine, His
H_2	molecular hydrogen
H_2O	water
$H_2O^{Mol.Biol.}$	molecular biology grade water
H_2SO_4	Sulfuric acid
H_3PO_4	Phosphoric acid
HCl	Hydrochloric acid
HCO_3^-	Hydrogen carbonate
HF	high-fidelity
HGT	high glucose throughput mutant strain
hipA	Serine/Threonine kinase 'high persistence factor A'
HPLC	High Performance Liquid Chromatography
HS	High Synthetase mutant strain
IclR	Isocitrate Lyase regulator
bIF-2	bacterial translation initiation factor IF-2, encoded by the *infB* gene
IMP	inosine 5'-phosphate
IPTG	Isopropyl-β-D-1-thiogalactopyranoside
IS	insertion sequence
ISO	isothermal
I.U.	International Unit
K	Lysine, Lys
K_S	Monod substrate affinity constant [g L^{-1}]
K	Kelvin
K_2HPO_4	di-Potassium hydrogen phosphate
Kan	Kanamycin
KH_2PO_4	Potassium dihydrogen phosphate
KM	Kornberg Medium

KOH	Potassium hydroxide
LamB	maltose outer membrane channel, maltose high-affinity receptor, phage lambda receptor protein
LB	Lysogeny Broth
LdhA	Lactate Dehydrogenase
m	mass of a compound [g]
m_P	amount of product [g]
m_S	amount of substrate [g]
m_X	amount of biomass [g]
m_S	maintenance coefficient [g $_{\text{Glc}}$ g_{CDW}^{-1} h^{-1}]
m_{tare}	tare weight of a compound [g]
MCS	multiple cloning site
MD	middle domain
Mg^{2+}	Magnesium ion
Mn^{2+}	Manganese ion
MglBAC	D-galactose/methyl-β-D-galactoside ABC transporter
$MgCl_2$	Magnesium chloride
$MgSO_4$	Magnesium sulphate
MMR	methyl-directed mismatch repair pathway
$MnSO_4$	Manganese(II) sulfate
mRNA	messenger RNA
$\dot{n}$	molar amount of a compound [mol]
N	agitation speed [min^{-1}]
N	nitrogen
N_2	nitrogen, elementary
N-lim	nitrogen-limited
Na	Sodium
NaCl	Sodium chloride
NAD^+	β-Nicotinamide adenine dinucleotide
NADH	β-Nicotinamide adenine dinucleotide (reduced)
NADPH	Nicotinamide adenine dinucleotide phosphate (reduced)
NaH_2PO_4	Sodium phosphate monobasic

NaOH	Sodium hydroxide
Na_2SO_4	Sodium sulfate
NCBI	National Center for Biotechnology Information
NH_3	Ammonia
NH_4^+	Ammonium
NH_4OH	Ammonium hydroxide
$(NH_4)_2HPO_4$	di-Ammonium hydrogen phosphate
$(NH_4)_2SO_4$	Ammonium sulphate
nt	nucleotides
NTD	N-terminal domain of a protein
O_2	oxygen, elementary
OD_{600nm}	Optical Density at 600 nm
OmpCF	non-specific outer membrane porins for sugar, ion and amino acid intake
ORF	open reading frame
ori	origin of replication
OUR	oxygen uptake rate [mol L^{-1} h^{-1}]
p	pressure [Pa]
P	Proline, Pro
P_i	inorganic phosphate
PP_i	inorganic pyrophosphate
PCA	Perchloric acid
PCR	polymerase chain reaction
PDHC	Pyruvate Dehydrogenase complex
PEG	Polyethylene glycol
PEP	phosphoenolpyruvate
PFK	Phosphofructokinase
PFL	Pyruvate Formate Lyase
Pgi	Phosphoglucose Isomerase
PGK	Phosphoglycerate Kinase
Pgm	Phosphoglucomutase
pH	potential of hydrogen [negative decadic logarithm of the proton concentration]

PK	Pyruvate Kinase
PMMA	Polymethyl methacrylate (acrylic polymer)
PO_4^{3-}	orthophosphate
PoxB	Pyruvate Oxidase
PP	Pentose Phosphate pathway
Ppc	Phosphoenolpyruvate Carboxylase
ppGpp	Guanosine-3',5'-bisdiphosphate
pppGpp	Guanosine-3'-diphosphate,5'-triphosphate
PpsA	Phosphoenolpyruvate Synthase
PPX	Exopolyphosphatase
PTFE	Polytetrafluoroethylene
PTS	Phosphotransferase System
PykF	Pyruvate Kinase I
Pyr	pyruvate
q_{CO_2}	biomass-specific carbon dioxide emission rate [mol g_{CDW}^{-1} h^{-1}]
q_{O_2}	biomass-specific oxygen uptake rate [mol g_{CDW}^{-1} h^{-1}]
q_P	biomass-specific product formation rate [g_P g_{CDW} h^{-1}]
q_S	biomass-specific substrate consumption rate [g_{Glc} g_{CDW} h^{-1}]
Q_{CO_2}	volumetric carbon dioxide emission rate [mol L^{-1} h^{-1}]
Q_{O_2}	volumetric oxygen uptake rate [mol L^{-1} h^{-1}]
R	Arginine, Arg
R	universal gas constant, 0.08314 [J mol^{-1} K^{-1}]
RBS	ribosome binding site
RC	RNA control
rev	reverse
RID	refractive index detector
RNA	Ribonucleic acid
RNAP	RNA Polymerase
rRNA	ribosomal RNA
RP	reversed-phase
RQ	respiratory quotient
RSH	RelA and SpoT homologue
RT	room temperature (15 - 25°C)

S. cerevisiae	*Saccharomyces cerevisiae*
SDS	Sodium dodecyl sulphate
SF	shaking flask
SHX	DL-Serine hydroxamate
SIM	stress-induced mutagenesis
SQR	succinate-ubiquinone oxidoreductase
SR	Stringent Response mutant strain
ss	single-stranded
T	temperature
T	thymine (pyrimidine derivative)
TA	toxin/antitoxin
Taq	*Thermus aquaticus*
TAE	Tris-acetate-EDTA
TBAS	Tetrabutylammonium bisulfate
TC	total carbon
TCA	Tricarboxylic Acid Cycle
TE	Tris-EDTA
TES	Trace Elements Solution
TGS	Threonyl-tRNA Synthetase
ThDP	Thiamin diphosphate
TN	total nitrogen
TOC	Total Organic Carbon
tRNA	transfer RNA
TS	target sequence
U	enzyme units
UniProtKB	Universal Protein Resource Knowledgebase
UTase/UR	Uridylyltransferase/Uridylyl-Removing Enzyme
UV	ultraviolet light
V	volume [L]
$\dot{V}_G$	volumetric gas flow rate [L h^{-1}]
V_R	working volume of a bioreactor [L]

VIS	visible light
w/o	without
WT	wild-type
X-β-Gal	5-Bromo-4-chloro-3-indolyl-β-D-galactopyranoside
y	molar gas fraction
$Y_{P/S}$	yield coefficient of product from substrate [$g_P\ g_{Glc}^{-1}$]
$Y_{P/X}$	yield coefficient of product per biomass [$g_P\ g_{CDW}^{-1}$]
$Y_{X/N}$	yield coefficient of biomass from nitrogen [$g_{CDW}\ g_{NH_4^+}^{-1}$]
$Y_{X/S}$	yield coefficient of biomass from substrate [$g_{CDW}\ g_{Glc}^{-1}$]
$Y_{X/S}^{true}$	true yield coefficient of biomass from substrate [$g_{CDW}\ g_{Glc}^{-1}$]
YT	Yeast extract Tryptone
$ZnSO_4$	Zinc sulfate

Zusammenfassung

Großskalige Industrieprozesse zur kommerziellen Herstellung von Lebensmitteln, Futterzusatzstoffen, Probiotika, Treibstoffen und vielen anderen Substanzen zielen auf hohe Produktausbeuten ab. Das Erreichen solch hoher volumenbezogener Produktivitäten ist oftmals abhängig von erhöhten Biomassekonzentrationen, die verstärkt Produktkatalysatoren bereitstellen, oder von gesteigerten spezifischen Leistungsfähigkeiten der mikrobiellen Produzentenstämme selbst. Im Besonderen sind großskalige aerobe Kultivierungen von Mikroorganismen häufig durch die vorliegenden technischen Grenzen der industriellen Fermentationsanlagen begrenzt. Beispielsweise können der Sauerstoffübergang von der Gas- in die Flüssigphase sowie der Wärmeübertrag stark limitiert sein. Ebenso kann dadurch eine inhomogene Durchmischung der Nährstoffe im Reaktorraum herrschen. Verschiedene Ansätze stehen den heutigen Bioverfahrenstechnikern zur Verfügung, um die optimalen Kultivierungsbedingungen für die Mikroorganismen zu gewährleisten. Entweder, man reduziert den bakteriellen Stoffwechsel auf ein Minimum, indem man die Kultur einer kontrollierten Nährstoffverknappung aussetzt, oder man nimmt gezielt Eingriff in definierte metabolische Stoffwechselwege, um so den bakteriellen Phenotyp an die herrschenden Bedingungen anzupassen. Die vorliegende Arbeit befasste sich mit der Kombination beider zuvor vorgestellten Möglichkeiten und präsentiert die genetisch modifizierte Mutante *E. coli* HGT ('high glucose throughput') mit hohen Glukoseaufnahmeraten sogar im Umfeld von wachstumslimitierenden Kulturbedingungen, wie sie in industriellen Prozessen Standard sind. Die Mutante wies sehr geringe Wachstumsraten bei gleichzeitiger hoher Glukoseaufnahmerate im ruhenden zellulären Zustand auf, wobei sich der Sauerstoffbedarf gleichbleibend in der Größenordnung des Wildtypen und somit auch innerhalb der technischen Beschränkungen befand. Obwohl *E. coli* HGT lediglich mit einer weniger als halb so großen Wachstumsrate wie der *E. coli* WT wuchs, war die assoziierte biomassespezifische Glukoseaufnahmerate in exponentiell wachsenden Zellen nahezu identisch mit der des Wildtypen. Ein gesamtheitlicher Stillstand des Wachs-

tums der bakteriellen Kulturen wurde als Konsequenz eines gezielten Stickstoffmangels im Minimalmedium ausgelöst. Dieser Nährstoffentzug in *E. coli* HGT Zellen führte folglich zu vierfach erhöhten metabolischen Raten, verglichen mit dem Wildtypen, während einer Stickstofflimitierung. Letztendlich bewirkte eine herunterregulierte Aktivität des Pyruvat Dehydrogenase Komplexes (PDHC) in der HGT Mutante eine starke Ableitung des Glukoseüberschusses entlang des zentralen Kohlenstoffwechsels in Richtung einer Anreicherung von Pyruvat. Aus diesem Zusammenhang entstanden wesentliche Vorzüge einer wachstumsentkoppelten Produktion wie z.B. einer geringen Biomassesynthese sowie einer niedrigen Kohlendioxidabgabe in nicht wachsenden Zellen mit hohen zellulären Umsatzraten. Zusätzlich befasste sich die vorliegende Studie mit der Möglichkeit, die mikrobielle Kohlenstoffaufnahme für eine erhöhte Produktbildung weiter zu steigern, indem die intrazelluläre Signalweiterleitung der stringenten Kontrolle von den umgebenden stickstoffbasierten Stressbedingungen entkoppelt wurde. Das Auslösen der stringenten Kontrolle wird von der Verfügbarkeit des Signalmoleküls ppGpp bestimmt, welches ab einer kritischen Konzentration eine Neuorganisierung der transkriptionellen Vorgänge in der Zelle einleitet. Das Vorhandensein von ppGpp wird hauptsächlich durch das Zusammenspiel der beiden Schlüsselenzyme ppGpp Synthase RelA und ppGpp Hydrolase SpoT kontrolliert. In dieser Arbeit entstand eine Sammlung von neun rekombinanten Stämmen des etablierten Modellorganismus *E. coli*, welche einen schrittweisen Anstieg der maximalen Guanosin-3‘,5‘-bisdiphosphat (ppGpp) Konzentration am Übergang in die stickstofflimitierte Phase aufwiesen. Verschiedene genetische Strukturen der beiden Gene *relA* und *spoT* wurden kombiniert, um Mutanten mit weitreichenden Effekten in der Signalentstehung der stringenten Kontrolle zu erzeugen. Die Reihe solcher genetischer Komponenten mit synthetischen Eigenschaften umfasste sowohl kleinere Änderungen innerhalb der Aminosäuresequenz, die einen Einfluss auf die enzymatische Substrataffinität haben konnten, als auch Modifikationen gesamter katalytischer Bereiche, die höchstwahrscheinlich neuartige Enzymfunktionen hervorgerufen haben. Innerhalb dieser Reihe traten *E. coli* HGT und die nicht produzierende Variante davon *E. coli* SR durch ihren einzigartigen Signalmolekülverlauf während der Fermentationsprozesse hervor. Beide waren durch eine ausgeglichene Entwicklung der stringenten Kontrolle auf einem individuellen Basiswert in wachsenden und auch in nährstoffabgereicherten Zellen gekennzeichnet. Eine angepasste Synthese- und Hydrolyserate von ppGpp ermöglichte es, das typisch stressbedingte Reiz-Reaktions-Schema der Stickstoffknappheit von den reellen Umweltbedingungen zu entkoppeln. Auf diesem Wege konnte zusätzlich der Verlust von Energieträgern zur Umstrukturierung metabolischer Prozesse und regulatorischer Aufgaben vermieden

werden. Die sich im Gleichgewicht befindliche Stressantwort des genetisch veränderten Stammes *E. coli* HGT bietet eine Vielzahl an charakteristischen Merkmalen in Bezug auf eine höhere Stresstoleranz unter nährstoffreduzierten Kultivierungsbedingungen zusammen mit einer erhöhten Glukoseaufnahme- und Produktbildungsrate in ruhenden Zellen. Aufgrund dessen wird hierdurch *E. coli* HGT als neue bakterielle Produktionsplattform für pyruvatbasierte Verbindungen vorgestellt, welche ein hohes Potenzial aufweist durch gezielte Weiterentwicklung in zukünftigen industriellen Anwendungen ihren Einsatz zu finden.

Abstract

Large scale industrial processes for commercial production of food, feed, probiotics, enzymes, fuels and many other substances are targeted on high product yields. The achievement of such high volumetric productivities is often dependent on elevated biomass formation to gain more product catalysts or increased specific productivities of the microbial producer strain itself. Especially large-scale aerobic microbial cultivations are often subject to the prevailing technical restrictions of such industrial fermentation systems in terms of limited oxygen transfer, mixing inhomogeneities and heat exchange. To meet the microbial activity requirements of the culture, biochemical engineers have several choices. Either they can reduce the bacterial metabolism to a minimum rate by applying a controlled limited nutrient supply or they can manipulate the bacterial phenotype by engineering certain metabolic pathways to their special needs. The present study demonstrates a combination of these two approaches and introduces the genetically engineered *E. coli* high glucose throughput (HGT) mutant with high glycolytic turnover rates even under growth-limited culture conditions as these are representative for industrial processes. With its slow growth rate and the accompanying high glucose consumption at a resting cellular state, the oxygen demand of the mutant remained constantly at a WT-like level and thus within the technical constraints. In *E. coli* HGT, the biomass-specific glucose consumption rate of exponentially growing cells was almost identical to the *E. coli* WT although HGT was growing at less than halve the WT growth rate. Growth-arrested cultures were induced as consequence of nitrogen starvation in the minimal medium. Such nutrient depleted *E. coli* HGT cells consumed glucose at four-times higher rates compared to WT cells in nitrogen-limitation. Finally, a downregulated Pyruvate Dehydrogenase complex (PDHC) activity in the HGT mutant facilitated a strong drain of the carbon surplus along the central carbon metabolism to pyruvate accumulation. Hereby, the major benefits of growth-decoupled product formation were low biomass synthesis and carbon dioxide (CO_2) respiration in non-growing cells that performed growth-like cellular activi-

ties. Besides this metabolic pathway adjustment, the central idea of this study focused on further enhancing microbial carbon uptake rates towards higher productivities by uncoupling the intracellular stringent response signaling from the surrounding nitrogen stress conditions. Stringent response induction is dependent on the degree of Guanosine-3',5'-bisdiphosphate (ppGpp) availability, that controls induction of transcriptional rearrangements in the cell, which is mediated by the interplay of the two key enzymes - the ppGpp Synthase RelA and the Hydrolase SpoT. In the course of this study, a collection of nine recombinant mutants of the well-known *E. coli* model strain with gradually increasing maximum ppGpp levels upon transition into nitrogen-stress was established. Different genetic structures of the *relA* and *spoT* genes were assembled to generate mutants that reacted with wide-ranging stringent response regulations when an internal stress signal transduction commenced. Such synthetically designed stringent response components included small amino acid sequence variations that probably affected enzymatic substrate affinities up to entire catalytic motif substitutions that most likely created new-to-nature enzymatic properties. *E. coli* HGT and its non-pyruvate producing variant *E. coli* SR presented quite unique alarmone progressions along the two process stages. Both mutant strains were characterized by a balanced stringent response performance during growth and starvation at their own individual basal ppGpp levels. These adjusted alarmone hydrolysis and synthesis rates empowered the bacterial cells to uncouple their nitrogen-stress induced stimulus-response cascade from nutritional realities in the environment. In this way, the loss of energy molecules for arising reorganization processes of metabolic and regulatory activities would be prevented. According to its characteristic stress-balanced features, *E. coli* HGT offered a higher stress tolerance at nutritional starvation conditions together with elevated glucose consumption and product conversion rates of non-growing cells. Thus, *E. coli* HGT is introduced as novel bacterial production platform for pyruvate-derived compounds and holds a considerably great potential to be further engineered into a future chassis for industrial production applications.

1. Motivation and Objectives

The United Nations defined the term Biotechnology as '*any technological application that uses biological systems, living organisms, or derivatives thereof, to make or modify products or processes for specific use*' (United Nations 1992). Whereas the origin of the term is traced back to the Hungarian agricultural engineer Karl Ereky, who coined it back in 1919 in a book he wrote during his time as Hungarian Minister of Food (Ereky 1919). Basically, he described the need of science to transform raw materials into products by exploitation of living organisms (OECD 1999). In general he referred to a process, that mankind profited from - knowingly or unknowingly - over centuries. It is common knowledge, that throughout history humans of all different ethnical roots availed themselves of the advantages of microbial fermentation mechanisms primarily in terms of food preservation. Especially as regards of taste improvement of food and beverages and provisions conservation manifold methods evolved over time. Later on, those practices were no longer limited to the processing of nutritional components. Studies on biological and biochemical backgrounds of bacterial fermentations contributed to clarification of metabolic pathways and formation of fermentation products. These findings also led to the identification of various application-specific microorganisms, which from that point on were subject to controlled biosynthetic procedures. From the middle of the 19^{th} century on, fermentative productions extended to the specific synthesis of organic compounds such as lactic and butyric acid. Within the next hundred years this metabolic spectrum already covered a wide range of areas of applications including provisioning of antibiotics for the health-care sector, organic solvent fermentation for the defense industry and biotechnological production of citric acid and gluconic acid as acidifying and chelating agents for food manufacturing (Sahm et al. 2014). In the period that followed, microbial production processes were conditioned to be well-implemented in the industrial field. The power of bacterial conversion reactions was used in an opulent range of applications. Product varieties span from food to feed industries, variants of green fuels, fine chemicals, biopharmaceuticals and fur-

ther added-value products. Higher demands for medical treatments, alternative energy sources, waste biodegradation and others came along with increasing reaction volumes of large-scale industrial processes to serve the markets. To meet the evolving complexities and requirements of those commercially-driven productions, particularly today, successful scale-up strategies and bioprocess designs are essential in biotechnological applications.

1.1. Microbial Processes at Industrial Scale

Large-scale industrial processes include cultivation of different microorganisms in qualified fermentation vessels, the associated formation of a product of choice and likewise subsequent purification steps for sufficient product recovery. On the manufacturing approach level, such microbial processes can take on production scales ranging from some 10,000 L to 1,000,000 L and more (Crater and Lievense 2018). Nevertheless, development of large-scale industrial application strategies usually starts at laboratory scale. A small vial containing seeding cells from the working cell bank is used as starting material for further up-scaling activities of the microbial process, reaching final enlargement factors from hundreds to millions in size, amount or reaction volume. This so-called upstream process development concentrates on expansion of living prokaryotic or eukaryotic cultures in principle and therefore has recourse to several obviously mandatory cultivation techniques. Since industrial scale processes are often susceptible to inhomogeneities of cultivation parameters, consistent bioprocess developments need to be supported by applied technical and scientific tools (Neubauer et al. 2013). For successful lab-to-production transfer, each scenario has to be examined individually. The supreme goal of process engineering is consequently maintenance of a high efficacy throughout the process in order to minimize or prevent performance loss and to meet product expectations. Deviations from anticipated process performance and success can be described by cultivation-derived parameters like e.g. a reduction of carbon-to-product conversion yields, increased by-product formation, altered growth rates, or reduced space-time yields (Takors 2016). In this context, integration of methods from different disciplines is indispensable to provide control strategies for all stages of process development and scale-up. In his article, Takors 2012 reviewed current obstacles and restraints of industrial large-scale fermentations and thereby proposed a classification of the crucial impacts on microbial processes into chemical, physical and biological factors.

Chemical factors: Going from small laboratory test fermentors to large-scale industrial production conditions, chemical compounds in the cultivation medium or in titration solutions may have unexpected effects on cell activities due to bulk preparation. Hence, production media recipes should be kept simple at best and low-salt or even salt-free titration agents (or better gases) should be applied. Solubility of the two typical process gases oxygen (O_2) and CO_2 is increased at higher hydrostatic pressures, as it is the case with growing reactor heights. Higher dissolved CO_2 fractions involve higher amounts of bicarbonate at a ratio of about 1:4, which in turn has an influence on the total buffer capacity of the CO_2/HCO_3^- system. Other medium additives, like anti foaming agents, are often used to reduce foam formation in the bioreactor effectively at lab-scale. With increasing vessel sizes and cultivation volumes such hydrophobic substances might be less effective. Difficulties with bioprocess concepts, product formation yields and follow-up downstreaming steps can occur, such that measures in terms of process design and engineering need to be considered.

Physical factors: As mentioned before, industrial fermentors at manufacturing-scale rapidly reach working volumes of 100,000 L and more. At such dimensions, physical properties of these facilities bring along fundamental discrepancies in comparison to well-studied lab-scale bioreactors with volumes up to only some dozen liters. Gas solubilities are elevated with increasing hydrostatic pressure (>1 bar), resulting in vertical and radial gradients of dissolved gases as a consequence of technical limitations of oxygen transfer among other impacts. Fluctuating availability is not restricted to oxygen supply alone. Extended mixing times in large-scale industrial processes implicate inhomogeneities in substrate and temperature distribution as well as pH regulation (Junker 2004, Onyeaka et al. 2003, Enfors et al. 2001, Langheinrich and Nienow 1999, Bylund et al. 1998). Such heterogeneities of process conditions enforce sectional micro-environments with different availability of e.g. nutrients or oxygen. Exposure of the bacterial culture to various types of external stress triggers the formation of microbial population heterogeneity which in turn affects the performance of industrial processes. With high resolution techniques, Müller et al. 2010, described the origin and the significant impact of inefficient subpopulations in industrial cultures on bioprocess underperformance. Other research contributions integrate cellular needs for nutrients or properties of cell cycle adaptations into their physical scale-up criteria. An *in silico* method was presented to predict the formation of such named bacterial population heterogeneities. Simulated substrate gradients under large-scale mixing conditions revealed co-existing subpopulations of bacteria un-

dergoing different growth and productivity states and thus showing distinct demands for energy. About three-quarters of those cells were described to switch between standard and multifork replication phases. As a consequence of fluctuating external starvation conditions, massive transcriptional adaptations were required for growth continuation and cell survival. In fact, strong population heterogeneities were observed in terms of enhanced adenosine triphosphate (ATP) maintenance demands of up to 1.5-fold compared to average population demands (Kuschel et al. 2017).

Biological factors: Volume enlargement from small-scale bench top cultivations to large-scale industrial applications affects the microbial culture in seed train expansion manners and also has associated impacts on strain performance. Inoculum development for a successful biotechnological process needs consideration of a significant increase in the bacterial generation number with higher cultivation volumes due to a longer course of the seed and production phases. Stability of introduced recombinant manipulations in the production hosts has to be ensured over the expected bioprocess duration by selective pressure evaluation. Further factors like mutation probability, contamination vulnerability of the culture and changing stress conditions have to be contemplated in long-term industrial productions as well (Takors 2012, Junker 2004). By modern standards, microbial strain design is no longer subject to the principle of random trial-and-error approaches. Biochemical engineers all over the world now have plenty of state-of-the-art genetic tools to choose from. Lately, the call for innovative holistic concepts for sufficient industrial strain engineering is becoming ever louder. A recent review demonstrates various ways how systems biology provides the deep understanding of complex microbial systems that can be dissected into their smallest parts and reconstructed in the field of synthetic biology. Those systemic approaches deploy dynamic metabolic modeling of regulatory units in the host to find interacting modules that can be engineered for novel functions. In this way, natural cellular answers to local changes in the system in form of multi-level responses (metabolic, transcriptional and translational controls) could be circumvented (Takors and de Lorenzo 2016). This process is taken to an even higher level through systems metabolic engineering strategies for developing industrial overproduction strains at large-scale. Such approaches incorporate the basic techniques of systems biology, synthetic biology and evolutionary engineering at the systems level. Efficient synthetic biology tools such as Clustered Regularly Interspaced Short Palindromic Repeats (CRISPR)-based manipulations (Jinek et al. 2012) or genome editing (Csörgő et al. 2016) pave the way for advanced biotechnological microbe designs. The combination of these progressive methodologies

will give the researchers access to a broader carbon substrate utilization range. It will enable the use of less-known and less-characterized species apart from the well-described industrial workhorses like *Escherichia coli* and *Saccharomyces cerevisiae*. Also it will extend the palette of biobased productions of non-natural chemical compounds amongst many other beneficial advances (Lee and Kim 2015).

1.2. Limitation Strategies in Microbial Processes

Microbial production processes at large-scale face a vast series of physical, chemical and biological obstacles with increasing bioreactor dimensions. The most common restraints at higher volume scales are correlated to insufficient oxygen supply of the culture, barely adequate heat removal due to extensive vessel sizes and spatial inhomogeneities in e.g. nutrients, dissolved gases and pH mixing caused by limited power input. As generally known, the transfer rate of oxygen into an aqueous cultivation medium is limited to about 150 – 180 mmol L^{-1} h^{-1}. To avoid the risk of running into oxygen-limited conditions during aerobic industrial production processes, a fed-batch or continuous cultivation mode is initiated after biomass formation is completed with exponential growth. As a result, highest product titers, substrate conversion yields and product purity are achieved (Takors 2012). Alternatively, anaerobic cultivation conditions can be applied to circumvent the technical limitations of a system. By providing an electron acceptor other than oxygen, the Tricarboxylic Acid Cycle (TCA) is downregulated and facultative anaerobic microbial cells like *E. coli* switch from respiration to fermentation. Under anoxic conditions different sugars are oxidized incompletely such that a mixture of fermentation end products as acetate, lactate, succinate, formate and ethanol is consequently produced with high yields. However, the reduced spectrum of feasible products, anaerobic host microorganisms and the maintenance of the redox balance are severe drawbacks of oxygen-limited fermentation processes that researchers are still confronted with (reviewed in Förster and Gescher 2014).

In order to reduce high metabolic activities and growth of aerobic microbial cultures, availability of essential nutrients in the cultivation environment is limited and often controlled by a nutrient-feeding strategy. Key elements, such as carbon (C), hydrogen (H), oxygen (O), nitrogen (N), phosphorous (P) and sulfurous (S) are central representatives within

major biochemical cycles of the microbial metabolism (Egli 2015). Uptake, assimilation and degradation of sugars, other carbohydrates, proteins, lipids, nucleic acids, water and oxygen provides most substantial components for cellular processes like catabolic and anabolic reactions, respiration, energy preservation, building blocks and macromolecules formation, cell wall synthesis, reproduction and so on. The average elemental cell composition of a growing microorganism such as *E. coli* is composed of about 44.3 % C, 7.4 % H, 28.4 % O, 12.1 % N and 0.5 % S (Taymaz-Nikerel et al. 2010). This sums up to approximately 93 % of the total bacterial cell dry weight, leaving the residual 7 % to further nutritional requirements of phosphorous compounds, other macro elements (potassium, sodium, calcium, magnesium, iron and others) and trace elements (manganese, zinc, cobalt, molybdenum, nickel and copper).

Metabolic control of the microbial growth rate is typically achieved by limitation of cell nourishment with one of the named basic biochemical elements. Although bacterial growth and cellular activities can be decelerated in this way, these generated systems need to be characterized with all their associated ramifications. Most commonly, the microbial culture is investigated at steady-state under nutrient depleting conditions such as carbon and nitrogen limitations. In slow-growing cells (specific growth rates $\mu \leq 0.10$ h^{-1}) of nutrient-limited chemostat cultures, metabolic activities as well as substrate and product fluxes are reduced compared to non-limited cell growth cultivations. By making use of the Herbert-Pirt equation, substrate consumption and product formation rates can be described to have a linear relation to the specific growth rate of a culture. Generally, consumed substrate is distributed over cellular functions contributing to growth, product synthesis and energy supply for maintenance (m_S). If biomass synthesis and hence product formation are limited to a static degree, the carbon source flux of a microorganism is exclusively directed to non-growth related maintenance functions that prolong survival of starved cells (Herbert 1958, Pirt 1965, Hua et al. 2004). From literature m_S values of 0.024, 0.057 and 0.083 g_{Glc} g_{CDW}^{-1} h^{-1} are documented for non-growing *E. coli* cells in aerobic carbon-limited chemostat cultivations (Villadsen et al. 2011, Taymaz-Nikerel et al. 2010, Chubukov and Sauer 2014).

A recent study on fluctuating substrate availabilities in the cellular microenvironment of *E. coli* revealed significant changes in transcriptional dynamics as reaction to frequent activation of regulatory programs in the cell. While periodically passing from a carbon (glucose) limited cultivation scenario into nitrogen (ammonia) limitation, these cells ac-

tivated 'housekeeping' σ^{70} (*rpoD*), σ^{38} (*rpoS*) and σ^{54} (*rpoN*) regulatory cascades, which were assigned to carbohydrate and amino acid transport as well as metabolism. Under dual limitation conditions the long-range stress response was dominated by the alternative sigma factor σ^{24} (*rpoE*). Therefore, the data suggested an orchestrating role for σ^{24} in the complex regulatory network of the interplay between carbon and nitrogen-specific hunger responses (Löffler et al. 2017). Further research on genome-wide transcriptional responses to environmental changes (glucose or ammonia limitation) is in good agreement with these findings. Directly compared to cell specific carbon uptake rates under glucose-limited conditions, cells in a nitrogen depleted environment have been found to show even increased levels of substrate consumption (Hua et al. 2004, Kumar and Shimizu 2010). In fact, limitation of non-carbon nutrients for growth is a highly desirable scientific approach for microbial production process designs. Endogenous carbon-excess enables product formation and maintenance in growth-arrested cultures at a full catabolic extent where the majority of metabolic programs are available to the cell (Rühl et al. 2012). Limitations of phosphorous or sulfurous compounds are only two more options to control the growth rate of the culture without limiting elements of the target molecules at the same time. Such starvation for essential non-carbon nutrients was shown to elevate glucose consumption rates to values of 0.16 $g_{Glc}\ g_{CDW}^{-1}\ h^{-1}$ at phosphate depletion and 0.23 $g_{Glc}\ g_{CDW}^{-1}\ h^{-1}$ under sulfur lacking conditions (Chubukov and Sauer 2014). An elaborate study from 2014 highlighted the interplay of process-induced phosphate starvation and microbial product formation performance of an L-Tryptophane overproducer. The group proposed a matching glucose uptake rate of a non-growing *E. coli* WT strain at 0.17 $g_{Glc}\ g_{CDW}^{-1}\ h^{-1}$ and an elevated rate of 0.25 $g_{Glc}\ g_{CDW}^{-1}\ h^{-1}$ in the growth-arrested production strain. These data suggested, that installing nutrient limitations in industrial relevant processes might be a very efficient approach to ensure high product titers and overcome technical restraints at the same time. However, they also considered inherent drawbacks that proper phosphate limitations could have on highly energy demanding processes from an industrial application position. At reduced phosphate availability, they found a deteriorating stoichiometric ratio of ATP formation to proton translocation which in turn meant decreasing activities of the respiratory chain and ATP Synthase complex (Schuhmacher et al. 2014).

1.3. Genetic Modification Approaches Towards Higher Productivity

As far as this, controlled and preset process-dependent nutrient supply strategies were considered as truly useful tool for yield increase in microbial productions. Indeed, such process-induced limitations of one essential element, exactly like the presented approaches in the former section, hamper the channeling of carbon fractions and precursors into biomass formation. Thus, besides providing basic energy levels for cell maintenance, substrate is almost exclusively available for product synthesis reactions in the first place. Even more remarkable is the fact that some limitation conditions automatically implicate elevated substrate consumption rates, especially for glucose, in such growth-arrested cultures which is a very comfortable side benefit. Nevertheless, these biotechnological production conditions often come along with serious ramifications on the microbial physiological state on the downsite. Not only are nutrient restrictions and feeding strategies technically limited in some degree, environmental stress situations affect global intracellular regulatory systems which in turn lead to physiological and morphological modifications. The underlying mechanisms of stress sensing, integration of extracellular signals and adjustment of metabolic responses are highly variable depending on the nature of different environmental perturbations. Eventually, living organisms must adapt efficiently to changes in their direct surrounding in order to survive nutritional or process-induced limitations (Shimizu 2013). Several studies already demonstrated how genetically engineered bacterial cells managed to compensate for nutritional shortage by rearranging their metabolic fluxes and adjusting catabolic pathways. Especially mutations in genes related to proteins and enzymes of the central metabolic pathways are known to cause redirection of glucose into glycolytic branches other than the Embden-Meyerhof-Parnas pathway (EMP), as e.g. the Pentose Phosphate (PP) pathway, TCA, mixed acid fermentation, glycogen synthesis and so on (Figure 2.14). In 2008, researchers found increased glucose uptake rates of an *E. coli* pyruvate producer containing several deletions of key enzymes participating in carbon distribution steps, like Pyruvate Dehydrogenase complex, Pyruvate Formate Lyase, Pyruvate Oxidase, Phosphoenolpyruvate Synthase and Lactate Dehydrogenase. Carefully selected substrate limitation processes and further genetic manipulations even heightened glucose consumption and product titers. More precisely, deletion of the (F_1F_0) H^+-ATP Synthase Complex (*atpFH*) led to increased intracellular levels of ADP and AMP, which activated specific glycolytic enzymes and resulted in further elevated glucose uptake rates and a

reduced biomass from carbon yield of the cells (Zhu et al., 2008). Another metabolic engineering approach led to a similar phenomenon. Glycolytic fluxes in *E. coli* mutants with a disrupted Phosphotransferase System (PTS) were observed to be highly elevated, although actual glucose consumption rates were not calculated directly. Since the assimilation of glucose through the native transport pathway was blocked, glucose internalization was accomplished via the PEP-independent transporter Galactose Permease (GalP) and immediately phosphorylated by Glucose Kinase (Glk)-specific enzyme activity once inside the cell (Flores et al. 2002, Steinsiek and Bettenbrock 2012).

Several other studies reported variations in glucose consumption based on approaches affecting intracellular stress sensing mechanisms. Small global regulators or signaling molecules, such as cyclic-AMP (cAMP), cyclic-GMP (cGMP) or ppGpp, are synthesized immediately upon transition into nutrient starved conditions, thus activating catabolic regulatory pathways consequently. A very recent study highlighted the interplay of stringent response activation in *E. coli* and the heterogeneous conditions the culture might be confronted with in a large-scale fermentation scenario. At a certain scale, limited mixing capacities of the bioreactor system also involve poor substrate distribution and vessel zones with changing nutrient supply. Cells which were circulating through periodically varying levels of glucose availability reacted with multilayered regulatory programs to the nutritional heterogeneities. As a consequence to adapt to such frequently activated stress conditions, short- and long-term strategies were observed in those cells. At a short-term dimension, transition from carbon limitation to mere starvation quickly activated a range of metabolic cascades. This tactical response caused a rapid accumulation of ppGpp that triggered transcriptional changes like induction of the stationary phase sigma factor σ^{38} - commonly known as σ^{S} (*rpoS*) - and the amplification of amino acid biosynthesis genes. After repeated glucose shortage cycles, cells adapted to the general σ^{S}-dependent stress reaction and performed a strategic long-term response. Genes involved in cell motility, carbon and energy metabolism were downregulated, those attributed to macromolecule synthesis were upregulated (Löffler et al. 2016). With respect to the principles that ppGpp has an effect on microbial productivity, the question arises as to what extent the influence of the stringent response related proteins RelA and SpoT can be manipulated to increase product yields. Former research data already set the basis for the integration of biotechnological productions and intracellular stress regulation responses. In 2006 Imaizumi et al. investigated the effect of different intracellular ppGpp levels on amino acid synthesis in *E. coli*. They found increased accumulation of L-Lysine and L-glutamate in bacterial

cells overexpressing the *relA* gene, encoding for (p)ppGpp Synthase I, from an extra-chromosomal DNA sequence. Furthermore they observed a dependency of rising ppGpp levels on the degree of Glutamate overproduction in particular. However, a minimal intracellular ppGpp concentration seems to be indispensable for amino acid overproduction since *relA* knock-out mutants were described to show poor growth and low formation of amino acids as well. Back then it still remained a central issue whether increased ppGpp levels directly promoted positive upregulation of amino acid gene transcription (stated by Paul et al. 2005) or if enhanced amino acid concentrations were only a secondary effect of rRNA transcription inhibition (suggested by Zhou and Jin 1998). Interestingly, contradictory findings were published for overexpression of recombinant proteins in limited microbial processes. Apparently a severe reduction of intracellular ppGpp levels was crucial for significantly increased recombinant protein yields. Various research groups succeeded in improved heterologous protein expression under conditions of minimal cell growth using manipulated *E. coli* strains with deficient ppGpp formation abilities (Dedhia et al. 1997, Harcum and Bentley 1999). Further insights were gained from metabolic footprint analysis in an *E. coli* Δ*relA* strain showing enhanced growth-uncoupled Green Fluorescent Protein (GFP) expression. In nutrient deprived cultivations this stringent response impaired mutant facilitated about three-times higher product formation rates of the heterologous GFP protein than the WT accompanied with two-times elevated glucose consumption rates (Carneiro et al. 2011). An entire elimination of a stringent response reaction to nutrient limitation was achieved in an *E. coli* $ppGpp^0$ strain (deletion of the *relA* and *spoT* genes). It was observed that the lack of ppGpp had an immense impact on Ribonucleic acid (RNA) and biomass synthesis (~50 % progression) in the mutant compared to a WT control strain during amino acid starvation. On the transcriptional level, genes of glycolytic key elements like the PTS, Phosphoglucose Isomerase (Pgi) and the PDHC were downregulated such that glycolytic flux through the central metabolic pathway was diminished drastically (Traxler et al. 2008).

1.4. Metabolic Engineering of *E. coli* towards higher Glycolytic Turnover Rates

The previous sections exemplary introduced various ways and experimental concepts how bacterial organisms can be manipulated either externally by using technical applications or internally by using phenotype alterations. In the present study, those documented valuable findings and research insights served as the basis to specifically engineer the industrial workhorse *E. coli* into a microbial chassis with high glucose turnover under industry-related growth conditions. Usually, high metabolic activities of a microbial culture demand high nutritional supply of the cells as well as high provisioning with other essential growth factors e.g. needed for respiration. In order to circumvent possibly resulting restrictions, a nutrient-limited cultivation environment was implemented to ensure intensely reduced bacterial cell growth and oxygen assimilation rates during the process. This stationary growth phase was artificially induced at the transition from nutrient-abundant into nitrogen-deprived cultivation conditions, while the carbon source was in excess all along. Surely such a constructed fermentation scenario is of great interest for industrial biotechnological and microbiological productions. The major benefit of non-carbon nutrient limitations is the fact that a full carbon catabolism is available which allows for sufficient energy generation even in non-growing cells (Shaikh et al. 2009, Rühl et al. 2012). Energy surplus, that is not required for cell maintenance, could be directly channeled into product formation of heterologous metabolites. In theory this could maximize cell-specific productivities and substrate to product conversion yields during stationary phase productions (Boender et al. 2009).

The here presented *E. coli* HGT chassis was designed with a special focus on significantly elevated consumption rates for carbon-based substrates at very slowly growing or resting cellular states. At best, a precursor strain like this can be advanced to have further properties like high product conversion rates combined with a relaxed intracellular stress response at nutrient starvation. Thus, the central idea of this study was to uncouple the stringent response network of *E. coli* from carbon uptake under environmental stress conditions towards an enhanced productivity. In terms of bioprocess engineering this means, such an *E. coli* chassis would achieve growth-like cellular activities for product formation in the late process phase when actual growth rates are at a minimum. Hence, state-of-the-art genetic engineering tools could be applied to insert stable chromosomal

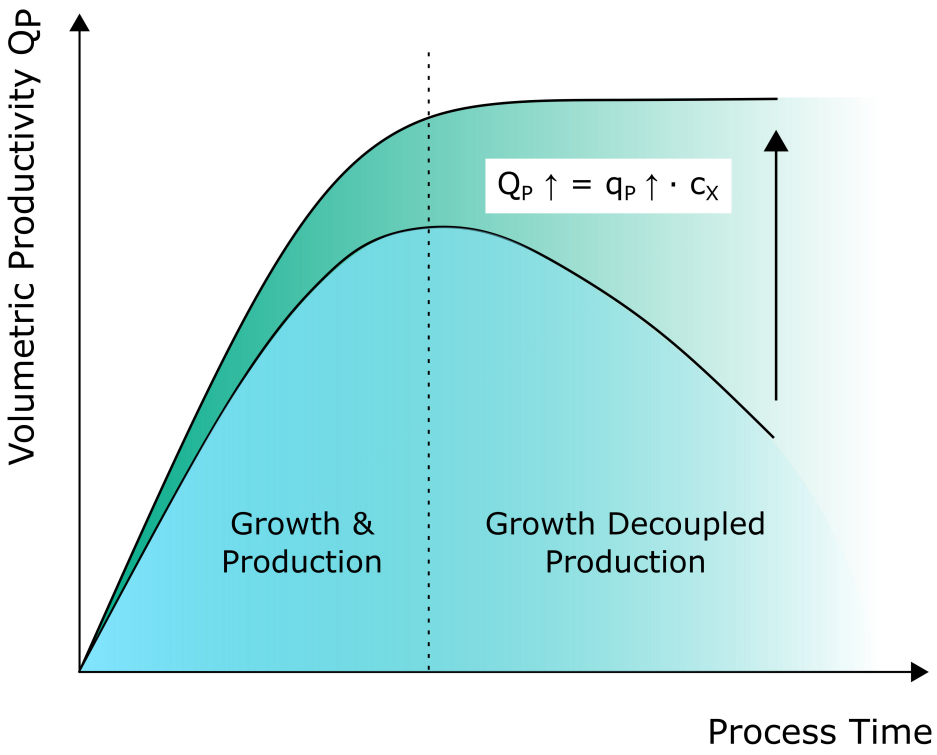

Figure 1.1. Microbial Productivity during Biotechnological Processes. The graph shows the typical progression of growth-coupled product formation during an aerobic microbial fermentation process. The research efforts in this study are yielding at a significantly increased volumetric productivity (Q_P) of the bacterial culture in late process phases with growth-limited conditions. By elevating the biomass-specific glucose uptake rate (q_S), the biomass-specific product synthesis rate (q_P) will be increased correspondingly in the cells.

modifications into the *E. coli* host that lead to highly increased biomass-specific glucose consumption rates and therefore product synthesis rates as a consequence. In non-growing cells the oxygen demand and increased glucose uptake solely would be related to product formation and few maintenance functions of the cells. In this way, growth-uncoupled volumetric productivity rates of the microbial culture (Q_P) could remain at a plateau level after the maximum yield is reached instead of the typically observed dropdown (Figure 1.1). Furthermore, unwanted carbon loss for cell growth and biomass synthesis as well as by-product formation due to stress occurrence of any kind would be reduced. More precisely, the chassis strain should be improved towards a better stress resistance at nutritional starvation conditions. The bacterial stringent response signaling could be uncoupled from carbon and nitrogen metabolism to gain a balanced intracellular regulation upon limitations. A high cellular activity of non-growing cells that is comparable

to exponential growth could guarantee a steady supply of intermediates and precursor molecules for product formation. The interference of direct connections between recognition of environmental limitation conditions and the intracellular response system could be targeted. One such regulatory node could be the signal transduction of the small alarmone ppGpp to the translational apparatus and the transcriptional initiation complex. The ppGpp-mediated interaction of stress signaling and stress response could be controlled by an engineered adjustment of hydrolysis and synthesis activities of the two stringent response protagonists RelA and SpoT towards a balanced level of intracellular ppGpp (Figure 1.2). New-to-nature properties like higher stress tolerance, high level substrate uptake rates and enhanced productivity in nutrient limited environments could be the result of this restructured production strain.

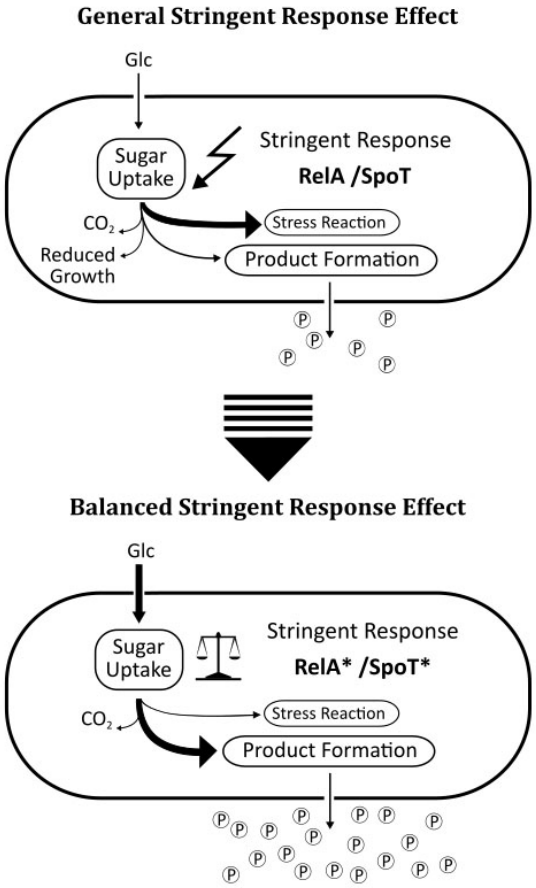

Figure 1.2. Balanced stringent response with enlarged stress tolerance. The graph demonstrates a general approach for a prospective microbial stringent response regulation during industrial productions. The bacterial cell is designed to be released from environmental stress signals such that a high carbon-drain will be channeled towards product synthesis.

2. Theoretical Background

2.1. Nutritional States of Bacteria

The well-known classic Monod's bacterial growth model considers the lifecycle of microorganisms as a causal relationship between the nutrient concentration in the environment and the bacterial growth rate (section 3.2.8 for further details). At substrate abundance microbial cells tend to grow with a growth rate μ at their individual specific upper limit. Whereas, declining nutrient concentrations entail emerging growth deficiencies until the substrate becomes limiting, which obviously implies the end of growth (Monod 1942; 1949, Lobry et al. 1992). In natural microbial habitats availability of essential nutrients such as substrates and co-factors is usually restricted to a very short lapse of time and long periods of starvation are prevalent. During these deprivation periods sustaining of life becomes a vital task. Commonly, it is assumed that starving microbes follow simple first order kinetics and cells die at a constant exponential decay rate (Moats 1971, Peled et al. 1977). Phaiboun and his colleagues recently characterized the dynamics of cell survival in starving microbial cultures. Using *E. coli* as model system, they revised the familiar textbook knowledge of exponential decay in nutrient limited cells with a phenomenology-to-mechanism approach. They accepted the assumption that starving cells die exponentially as true in principle, but only for microbial cultures at high cell densities. The investigated cultures showed declining growth rates immediately at transition into starvation periods. In contrast, low density cultures maintained their viability longer and persevered energy for an extended period of time before dying exponentially at a comparable decay rate. They described the observed survival kinetics to be density-dependent and biphasic. At low nutrient levels they also found mutants of the general stationary phase regulator σ^S ($\Delta rpoS$) to exhibit cell death at twice the exponential decay rate as a WT control culture. In such a case, continued growth and cell activity at

an expense of survival and resource conservation might be beneficial in terms of short period starvations (Phaiboun et al. 2015) like fluctuating nutrient supply conditions in biotechnological large-scale productions.

2.1.1. Hunger Response in *E. coli*

What are the minimal preconditions required for microbial life? For bacterial organisms to grow, a natural habitat must provide an aquatic environment with access to liquid water, an appropriate carbon-based organic source of energy as well as all other essential chemical elements, ions, co-factors and if necessary electron acceptor molecules for respiration. Usually those natural habitats are characterized by their heterogeneity in availability of all the different components, which commonly evolve themselves in the form of gradients. In this way a high diversity of ecological niches is created that mirrors the complexity and multitude of microbial species. Within such environments nutrient fluctuations can be very fast and temporal which is why evolutionary processes in microorganisms generated a variety of strategies to cope with these changing conditions. While waiting for favorable conditions most microorganisms linger in a metabolically inactive state (Koschorreck 2005).

For the majority of bacteria, living in their habitual state means to spend most of their life somewhere between 'feast and famine' as Arthur Koch described this existence in the early 1970ies (Koch 1971). Some 20 years later Thomas Ferenci and colleagues expanded this span of nutritional states and established the hypothesis of a hunger response in bacterial cells. They proposed a further distinction between nutrient-excess conditions (feast) and starvation (famine). Under suboptimal levels of nutrients, but still apart from total nutrient depletion, microbes express a cellular hunger response that can be distinguished from the well-known starvation reactions. The scope of such stress regulation cascades is highly dependent on the nature of the nutrient source that becomes depleted (C, N or P etc.). A batch culture passes through both, hunger and starvation responses, if grown to complete limitation of a nutrient. Starting at a saturated excess-nutrient concentration the culture grows at a maximal attainable rate ($\mu_{\max}$). With declining nutrient concentrations over time the specific growth rate of the culture decreases. Still the hungry organism is growing at very low growth rates and scavenging nutrients at nanomolar levels. Once

the nutrient supply becomes definitely limited, cell growth stops and a protective starvation response superimposes all previous physiological and regulatory reactions (Death and Ferenci 1994, Ferenci 2001). The relationship of nutrient shortage derived stress responses and the corresponding specific growth rates are plotted in Figure 2.1 for the model strain *E. coli*.

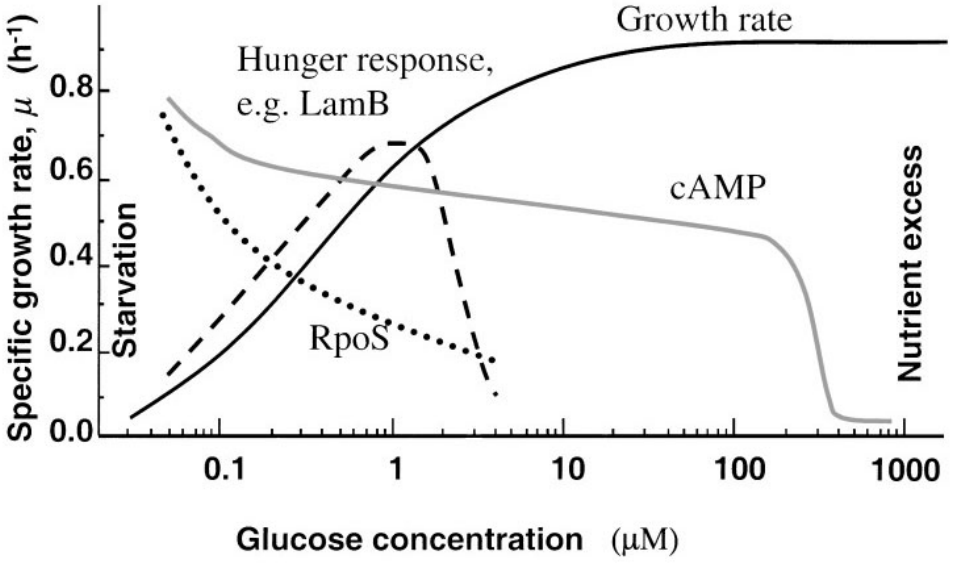

Figure 2.1. Hunger response in *E. coli*. In this review, the author summarized the behavior of different stress signal molecules and the bacterial growth rate at varying carbon source levels ranging from nanomolar to micromolar concentrations. For this graph he compiled data sets from several references. Along the way from nutrient excess to starvation the specific bacterial growth rate μ (from Senn et al. 1994) declines while the levels of all three signal molecules cAMP (gray line, from Notley-Mcrobb et al. 1997), LamB (dashed line, from Notley and Ferenci 1995) and RpoS (dotted line, Notley and Ferenci 1996) have their maximum at different concentrations of glucose. The illustration was modified after Ferenci 2001.

According to Ferenci, the hunger response is defined as the bacterial growth behavior at very low glucose concentrations (< 10 µM) before starvation is established. In this hunger situation, the specific growth rate of *E. coli* is neither zero nor at its maximum rate during exponential growth as can be seen in Figure 2.1. The onset of cAMP synthesis is initiated when glucose is still in abundance (~300 µM) and the culture is growing at almost μ_{max}. This might represent the beginning of the hunger response since elevated cAMP levels are a signal for declining glucose availability (Ferenci 2001). From literature it is known that 1/2 μ_{max} is reached at a critical substrate saturation which has a published value around 40 – 50 µM for *E. coli* grown on glucose at 37 °C (Dykhuizen 1978, Owens and

Legan 1987, Senn et al. 1994, Villadsen et al. 2011). As a consequence, this is also the point of decreasing bacterial growth rates. In the interphase between limitless growth and true starvation second messenger molecules become dominant and cellular responses for substrate scavenging are stimulated. At transition from growth into nutrient-limited preservation, the central regulator of the stationary phase stress response σ^S (RpoS) coordinates intracellular preparations for the imminent hunger phase. The closer the glucose concentration reaches total depletion, the more RpoS sigma factors become expressed in the cells. The σ^S-mediated stress signaling has a direct or an indirect regulatory effect on a number of key molecules at multiple levels like transcription, translation, degradation and regulation of specific activities (Gentry et al. 1993, Battesti et al. 2011).

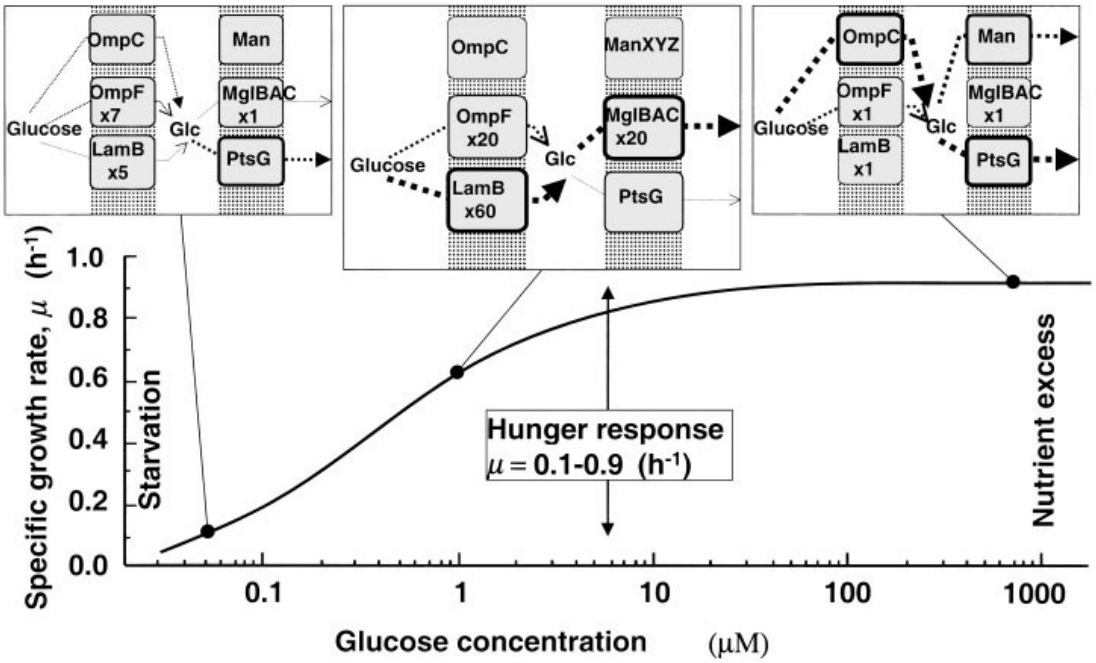

Figure 2.2. Glucose transport pathways in *E. coli*. Glucose consumption systems are displayed at varying levels of carbon availability. The three boxes indicate activity and expression levels of glucose transports across the inner and outer membrane of *E. coli* at nutrient excess, starvation and an intermediate glucose level. Relative gene expression alterations are given as multiplicity-value of the nutrient-excess condition. The illustration was modified after Ferenci 2001.

For example, an elevated RpoS expression has a negative effect on the high-affinity glucose transport pathway which includes members of the sugar porin family (LamB) and superfamily of ABC transporters (MglBAC) amongst others. Such scavenger transporters are mainly induced in accordance with the peak of the hunger response at intermediate

growth rates ($\mu = 0.4 - 0.7$ h^{-1}) and glucose concentrations. The different activity levels of glucose transport pathways into the cell are displayed along various concentrations of glucose in Figure 2.2. Interestingly, gene expression levels of glucose transporters of the outer (OmpCF) and inner membrane involving the PTS, maltose, galactose and mannose systems and their activity spectrum change at different growth rates (Ferenci 2001).

2.1.2. Stress-induced Mutagenesis

Exposure to environmental stress of any kind causes a metabolic regulatory response on the one hand. On the other hand, intracellular mechanisms of stress-induced mutagenesis (SIM) are exhibited at the molecular level as further reaction to the stress signal. The result is a transient accumulation of various mutations within the bacterial genome for the period of the stress burden. An increased mutation rate under stress enables a swift reaction upon changing conditions and a rapid genetic variation that is critical for adaptation. So-called mutators, bacteria with fairly high mutation rates, therefore have a growth advantage in a temporarily unfavorable environment. However, at a long-term perspective those cells accumulate deleterious mutations such that their advantageous position will be diminished in another stress situation (Bjedov et al. 2003, Agashe 2017). From an evolutionary point of view, SIM could be a site effect of selection in bacterial cells preparing for improved survival. This temporary dominance of increased genome-wide mutation rates represents a trade-off between the conditional necessity to adapt to an imposed situation and the intracellular costs of repair and protection (Tenaillon et al. 2004). Damages to the bacterial DNA, which can be directly assigned to a stress-associated origin, trigger the global SOS response in living cells (Radman 1975). Those stress-resistance mechanisms include a cell cycle arrest in the first instance. Consequently, the error-prone DNA repair machinery is highly upregulated while the methyl-directed mismatch repair pathway (MMR) is suppressed at the same time. In this way damaged DNA is repaired by the non-replicative DNA polymerases Pol II (encoded by *dinA*), Pol IV (*umuDC*) and Pol V (*dinB*). In combination these three polymerases can bypass different types of DNA lesions in the template genome such that replication can be restarted and extended at stalled replication forks (Tippin et al. 2004, Fuchs et al. 2004, Foster 2007). This large and complex network of survival functions is accompanied by the RpoS-mediated general stationary phase stress response as it is typical for a nutrient starved culture for instance.

The sole perception of high σ^S expression levels seems to be enough for a bacterial cell to significantly change its mutational spectrum. Mutagenesis pathways are activated in response to an environmental shift in nutrient availability. Depending on the nutritional stress catalyst (carbon, phosphate, nitrogen, oxygen or iron limitation) a distinct mutational profile is produced each of which is characterized by an individual DNA mutation type. Apparently, phosphate and carbon starvations are the most mutagenic and mainly involve a large number of base pair substitutions. Under nitrogen, oxygen or iron starvation conditions remarkably lower mutation rates are observed. Such stress-affected genetic variations are attributed to insertion sequence (IS) transpositions, deletion and insertion indels and partly high occurrence of base-pair substitutions (Maharjan and Ferenci 2017). Prolonged and repeated periods of a distinct nutritional stress may eventually increase the capacity for adaptive changes due to an accumulation of unique stress-specific mutations. Especially at extended hunger conditions those mutations may provide fitness advantages of the mutator cell in comparison to the less competitive wild-type (WT) opponent. In the long term, those bacterial cells exposed to an exceptionally high mutation rate may potentially be affected irretrievably in their ability of survival and nutrient scavenging capabilities (Ferenci 2001).

2.1.3. Bacterial Persistence and Long-Term Survival

Persistence is one of the bacterial long-term survival strategies. The phenomenon can be observed in an exponentially growing population of wild-type *E. coli* cells. Among the growing culture, a very small subpopulation arises that switches stochastically from normal exponential cell division into a slow-growing state from which it can resuscitate. Persistence gives the cells the capability to overcome environmental insults by entering dormancy until favorable conditions are restored. During this transient growth-arrest, the persister cells are able to tolerate multiple antibiotics and other bacteriostatic drugs. This dormant state of the cells should not be confused with extra chromosomal antibiotic-resistance or mutations on the genome. Persisters are isogenic to their wild-type counterparts, except, however lethal concentrations of antibiotics cause no harm to survival of the subpopulation (Gerdes and Maisonneuve 2012). Mechanistic and functional backgrounds on the emergence of bacterial persisters has long been studied. Over the last decades researchers revealed a possible correlation between controlled induction of the stringent

response and the onset of bacterial persistence. Since the stringent response alarmone ppGpp is the main determinant for growth rate control and metabolism during starvation in *E. coli* (Potrykus et al. 2011), it most likely also has a key role in persistence. A direct and inducible transition of active cells into a dormant state was described for a Serine/Threonine kinase (*hipA*) mutant (Korch et al. 2003). The HipA protein, which is also known as the 'high persistence factor A', together with HipB represent the two factors of a toxin/antitoxin (TA) module. By definition of a type II TA system, overexpression of the HipA-toxin immediately leads to growth arrest, which can be reversed by expression of the HipB-antitoxin (reviewed in Hauryliuk et al. 2015).

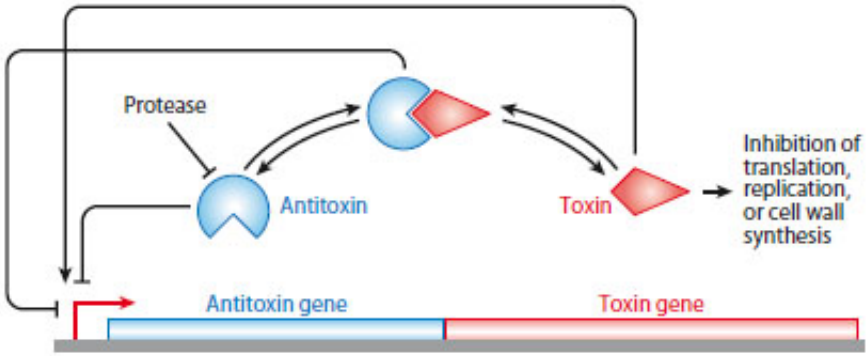

Figure 2.3. Function of a Type II toxin/antitoxin module in *E. coli* K12. The prototypical type II TA locus on the *E. coli* genome is constituted of an antitoxin gene (blue) and a downstream encoded toxin gene (red). In presence of the antitoxin the TA operon promoter is repressed by the TA complex which is typical during rapid growth. High concentrations of free toxin derepress promoter activity and expression of the TA operon is initiated to increase the toxin/antitoxin ratio in the cells. The illustration was modified after Gerdes and Maisonneuve 2012.

Figure 2.3 illustrates how the toxin component inhibits cell growth by repressing translation, replication and cell wall synthesis and the protein-antitoxin autoregulates expression of the *hip* operon and toxin activity. A mutant version of the *hipA* allele (*hipA7*) in *E. coli* was found to have an impact on intracellular ppGpp basal levels upon transition into stress circumstances. Those mutant cells were able to generate a significantly increased ratio of persistence phenotypes depending on their ppGpp synthesis extents. Whereas in stringent response knock-out variants of the mutants, an establishment of the persister state was eliminated, what corroborated the interplay between nutrient stress signaling and

rapid transition into dormancy (Korch et al. 2003). A decade later, these findings were approved by further investigations on the significant role of ppGpp in toxin/antitoxin networks. The tendency of persister formation elimination was confirmed in $ppGpp^0$ strains ($\Delta relA\Delta spoT$) and *E. coli* mutants deficient for the RNA Polymerase-binding transcription factor DksA. Furthermore, a new TA module was introduced in which ppGpp plays the role of the toxin substance that provokes bacteriostasis and persistence at high levels and the SpoT protein that acts as its enzymatic antitoxin (Amato et al. 2013). Equally, HipB is assumed to interact with multiple promoters in *E. coli* on the transcriptional level. Likewise other DNA-binding proteins, the transcriptional repressor HipB binds to a specific palindromic structure within a number of promoter regions and thereby suppresses transcription initiation. In the special case of *relA* transcription inhibition, HipB is able to reduce *relA* promoter activity to a residual amount of about 70%. In a complex together with HipA this repressor function is even elevated to some remaining activity of less than 40% (Lin et al. 2013).

Controversial proposals for the underlying interactions between the TA components and cell growth arrest are found throughout literature. One of these theories suggests a mechanism whereby persistence is a consequence of cell stasis. The persistence factor HipA is described to act as a Serine/Threonine kinase, that catalyzes the phosphorylation of the translation elongation factor EF-Tu, the most abundant protein in *E. coli* and key player in protein biosynthesis. The consequential inhibition of protein synthesis causes instant cell growth arrest and dormancy. The transcriptional regulator HipB-antitoxin interacts with HipA under standard growth conditions and neutralizes its toxin-activity. However, antitoxins are labile proteins if they are not stabilized in a complex with their corresponding toxin and thus prone to cytosolic ATP-dependent protease degradation. In the case of the HipB-antitoxin, the Lon protease is mainly responsible for proteolysis since it is the universal protease for a number of rapidly degraded regulatory proteins. This models implies that the total level of antitoxins is determined by Lon protease activity and in turn the antitoxin level regulates the amount of free toxin compounds (Schumacher et al. 2009, Hansen et al. 2012). The regulatory cascade that underlies this persistence phenotype depends hierarchically on an intracellular increase in ppGpp levels in the first place. High ppGpp concentrations strongly inhibit Exopolyphosphatase (PPX) activity which commonly degrades inorganic polyphosphates (polyP). Accumulation of such PolyP polymeric structures finally activates Lon proteases and type II antitoxins, like e.g. HipB, are degraded as a result (Maisonneuve et al. 2013). Another theory claims the

position that although HipA is also considered as Serine-Threonine kinase, EF-Tu is not a target of HipA activity. Instead, HipA phosphorylates the glutamyl-tRNA Synthetase (GltX) and inhibits aminoacylation of Glutamate in this way. Uncharged $tRNAs^{Glu}$ are generated and accumulate in the cells. Such hungry codons increase the frequency of hungry ribosomal A sites as it is typical for amino acid starvation (Germain et al. 2013). Consequently, translation at the ribosomes pauses and RelA-dependent ppGpp synthesis is triggered (full mechanism described in English et al. 2011). Translational inhibition is a product of high activity of the persistence factor HipA together with the stringent response factor RelA. A few years ago the metabolic activity and nutrient consumption in those growth arrested persister cells were examined. The tests revealed continuing glucose consumption, oxygen respiration and amino acid accumulation during a cultivation of HipA-induced cells which were obviously obstructed in biomass formation (Bokinsky et al. 2013).

2.2. Stress Signaling in Starved *E. coli* Cells

Nutrient poor environments have a determining role in bacterial growth characteristics. Lack of the most essential elements including carbon, nitrogen, phosphorous and amino acid molecules may arrive at the same result eventually. Confrontation with any type of nutrient starvation is sensed by the bacterial cells and a dormant growth mode with static cell numbers is initialized. However, the underlying regulatory and metabolic strategies to cope with different sources of nutrient starvation are largely distinct. Although a protective policy of the cells against nutrient depletion in general may superimpose the individual response to a certain starvation (Ferenci 2001), the initial action steps are tailored for each stress sensing and signaling pathway. Often demands for nutrient scavenging and energy regeneration face metabolic closedown activities upon environmental stresses. Glucose limitation is a typical model for the interplay of opposing strategies and coupling of regulatory control units on different intracellular levels (section 2.2.1).

2.2.1. Carbon Catabolite Control

The bacterial metabolism and growth rate are under control of global superior regulatory systems. A group of genes can be encoded as one genetic unit and also be controlled such as the same. In this case the term of an operon is used in reference to prokaryotes. Several such operons can be organized into a regulon and thus can be located at disparate sites on the bacterial genome. Generally, a regulon is controlled by the expression or interaction of a repressor or activator molecule that either inhibits or induces transcription initiation at a specific gene promoter locus. Furthermore, a set of regulons and operons can be combined into a stress response modulon that acts on a global regulatory level to change the state within the prokaryotic cell. An apparently unrelated number of genes is collectively regulated upon changing environmental conditions and affects overall metabolic processes by control of different regulatory cascades (Neidhardt et al. 1996, Lengeler et al. 1999). The cAMP receptor protein (CRP) modulon in *E. coli* is a prominent example for a globally regulated stimulus response cascade. *E. coli* and other bacterial strains share a certain descending order in which various carbon sources are consumed. Since glucose is preferred as the primary energy source, the sheer presence of glucose in a bacterial habitat or cultivation environment will lead to uptake inhibition of any other carbon-based substrates. Carbon catabolite repression together with carbon catabolite activation are mutually termed as carbon catabolite control. This global regulatory system senses alterations of metabolic fluxes, in particular fluctuations of an extracellular carbon source. An intracellular sensor (catabolite) takes action as facilitator of catabolic gene derepression (catabolite activation) or catabolic gene deactivation (catabolite repression). In other words, the presence of a preferred carbon source (glucose in most model organisms) prevents utilization of secondary carbon sources and determines reduced expression and activities of the corresponding enzymes (Pastan and Adhya 1976, Botsford and Harman 1992). The transport of glucose and other sugars into the bacterial cell is mediated by the multicomponent system of the PTS involving membrane-bound and cytoplasmatic enzymes (reviewed in Deutscher et al. 2006, Cases et al. 2007). The underlying intracellular catabolite repression mechanisms of phosphate translocation, enzyme activation and repression respectively are summarized in Figure 2.4. The glucose molecule passes the cell membrane through the saccharide transporter Enzyme IIC (EIIC). Once inside the cytoplasm, a phosphate group is translocated from phosphoenolpyruvate (PEP) as energy donor to the glucose acceptor molecule to form Glucose-6-Phosphate (G-6-P) via

several proteins of the PTS (EI, HPr, EIIA^{Glc}, EIIB^{Glc}). This phosphorylation event adds a charged residue to the glucose molecule and thus prevents its diffusion out of the cell. All together, the phosphorylation state of EIIA^{Glc} plays a key role in the regulation of carbon metabolism in *E. coli*. If the extracellular glucose concentration is high, the high glycolytic flux into the cell drains the phosphate towards the sugars and leaves the enzyme EIIA^{Glc} predominantly dephosphorylated. Binding of EIIA^{Glc} to various transporters and proteins of non-PTS carbohydrates induces negative regulation of e.g. galactoside transport (LacY), glycerol kinase (GlpK) or melibiose symport (MelB).

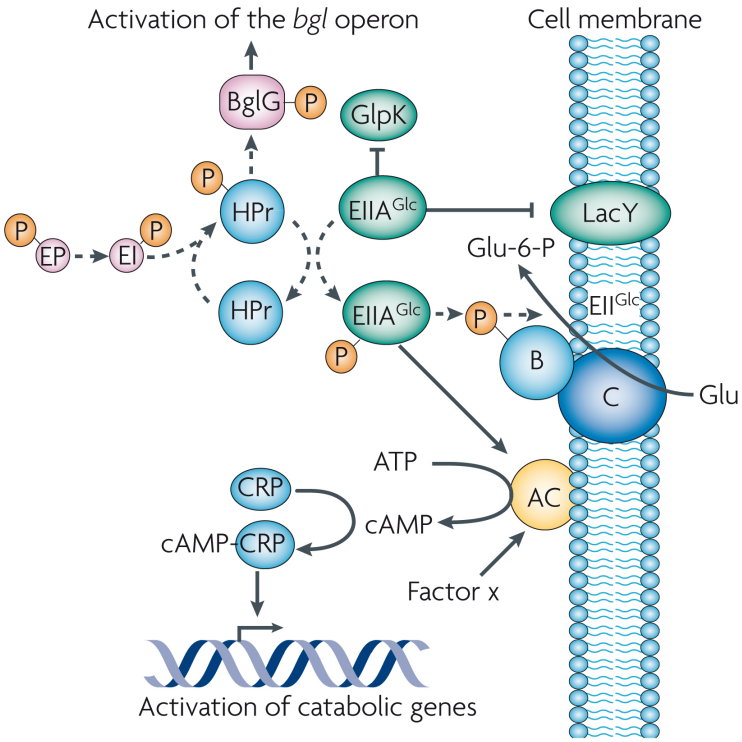

Figure 2.4. Carbon Catabolite Repression in *E. coli*. Glucose enters the cell via the EIIC^{Glc} transmembrane transporter. In the cytoplasm, the glucose molecule immediately becomes phosphorylated by a series of phosphate translocation events involving various enzymes like EI, HPr, EIIA^{Glc}, EIIB^{Glc} and PEP as donor molecule. The phosphate translocation route is marked with several dashed arrows. At high glucose concentrations EIIA^{Glc} is dephosphorylated and represses activities of enzymes participating in secondary carbon source metabolism such as LacY and GlpK. In a phosphorylated state, EIIA^{Glc} activates Adenylate Cyclase (*cyaA*) and the second messenger cAMP is synthesized from ATP. In combination with its receptor protein, a cAMP-CRP complex is formed and the expression of catabolic genes is activated. P: Phosphate; Glu: glucose; Glu-6-P: Glucose-6-Phosphate; GlpK: Glycerol Kinase; CyaA: Adenylate Cyclase; BglG: transcriptional antiterminator. The illustration was modified after Görke and Stülke 2008.

The process that prevents alternative sugar uptake and inhibits the interaction of transporters with their sugar substrates is called inducer exclusion (Postma et al. 1993, Stülke and Hillen 1999). High rates of glucose-mediated carbon metabolism consequently also ensure high enzymatic activities within the Embden-Meyerhof-Parnas pathway (Glycolysis), high pyruvate and in contrast low phosphoenolpyruvate levels. The regulator in the control of the phosphorylation state of $EIIA^{Glc}$ is the PEP to pyruvate ratio in the presence of non-PTS carbon sources. In the absence of glucose the PEP levels decrease while pyruvate accumulates in the cells. Such a low PEP-pyruvate ratio shifts the balance towards the phosphorylated form of $EIIA^{Glc}$ ($EIIA^{Glc}$-P) and thus turns off the catabolite repression function of the PTS. $EIIA^{Glc}$-P activates the membrane-associated enzyme Adenylate Cyclase (CyaA) which synthesizes the signal metabolite cAMP from the purine nucleobase ATP (Hogema et al. 1998). Together with its cognate receptor CRP (cAMP receptor protein - also called CAP: Catabolite Activator Protein), the cAMP-CRP complex directly activates transcription of catabolic genes and operons at usually weak promoter sites (Busby and Ebright 1999, Malan et al. 1984). The complex also has an indirect effect on gene expression as it moreover regulates the action of small non-coding regulatory RNAs (Papenfort et al. 2008, Polayes et al. 1988). Besides $EIIA^{Glc}$, cAMP and CRP, catabolite control is additionally performed by Cra - another catabolite repressor/activator protein. Independent from the cAMP-CRP regulator, the Cra modulon determines the direction of carbon fluxes through central pathways of the carbon and energy metabolism. As DNA-binding transcriptional dual regulator, it positively regulates the expression of numerous genes and operons involved in gluconeogenesis, TCA and glyoxylate shunt. At the same time it exerts inhibition of genes encoding for glycolytic enzymes and the Entner-Doudoroff (ED) pathway (Saier and Ramseier 1996, Ramseier 1996). In 2007 a hypothesis for the possible contribution of the cAMP-CRP complex and the Cra modulon to enzymatic coordination and glycolytic fluxes during nutrient limitation was proposed (Hardiman et al. 2007). The group supported their assumptions by results from glucose-limited fed-batch cultivations of *E. coli* at low growth rates. Apparently the bacterial cells pursued an offensive strategy in catabolite control at the level of precursor supply regulation. During carbon-limited growth, the Cra modulon was shown to regulate large parts of glycolysis, TCA and glyoxylate shunt in harmonization with the cAMP-CRP complex. Coordinative positive and negative regulation modulated the carbon flow into branches of the central carbon metabolism (Figure 2.14) such that precursor and energy supply for biomass synthesis were at a good economic balance.

2.2.2. Nitrogen Regulatory Network

Since the cumulative ammonia content in a standardized bacterial cell like *Escherichia coli* amounts to 20 – 25% of the total cell mass, obviously nitrogen belongs to the group of the most abundant elements in a living cell besides carbon, hydrogen, oxygen and phosphorous (Villadsen et al. 2011). Nitrogen is incorporated into a multitude of biochemical components and cellular macromolecules. For instance, it is an essential part of the amine functional group in all amino acids and thus is involved in the formation of the polypeptide backbone structure in proteins. Furthermore, nitrogen appears as structural component in DNA nucleobases or their derivatives from RNA synthesis, in amino sugars as *N*-acetylglucosamine and many more (Reitzer 1996). Hence, it is not surprising that more than one third of the total nitrogen in a bacterial cell can be found in form of guanine and adenine nucleotides as well as the amino acids arginine and lysine. In view of available external inorganic nitrogen sources, the model organism *E. coli* preferably consumes ammonia, among a variety of other N-containing compounds, for nitrogen assimilation. This choice offers the cells the fastest growth rate of the nitrogen spectrum under aerobic conditions. Assimilated ammonium is fixed by two major intracellular metabolic pathways (Figure 2.5) to form the primary products glutamine and glutamate that serve as nitrogen donors for numerous biosynthetic reactions (Reitzer 2003). One of both routes is constituted of the cyclic catalytic actions of the two synthases Glutamine Synthase (GS) and Glutamate Synthase (GOGAT). First, L-glutamine is formed by GS in an ATP-consuming ammonia assimilation reaction. Then, the cycle is closed when GOGAT catalyzes the formation of two L-glutamate molecules and hence delivers one new substrate for GS. The high affinity of GS for ammonium together with the fact that one molecule ATP is spent per molecule L-glutamate rises the assumption that the GS-GOGAT pathway is prevalent used during growth when nitrogen becomes limited but the energy state of the cell is high due to carbon excess (Meek and Villafranca 1980, Helling 1994; 1998). The second metabolic route includes the amination reaction of 2-ketoglutarate to form L-glutamate by the enzyme Glutamate Dehydrogenase (GDH) (details on nitrogen assimilation are reviewed in Merrick and Edwards 1995, Reitzer 2003, Shimizu 2013, Van Heeswijk et al. 2013). Given the relatively low affinity of GDH for ammonium, the enzymatic activity apparently rather emerges during growth in nitrogen-rich media when the carbon level is low and nitrogen must be assimilated in an energy-saving manner (Sakamoto et al. 1975, Sharkey and Engel 2008).

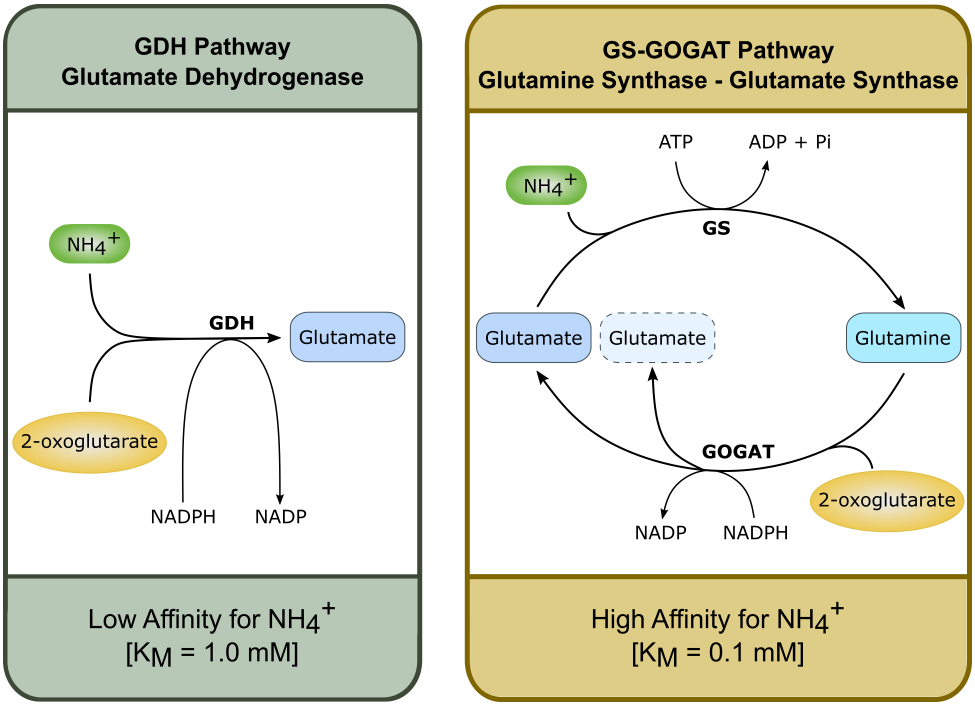

Figure 2.5. Nitrogen assimilation in *E. coli*. In *Escherichia coli* two independent pathways for nitrogen assimilation are available. On the left side, the Glutamate Dehydrogenase pathway is shown. GDH catalyzes the amination (addition of NH_4^+) of 2-ketoglutarate to L-glutamate in a NADPH-dependent reaction. The graph on the right side shows the cyclic GS-GOGAT pathway. Within this cyclic transfer of ammonium, the Glutamine Synthase combines a L-glutamate molecule with NH_4^+ to one L-glutamine in an ATP-dependent amination. Subsequently, L-glutamine together with 2-ketoglutarate is converted into two molecules of L-glutamate, one of which serves directly as substrate for GS in the next round of L-glutamate synthesis. The illustration was modified after Van Heeswijk et al. 2013.

Intracellular nitrogen levels result from nitrogen assimilation at high or low ammonium abundance in the nutritional environment of the bacterial culture. Whenever the availability of the nitrogen source changes, especially when it tends towards nitrogen starvation, the cell rapidly adapts its metabolic organization and initiates the global nitrogen-regulated (Ntr) stress response. In this context, the interplay of the four involved proteins Uridylyltransferase/Uridylyl-Removing Enzyme (UTase/UR) (encoded by *glnD*), protein PII (encoded by *glnB*) and the two-component system NtrB/NtrC (encoded by *glnL* and *glnG*) coordinates the regulation of several transcriptional and enzymatic activities within the Ntr regulon of *E. coli* at nitrogen limited growth. The effects of this Ntr regulatory cascade extend from various ammonia assimilation routes to taking the advantage of alternative nitrogen sources and integrating the nitrogen metabolism with other central processes like carbon assimilation (reviewed in Merrick and Edwards 1995, Reitzer 2003,

Van Heeswijk et al. 2013). At conditions of deficient nitrogen supply, the intracellular glutamine level is low which activates the Ntr cascade by uridylylation of the two signal proteins PII (GlnB) and PII2 (GlnK) as result of UTase/UR stimulation. These two signal proteins in turn activate the kinase/phosphatase properties of the two-component NtrB/NtrC regulator system. As a result, NtrB - also called the Nitrogen Regulator II (NRII) - activates the global transcriptional regulator NtrC - the Nitrogen Regulator I (NRI) - by phosphorylation and thus relocates the transcriptional control of the cell towards a σ^N-dependent expression of genes. Numerous genes and operons participating in nitrogen and amino acid assimilation like transporters and permeases, nitrogen metabolism like glutamine synthetase and various catabolic enzymes are affected by this regulatory rearrangement (reviewed in Hunt and Magasanik 1985, Magasanik 1993, Ninfa et al. 2001, Reitzer 2003). Prior to transcription initiation, binding of the transcriptional dual regulator NtrC-P to the DNA is required for the association of the RNAP-sigma N holoenzyme ($E\sigma^N$) to the nitrogen promoter (reviewed in Reitzer and Schneider 2001, Wigneshweraraj et al. 2008). The twenty-one well-known σ^N-dependent nitrogen promoters relate to genes of the central intermediate and energy metabolism, the amino acid biosynthesis pathway as well as general transport functions and flagellar biosynthesis and others (Zhao et al. 2010, Brown et al. 2014b). Intriguingly, about half a decade ago a connection between the Ntr stress regulon and the stringent response network was established via a newly identified promoter binding site for σ^N upstream of the *relA* gene region (section 2.3.4). However, a recent study revealed the short-term transcriptional response of *E. coli* cells continuously fluctuating between ammonia shortage and full ammonia depletion did not increase *relA* mRNA levels in the first instance. Apparently, within the first 70 seconds of nitrogen limitation the σ^N-mediated Ntr stress response was initiated together with the stringent response via highly elevated ppGpp levels. Synthesis of the small alarmone molecules was possibly accomplished by alternative rapid cellular reactions. The correspondingly upregulated gene expression patterns contributed to amino acid metabolism and transport, protein degradation and modification as well as catabolic pathways. Typically for stringent response-mediated gene expression patterns, translation, replication, cell motility and nucleotide biosynthesis were downregulated (Simen et al. 2017). In general, the intracellular carbon and nitrogen status is signaled by a limited amount of glutamine accompanied by a high 2-ketoglutarate level at the same time (Zimmer et al. 2000, Chubukov and Sauer 2014 and reviewed in Van Heeswijk et al. 2013). A metabolomics study of ammonia deprived *E. coli* provided further evidence for the presence of an internal glutamine/2-ketoglutarate indicator of nitrogen limitation.

They reported a decrease in the glutamine concentration of more than 60-fold and a simultaneous increase in the 2-ketoglutarate concentration of approx. 16-fold after transferring the cells to an ammonium-free culture media (Brauer et al. 2006). Moreover, glutamine and 2-ketoglutarate levels provide a regulatory common link between the two intrinsically independent carbon and nitrogen assimilation networks. Nitrogen acquisition from different sources is tightly regulated by glutamine synthetase and the Ntr regulon. Variations in carbon supply are sensed by the cAMP-CRP complex which regulates transcriptional control of genes from carbon catabolism. Both networks are linked by the direct cAMP-CRP-dependent activation of gene expression from the *glnHPQ* operon promoter which immediately results in enhanced glutamine uptake. Rising glutamine concentrations cause a deuridylylation of the two PII proteins which in turn decrease the availability of the NtrC activator and consequently transcription at σ^N-dependent promoters is deactivated (Mao et al. 2007 and reviewed in Shimizu 2013, Van Heeswijk et al. 2013).

2.2.3. RpoS-mediated General Stress Response

Various responses have been developed throughout the bacterial systematics to evade changing environmental conditions as for instance nutritional difficulties or abrupt shifts in temperature, pH and osmolarity. Adaptation to unfavorable situations requires a stress detecting sensor in the first place, a signal redirection cascade, a set of collectively regulated genes and operons and finally an inducible metabolic pathway to react upon the stress. In *E. coli* one of the global stress responses is triggered by the general stress regulator and alternative sigma factor σ^S (RpoS). Acting at multiple levels of regulation (transcription, translation, degradation and activity adjustment), the RpoS regulon mediates high bacterial resistance towards a vast amount of external factors. Today, a whole series of scientific references on this subject is available throughout literature, that helped to define the RpoS regulon during the past 30 years (Groat et al. 1986, Lange et al. 1995 and many others). Possibly one of the particularly important attributes of such general stress responses is to provide a highly resistant state to the cell. By this means, the encounter of an inducing stress source enables the microorganism to additionally benefit from a programmed cross-protection phenomenon which ensures a more global metabolic restructuring and gene expression control (Battesti et al. 2011). In the case of RpoS, entry into stationary phase or other environmental stress-inducing changes

strongly elevate intracellular σ^S levels by activation of transcription from its promoter rpoSp. In high abundance, the alternative sigma factor σ^S interacts with the core RNA Polymerase (RNAP) at growth arrest and redirects transcription towards the regulation of the general stress response. A well-defined but large set of approx. 500 different genes in *E. coli* K-12 (~10 % of the genome) was demonstrated to be under direct or indirect control of RpoS. The research group around R. Hengge described a hierarchical regulatory network of positively and negatively σ^S-dependent genes that underlie a modular structure of regulation. A high number of those genes were identified to encode regulatory proteins which apparently led to the assumption that these molecules could act as signal integrators for transcriptional fine-tuning or overexpression (Weber et al. 2005a). The default role of RpoS is characterized by an insignificant concentration during exponential growth as consequence of low synthesis combined with high and rapid degradation rates. Only at the onset of a variety of starvation and stress conditions, the repressing mechanism is overcome and RpoS accumulates in the cell. Despite these generally valid principles, the stationary phase sigma factor (σ^S) was equally reported to contribute in the transcription of many central carbon metabolism-related genes at logarithmic growth together with the primary or 'housekeeping' sigma factor (σ^D). The presented data indicated some considerable changes in the activity levels of the acetate metabolism, the TCA cycle and others in logarithmically growing cultures of an *rpoS*-deficient *E. coli* strain. Consequently, RpoS most likely functions as a kind of repressor-like controlling switch not only during starvation conditions (Rahman et al. 2006). Moreover, the presence of RpoS seems to be highly important in the context of bacterial growth and glucose consumption. By disabling the PEP:Carbohydrate Phosphotransferase System of an *E. coli* culture in minimal medium on glucose, transcription was shown to be downregulated for many genetic sites including most glycolytic genes. As a consequence, this σ^S inactivation in a *pts*$^-$ background also resulted in a decreased culture growth rate of 50 % (Flores et al. 2008). Such mutations in the *rpoS* gene, may they occur in a natural or a laboratory population, are indeed a common molecular biological tool for a microorganism to profit from the selective advantage of a deficient sigma factor during nutritional stress. Losing RpoS and thus the ability of the general stress resistance under limited conditions that force selection enabled these mutants to rapidly displace the wild-type population. Lower or even missing levels of σ^S during starvation apparently gave a different picture of sigma factor competition for core RNA polymerase. In fact, increased transcription of genes involved in the hunger response and such contributing to the high-affinity glucose scavenging system was observed. Nevertheless, the true scale of the RpoS mutation was

found to be partially dependent on the stress-level and stress-origin. Since an impaired maintenance of the general stress resistance is in permanent conflict with the hunger response this survival benefit could only be a temporarily lasting advantage to the affected subpopulation (Notley-Mcrobb et al. 2002). The beginning of a nutrient limitation is not necessarily the initial signal for the general stress response to commence. At first, decreasing carbon concentrations are characterized by the onset of the hunger phase which is mainly identifiable by considerably rising intracellular cAMP levels and no detectable σ^S-mediated stress and starvation response. During hunger, the CRP-cAMP modulon basically regulates gene expression in the cell and thus mRNA transcription from the *rpoS* locus is inhibited by the complex. This situation is of special interest upon fed-batch cultivations in a bioreactor where starvation stress can be omitted because the applied constant nutrient feeding strategies mainly contribute to the hunger state (Lemuth et al. 2008). A further description on the hunger response and its detailed actions can be found in section 2.1.1 (Hunger Response in *E. coli*). Whenever nutrient availability passes over from the hunger state into a severe limitation condition, synthesis of the stationary phase sigma factor is initiated. RpoS levels are described to increase following e.g. glucose, phosphate and ammonia starvation, whereby the extent of the resulting σ^S concentration can differ in an order of magnitude. This effect is supported by the antagonistic actions of various anti-sigma factors that inhibit all relevant transcriptional activities. For instance, a vast accumulation of RpoS upon glucose starvation was found to be a consequence of induced *rpoS* transcription and full inactivation of the anti-sigma factor SprE, which normally promotes regulated RpoS proteolysis at the ClpXP protease. In contrast, the RpoS level under ammonia starvation was 10-fold below the observed glucose-limited level and thus remained very close to the value obtained from exponentially growing cells (Mandel and Silhavy 2005). At the onset of starvation, the anti-sigma factor Rsd additionally helps reprogramming the intracellular transcription profile from logarithmic to stationary growth. The interaction of Rsd with sigma factor σ^D and the core enzyme of RNAP inhibits an open complex formation of the holoenzyme at promoters of the housekeeping genes. Hence, the transcription specificity of the cell changes in favor of $E\sigma^S$ dependent promoters (Ilag et al. 2004, Piper et al. 2009, Hofmann et al. 2011). The stationary phase network regulator RpoS is itself controlled by the presence of the small regulator ppGpp amongst other positively or negatively operating molecules. RpoS synthesis in *E. coli* cells entering stationary phase due to nutrient sufficiency or other limitations was reported to be activated by an intracellular alarmone accumulation. An incremental enlargement of the basal ppGpp level was achieved with different spoT mutant strains which produced

abnormally high σ^S concentrations during exponential growth. This sigma factor stimulation was then greatly reduced in ppGpp-deficient mutants on the contrary (Gentry et al. 1993). In later studies on this subject further details on the interplay between the stringent control and transcription regulation by sigma factors were elucidated. The presence of ppGpp is not mandatory for the active transcription at an σ^S-dependent promoter. Rather a new function for ppGpp as a master regulator of the relative σ-factor competitiveness was presented. Alternative σ-factors can become prevalent at the corresponding transcription sites when the stringent alarmone level increases. Other circumstances also conduce to the competition for RNAP core enzyme. The underproduction of σ^D due to mutations in the gene sequence or the overproduction of the anti-σ^D factor Rsd rescued σ^S-dependent promoters even in the absence of ppGpp (Jishage et al. 2002).

2.2.4. Stringent Control by the Alarmone ppGpp

The bacterial stringent control together with its stringent response mechanism, is another microbial element of global regulatory cooperation and signal transduction at different physiological levels. Intracellular stress signal molecules sense a variety of environmental changes and react upon these nutritional stress conditions with a rapid metabolic adaptation. These second messengers detect external growth-impairing factors and function as alarmones that regulate gene expression at the transcriptional level and control central metabolic activities in this way. Often such alarmone molecules are derivatives of nucleotides. Back in the late 60'ies of the last century the two researchers Michael Cashel and Jonathan Gallant made a major scientific breakthrough during their studies on the function of the stringent control gene. They discovered two by then unknown compounds on two-dimensional autoradiograms presenting radio-labeled nucleotides from amino acid-starved *E. coli* culture extracts and proposed a possible involvement of these nucleotides in the inhibition of RNA synthesis. They named their findings magic spot I (ppGpp) and magic spot II (pppGpp) according to the rather unanticipated appearance (Cashel and Gallant 1969). Nowadays these chemical molecules are identified and the metabolic pathways around the stringent response were studied extensively. The formation and degradation cycle of the two magic spots - Guanosine-3',5'-bisdiphosphate (ppGpp) and Guanosine-3'-diphosphate,5'-triphosphate (pppGpp) (together referred to as ppGpp) - is illustrated in Figure 2.6. In principal, ppGpp is synthesized by the 5'-phosphohydrolase

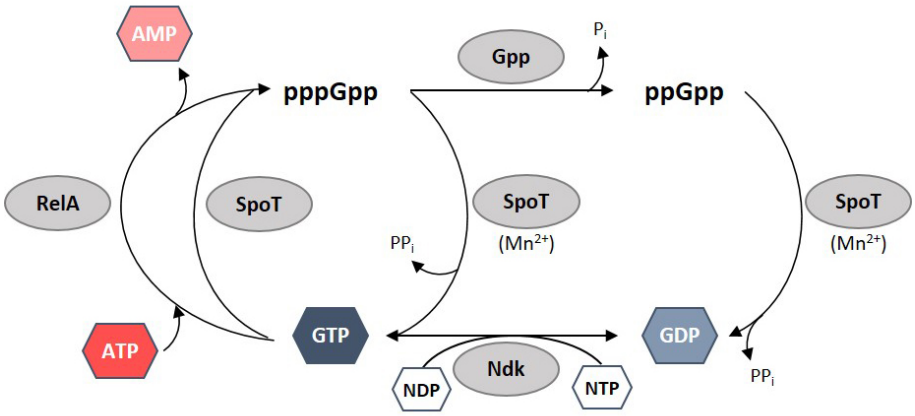

Figure 2.6. General scheme of the intracellular ppGpp metabolism. Formation and degradation of ppGpp and pppGpp are shown under physiological conditions. The RelA and the SpoT enzymes synthesize pppGpp from Guanosine triphosphate (GTP) and Adenosine triphosphate (ATP). The 5'-phosphohydrolase Gpp converts Guanosine-3'-diphosphate,5'-triphosphate (pppGpp) to ppGpp which then is degraded to Guanosine diphosphate (GDP) by SpoT with the help of Mn^{2+} - inorganic phosphate (P_i) and inorganic pyrophosphate (PP_i) is released from the named reactions. The nucleotide phosphokinase Ndk transforms free GDP nucleotides to GTP and provides new substrates for RelA and SpoT. The illustration was modified after Cashel et al. 1996.

Gpp from pppGpp molecules which were previously provided by RelA and SpoT enzymes in an energy consuming reaction that requires ATP and GTP. New substrates for ppGpp formation are provided by the nucleotide phosphokinase Ndk that converts GDP nucleotides to GTP. Degradation of ppGpp occurs by the exclusive action of SpoT. Whereas e.g. cAMP acts as alarmone within the CRP modulon for the general performance of catabolic functions, the small nucleotide ppGpp is the alarmone of the global regulatory system for anabolic reactions. In an exponentially growing bacterial culture with unlimited nutrient supply, the basal ppGpp concentration is kept at a constant low level. Nutritional deficiencies in the environment like starvation for amino acids, fatty acids or diverse carbon and ammonium sources induce a stress-mediated growth arrest and trigger the stringent response as result of a sudden ppGpp level increase. This small alarmone is produced in high amounts by the *relA* gene product, the (p)ppGpp Synthase I, when the available aminoacyl-transfer RNA (tRNA) pool declines to maintain the demands of protein biosynthesis and allow for prolonged survival in periods of nutrient limitation (Cashel et al. 1996). The general characteristics of the stringent response during isoleucine starvation as example are outlined in a physiological model in Figure 2.7. This regulatory network of metabolic activities is equally valid for nutritional stress con-

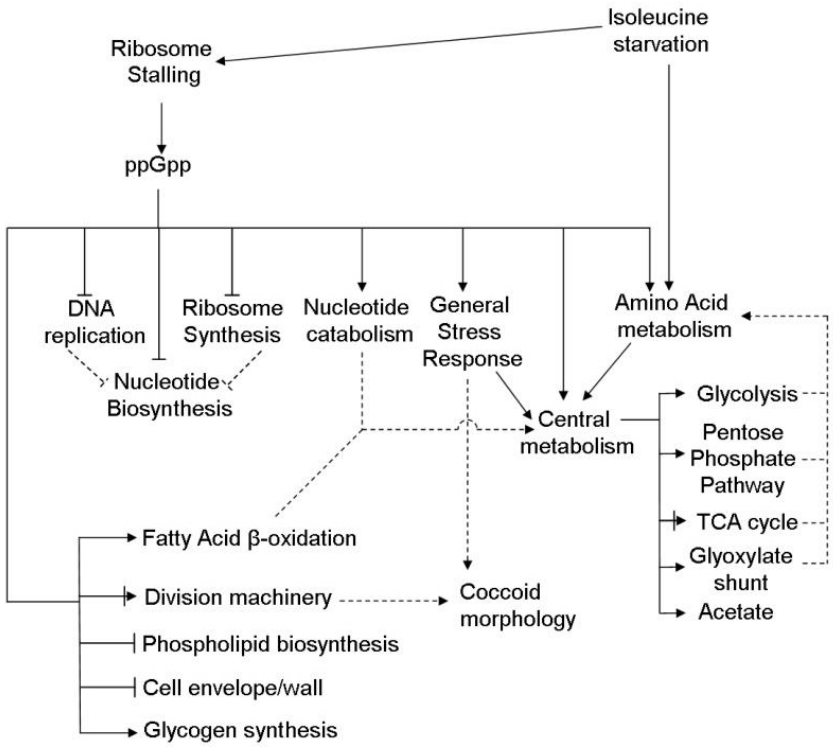

Figure 2.7. Data-driven model of the ppGpp-dependent stringent response to isoleucine starvation in bacteria. The regulatory effects on the bacterial metabolism upon starvation for the amino acid isoleucine are represented by different types of arrows. Solid lines with an arrow head or a flat end imply positive and negative regulatory connections, respectively, or a complex combinatorial regulation involving both. The same description applies to the dashed lines, whereas these refer to indirect functional effects of the generated intermediates. The illustration was modified after Traxler et al. 2008.

ditions of other origin, as described above. Starvation for a nutrient source, especially for amino acids, provokes low affinity binding of deacylated tRNAs to the ribosomal acceptor site which leads to ribosome stalling. The RelA protein is associated to the ribosome through an interaction with the L11 protein (*relC* gene product). It detects the blocked ribosome state and mediates ppGpp synthesis, which in turn at high levels activates the stringent response. The entire process of this mechanism of action for the stringent factor RelA is specified in detail in the publications from Haseltine and Block 1973, Wendrich et al. 2002, Elf and Ehrenberg 2005 as well as English et al. 2011. Accumulation of ppGpp affects many intracellular activities at the transcriptional level. Resource-consuming cell processes like DNA replication, biosynthesis of stable RNAs (rRNA and tRNA), ribosome and phospholipid synthesis as well as cell division proceedings are downregulated. Previ-

ously assimilated metabolites in the form of nucleotides and fatty acids are redistributed into amino acid biosynthetic pathways (Traxler et al. 2008). By interacting with the RNA polymerase core enzyme, ppGpp shifts the transcriptional profile in favor of alternative sigma factor binding and thus acts as a positive regulator of stress-induced gene expression. Several elements of the general stress response, the central carbon metabolism, the nucleotide catabolism as well as the amino acid biosynthesis and protein degradation are activated by the small alarmone. This metabolic restructuring includes extensive preventive actions to prepare the bacterial culture for long-term survival in stationary phase (reviewed in Chatterji and Ojha 2001, Magnusson et al. 2005, Jain et al. 2006, Potrykus and Cashel 2008, Dalebroux and Swanson 2012, Shimizu 2013, Hauryliuk et al. 2015, Ronneau and Hallez 2019).

2.3. Stringent Response Regulation

Some of the previous chapters provided a brief insight into the basic functional principles of bacterial strategies towards the omnipresent fluctuations amongst nutrient excess (feast) and nutrient deprived (famine) conditions in their living environments. Within the scope of this sustained trade-off between fast reproduction and intensive stress defense for cell maintenance, the stringent response regulatory network plays a leading role in microbial existence due to its tremendous abilities in resource reallocation and energy conservation. Hence, the following section refers to the detailed functions of the participating enzymes and targets of the stringent control and their respective regulation.

2.3.1. ppGpp Homeostasis in Bacteria

Whenever the small effector molecule ppGpp accumulates upon limitation, cellular functions in terms of growth rate control and nutrient distribution are the main targets of transcriptional regulation in an activating or an inhibitory manner as visualized in the general scheme in Figure 2.8. Primarily, ppGpp is produced by the two major catalytic factors of stringent response - RelA and SpoT - from ATP and GTP or GDP as described above (section 2.2.4). Both key enzymes entail the ability of ppGpp synthesis in principle

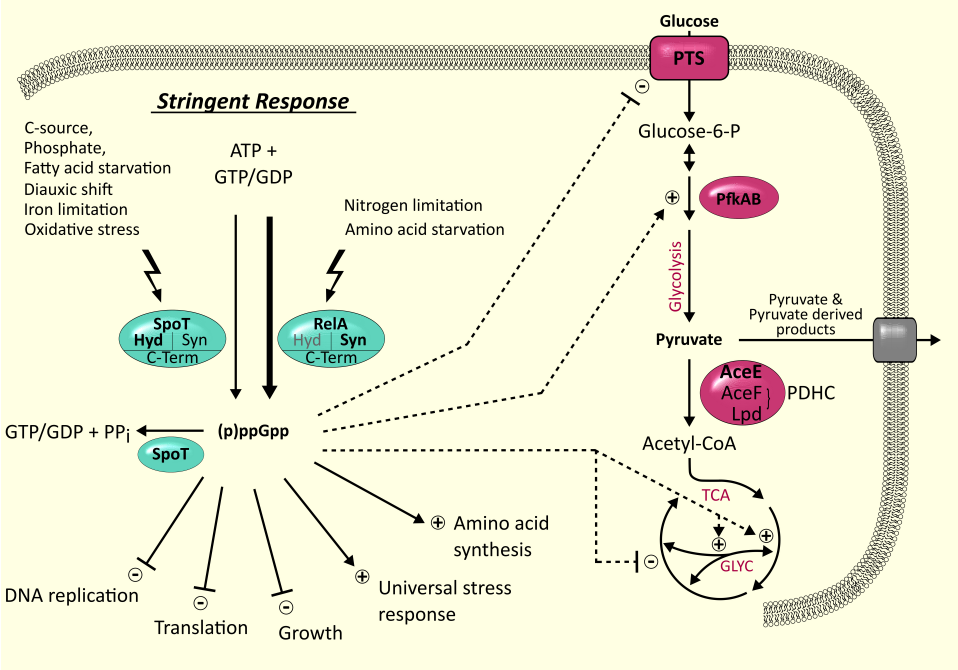

Figure 2.8. General stringent response regulation in *Escherichia coli*. A broad variety of environmental stress-factors is known to initiate the intracellular stringent response to starved conditions. While nutrient starvation for amino acids or a N-source directly increase the activity of the (p)ppGpp Synthase I (RelA), varying limitations activate the (p)ppGpp Synthase II and Pyrophosphohydrolase (SpoT). Both enzymes catalyze the alarmone ppGpp from ATP and GTP or GDP, respectively, but with highly different catalytic affinities (Kanjee et al. 2012). RelA contributes the major proportion of ppGpp upon its activation, whereas SpoT has both - weak synthesis (Syn) and strong hydrolysis (Hyd) abilities. Positive (plus symbol) or negative (minus symbol) regulatory effects of increased ppGpp levels are indicated with solid arrows for acknowledged transcriptional arrangements of cell growth and maintenance and with dashed arrows for possible regulatory targets in the central carbon metabolism as suggested by Durfee et al. 2008 and Traxler et al. 2008. The illustration was modified after Michalowski et al. 2017.

but their individual activity profile, enzyme stability as well as their specific substrate affinity disagree substantially (see below). The RelA protein, also called the (p)ppGpp Synthase I, provides the main fraction of ppGpp during nitrogen- and amino acid-based limitations due to its highly active synthase domain. Whereas SpoT is described to be relatively inactive during amino acid starvation. Other sources of nutrient deprivation (carbon, phosphate, fatty acid, iron starvation) or external stress signals (diauxic shifts or oxidative stress) are necessary for SpoT activation. Furthermore, the basal level of ppGpp, determined in exponentially growing bacterial cultures, was attributed to a logarithmic growth activity of SpoT. Studies with an *E. coli* Δ*relA* strain revealed a balanced ppGpp synthesis and degradation during exponential growth and referenced this alarmone occurrence to the dual functionality of SpoT, which provides both ppGpp formation by

the (p)ppGpp Synthase II and degradation of the same by the Pyrophosphohydrolase. At transition into conditions of physiological stress the intensity of ppGpp hydrolysis by SpoT is downregulated (Harshman and Yamazaki 1971, Sarubbi et al. 1988, Spira et al. 1995, Murray and Bremer 1996, Vinella et al. 2005, Battesti and Bouveret 2006, Bougdour and Gottesman 2007). These individual contributory effects of RelA and SpoT to the stringent response were subject to a whole range of studies that examined growth characteristics in a variety of bacterial mutants. Basically, *E. coli* cells lacking a catalytically active *relA* gene product were found to be either fully or partially restricted in ppGpp accumulation. Several decades ago, the terms of a 'relaxed phenotype' and a 'relaxed mutant' were established for *E. coli* cultures presenting such characteristic behavior. Back then the main implication of a relaxed phenotype was focused on the critical regulatory control of ribosomal RNA (rRNA) expression by the stringent response. In contrast to the stringent amino acid regulated synthesis of rRNA in the wild-type strain carrying the RNA control (RC) stringent allele, the relaxed mutant was unresponsive to amino acid starvation (Alföldi et al. 1962). Additional deletion of the *spoT* encoding genetic region in such an *E. coli* Δ*relA* strain eventually eliminates ppGpp accumulation and disrupts stringent response permanently. A so called ppGpp^0 (Zero, Δ*relA*Δ*spoT* strain) mutant displays a pleiotropic starvation-dependent phenotype which is often accompanied by a range of undesirable growth-related features. Usually, the physiology of these cultures can be well distinguished by their lack of growth in minimal synthetic medium due to multiple amino acid requirements, their difficulties in regular cell division and resulting poor survival of aged cultures as well as their immotility. Beyond these disadvantageous features, an aberrant stationary phase morphology that consequently disables the cultures in stable nutrient starvation survival was published independently by different scientific groups. The corresponding articles discussed the impacts of a defective cell-cell aggregation, which typically leads to sedimentation, an absent filament formation, a failure in inducing the coccoid bacterial shape and an impaired ability to synthesize the alternative sigma factor σ^S in cells entering stationary phase (Xiao et al. 1991, Gentry et al. 1993, Gentry and Cashel 1996, Tedin and Norel 2001, Magnusson et al. 2007). All these findings emphasized physiological changes and metabolic adjustments in different mutants with gradually decreasing ppGpp levels. In return, modifications within the gene locus of *spoT* like insertions of a second actively transcribed variant or deletion of the *spoT* open reading frame (ORF) on the chromosome were described to be lethal in a *relA*$^+$ background as consequence of an enormously high intracellular alarmone concentration in the cells (Xiao et al. 1991, Gentry and Cashel 1996).

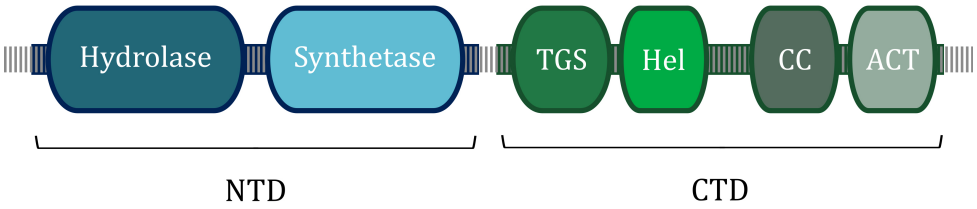

Figure 2.9. Domain Structure of RSH Proteins in *E. coli*. The structure of the RSH protein is divided into a conserved N-terminal domain (NTD) including the Hydrolase and Synthase regions with catalytic activities. The regulatory C-terminal domain (CTD) halve consists of the Threonyl-tRNA Synthetase (TGS) domain, helical sites (Hel), a conserved Cysteine (CC) domain and the Aspartokinase, Chorismate Mutase and TyrA (ACT) motif. The illustration was modified after Atkinson et al. 2011.

The widely known group of RelA and SpoT homologue (RSH) proteins, which were named after their *E. coli* enzyme sequence similarity, nowadays reached an impressive amount of categorized and proposed members. This large superfamily of ppGpp synthesizing and hydrolyzing enzymes extends over a variety of subgroups across the tree of life including most free-living bacteria and archaea as well as eukaryotes like plants (*Arabidopsis thaliana*) and animals. As opposed to this, RSH protein species were not yet discovered in mostly obligate intracellular parasites and endosymbionts (Van Der Biezen et al. 2000, Mittenhuber 2001, Tozawa and Nomura 2011). A few years ago, amino acid sequences of those RSH variants were classified by phylogenetic analyses into three superordinate protein groups according to their domain architecture. In this context, the hypothesis of small stand-alone alarmone synthases and hydrolases arose. During evolution they could be gained and lost to enable bacteria to benefit from a dynamic stress response physiology on the one hand. Long RSH sequences comprising all six structural regions of a bifunctional protein, as can be obtained from Figure 2.9, were identified on the other hand. Apparently this RSH subgroup originated from a gene duplication event early in bacterial evolution and specialized its functions due to highly conserved regions (Atkinson et al. 2011, Atkinson and Hauryliuk 2012). RSH proteins with a single or with dual functions can be dissected into a catalytic N-terminal domain harboring the ppGpp synthase and hydrolase enzyme regions as well as the regulatory C-terminal domain. The primary functions of the conserved C-terminal Threonyl-tRNA Synthetase (TGS) domain and Aspartokinase, Chorismate Mutase and TyrA (ACT) motif are exclusively attributed to regulation of SpoT activity as a mediator of starvation signaling. An interaction between the central TGS domain of SpoT with acyl carrier protein (ACP), one of the cofactors in fatty acid synthesis, could be the long-awaited answer to the question how SpoT can

manage to switch from its strong hydrolase to its rather weak synthase activity. The proposed hypothesis by A. Battesti and E. Bouveret suggests different forms of SpoT bound to an ACP molecule. A changing ratio of acylated to unacylated ACP has an impact on the conformational modification of the SpoT-ACP complex which serves as intracellular sensor for fatty acid and carbon-source limitations, respectively. The resulting allosteric transition of SpoT turns the balance of enzyme functions towards a low ppGpp synthesis rate and thus initiates the SpoT-mediated stringent response (Battesti and Bouveret 2006, Potrykus and Cashel 2008). In the RelA protein, C-terminal sequence elements are involved in its catalytic enzyme regulation in an equal manner. A model for the regulatory control of RelA ppGpp synthesis activation by its oligomerization state was proposed. This model supports the theory that two Cysteine (C) residues and one Aspartate (D) within the C-terminal conserved region (aa 612 to 638) facilitate oligomer formation between ribosome-bound and free RelA monomers which keeps RelA in an inactive form. Upon amino acid deprivation the oligomer dissociation is induced and RelA obtains its active state (Gropp et al. 2001, Yang and Ishiguro 2001).

Although the RelA and SpoT proteins from *E. coli* share a structurally common architecture, the similarity of both amino acid sequences within the two peptides is only at a value of ~30 % (Figure 2.10) and catalytic activities of the N-terminal protein features are substantially disparate. The RSH family is divided into bifunctional enzymes which possess both, synthase and hydrolase activity, such as SpoT and monofunctional enzymes with only synthesizing abilities like RelA. In gram-negative bacteria like the model microorganism *E. coli*, the monofunctional RelA is responsible for the major ppGpp accumulation performance on occasions of starvation. The bifunctional SpoT protein is rather viewed as main protagonist of high-affinity ppGpp hydrolysis that can switch to a weak synthase activity on demand (Mittenhuber 2001). The presence or absence of the protein‘s ppGpp degrading function is determined by a well conserved HD domain within the hydrolase part of the NTD. This specialized conserved catalytic site was ascribed to characterize the superfamily of Mn^{2+}-dependent pyrophosphohydrolases of which SpoT is naturally a member. These metalloenzymes contain a combination of metal-chelating residues including the eponymous amino acids Histidine (H) and Aspartate (D) in their HD domain. The corresponding amino acid residues are substituted to Phenylalanine (F) and Proline (P) in the RelA sequence, which turns the RelA hydrolase into an inactive form but still retains its native protein structure (Aravind and Koonin 1998, Sajish et al. 2009). The other exceptionally important catalytic site of the NTD is situated within

the ppGpp synthesizing protein region. The research group around B. Prakash were the first to report a charge reversal in the ppGpp synthesis domain of monofunctional (ExDD motif) and bifunctional (RxKD motif) RSH proteins, which is highly conserved across a variety of species. The ExDD (Glu-x-Asp-Asp) motif of the RelA protein contains the two negatively charged amino acid residues Glutamate (E) and Aspartate (D). This dual negative charge qualifies the RelA synthase to provide a second Mg^{2+} binding site that stabilizes the phosphates of the GTP nucleotide and offers variable substrate affinities to the enzyme. Although both guanosine derivatives, GDP and GTP, can serve as acceptor molecule for pyrophosphate transfer during (p)ppGpp synthesis, the binding capacities allowed by the ExDD motif highly prefer GDP as main substrate over GTP. The calatytic synthase reaction from ATP and GDP directly creates ppGpp such that the hydrolysis activity to convert pppGpp into ppGpp by Gpp (phosphohydrolase) is bypassed. Correspondingly, the charge reversal explains the weak synthase activity in bifunctional RSH proteins like SpoT which contain the positively charged RxKD (Arg-x-Lys-Asp) motif based on the two residues Arginine (R) and Lysine (K). In opposition to RelA, SpoT shows a distinct substrate preference for GTP. Apparently binding of a Mg^{2+} ion to the RxKD motif promotes a structural loop-to-helix transition in close proximity to the active site and the substrate binding pocket is locked. The two substrate molecules ATP and GTP are excluded from the enzyme complex in a way that pppGpp formation is prevented. The effective interaction of these catalytic sites with Mg^{2+} and the nucleotide substrates was further investigated by exchanging the conserved amino acid residues in the RelA and SpoT protein, respectively. This means, the ExDD motif in the monofunctional RelA was substituted to a RxKD amino acid order and vice versa for the bifunctional SpoT. Promptly, the effect of Mg^{2+} ions to the enzyme-substrate complex formation of a mutant monofunctional protein (ExDD $\rightarrow$ RxKD) was reversed and GTP/ATP nucleotide binding was severely inhibited with higher Mg^{2+} concentrations. Intriguingly, a bifunctional protein (RxKD $\rightarrow$ ExDD) attained a GTP and ATP binding behavior due to the motif reversal that was comparable to the wild-type RelA nucleotide binding, even at ascending Mg^{2+} concentrations. An in vitro (p)ppGpp synthesis assay with the named ExDD/RxKD domain reversal mutants finally uncovered the individual properties of the conserved enzyme sites to the small alarmone accumulation. The substitution mutation of RxKD to ExDD in the bifunctional protein caused a drastic reduction in ppGpp synthesis by 90% compared to the wild-type performance. On the contrary, the ExDD to RxKD reversal in the monofunctional mutant in fact resulted in a ~2.5-fold higher ppGpp formation than observed in for the WT protein (Sajish et al. 2007; 2009).

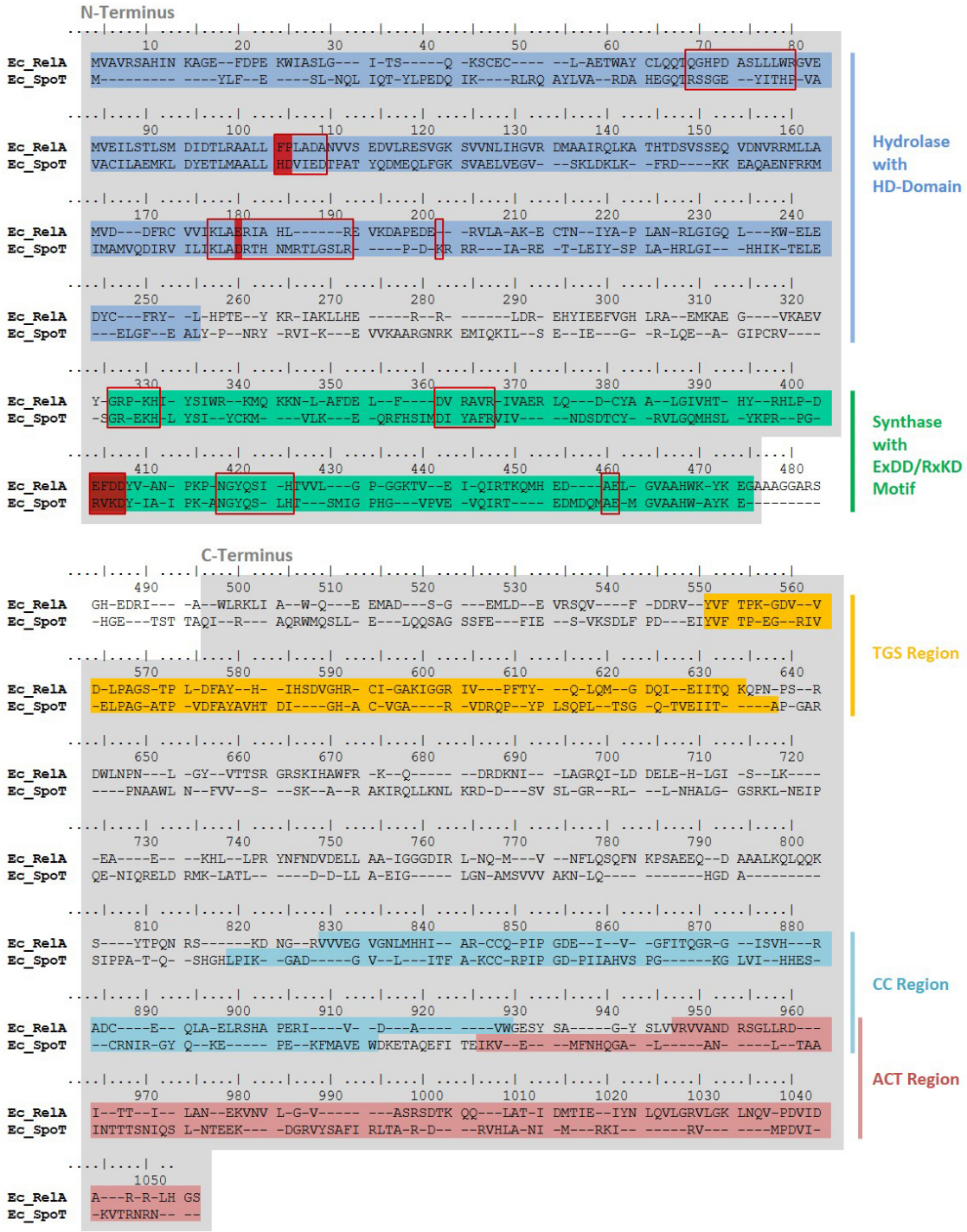

Figure 2.10. Alignment of functional domains in RSH from *E. coli* K-12 MG1655. Amino acid sequences of RelA and SpoT are aligned and show a similarity of ~30 %. The C-terminal and N-terminal halves of both peptide sequences are highlighted in gray. Within the N-terminal region the Hydrolase sequence including the HD motif and the Synthase sequence with the ExDD/RxKD domain are highlighted in blue and green, respectively. As depicted, the C-terminus contains the TGS region (yellow) as well as the CC (violet) and the ACT (orange) regions. Sequence information is based on Atkinson et al. 2011.

2.3.2. Intracellular targets of ppGpp

Only one small molecule is the master effector for the global regulation of a plethora of metabolic pathway rearrangements, structural reorganisations and transcriptional reprioritizing. To put it briefly, ppGpp can either act as indirect regulator of gene expression by modifying transcription profiles or it can directly target enzymes of metabolic and stress responses. Despite the obvious spectrum of proteins participating in stringent response as to be named RelA, SpoT, Gpp and as a matter of course RNA Polymerase - the main intracellular target of ppGpp regulation (further details in section 2.3.3), the alarmone binds directly to a variety of specific target enzymes as well.

GTP Pathway and GTPases

Upon the bacterial reaction to amino acid depletion, ppGpp is produced from GTP and ATP molecules up to the micromolar concentration level within a very short time frame. Consequently, the intracellular nucleoside triphosphate pool is subject to rapid alterations and the GTP availability diminishes as a result of its indirect mechanism of action. In the course of GTP biosynthesis, the Guanosine triphosphate nucleotide is synthesized via two different pathways. Although both conversion processes differ in their starting compound assortment as well as in their catalytic enzymes, they share inosine 5'-phosphate (IMP) as a common key intermediate in purine nucleoside triphosphate synthesis. An involvement of the regulator in GTP provisioning transpires through direct regulation of the first enzymes of the guanylate and adenylate biosynthetic pathways. The activity of the two enzymes IMP dehydrogenase and adenylosuccinate synthetase was reported to be strongly inhibited by interaction with ppGpp (Gallant et al. 1971, Pao and Dyes 1981). Regulatory effects of ppGpp on the guanosine metabolism, nucleotide uptake and interaction mode are undoubtedly further reaching than explained here. An outstanding review on this topic is available in Kanjee et al. 2012.

The GTPase superfamily in prokaryotes is a large group of hydrolitic enzymes that in particular degrade GTP to GDP. In bacteria their main functions contribute to translation, cell cycle regulation, intracellular protein transport, cellular motility and signal transduction (Leipe et al. 2002). Ribosome-associated GTPases are molecular switches of

translation as they have a reputation for acting like the checkpoints to ribosome assembly in a GTP-attached complex. They bind at specific immature sections within the precursor ribosome conformation and ensure by steric hindrance a precise structure maturation before further subunit assembly occurs (Britton 2009, Verstraeten et al. 2011). Through direct inhibition of this GTPase activity by ppGpp, accurate ribosome assembly is discontinued and the decreasing cellular pool of 70S ribosomes is followed by a reduced growth rate (Zhang et al. 2018). Other cellular GTPases modulate the protein biosynthesis process as they exert roles in translation elongation and initiation. The bacterial translation initiation factor IF-2 (bIF-2) mediates the initiation of protein synthesis by coordinating base pairing between the initiator $tRNA^{fMet}$ and the mRNA start codon when the translating ribosome is assembled. Binding of ppGpp to bIF-2 happens with the same affinity as GDP association. This ppGpp-bound form of bIF-2 is fairly inactive and thus hinders the initial dipeptide bond formation and association of the initiator tRNA under stress conditions (Milon et al. 2006, Mitkevich et al. 2010). After the mature ribosome is assembled and translation is initiated the GTP-bound translation elongation factor Tu (EF-Tu) ferries aminoacylated-tRNAs to the ribosomal A-site where EF-Tu hydrolyzes GTP upon proper tRNA incorporation (Sprinzl 1994, Song et al. 1999). During the active protein synthesis process activity of the translation elongation factor G (EF-G) provides the necessary energy for mRNA and tRNA translocation at the ribosome (Zhou et al. 2019). The activities of both essential GTPases can be inhibited by direct competitive binding of ppGpp (Rojas et al. 1984, Dix and Thompson 1986 and reviewd in Kanjee et al. 2012, Bennison et al. 2019).

(p)ppGpp Synthase I - RelA

RelA activation occurs fast once a deacylated tRNA enters the A-site on a ribosome. The resulting dramatic increases of the intracellular ppGpp level directly regulates its own turnover rate at the ribosome-associated RelA proteins. Direct binding of ppGpp to RelA triggers a positive allosteric feedback loop, activates the enzymatic synthase function and finally intensifies the cellular reaction to stress (Shyp et al. 2012). Based on this positive regulation mechanism, small individual outputs of RelA activity all over the cytoplasm can be amplified and synchronized to a potent metabolic signal strength that rapidly coordinates stringent response (Traxler et al. 2008). However, small fluctuations of ppGpp beneath the threshold level also require regulation so that avalanche-like releases of the

effector molecule are suppressed. In this context, the indispensable role of SpoT during cell proliferation and exponential growth becomes evident (Xiao et al. 1991). Fluctuations between high and poor nutritional states of the cell provides a further control level. When amino acid availability recovers, the translation apparatus restarts its action and ppGpp accumulation by RelA is abruptly inhibited. A slow negative feedback loop is generated that in combination with the fast positive feedback loop efficiently switches from starved to non-starved responses (Kim et al. 2007, Traxler et al. 2011).

Nucleotide Metabolism

Metabolic rearrangements during stress include the downregulation of many enzymes involved in nucleotide metabolism and cell division due to the decreasing demand for stable RNA synthesis and DNA replication. The DNA primase DnaG is a key enzyme of replication and consequently an important component of the bacterial replisome. Interaction of DnaG with the helicase DnaB forms the so-called primosome which is responsible for the synthesis of a short RNA primer complementary to a single-stranded (ss) DNA template. This short nucleotide sequence is then used by the DNA polymerase to initiate DNA strand replication at a origin of replication on the chromosome or a plasmid (reviewed in Frick and Richardson 2001). In *E. coli*, ppGpp was reported to be a strong competitive inhibitor of DnaG since it binds at the intrinsic nucleotide binding site of the enzyme. The resulting arrest of the replication fork in the process of *de novo* DNA synthesis is a crucial factor during stringent control (Keck et al. 2000, Maciąg et al. 2010).

Lipid Metabolism

Similar to the regulatory events in stress-induced nucleotide metabolism, the demand for new membranes to form cell envelops as part of cell proliferation is lowered in bacterial cultures exposed to nutrient deprivation. Under circumstances of high cellular growth rates, the two membrane-associated enzymes glycerol-3-phosphate acyltransferase (PlsB) and phosphatidylglycerophosphate synthase (PgsA) supply their corresponding cellular processes with lipids and phospholipids, respectively. The catalytic activities of both membrane proteins are directly inhibited by ppGpp (Merlie and Pizer 1973, Heath et al.

1994). Within the bacterial type-II fatty acid biosynthesis pathway, the acetyl-CoA carboxylase (ACC) complex plays a major role. The catalytic units together with the carrier protein of the ACC complex facilitate the intermolecular transfer of a carboxy group to acetyl-CoA to generate malonyl-CoA (Bilder et al. 2006). The heterotetrameric acetyl-CoA carboxytransferase subunit of the complex was reported to be specifically inhibited by physiological ppGpp concentrations (Polakis et al. 1973).

Carbon and Nitrogen Metabolism

Throughout literature, most articles refer to ppGpp having a cellular effect on carbon metabolism on the gene transcription level by acting as a positive or negative regulator. Publications of direct intracellular protein targets within the central carbon pathway are rather rare. One of these described interaction partners is the NADPH-dependent glutamate dehydrogenase (GdhA) enzyme. In *E. coli*, L-glutamate is synthesized from ammonia, NADPH and 2-ketoglutarate in an amination step catalyzed by GdhA induced by growth on glucose and ammonia (Veronese et al. 1975 and reviewed in Reitzer 2004). At transition from nutrient excess conditions to carbon or nitrogen deprivation intracellular concentrations of ammonia or 2-ketoglutarate decline while NADPH accumulates in starving cells. The enzymatic structure of the L-glutamate dehydrogenase with NADPH alone in instable and subject to degradation by ATP-dependent proteases like ClpAP, ClpXP, Lon and others. By allosteric binding, the guanosine nucleotides GTP and ppGpp can stabilize the GdhA-NADPH complex and reverse its sensitivity for proteases (Maurizi and Rasulova 2002, Weichart et al. 2003). Another central metabolic enzyme being reported a direct interaction target for the stringent response alarmone is the phosphoenolpyruvate carboxylase (Ppc). The enzyme utilizes the pivotal intermediate PEP of the central carbon metabolism together with P_i and Mg^{2+} or Mn^{2+} as a cofactor to catalyze the carboxylation reaction to form oxaloacetate which replenishes the TCA (Kameshita et al. 1978, Terada and Izui 1991). In opposite to many other studied enzyme regulations described here, ppGpp was reported to provoke Ppc activity upon binding even at its physiological concentrations during starvation (Pao and Dyes 1981).

2.3.3. Interaction with RNA Polymerase

Probably the most important interaction partner for the ubiquitous stress signal molecule ppGpp in prokaryotes is the RNA Polymerase (RNAP) multi-subunit protein complex. This sophisticated enzyme is essential to life since its activity drives bacterial as well as advanced living organisms to grow, to reproduce and to survive through excess and starvation conditions. Typically, RNAP performs the well-known physiological process of RNA transcription from a genetic DNA template that generates mRNA sequences which are then subject to translation into an amino acid polypeptide at the ribosomes. In its functionally assembled structure, the core RNAP binds a specific sigma factor protein and finally initiates transcription at a target promoter on the chromosome. During periods of nutritional deprivation of various origins, bacteria especially manage to overcome the trade-off between cell growth and maintenance by altering the RNAP availability at defined genetic sites. The gene expression profile shifts from growth to growth-arrest and these transcriptional adjustments are facilitated via direct interaction of the small effector ppGpp with the RNAP core enzyme. Competition of sigma factors for RNA Polymerase acquisition is regulated by ppGpp and the specific transcription factor DksA in order to repress transcription of stable RNAs (rRNA and tRNA), cell proliferation genes and others. Simultaneously, transcription of biosynthetic operons, amino acid biosynthesis genes, protein hydrolysis genes and central carbon pathway genes is promoted. ppGpp additionally activates transcription from promoters of many alternative sigma factor-dependent genes (RNAP action and regulation is reviewed extensively throughout literature in e.g. Nyström 2004, Magnusson et al. 2005, Potrykus and Cashel 2008, Hauryliuk et al. 2015, Gourse et al. 2018). The modular structure of the *E. coli* RNA Polymerase assembles from its five subunits to form the core enzyme comprising two alpha subunits, the beta and beta prime subunits as well as the small omega subunit. This $\alpha_2\beta\beta'\omega$ complex is coordinated at a specific promoter on the genome by a transcriptional sigma factor, e.g. the most abundant σ^D, resulting in the RNAP holoenzyme ($E\sigma^D$) that is required for transcription initiation. Binding of the holoenzyme to the chromosome unwinds the promoter DNA duplex strand and establishes the transcription bubble of the open promoter complex (Burgess et al. 1969, Hinkle and Chamberlin 1972). In recent times, different studies of the *E. coli* RNAP in complex with ppGpp and partially with DksA were published (Ross et al. 2013, Zuo et al. 2013). Apparently, both guanosine alarmone derivatives, ppGpp and pppGpp, bind to the same interface on RNAP whereas the latter showed

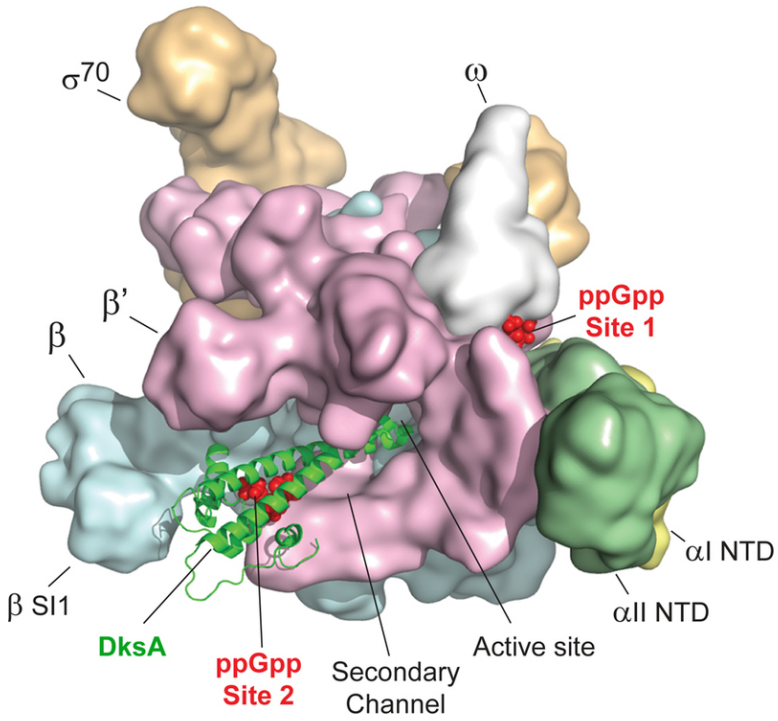

Figure 2.11. Surface structure of the *E. coli* RNAP in complex with ppGpp and DksA. The prokaryotic RNA Polymerase holoenzyme of *E. coli* is shown with each subunit highlighted in a different color. The main core enzyme subunits consist of the two alpha subunits αI NTD (yellow) and αII NTD (green), the beta subunit β (light blue) and the beta prime subunit β' (rose) as well as the small omega subunit ω (white). In combination with a specific sigma factor like σ^{70} (golden) the holoenzyme is complete. The two ppGpp binding sites 1 and 2 associated with the small alarmone and DksA are colored in red. The illustration was modified after Gourse et al. 2018.

a much lower potency in transcriptional regulation (Mechold et al. 2013). Although a possible interaction between ppGpp and the β-subunit was demonstrated already more than two decades ago (Chatterji et al. 1998, Toulokhonov et al. 2001), detailed insights into alarmone-RNAP binding remained unclear for a long time. However, latest crystal structures of the holoenzyme-ligand complex, obtained by high-resolution X-ray imaging, revealed with great precision two architectural binding sites for ppGpp on RNA Polymerase (Figure 2.11). One alarmone molecule interacts at the interface between the β'-subunit and the ω N-terminus in site 1. The other ppGpp molecule binds in the secondary channel at a different location of the β'-subunit and associates with DksA in the binding site 2 (Ross et al. 2016, Gourse et al. 2018). Both sites exhibit different regulatory requirements and the actual binding of ppGpp to one or both sites is highly dependent on

the present ω and DksA concentrations in the cell. Occupation of both sites is necessary for full inhibition of rRNA transcription whereas the combined binding of ppGpp together with DksA has a widespread effect on transcription control since it directly affects gene expression at a much larger amount of various promoters (Ross et al. 2016). Thus, the synergistic effect of the protein factor DksA on ppGpp-mediated transcriptional control is the key to amplification of the stringent response signal at the level of RNAP activity stimulation or inhibition (Paul et al. 2004). First incorrectly reported as a suppressor for the chaperone protein DnaK (Kang and Craig 1990), it has taken some time to eventually define DksA correctly as RNA Polymerase-binding transcription factor and enhancer (Paul et al. 2004; 2005). Taken together, the binding of ppGpp and DksA to the RNA Polymerase open complex destabilizes the anyhow short-lived promoter binding capacities of the holoenzyme. In addition, the promoter sequence itself at which the holoenzyme is formed prior to transcription initiation, appears to encode an intrinsic regulation of promoter selection. DNA sequences with AT-rich discriminator regions between the Pribnow box (-10 sequence) and the transcriptional start (+1 nucleotide of a promoter) are evidently allied with promoter activation of e.g. amino acid biosynthesis operons. Likewise, such promoters containing a GC-rich discriminator sequence are strongly inhibited as it is the case for e.g. rRNA operons (Barker et al. 2001b,Barker et al. 2001a, Sanchez-Vazquez et al. 2019). The preceded promoter recognition mechanism is conducted by an impressive intracellular repertoire of various σ-factors that guide the RNAP to specific target sites on the chromosome (Burgess et al. 1969, Burgess 1971). Despite the primary σ-factor (σ^{D}) that regulates the majority of gene expression activities during growth, recruitment of an alternative σ-factor is essential at starvation and stress to achieve an appropriate reaction to different environmental factors. In *E. coli*, the six alternative σ-factors σ^{N} (nitrogen limitation), σ^{S} (stationary phase), σ^{H} (heat shock), σ^{F} (flagellar synthesis and chemotaxis), σ^{E} (extracellular proteins) and σ^{FecI} (iron transport and metabolism) manage to shift the transcriptional balance towards their individual cellular requirements for stress resistance. The RNA Polymerase core enzyme in complex with ppGpp and DksA enables a modified competitiveness of σ-factors towards the assembly of the holoenzyme (Jishage et al. 2002). In unfavorable conditions, the majority of free core RNAP is available for alternative sigma-factor binding. The primary σ-factor σ^{D} is replaced such that a systematic reprogramming of gene expression at particular stress-related operons can be promoted (reviewed in Burgess and Anthony 2001, Gruber and Gross 2003, Sharma and Chatterji 2010, Paget 2015).

2.3.4. Nitrogen-Regulated *relA* Transcription

The catalytic product of the *relA* gene has many names like GDP/GTP pyrophosphokinase, stringent factor or ppGpp synthetase I (UniProt Entry - P0AG20). Nonetheless, all these synonyms reference to the genetically encoded ORF of the well-known key enzyme RelA, the mediator of ppGpp synthesis and stringent response to amino acid starvation. The *relA* gene is located in between the 23S rRNA methyltransferase (*rlmD*) and the MazF-MazE toxin-antitoxin system operon (*mazEF*) on the *E. coli* K-12 chromosome (Figure 2.12). Initially, two individual σ^{70}-dependent promoters were reported to coordinate gene expression of the *relA* transcription units. The constitutive transcriptional control of the *relA*p1 promoter ensures a steady production of the RelA enyzme during exponential growth (Metzger et al. 1988). A second RNAP binding site is provided by the *relA*p2 promoter which is located further upstream of the *relA* transcriptional start. Induction of *relA*p2 occurs during the transition from growth into stationary phase (Nakagawa et al. 2006). Global transcriptional regulators like H-NS, CRP and the interaction of the toxin-antitoxin module HipA/HipB are furthermore involved in the control of both *relA* promoters (reviewed in Irving and Corrigan 2018, Ronneau and Hallez 2019). Direct

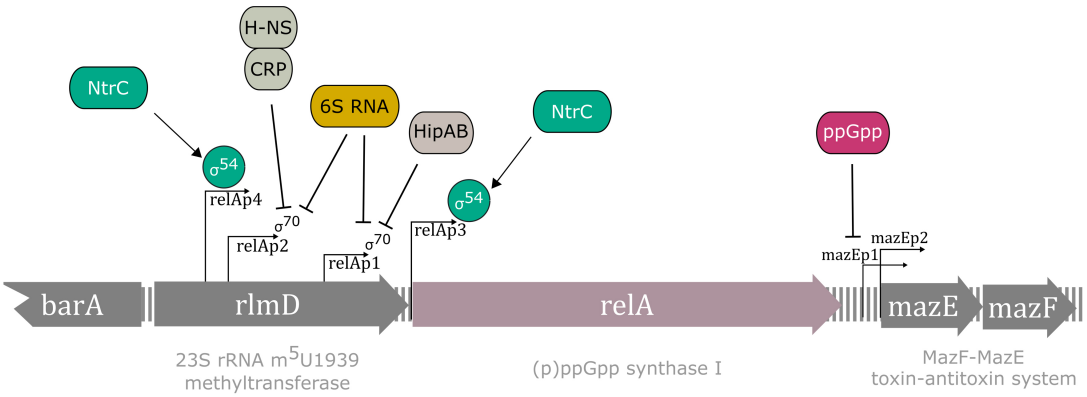

Figure 2.12. *relA* operon and promoter regulation at the *relA* ORF. The genetic context of the *relA* gene is situated between the *rlmD* gene (23S rRNA m^5U1939 methyltransferase) and the *mazEF* operon (MazF-MazE toxin-antitoxin system). At the two σ^{70}-dependent promoters *relA*p1 and *relA*p2 transcription is regulated by H-NS, CRP, HipA/HipB and 6S RNA interactions with the DNA or with RNAP. Promoter regulation of the σ^{54}-dependent promoters *relA*p3 and *relA*p4 occurs via binding of the master regulator NtrC during nitrogen starvation. This graph was designed based on regulatory information according to Irving and Corrigan 2018 and genetic information received from the EcoCyc webpage (BioCyc Database Collection 2020).

downregulation of transcription from *relA*p1 and *relA*p2 can be achieved by accumulation of the small non-coding 6S RNA in late stationary phase (Cavanagh et al. 2010). Molecules of 6S RNA are described to build stable associations between the core RNA polymerase and the primary sigma factor. Such highly specific interactions modulate the σ^{70}-holoenzyme activity during stationary phase in a way that gene expression from σ^{70}-dependent promoters is repressed and thus transcription of a wide range of key pathways diminishes in non-growing cells (Wassarman and Storz 2000). The existence of two additional *relA* promoters was discovered very recently (Brown et al. 2014a). While studying potential binding sites of RNAP in association with the global transcriptional regulator NtrC on the *E. coli* genome, new sites of *relA* transcription initiation were mapped within the upstream region. Both σ^{54}-dependent promoters (*relA*p3 and *relA*p4) are activated in conditions of nitrogen starvation via NtrC (Figure 2.13). In general, the master regu-

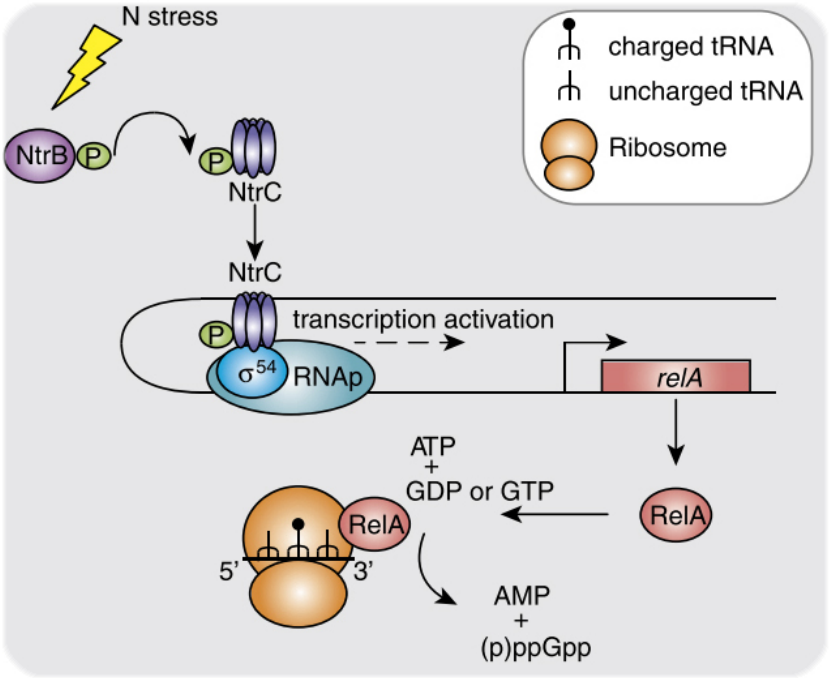

Figure 2.13. Nitrogen starvation-mediated activation of stringent response in *E. coli*. The connection between the Ntr stress response and the stringent response in nitrogen-starved *E. coli* cells is established via the the global transcriptional regulator NtrC. In its phosphorylated and thus activated form, NtrC-P mediates activation of *relA* gene expression at the novel σ^{54}-dependent promoter binding sites upstream of the *relA* transcription start. The consequently rising RelA protein pool is responsible for ppGpp accumulation. The illustration was modified after Brown et al. 2014b.

lator Ntr responds to declining glutamine concentrations by directly activating σ^{54}-driven gene expression from nitrogen promoters to scavenge nitrogen from alternative sources (section 2.2.2). These new *relA* promoter binding sites now integrate two major bacterial responses caused by different external nutritional stress factors. Hence, the intracellular stringent response reaction upon nitrogen deprivation is triggered by the limitation signal itself due to σ^{54}/NtrC controlled *relA* transcription without any detours. The resulting ppGpp accumulation in the cells is eventually the product of enhanced RelA protein levels and alarmone synthesis (Brown et al. 2014b). Indeed, formation of the stringent regulator molecule could be evidently detected in nitrogen-starved *E. coli* persister cells (Brown 2019). Although ppGpp levels were increased, occupancy of RNA Polymerase at stringent promoters was found to be merely at 60 % which led to the assumption that nitrogen starvation activates a smaller subset of stringent response-related genes than the native stimulus (Brown et al. 2014b).

2.4. Central Carbon Metabolism in *E. coli*

In natural microbial habitats, the most abundant carbon sources are polymeric sugars bound in complexes like starch, cellulose, pectin and similar related polymers. Throughout the biological biosphere, autotrophic organisms, as e.g. plants, gain their energy from non-biological sources and are able to donate such polymeric carbon-based substrates to the carbon cycle. Most heterotrophic organisms act like recipients since they rely on these biopolymers to cover their nutritional and energetic requirements from oxidation of organic compounds like carbohydrates, lipids and proteins (Antranikian 2006). To make those sugar complexes accessible as good substrates for bacterial growth, specialized extracellular enzymes degrade the polymers into di- and monomeric saccharide units. One such major digestive enzyme in *E. coli* is the α-amylase AmyA, the second known α-amylase is the periplasmic enzyme MalS. Both degrade linear substrates as dextrins, amylose, starch or amylopectin to sugar residues (Freundlieb and Boos 1986, Raha et al. 1992). These sugars are either transported into the cytoplasm by different PTS group translocation systems (glucose-PTS, mannose-PTS, fructose-PTS) that combine transportation with phosphorylation or by direct unphosphorylated uptake via the galactose ABC transporter (*mglBAC*), the galactose permease (*galP*) and the maltose ABC transporter (*malEFG*) (Hunter and Kornberg 1979, Notley and Ferenci 1995 and also reviewed

in Postma et al. 1993, Boos and Shuman 1998). The chemically bound energy in glucose and its derivatives is harvested from bacterial cells within the basically exergonic processes of the catabolic metabolism which provide the necessary energy for consecutive endergonic reactions. In a reaction chain of subsequent and interdependent enzymatic steps, hydrogen is released from a glucose molecule at different stages and finally transferred to oxygen under aerobic conditions. From the intermediate steps, biomass and CO_2 are formed (Berg et al. 2003, Chmiel 2011). Once activated to glucose-6-P, this central and prominent cellular metabolite enters various major metabolic pathways like the glycogen biosynthesis for glucose storage purposes (section 2.4.1), the glycolysis for regular carbohydrate oxidation or the Pentose Phosphate (PP) pathway for alternative glucose oxidation (Figure 2.14). A minor portion of glucose-6-P is channeled into the Pentose Phosphate pathway where essential precursors for cell expansion are synthesized. Numerous enzymatic reactions provide the cell with e.g. pentose and tetrose sugars that are metabolized into nucleotides, aromatic amino acids and others. At the same time, reducing equivalents in form of NADPH are generated which are the major source of electrons in reductive biosynthetic reactions (anabolism) as e.g. fatty acid synthesis (Neidhardt et al. 1996 and reviewed in Fuhrer et al. 2005). The major fraction of the consumed glucose is directed into the Embden-Meyerhof-Parnas pathway (EMP) which is the most recognizable and common type of glycolysis. The oxidation of one molecule glucose (C6) into two molecules pyruvate (C3) divides the pathway into an upper and a lower half. Within the steps of the upper section, glucose is phosphorylated by the PTS during its transport into the cytoplasm with PEP as donor molecule to form glucose-6-P. Glucose, which was converted in the cytoplasm from other sugars like maltose, is phosphorylated by the Glucokinase upon requirement of one molecule ATP.

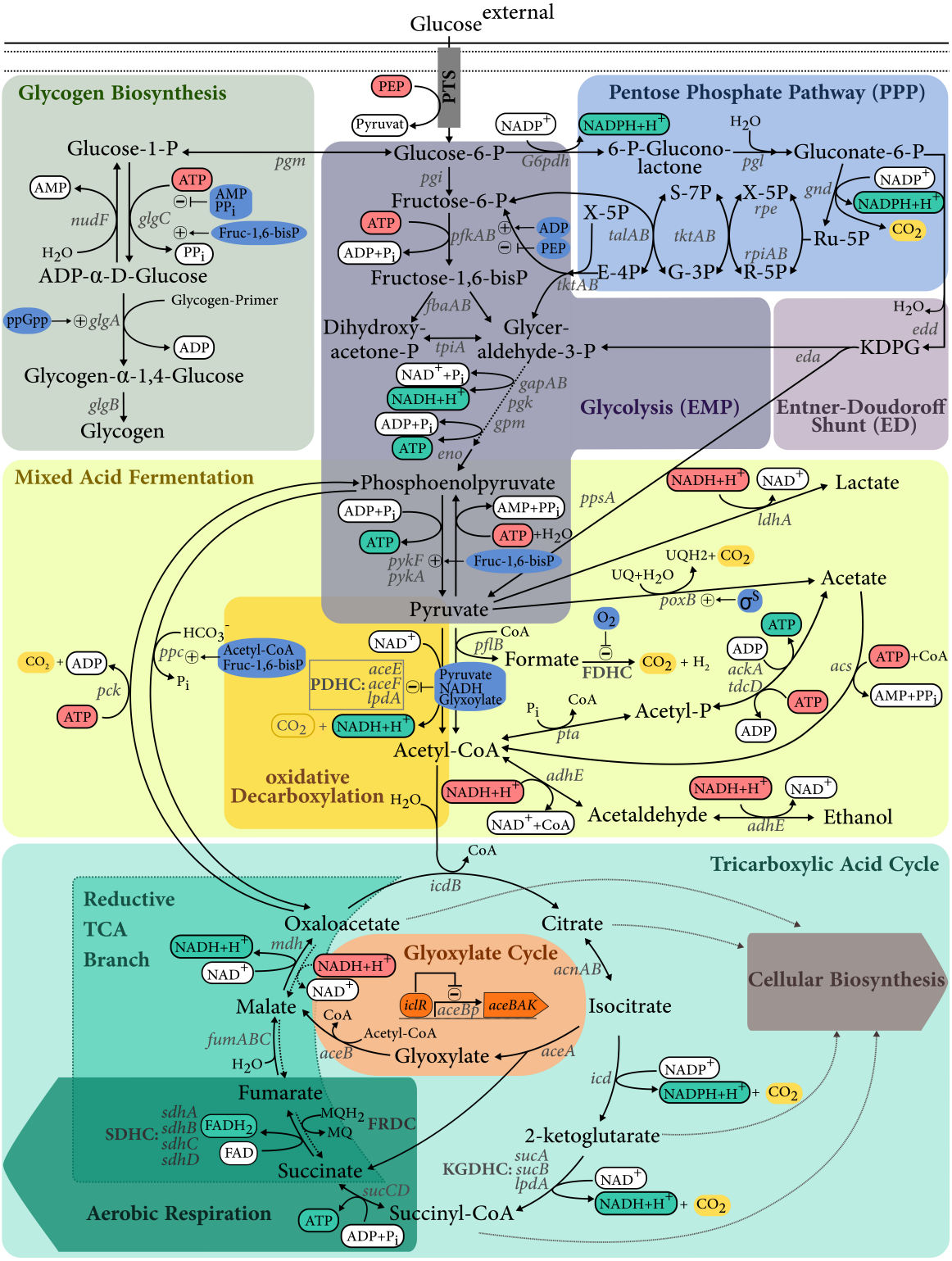

Figure 2.14. Central carbon pathway in *E. coli*. Glucose is transported into the cell and activated e.g. by the PTS. Glucose storage occurs in the glycogen biosynthesis pathway. The catabolic routes for glucose oxidation are either the glycolysis (EMP) or alternatively the Pentose Phosphate to obtain pyruvate. Oxidative carboxylation generates Acetyl-CoA which is substrate for the TCA including the subsequent aerobic respiration. At anaerobic or carbon overflow conditions, the mixed acid fermentation is active.

This activated form of the hexose ensures a steady low glucose concentration in the cell that promotes a continuous influx of carbons and simultaneously prevents the leaking-out of glucose-6-P due to missing specific transporters. The following steps provide the isomerization into fructose-6-P to stabilize the carbanion prior to its further phosphorylation by Phosphofructokinase (PFK) that involves the hydrolysis of a second ATP molecule. At this stage of glycolysis, the activation of the glucose molecule becomes irreversible what makes PFK the key regulatory enzyme of this rate-limiting step (Atkinson and Walton 1965, Reeves and Sols 1973, Babul 1978). Diphosphonucleosides like ADP and GDP activate the enzymatic function by allosteric binding in strong competition to the proper substrate ATP, while phosphoenolpyruvate acts as allosteric inhibitor by decreasing the affinity of PFK for fructose-6-P (Blangy et al. 1968). The product of this reaction is fructose-1,6-bisP. It activates Phosphoenolpyruvate Carboxylase (Ppc), the regulator of oxaloacetate flux into the reductive TCA branch (Izui et al. 1981), and Pyruvate Kinase I (PykF) that catalyzes the last step of glycolysis from PEP to pyruvate (Kornberg and Malcovati 1973, Markus et al. 1980 and reviewed in Muñoz and Ponce 2003). Up to now, the energy of two ATP molecules was invested to destabilize the hexose in order to eventually cleave fructose-1,6-bisP into the two triose sugars dihydroxyacetone-P and glyceraldehyde-3-P. In the following lower half of glycolysis, these triose sugars are further oxidised. The change in free chemical energy from the activity of a sequence of enzymes like isomerase (TpiA), oxidoreductase (GAPDH), transferase (PGK and PK), mutase (Pgm) and a lyase (Eno) either drives the subsequent reaction of an intermediate or is stored in form of the universal cellular energy sources ATP and NADH. The two transferases Phosphoglycerate Kinase (PGK) and Pyruvate Kinase (PK) catalyze the two substrate-level phosphorylations of the glycolysis by direct transfer of a phosphate group to ADP producing ATP without an external electron acceptor. Thus, the net energy outcome per glucose of the glycolysis pathway are two molecules NADH and two molecules ATP (reviewed in Mayer and Boos 2005, Romeo and Snoep 2005, Wolfe 2015). Proceeding from the PEP-pyruvate-oxaloacetate node which interconnects several major pathways of the central metabolism, the carbon precursor molecule can be distributed into catabolic, anabolic or energy generating processes (reviewed in Sauer and Eikmanns 2005). At a higher control level, the general direction of this carbon flow is modulated by the DNA-binding dual transcriptional regulator Cra, which acts independently of the CRP receptor protein (section 2.2.1). Intriguingly, an intermediate metabolite originating from a different metabolic route than glycolysis turns out to be the physiological effector of Cra. Recently, fructose-1-P was described being the only second messenger molecule

to interact with the Cra regulator, as it was already proposed almost one decade ago for *Pseudomonas putida* (Chavarría et al. 2011), despite the long believed view that fructose-1,6-bisP is the key effector of Cra actions in the cell (Bley Folly et al. 2018 and reviewed in Chavarría and de Lorenzo 2018). However, the high affinity of Cra for fructose-1-P prevents the binding of the transcriptional regulator at its target operons of glycolysis and ED pathway genes and therefore counteracts the repressing effect on transcription. This regulatory control is reversed in the absence of glucose when catabolite repression is suppressed and Cra activates gene expression related to the TCA pathway (Cozzone and El-Mansi 2006), the gluconeogenesis (Bledig et al. 1996) and the glyoxylate cycle (Ramseier et al. 1995, Ramseier 1996). Under aerobic glucose-rich conditions, the Pyruvate Dehydrogenase complex facilitates the direct access from glycolysis into the Tricarboxylic Acid Cycle by oxidative decarboxylation of pyruvate. The PDHC multi-enzyme complex ($[(AceE)_2]_{12}AceF_{24}[(Lpd)_2]_6$) is formed by self-assembly of numerous subunits of the three enzymes AceE (E1), AceF (E2) and LpdA (E3). The activity of the complex is regulated by the stoichiometric ratios of its metabolic intermediates ($NADH/NAD^+$ and acetyl-CoA/CoA) and the endproduct (ATP/ADP). High concentrations of reaction products generated by the PDHC inhibit the catalytic functions of the complex itself at different sites (Bates et al. 1977, Angelides et al. 1979, Berg et al. 2003). The catalyzed acetyl-CoA is then channeled into the Tricarboxylic Acid Cycle where it is completely oxidized to two molecules of CO_2 with the help of water. Within this process, two carbons enter the cycle in form of acetyl-CoA. In the first reaction step, this C2-acetyl group and H_2O are transferred on the C4-substrate oxaloacetate in a condensation reaction to produce the C6-compound citrate. Over the TCA course, the citrate molecule is converted in several partially irreversible catalytic steps including oxidation reactions to release electrons for NAD^+ and FAD reduction as well as decarboxylations to generate CO_2 among other reactions. Finally, the initial oxaloacetate substrate is regenerated and the cycle is repeated from the beginning with another acetyl-CoA molecule. Many of the TCA intermediates are regularly removed from the cycle in cataplerotic reactions that transfer these precursors into various anabolic biosynthesis pathways like e.g. amino acid, fatty acid, purine, pyrimidine synthesis reactions and others. In contrast to this, anaplerotic reactions replenish the TCA at different entry sites and thus can increase the cycle efficiency including the resulting ATP synthesis yield during oxidative phosphorylation. For instance, amino acids which derive from protein degradation can be specifically converted and enter the TCA at the level of 2-ketoglutarate or acetyl-CoA. Additional oxaloacetate can be converted by the Phosphoenolpyruvate Carboxylase from PEP and HCO_3^- and channeled into

the TCA to increase the flux. The two regulatory molecules acetyl-CoA and fructose-1,6-bisP activate Ppc at an allosteric enzyme site and induce a positive feed-forward signal of elevated glycolysis levels in the cell (Kameshita et al. 1978, Izui et al. 1981). An entirely different pathway of anaplerotic TCA replenishment is categorically repressed as long as glucose is present in the environment. The Isocitrate Lyase regulator (IclR) is a transcription factor that negatively controls gene expression from the *aceBAK* operon with glucose as carbon source. Whenever the bacterial growth conditions switch to a C2-substrate-based nutrition (e.g. acetate), the interaction of IclR with the *aceBAK* promoter site is disrupted and the glyoxylate cycle (AceA, AceB, AceK) is activated for the synthesis of carbohydrates. In this way, the carbon source enters the TCA at the level of acetyl-CoA where it is transferred on oxaloacetate as described before. Contrary to the regular sequence of enzymatic transformation reactions, isocitrate is converted to glyoxylate and succinate by isocitrate lyase (AceA). The formed two-carbon glyoxylate molecule is further modified to the four-carbon compound malate by the malate synthase A (AceB) in a condensation reaction with another acetyl-CoA substrate. Both oxidative decarboxylation steps of the TCA are bypassed such that these carbons are conserved. The necessary oxaloacetate molecule for another cycle passage is regenerated from the produced malate compound and another acetyl-CoA can enter the reaction sequence all over again (LaPorte et al. 1984, Cortay et al. 1989). To meet the cellular requirement of a steady precursor supply for biosynthesis, the actions of this central metabolic allocator are tightly controlled by substrate activation and product inhibition. An accumulation of acetyl-CoA indicates the demand for oxaloacetate in the TCA that can be caused e.g. by a high energy charge of the cell. A high energetic status is characterized by high ATP levels, a reduced amount of ADP and a backlog of NADH compounds. The energy-rich molecules NADH and ATP inhibit a number of enzymes as for instance pyruvate dehydrogenase, 2-ketoglutarate dehydrogenase and citrate synthase (Swim and Krampitz 1954, Neidhardt et al. 1996, Berg et al. 2003). The overall net reaction of one TCA cycle yields three molecules of NADH and one molecule $FADH_2$ and GTP each per acetyl group that is oxidized. From this view, the emphasis of the main cycle function is rather on capturing electrons from the carbons in high-energy compounds like reducing equivalents than generating energy molecules by substrate-level phosphorylation. The electron donor molecules serve in subsequent reactions of the aerobic respiration process to efficiently synthesize large proportions of the intracellular energy pool. Based on the mechanism of oxidative phosphorylation electrons from NADH and $FADH_2$ are transferred to many different electron acceptor molecules in a sequence of redox reactions called the electron

transport chain. The energy from this electron flow drives in turn the transport of protons across the bacterial cytoplasmic membrane which produces an electrochemical gradient that eventually engages the phosphorylation of ADP at the ATP synthase complex. At the final stage the electrons are used to reduce the terminal acceptor molecule oxygen to form water from two additional protons (Ingledew and Poole 1984). In the absence of the final electron acceptor oxygen, bacterial members of the Enterobacteriaceae like *E. coli* perform an anaerobic fermentation of the glucose carbon source into a mixture of different acid compounds and gases. The end products of this so called mixed acid fermentation reactions include in particular acetate, lactate, ethanol, succinate, formate as well as CO_2 and H_2. First, the glycolysis pathway is used to oxidize glucose into two molecules of pyruvate and thereby generate two energetic units each of ATP and NADH. Without the activity of the oxidative phosphorylation complex, ATP is mainly synthesized by substrate-level phosphorylation during oxidation reactions of various intermediates. The second stage of fermentation produces additional ATP molecules by conversion of acetyl-phosphate to acetate by Acetate Kinase (AckA) while NADH is recycled to NAD^+ in several steps of lactate and ethanol synthesis as well as in succinate fermentation along the reductive TCA branch (reviewed in Holms 1996, Neidhardt et al. 1996, Wolfe 2015). However, those bacterial cultures are also capable of mixed acid fermentation instead of respiration in the presence of oxygen. This phenomenon is termed the overflow metabolism and occurs at conditions of high glucose concentrations especially in fast-growing cells. It is assumed that the decision of fermentation over respiration at aerobic growth is a global regulatory response which balances the energetic costs of proteomic resources needed for both metabolic pathways (Basan et al. 2015).

2.4.1. Glycogen Biosynthesis

Glycogen is a branched homopolysaccharide consisting of glucose residues linked together in linear polymer chains and represents the major compound of carbon storage in a variety of organisms including the prokaryote *E. coli*. It accumulates upon conditions of unrestricted access to a carbon source while the availability of other essential nutrients in the environment is limited (Holme and Palmstierna 1956, Dietzler et al. 1973). Consequently, the activity of glycogen formation is highest at transition from growth into a nutrient-starved stationary phase. Thus, the accumulation rate behaves inversely to the growth

rate and varies widely with the growth phase (Preiss 1984). The pathway of glycogen build-up starts with a glucose-1-P molecule that was beforehand transported into the cell and activated to glucose-6-P by the PTS and subsequently phosphate group modulated at the 1' and 6' positions by Phosphoglucomutase (Pgm). The following adenylyltransferase (GlgC) reaction converts this glucose-1-P into ADP-α-D-glucose by consuming one molecule of ATP and holds control of the rate-limiting step in glycogen biosynthesis. Regulatory molecules like the glycolytic intermediate fructose-1,6-bisP, the nucleotide AMP and the inorganic anion pyrophosphate have either an activating or inhibiting allosterical binding effect on GlgC. In this way, these compounds transfer the signals of the intracellular energy state to the catalytic regulator GlgC which in turn responds to growth and maintenance conditions determined by the nutrient availability of the surrounding (reviewed in Neidhardt et al. 1996, Wilson et al. 2010, Preiss 2014). The metabolic flow of nucleotide hexose precursors like ADP-glucose towards glycogen biosynthesis is additionally regulated in *E. coli* and other bacteria. In situations of ADP-glucose accumulation, further glycogen synthesis is non-essential and this precursor molecule is hydrolyzed to glucose-1-P by ADP-sugar Pyrophosphatase (AspP). Especially upon decreasing carbon supply in stationary phase, the microbial cells prepare for the imminent adverse conditions and glycogen degradation activity of ADP-sugar Pyrophosphatase (AspP) is stimulated by signaling metabolites like nucleotide-sugars, glucose-1,6-bisP and also by high total intracellular concentrations of macromolecules. The carbon flux direction is reversed towards glycogen catabolism and other metabolic pathways depending on the individual cellular needs (Moreno-Bruna et al. 2001, Morán-Zorzano et al. 2007). The eventual formation of the carbon storage polymer glycogen is accomplished by elongation of the glucose units in α-1,4-glucosidic linkages to a oligosaccharide chain by Glycogen Synthase (GlgA) using the ADP-glucose monomers as sugar donor nucleotides. Afterwards, the Glycogen Branching Enzyme (GlgB) extends these glucose chains with α-1,6-glucosidic linkages to form a branched oligosaccharide polymer (reviewed in Neidhardt et al. 1996, Wilson et al. 2010, Preiss 2014).

Glycogen biosynthesis is further regulated at the level of gene expression, translation initiation and mRNA stability, as well. The bacterial Carbon Storage Regulator (CsrA) is a RNA-binding protein that controls a variety of biological pathways (Romeo et al. 1993). In terms of glycogen accumulation, it promotes decay of specific *glgCAP* mRNA and prevents translation of such *glgCAP* transcripts during the initiation step (Liu et al. 1995, Baker et al. 2002). Involved gene products of downregulation are Glucose-1-P Adeny-

lyltransferase, Glycogen Synthase, Glycogen Phosphorylase and the Surface Composition Regulator (GlgS) (Yang et al. 1996). Other catabolic pathways like the central carbon metabolism are activated by the CsrA regulator. In contrast, anabolic synthesis such as gluconeogenesis is repressed (reviewed in Romeo and Babitzke 2018). CsrA was also described to have a negative regulatory effect on the stringent response. It binds *relA* mRNA with high affinity and thus interferes with RelA protein biosynthesis and consequently in the extent of ppGpp formation at the induction of stringent response. The opposing regulatory cascade involves an inhibitory effect of high ppGpp levels on CsrA activity by in turn activating the two small regulatory RNAs CsrB and CsrC which are antagonists to CsrA (Edwards et al. 2011). Transcription of the key enzyme of glycogen synthesis GlgC is activated by ppGpp at transition into stationary phase in particular under conditions of amino acid starvation. The involvement of the stringent response regulator in glycogen synthesis was mainly concluded from observations of ppGpp-deficient strains that failed to induce glycogen metabolism even at favorable conditions (Taguchi et al. 1980, Romeo et al. 1990, Traxler et al. 2008). A detailed summary of varying glycogen accumulation phenotypes was reported recently for an *E. coli* stringent response mutants collection. Apparently, a series of different variations in *relA* and *spoT* mutations ($\Delta relA\Delta spoT$, $\Delta relA$, $\Delta spoT$ and associated *relA* suppressor mutations) revealed a significant ascending order of intracellular glycogen amounts. The spectrum ranged from glycogen-free to WT level mutants. Their findings conclude that ppGpp in fact constitutes a major positive effector of glycogen gene expression and glycogen biosynthesis regulation in *E. coli* (Montero et al. 2014).

2.4.2. Regulation of Energy

Distribution of metabolites over a variety of cellular pathways and cooperative networks requires well-orchestrated higher-level regulation that integrate signal entries from different cellular systems. Metabolic fluxes are coordinated as multi-layer concepts. For instance, the lowest level of control is represented by the enzymatic function of substrate catalysis. This can be extended to higher level systemic functions like the control of metabolite concentrations and fluxes. Hofmeyr and Cornish-Bowden described this intracellular metabolic processes as molecular economy in which the biosynthetic fluxes are controlled by supply and demand. They organized the metabolic network into three

general blocks. Namely, (i) a catabolic block for carbon and energy supply, (ii) a biosynthetic block for macromolecular synthesis and (iii) a growth block for cell envelope and biomass formation. According to them, all these individual events are interconnected by a pair of common cofactors that cycle through the supplying mechanisms (producers) and demanding reactions (consumers). The intracellular ubiquitous high-energy cofactors NADH and ATP hold the potential to integrate signals from catabolism and anabolism and thus to modify cellular metabolism into a preferred direction (Hofmeyr and Cornish-Bowden 2000, Holm et al. 2010). Their individual contribution to metabolic flux control by demand was studied over the past decades with many microbial mutants exerting either energy excess or energy deficiency phenotypes. The collective goal of the genomic engineering approaches was a stimulation of the host cell target product biosynthesis by improving the energy balance between synthesis and consumption. Naturally, the intracellular ATP levels were regulated in a way that a constant degree of synthesis and degradation was maintained. However, the unnatural nature of such overproducing bacterial cells required an unnatural energy balance and ATP supply had to be artificially regulated. Strategies to influence the energy input from the outside of the cell included e.g. the supplementation of the medium with energy substrates like citric acid. This artificial anaplerotic replenishing of the TCA cycle activated the expression of the corresponding TCA-related genes which regenerated NADH in dehydrogenase reactions and enhanced the electron transfer for respiratory ATP synthesis. Alternatively, the extracellular pH could be maintained at an acidic value. This enabled an increasing intracellular ATP supply since the lower energetic costs to preserve the proton-motive force at the cytoplasmic membrane drove the activity of the F_0F_1-ATP synthase. From the inside of the cell, endogenous energy pathways could be manipulated as for instance by interrupting components of the aerobic respiration. Targeted deletion of genes encoding enzymes of the respiratory chain caused a shift of ATP synthesis from the oxidative phosphorylation towards the glycolytic substrate-level phosphorylation even at aerobic conditions. These increased activities in glycolysis entailed further transcription of glycolytic enzymes and consequently an accelerated glycolytic flux that was regulated by the intracellular energy demand rather than by activities of the central carbon pathway. Under carbon-rich conditions, the ATP supply was determined by the cellular energy consumption and the degree to which ADP was available for de novo ATP formation (reviewed in Hara and Kondo 2015). With regard to this, a remarkably effective possibility to maintain high ATP synthesis rates was suggested by constantly degrading this energetic molecule with auxiliary demand processes. The phenomenon of artificial ATP drains was proposed by different

research groups under different names like 'enforced ATP wasting' or 'futile energy cycling' and others. Such engineered microbial cells had in common that e.g. the NADH oxidase or the soluble F1 part of the H^+-ATPase were overexpressed which introduced a steady hydrolysis of energy molecules. All these approaches based on an artificial ATP and NADH demand that strongly stimulated glycolytic flux into the cell up to a two-fold of the corresponding WT reference strain (Koebmann et al. 2002, Causey et al. 2003, Boecker et al. 2019). However, continuous hydrolysis of both energy molecules decreased their individual intracellular levels and thus gave rise to their antagonistic modes of operation. While lowered ATP concentrations had negative regulatory effects on protein, nucleotide and lipid biosynthesis and resulted in an increased acetate overflow, decreasing NADH levels positively regulated the biosynthesis of lipids and amino acids (Holm et al. 2010). Similarly, futile metabolic cycles were created by transcriptional modifications of genes related to the central carbon network that unnecessarily consumed ATP. A futile cycle involved the concurrent activities of glycolytic and gluconeogenic reactions within a carbon converting pathway. For instance, the upregulation of Phosphoenolpyruvate Synthase (PpsA) transcription caused a steady synthesis and degradation cycle between PEP and pyruvate. This increased PEP/pyruvate ratio enhanced the glucose uptake rate at the PEP:sugar Phosphotransferase System in *E. coli* (Patnaik et al. 1992). Moreover, this phenomenon was equally described for prokaryotes as well as for eukaryotes (Sauer et al. 1999, Hädicke et al. 2015, Semkiv et al. 2016).

3. Materials and Methods

3.1. Materials

3.1.1. Bacterial Strains and Target Genes

Table 3.1. Overview of used *E. coli* strains for cloning and growth studies.

Strain	Genotype	Source/Reference
E. coli K-12 MG1655	F^-, λ^-, *ilvG*$^-$, *rfb*-50, *rph*-1	DSM:18039[a] (Neidhardt et al. 1996)
E. coli K-12 BW25112 *glgC::kan*	F^-, λ^-, Δ(*araD-araB*)*567*, Δ*lacZ4787* (::rrnB-3), Δ*glgC763::kan*, *rph*-1, Δ(*rhaD-rhaB*)*568*, *hsdR514*	CGSC:10526[b] (Baba et al. 2006)
E. coli DH5αλ*pir* pEMG	*supE44*, Δ*lacU169*(Φ80lacZΔM15), *recA1, endA1, hsdR17, thi-1, gyrA96, relA1*, λ*pir* phage lysogen	Víctor de Lorenzo Lab[c] (Martínez-García and de Lorenzo 2011)
E. coli JM109 pACBSR	F', *traD36*, $proA^+B^+$, $lacI^q$, Δ(*lacZ*) *M15* / Δ(*lac-proAB*), *glnV44*, *e14*$^-$, *gyrA96*, *recA1*, *relA1*, *endA1*, *thi*, *hsdR17*	Víctor de Lorenzo Lab[c] (Herring et al. 2003)

a: German Collection of Microorganisms and Cell Cultures (DSMZ)
b: single-gene knockout mutant from KEIO Collection
c: Centro Nacional de Biotecnología (CNB) - Consejo Superior de Investigaciones Científicas (CSIC), Madrid, Spain

Table 3.2. *E. coli* target genes for genomic modifications and their corresponding enzymes.

Gene/Enzyme	Description	UniProtKB Accession #
relA / RelA	(p)ppGpp Synthase I / ATP:GTP 3'-Pyrophosphotransferase	P0AG20
spoT / SpoT	(p)ppGpp Synthase II / (p)ppGpp 3'-Pyrophosphohydrolase	P0AG24
aceE / AceE	Pyruvate Dehydrogenase, Decarboxylase component E1	P0AFG8
iclR / IclR	Isocitrate Lyase Regulator	P16528
sdhA / SdhA	Succinate Dehydrogenase flavoprotein subunit	P0AC41
sdhB / SdhB	Succinate Dehydrogenase, FeS subunit	P07014

3.1.2. Cloning Plasmids

Table 3.3. Target sites for restriction endonucleases within the MCS of pEMG.

Restriction enzyme	Restriction site	Restriction ends
SalI	5' G ↓ TCGAC 3'	sticky
XbaI	5' T ↓ CTAGA 3'	sticky
BamHI	5' G ↓ GATCC 3'	sticky
XmaI (Cfr9I)	5' C ↓ CCGGG 3'	sticky
SmaI	5' CCC ↓ GGG 3'	blunt
KpnI	5' GGTAC ↓ C 3'	sticky
SacI	5' GAGCT ↓ C 3'	sticky
EcoRI	5' G ↓ AATTC 3'	sticky

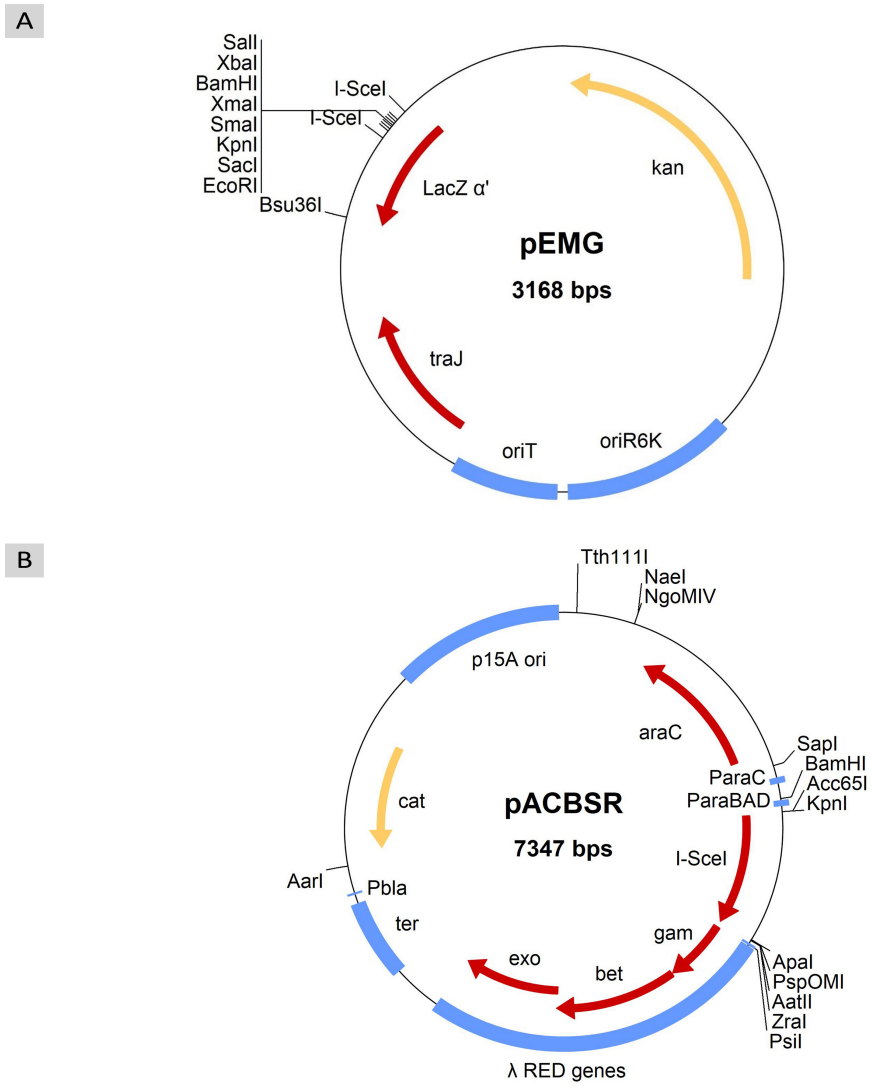

Figure 3.1. Vector maps of the used cloning plasmids pEMG and pACBSR.
A: During chromosomal gene replacement, pEMG (3168 nt) is the first executing cloning plasmid in the process as it delivers DNA segments to specific genomic loci of the host chromosome by homologous recombination. Since the *ori*R6K origin of replication is only able to function in a *pir* negative host strain, survival in Kanamycin (Kan) can be obtained e.g. in the *E. coli* DH5αλ*pir* strain. Furthermore, the plasmid is equipped with a origin of transfer region (*ori*T), *traJ* for conjugal mobility and a *lacZ*α fragment including the multiple cloning site (MCS). B: The helper plasmid pACBSR (7347 nt) facilitates arabinose-induced (P_{araBAD}) recovery of the pEMG plasmid backbone from the host chromosome by a λ RED genes (*gam, bet, exo*) mediated DNA recombination event. Additional features of this plasmid include the encoded I-SceI homing endonuclease from *S. cerevisiae*, transcriptional terminator (ter), arabinose operon regulator (*araC*), chloramphenicol acetyltransferase gene (*cat*) and p15A origin of replication.

3.1.3. Kits for Molecular Biology and Analytics

Table 3.4. List of applied test kits.

Kit	Manufacturer
NucleoSpin® Gel and PCR Clean-up Kit	Macherey-Nagel, DE
E.Z.N.A.® Plasmid DNA Mini Kit I	Omega Bio-tek, US
QIA®prep Spin Miniprep Kit	QIAGEN, DE
DN®easy Blood & Tissue Kit	QIAGEN, DE
Acetic acid enzymatic test	R-Biopharm, DE
D-Glucose enzymatic test	R-Biopharm, DE
Ammonium cuvette test kit LCK303	Hach, DE
Ammonium cuvette test kit LCK304	Hach, DE
Phosphate cuvette test kit LCK348	Hach, DE
Phosphate cuvette test kit LCK349	Hach, DE

3.1.4. Enzymes & Reaction Buffers

Table 3.5. List of enzymes and ready to use reaction buffers.

Enzyme / Buffer	Stock Solution	Manufacturer
FastAP thermosensitive alkaline phosphatase	1 [U μL^{-1}]	Thermo Fisher Scientific, US
Lysozyme	10 [mg mL^{-1}]	Sigma-Aldrich, US
Phusion® HF DNA polymerase	2 [U μL^{-1}]	New England Biolabs, US
Phusion® Hot Start II DNA polymerase	2 [U μL^{-1}]	Thermo Fisher Scientific, US
Proteinase K	10 [mg mL^{-1}]	Carl Roth, DE
diverse restriction enzymes	10 [U μL^{-1}]	Thermo Fisher Scientific, US
RNase A	10 [mg mL^{-1}]	Thermo Fisher Scientific, US
T4 DNA ligase	5 [U μL^{-1}]	Thermo Fisher Scientific, US
T5 exonuclease	10 [U μL^{-1}]	New England Biolabs, US
Taq DNA ligase	40 [U μL^{-1}]	New England Biolabs, US
Taq DNA polymerase	5 [U μL^{-1}]	Genaxxon bioscience, DE

Table 3.5. List of enzymes and ready to use reaction buffers (continued).

Enzyme/Buffer	Stock Solution	Manufacturer
Buffer S (incl. 15 mM MgCl)	10×	Genaxxon bioscience, DE
FastAP buffer	10×	Thermo Fisher Scientific, US
isothermal (ISO) reaction buffer (Gibson 2011)	5×	Lab stock
Phusion® HF buffer (incl. 7.5 mM $MgCl_3$)	5×	Thermo Fisher Scientific, US
diverse restriction enzyme buffers	10×	Thermo Fisher Scientific, US
T4 DNA ligase buffer	10×	Thermo Fisher Scientific, US

3.1.5. Complex and Minimal Media

Table 3.6. Complex and minimal media for bacterial growth.

Medium	Recipe
Lysogeny Broth (LB)-Lennox medium:	
10 g L^{-1}	Bacto™ Tryptone
5 g L^{-1}	Bacto™ Yeast Extract
5 g L^{-1}	NaCl
2× Yeast extract Tryptone (YT) medium:	
16 g L^{-1}	Bacto™ Tryptone
10 g L^{-1}	Bacto™ Yeast Extract
5 g L^{-1}	NaCl
Kornberg Medium (KM): (Govons et al. 1969, Lehman et al. 1958)	
8.5 g L^{-1}	KH_2PO_4
11 g L^{-1}	K_2HPO_4
6 g L^{-1}	Bacto™ Yeast Extract
	Adjust to pH 7.0, add 1.0 % (v v^{-1}) glucose prior to use.
Brain Heart Infusion (BHI) medium:	
37 g L^{-1}	Brain Heart Infusion

Table 3.6. Complex and minimal media for bacterial growth (continued).

Medium	Recipe
Agar plate supplements:	
50 µg/mL	Chloramphenicol (dissolved in ethanol^{abs})
50 µg/mL	Kanamycin
1.0 mM	IPTG
40 µg/mL	X-β-Gal
Agar plates:	
18 g L^{-1}	European agar Add appropriate amount of agar and a stirring bar to the medium and autoclave. Mix the hot solution gently on a magnetic stirrer and supplement antibiotics when agar medium is warm to the touch.
10× Minimal medium:	
98.44 g L^{-1}	$NaH_2PO_4 \cdot 2\ H_2O$
46.86 g L^{-1}	K_2HPO_4
13.21 g L^{-1}	$(NH_4)_2HPO_4$
26.80 g L^{-1}	$(NH_4)_2SO_4$
8.81 g L^{-1}	Na_2SO_4
	Adjust to pH 7.0 with KOH or HCl.
10× Minimal medium nitrogen-limited (N-lim) [40 mM]:	
98.44 g L^{-1}	$NaH_2PO_4 \cdot 2\ H_2O$
46.86 g L^{-1}	K_2HPO_4
13.21 g L^{-1}	$(NH_4)_2HPO_4$
12.68 g L^{-1}	$(NH_4)_2SO_4$
8.81 g L^{-1}	Na_2SO_4
	Adjust to pH 7.0 with KOH or HCl.
Minimal medium supplements:	
5 – 30 g L^{-1}	α-D(+)-glucose
0.10 mM	$CaCl_2$
1.00 mM	$MgSO_4$
0.03 mM	Thiamine
1x	TES

Table 3.6. Complex and minimal media for bacterial growth (continued).

Medium	Recipe
2000× Trace Elements Solution (TES):	
16.70 g L^{-1}	$FeCl_3 \cdot 6\ H_2O$
20.10 g L^{-1}	Na_2-EDTA
0.18 g L^{-1}	$ZnSO_4 \cdot 7\ H_2O$
0.10 g L^{-1}	$MnSO_4 \cdot H_2O$
0.16 g L^{-1}	$CuSO_4 \cdot 5\ H_2O$
0.18 g L^{-1}	$CoCl_2 \cdot 6\ H_2O$
	Sterile filter solution with a syringe filter 0.2 µm pore size.

3.1.6. Solutions and Buffers

Table 3.7. Solutions and buffers.

Solution/Buffer	Recipe
Lysis buffer:	
1x	TE
1 % (w v^{-1})	SDS
100 mM	NaCl
	Adjust to pH 8.0, add 100 µg mL^{-1} Proteinase K prior to use.
alkaline Lysis buffer I:	
0.1 g L^{-1}	α-D(+)-glucose
25 mM	Tris-HCl pH 8.0
10 mM	EDTA pH 8.0
	Add 1 mg mL^{-1} Lysozyme and 0.1 mg mL^{-1} RNase A prior to use.
alkaline Lysis buffer II:	
200 mM	NaOH
1 % (w v^{-1})	SDS
alkaline Lysis buffer III:	
3 M	Potassium acetate
11.5 % (v v^{-1})	Acetic acid^{abs}

Table 3.7. Solutions and buffers (continued).

Solution/Buffer	Recipe
50× Tris-acetate-EDTA (TAE):	
242 g L^{-1}	Trizma® base
5.71 % (v v^{-1})	Acetic acid^{abs}
50 mM	EDTA
10× Tris-EDTA (TE):	
100 mM	Tris-HCl
10 mM	EDTA
	Adjust to pH 8.0.
5× ISO reaction buffer: (Gibson 2011)	
25 % (w v^{-1})	PEG-8000
500 mM	Tris-HCl pH 7.5
50 mM	$MgCl_2$
50 mM	DTT
1 mM	each dNTP (dATP, dGTP, dCTP, dTTP)
5 mM	NAD^+
	Aliquot and store at -20 °C.
Assembly enzyme-reagent master mix: (Gibson 2011)	
320 µL	5× ISO reaction buffer
0.64 µL	T5 exonuclease [10 U μL^{-1}]
20 µL	Phusion® HF DNA polymerase [2 U μL^{-1}]
160 µL	*Taq* DNA ligase [40 U μL^{-1}]
ad 1.2 ml	molecular biology grade water ($H_2O^{Mol.Biol.}$)
	Aliquot á 15 µL and store at -20 °C.
HPLC elution buffer for organic acids:	
5 mM	H_2SO_4 (HPLC grade)
	Prepare elution buffer in H_2O^{HPLC}.
4 M Ammonia (NH_3) solution:	
26.4 g L^{-1}	$(NH_4)_2SO_4$ (BioUltra)
30 % (v v^{-1})	NH_4OH (~25.0 % NH_3)
	Prepare solution in H_2O^{HPLC}, confirm the pH to be at 10.2 and secure the bottle with a PTFE seal.

Table 3.7. Solutions and buffers (continued).

Solution/Buffer	Recipe
1.2 M Magnesium sulphate ($MgSO_4$) incl. internal standard:	
295.8 g L^{-1}	$MgSO_4 \cdot 7\ H_2O$
2.52 g L^{-1}	L-Rhamnose monohydrate
	Prepare solution in H_2O^{HPLC}.
0.1 M H_2SO_4 solution:	
2 % (v v^{-1})	H_2SO_4 [5 mol L^{-1}]
	Prepare solution by adding the acid into H_2O^{HPLC}.
Organic acids and sugars standard mix for HPLC analytics:	
100 g L^{-1}	D(+)-Glucose (GC grade)
50 g L^{-1}	Sodium pyruvate
50 g L^{-1}	Succinic acid
100 g L^{-1}	Sodium L-lactate
50 g L^{-1}	Formic acid
100 g L^{-1}	Acetic acid
100 g L^{-1}	Ethanol LiChrosolv®
	Prepare standard mix in H_2O^{HPLC} and store aliquots at 4 °C.
Nucleotides standard mix for HPLC analytics:	
0.5 mM	AMP
0.5 mM	ADP
0.5 mM	ATP
0.5 mM	GMP
0.5 mM	GDP
0.5 mM	GTP
	Prepare standard mix in H_2O^{HPLC} and store aliquots at -70 °C.
HPLC elution buffer A for nucleotides:	
88 mM	KH_2PO_4
12 mM	K_2HPO_4
4 mM	TBAS
	Adjust to pH 6.0, prepare elution buffer in H_2O^{HPLC}.

Table 3.7. Solutions and buffers (continued).

Solution/Buffer	Recipe
HPLC elution buffer B for nucleotides:	
88 mM	KH_2PO_4
12 mM	K_2HPO_4
4 mM	TBAS
30 % (v v^{-1})	Methanol HiPerSolv CHROMANORM®
	Adjust to pH 7.2, prepare elution buffer in H_2O^{HPLC}.

3.1.7. Chemicals

Table 3.8. List of chemicals.

Chemical, Purity	Manufacturer
Acetic $acid^{abs}$, 100 %	Merck, DE
Acetic acid, ≥ 99.8 %	Sigma-Aldrich, US
Adenosine-5'-monophosphate disodium salt (5'-AMP-Na_2), ≥ 99.0 % (HPLC grade)	Sigma-Aldrich, US
Adenosine-5'-diphosphate disodium salt dihydrate (5'-ADP-Na_2 · 2 H_2O), ≥ 98.0 %	Gerbu, DE
Adenosine-5'-triphosphate disodium salt trihydrate (5'-ATP-Na_2 · 3 H_2O), ≥ 98.0 % (HPLC grade)	Gerbu, DE
Agar (European)	Becton Dickinson, US
Agarose Low Melt	Carl Roth, DE
Ammonium hydroxide (NH_4OH), ~25.0 % NH_3	Sigma-Aldrich, US
di-Ammonium hydrogen phosphate ($(NH_4)_2HPO_4$), ≥ 97.0 %	Carl Roth, DE
Ammonium sulphate ($(NH_4)_2SO_4$), ≥ 99.5 %	Carl Roth, DE
Ammonium sulphate ($(NH_4)_2SO_4$), ≥ 99.5 % (BioUltra)	Sigma-Aldrich, US
L(+)-Arabinose, ≥ 99.0 %	Carl Roth, DE
Bacto™ Tryptone	Becton Dickinson Biosciences, US
Bacto™ Yeast Extract	Becton Dickinson Biosciences, US

Table 3.8. List of chemicals (continued).

Chemical, Purity	Manufacturer
Brain Heart Infusion (BHI)	Becton Dickinson Biosciences, US
Calcium chloride dihydrate ($CaCl_2 \cdot 2\ H_2O$)	Sigma-Aldrich, US
chloramphenicol (Cam), $\geq$ 99.0 % (HPLC grade)	Sigma-Aldrich, US
Chloroform ROTISOLV®, (HPLC grade)	Carl Roth, DE
Cobalt(II) chloride hexahydrate ($CoCl_2 \cdot 6\ H_2O$)	Sigma-Aldrich, US
Copper(II) sulfate pentahydrate ($CuSO_4 \cdot 5\ H_2O$), $\geq$ 99.0 %	Sigma-Aldrich, US
Deoxyribonucleotide triphosphates (dNTP) Set [each 100 mM], PCR Grade	Thermo Fisher Scientific, US
Dimethyl sulfoxide (DMSO)^{abs}, $\geq$ 99.9 %	Sigma-Aldrich, US
1,4-Dithiothreitol (DTT), $\geq$ 99.0 %	Carl Roth, DE
DNA Gel Loading Dye	Thermo Fisher Scientific, US
Ethanol^{abs}, $\geq$ 99.8 %	Carl Roth, DE
Ethanol denatured, $\geq$ 96.0 %	Carl Roth, DE
Ethanol LiChrosolv®, $\geq$ 99.9 %	Merck, DE
Ethylenediamine tetraacetic acid disodium salt dihydrate (Na_2-EDTA $\cdot$ 2 H_2O), $\geq$ 99.0 %	Carl Roth, DE
Formic acid, $\geq$ 98.0 %	Sigma-Aldrich, US
GelRED™ nucleic acid gel stain [10,000x in water]	Biotium, US
α-D(+)-Glucose monohydrate, $\geq$ 99.5 %	Carl Roth, DE
D(+)-Glucose, $\geq$ 99.5 % (GC grade)	Sigma-Aldrich, US
Glycerol anhydrous, $\geq$ 98.0 %	Carl Roth, DE
Guanosine-5'-monophosphate disodium salt hydrate (5'-GMP-$Na_2 \cdot H_2O$), $\geq$ 99.0 % (HPLC grade)	Sigma-Aldrich, US
Guanosine-5'-diphosphate sodium salt (5'-GDP-Na), $\geq$ 96.0 % (HPLC grade)	Sigma-Aldrich, US
Guanosine-5'-triphosphate sodium salt hydrate (5'-GTP-Na $\cdot$ H_2O), $\geq$ 95.0 % (HPLC grade)	Sigma-Aldrich, US
Hydrochloric acid (HCl), $\geq$ 32.0 %	Sigma-Aldrich, US
Iron(III) chloride hexahydrate ($FeCl_3 \cdot 6\ H_2O$), $\geq$ 98.0 % (HPLC grade)	Carl Roth, DE

Table 3.8. List of chemicals (continued).

Chemical, Purity	Manufacturer
Isopropyl-β-D-1-thiogalactopyranoside (IPTG), ≥ 99.0 %	Carl Roth, DE
Kanamycin sulphate (Kan), ≥ 750 I.U. mg^{-1}	Carl Roth, DE
Sodium L-lactate, ≥ 99.0 %	Sigma-Aldrich, US
Magnesium chloride ($MgCl_2$), ≥ 98.5 %	Carl Roth, DE
Magnesium sulphate heptahydrate ($MgSO_4 \cdot 7\ H_2O$), ≥ 99.0 %	Carl Roth, DE
Manganese(II) sulfate monohydrate ($MnSO_4 \cdot H_2O$), ≥ 98.0 %	Sigma-Aldrich, US
Methanol HiPerSolv CHROMANORM®, ≥ 99.8 % (HPLC grade)	VWR, DE
β-Nicotinamide adenine dinucleotide (NAD^+), ≥ 97.5 %	Gerbu, DE
Perchloric acid (PCA), 70.0 – 72.0 %	Sigma-Aldrich, US
pH-buffer solution, pH 7.0± 0.02	Carl Roth, DE
pH-buffer solution, pH 4.0± 0.02	Carl Roth, DE
pH-buffer solution, pH 9.0± 0.02	Carl Roth, DE
Phenol:Chloroform:Isoamyl Alcohol (25:24:1), BioUltra	Sigma-Aldrich, US
L-Phenylalanine, ≥ 98.5 %	Carl Roth, DE
Phosphoric acid (H_3PO_4), ≥ 85.0 %	Sigma-Aldrich, US
ortho-Phosphoric acid (H_3PO_4), 50.0 %	Carl Roth, DE
Polyethylene glycol (PEG)-8000	Sigma-Aldrich, US
Potassium acetate	Sigma-Aldrich, US
Guanosine-3',5'-bisdiphosphate (ppGpp), ≥ 85.0 %	Trilink, US
Sodium pyruvate, ≥ 99.0 %	Sigma-Aldrich, US
di-Potassium hydrogen phosphate (K_2HPO_4), ≥ 98.0 %	Carl Roth, DE
di-Potassium hydrogen phosphate (K_2HPO_4), ≥ 99.0 % (HPLC grade)	VWR, DE
Potassium dihydrogen phosphate (KH_2PO_4), ≥ 98.0 %	Carl Roth, DE
Potassium dihydrogen phosphate (KH_2PO_4) HiPerSolv CHROMANORM®, ≥ 99.5 % (HPLC grade)	VWR, DE
Potassium hydroxide (KOH), ≥ 85.0 %	Carl Roth, DE
L-Rhamnose monohydrate, ≥ 99.0 %	Sigma-Aldrich, US
DL-Serine hydroxamate (SHX)	Sigma-Aldrich, US
Sodium chloride (NaCl), ≥ 99.5 %	Carl Roth, DE
Sodium dodecyl sulphate (SDS) ultra pure, ≥ 99.5 %	Carl Roth, DE

Table 3.8. List of chemicals (continued).

Chemical, Purity	Manufacturer
Sodium hydroxide (NaOH), ≥ 99.0 %	Carl Roth, DE
Sodium phosphate monobasic dihydrate ($NaH_2PO_4 \cdot 2\ H_2O$), ≥ 99.0 %	Sigma-Aldrich, US
Sodium sulfate (Na_2SO_4)	Sigma-Aldrich, US
Succinic acid, ≥ 99.5 %	Sigma-Aldrich, US
Sulfuric acid (H_2SO_4), 5 mol L^{-1}	Sigma-Aldrich, US
Sulfuric acid (H_2SO_4), 49.0 – 51.0 % (HPLC grade)	Sigma-Aldrich, US
Sulfuric acid (H_2SO_4), 98.0 %	Carl Roth, DE
Tetrabutylammonium bisulfate (TBAS), ≥ 99.0 %	Sigma-Aldrich, US
Thiamine hydrochloride, ≥ 98.5 %	Carl Roth, DE
Tris(hydroxymethyl)aminomethane hydrochloride (Tris-HCl), ≥ 99.0 %	Carl Roth, DE
Trizma® base (Tris base), ≥ 99.9 %	Sigma-Aldrich, US
Water ($H_2O^{Mol.Biol.}$), BioScience Grade	Carl Roth, DE
Water ROTISOLV® (H_2O^{HPLC}), (HPLC grade)	Carl Roth, DE
Water ($H_2O^{Mol.Biol.}$), BioScience Grade	Carl Roth, DE
5-Bromo-4-chloro-3-indolyl-β-D-galactopyranoside (X-β-Gal), ≥ 99.0 %	Carl Roth, DE
Zinc sulfate heptahydrate ($ZnSO_4 \cdot 7\ H_2O$), ≥ 99.0 %	Sigma-Aldrich, US

3.1.8. Consumables

Table 3.9. List of laboratory consumables.

Consumable	Manufacturer
N/C analyzer vial snap caps, 1 mm	CS-Chromatographie Service, DE
N/C analyzer vials 1.5 mL, glass, snap neck	CS-Chromatographie Service, DE
Electroporation cuvettes, 1 mm	PEQLAB, DE
Exhaust gas filter Midisart®2000, 0.2 µm, PTFE	Sartorius Stedim Biotech, DE
hollow-bore needle, 1 mm × 200 mm, reuseable	Unimed, CH
HPLC column Rezex ROA organic acid H^+ (8 %), 300 mm × 7.8 mm, 8 µm	Phenomenex, DE
HPLC column Supelcosil™ LC-18-T, 3 µm, 150 mm × 4.6 mm	Sigma-Aldrich, US
HPLC guard column Hypersil™ BDS C-18, 5 µm, 4 mm × 10 mm	Thermo Fisher Scientific, US
HPLC Hardware Kit, KJO-4282	Phenomenex, DE
HPLC SecurityGuard™ cartridge for Carbo-H^+ column, 4 mm × 3 mm	Phenomenex, DE
HPLC vials 1.5 mL, glass, screw neck	VWR, DE
HPLC vial crew caps, PP, with septum	VWR, DE
HPLC vial inserts, 100 µL	VWR, DE
Kryo vials with caps, 2 mL	Sarstedt, DE
Meliseptol®	Braun, DE
Membrane filter disks MF™, 0.025 µm	Merck Millipore, US
PCR tubes Multiply®-Pro, 0.2 mL	Sarstedt, DE
Petri dishes, 92 mm × 16 mm	Sarstedt, DE
Pipet filter tips Biosphere® 20 µL, 200 µL, 1000 µL	Sarstedt, DE
Pipet tips 10 µL, 200 µL, 1000 µL	Carl Roth, DE
Reaction tubes 1.5 mL, 2 mL, 15 mL, 50 mL	Sarstedt, DE

Table 3.9. List of laboratory consumables (continued).

Consumable	Manufacturer
Reaction tubes, safe-lock, 1.5 mL, 2.0 mL	Eppendorf, DE
Semi-micro cuvettes, 1.6 mL, PMMA	Sarstedt, DE
Semi-micro cuvettes, 1.6 mL, polystyrene	Sarstedt, DE
Serologic pipets 1 mL - 25 mL	Sarstedt, DE
Shaking flasks with baffles, 500 mL	Glasgerätebau Ochs
Sterillium® classic pure	BODE Chemie, DE
Syringe filters Rotilabo®, 0.22 µm, CME, sterile	Carl Roth, DE
Syringe Injekt®, sterile, 1 mL - 5 mL	Braun, DE
Syringe SOFT-JECT® Luer Lock, sterile, 5 mL - 50 mL	HSW, DE

3.1.9. Equipment

Table 3.10. List of laboratory equipment.

Instrument & Model	Manufacturer
Autoclave PACS 2000	Getinge, DE
Autoclave DX-23	Systec, DE
Balance AM 100	Mettler-Toledo, US
Benchtop orbital shaker TR-150	Infors HT, CH
Centrifuge 5430 R	Eppendorf, DE
Centrifuge 5804 R	Eppendorf, DE
Centrifuge Minispin®	Eppendorf, DE
Centrifuge rotor A-4-44	Eppendorf, DE
Centrifuge rotor F-45-30-11	Eppendorf, DE
Centrifuge rotor F-35-6-30	Eppendorf, DE
Centrifuge rotor FA-45-30-11	Eppendorf, DE
Centrifuge rotor F-45-12-11	Eppendorf, DE
Clean bench Variolab-Mobilien W 90	Waldner, DE
Desalination device NANOpure II	Barnstead, US

Table 3.10. List of laboratory equipment (continued).

Instrument & Model	Manufacturer
diode array detector (DAD)	Agilent Technologies, US
Dissolved oxygen sensor 6800 Series	Mettler-Toledo, CH
Electronic balance ABJ 120-4M	KERN, DE
Eporator® 4309	Eppendorf, DE
Exhaust air filter	Bioengineering, CH
Gel tray Mini-Sub® Cell GT	Bio-Rad, US
Gel-pH electrode InPro® 3100	Mettler-Toledo, CH
Glass fermenter 0.25 L, DN 60, borosilicate 3.3	HWS Labortechnik, DE
HPLC system 1200 Series	Agilent Technologies, US
Image analyzer LAS-3000 IDX4	Fujifilm, JP
Lightbox 13 10 10	Desaga, DE
Magnetic stirrer Cimarec™ Mobil 25	Thermo Scientific, US
Magnetic thermomixer IKAMAG® REO	IKA Werke, DE
Mass flow controller GFC 17	Analyt-MTC, DE
Microbalance XP 26 DeltaRange®	Mettler-Toledo, US
Multi N/C analyzer 2100 S	Analytik Jena, DE
PCR-Thermocycler Mastercycler **ep***gradient*	Eppendorf, DE
PCR-Thermocycler Biometra TAdvanced 96 G	Analytik Jena, DE
pH meter SevenEasy	Mettler-Toledo, US
pH meter InLab® Micro	Mettler-Toledo, US
Photoacoustic fermentation monitor 1313	Innova AirTech Instruments, DK
Pipet Multipette® plus	Eppendorf, DE
Pipets 10, 100, 1000 µL Research® plus	Eppendorf, DE
Power pack Biometra P25	Analytik Jena, DE
Refractive Index Detector (RID) 1200 Series	Agilent Technologies, US
Rotary incubator CMV-ROM	Ltf Labortechnik, DE
Spectrophotometer NanoDrop™ ND-1000	Thermo Scientific, US
Spectrophotometer GeneQuant® 1300	GE Healthcare, UK
Thermomixer Comfort 1.5 mL	Eppendorf, DE

Table 3.10. List of laboratory equipment (continued).

Instrument & Model	Manufacturer
Ultrasonic bath RK 510 H	Bandelin Electronic, DE
UV transilluminator	INTAS Science Imaging, DE
VIS spectrophotometer DR 3900	Hach, DE
Vortex mixer Vortex Genie® 2	Scientific Industries, US
Water bath MS	Lauda, DE

3.1.10. Software

Table 3.11. List of used software.

Software	Manufacturer
Chem Station B.03.01	Agilent Technologies, US
Clone Manager 9 Professional	Sci-Ed Software, US
INKSCAPE 0.91	Inkscape Community (GPL)
LabVIEW 2009 SP1	National Instruments, US
Mendeley Desktop 1.17	Mendeley, UK
Microsoft Office 2013	Microsoft, US
Origin Pro 9	OriginLab, US
Sigmaplot 12	Systat Software, US
TeXnicCenter 2.02	The TeXnicCenter Team (GPL)

3.2. Methods

3.2.1. Genetic Tools for Metabolic Engineering

Many tools are available for genetic manipulation procedures in a variety of different classes of bacteria. For the group of gram-negative bacteria like *E. coli*, a number of applicable genome modification techniques based on plasmid integration into the chromosome or enzyme-mediated homologous recombination are well known. Here, the pEMG cloning vector and its associated I-SceI mutagenesis system are of special interest. This combination of two mutagenesis strategies has various persuasive advantages over other commonly used molecular cloning approaches like, for instance, the bacteriophage λRed mediated system or the pKO3 gene replacement method. In general, the λRed DNA recombination method (Datsenko and Wanner 2000) is a powerful and prevalent tool for diverse targeted genetic manipulations of chromosomes, plasmids, or BACs and also a very straightforward method. Despite all the positive aspects, this cloning method may entail the risk of leaving an unfavorable 34 nucleotides (nt) long flippase recognition target (FRT) scar sequence in the genome after elimination of the antibiotic resistance marker cassette. In some cases such sequences can be disturbing for further chromosomal modification events. The strong homology of FRT sites in bacterial strains carrying multiple mutations, might possibly lead to interference of adjacent regions and consequently to unwanted recombination events. Another possible choice of gene replacement system is the pKO3 vector. It has been developed as a molecular tool for precise deletion and insertion of DNA from or into the genome of WT *E. coli* strains (Link et al. 1997). One of its features is an integration event into the chromosome by homologous recombination at the non-permissive temperature of 43 °C due to the temperature-sensitive origin of replication (*ori*) *repA* from P1 phage. From experience, this step is hugely critical since it sometimes needs several rounds of selection until a positive integration event can be observed. Furthermore, handling bacterial cultures at higher temperatures than conventional practices allow, can prove difficult under day-to-day laboratory circumstances.

3.2.2. Primer Design

Genetic modifications of the *E. coli* chromosome started with the design of appropriate primer sequences depending on the type of desired mutations. A computer-based designing process as well as primer analysis for GC contents, melting temperatures, stability and repeats were accomplished by using the Clone Manager 9 Professional software. In Figure 3.2 various concepts for cloning strategies like deletion, insertion or nucleotide substitution are visualized schematically. The upper part describes a general procedure of primer part assemblage to provide homologous sequences for sufficient recombination during Gibson Cloning (3.2.3). From the 5' end, each primer consists of about 25-30 nt complementary to the sequence left or right of the MCS in the pEMG cloning vector. If any endonuclease cleaving site was required, the corresponding recognition sequence for a certain restriction enzyme was copied next to the pEMG sequence or was directly chosen from the MCS of the vector (Table 3.3). The following 18-20 nt were complementary to the sequences framing the chromosomal cloning insert. In this way, the outer forward (TS1F) and reverse (TS2R) primers were designed. In between these two, shorter primers were constructed to generate DNA components according to the mutation type of choice. It was important to consider adequate overlapping regions of minimum 30 nt to allow the right order of assemblage. In the case of this work, designed primers had at least a length of 30 nt of which 24 nt determined the right position for primer annealing within the gene of interest (GOI). Nucleotide substitution mutations were introduced concentrically in the sequence of the forward and the reverse primer, equally. Total primer lengths varied from 18 to 90 base pairs. An entire list of all primers used in this study can be found in Table A.1. All oligonucleotides were purchased from biomers.net GmbH (Ulm, DE).

3.2.3. Preparation of Cloning Plasmids

The first step in the concept of generating a functional variant of the cloning vector pEMG (Figure 3.1) was always to decide upon the character of the cloning cassette and the origin of the appropriate DNA template. In this thesis, all targeted genetic constructs were genes inherent in the *E. coli* K-12 MG1655 chromosome. Thus, isolated genomic DNA of this host strain was used as template for all further DNA amplification procedures.

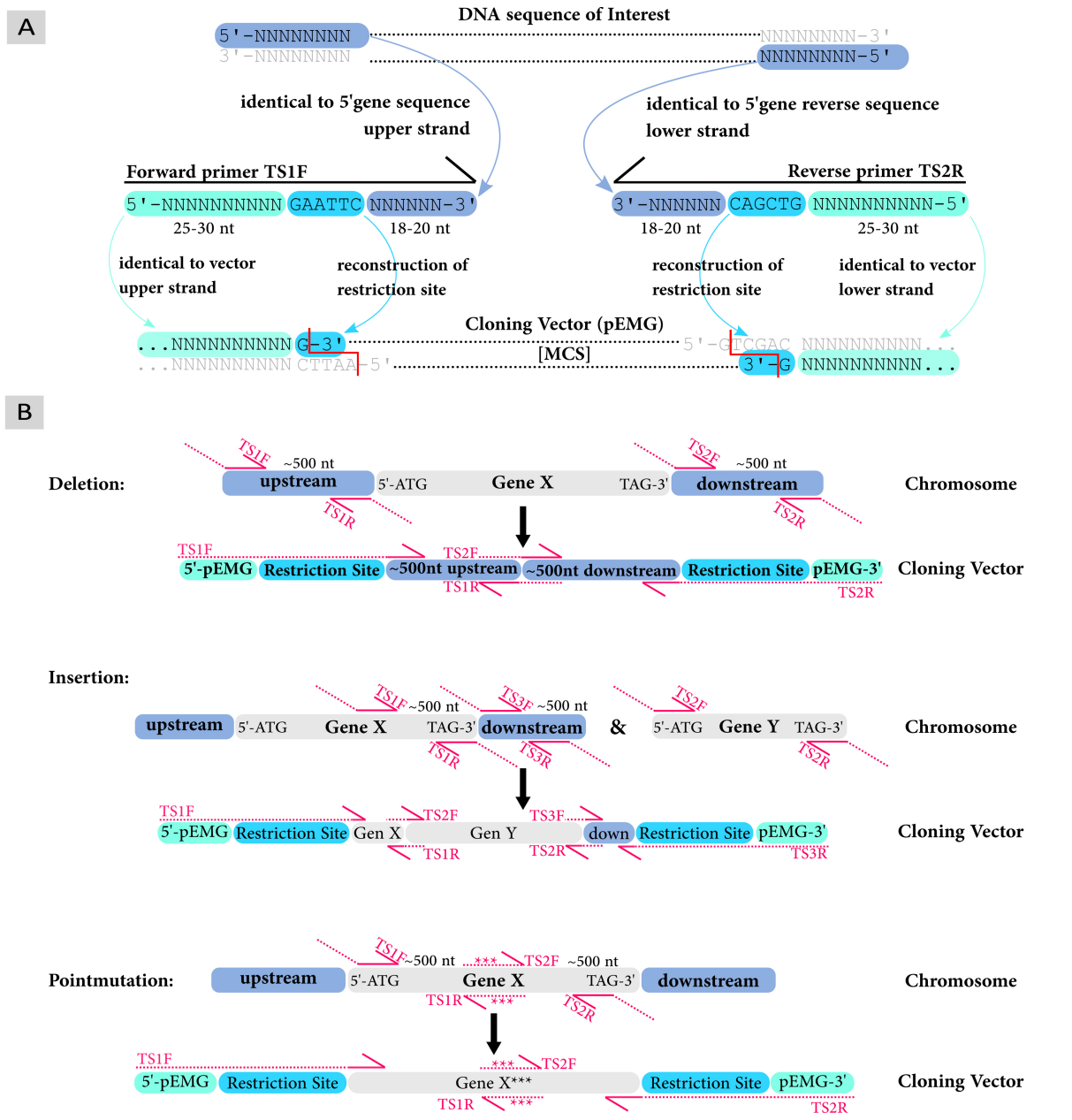

Figure 3.2. Schematic overview of primer design for Gibson Cloning. A: General approach for construction of primers, which can be applied for the Gibson Assembly Cloning method. Both outer primer sequences TS1F (target sequence 1, forward (fwd)) and TS2R (target sequence 2, reverse (rev)) share an identical configuration. Principal primer structures are a 5'-region of up to 30 nt complementary to the cloning vector pEMG sequence (cyan), a restriction recognition site (light blue) and a 18-20 nt long sequence complementary to the DNA of interest (blue). B: Detailed approaches for the cloning strategies of DNA deletion or insertion mutations as well as for nucleotide substitutions are demonstrated. Dotted lines represent homologous primer parts.

Extraction of Genomic DNA

To extract about 150 µg of genomic DNA from *E. coli* K-12 MG1655 , 2 mL of an overnight test tube culture centrifuged for 1 min at 12,000×g and room temperature (RT). After removing the supernatant, the bacterial cell pellet was resuspended in 800 µL lysis buffer and incubated for 30 min at 50 °C. Next, an equivalent volume of phenol:chloroform:isoamyl alcohol (24:25:1) was added to the suspension and the reaction tube was inverted several times until a bright emulsion was received. In the following centrifugation step at 12,000×g and RT for 5 min this emulsion separated into two liquid phases and a solid phase of denaturated proteins in between. The upper aqueous phase contained the extracted DNA and was carefully pipetted into an equivalent volume of phenol:chloroform:isoamyl alcohol (24:25:1), inverted and centrifuged as described above. This procedure was repeated three times in total to remove all protein residuals from the liquid phase. Subsequently, the DNA from the clear upper aqueous phase was precipitated for at least 1 h at -20 °C by filling the reaction tube to the 2 mL mark with cold ethanol^{abs} (-20 °C). The solution was centrifuged for 15 min at 20,800×g and 4 °C. After the supernatant was decanted, a gelatinous DNA pellet appeared and was resuspended in 396 µL TE buffer and 4 µL of RNase A [10 mg mL^{-1}] and incubated for 20 min at RT. Finally, the precipitation step with ethanol^{abs} was repeated one more time, the DNA was dried in a thermomixer at 50 °C for 1 min and dissolved in 50 µL of $H_2O^{Mol.Biol.}$ or TE buffer. All precipitation steps could also be extended overnight.

Amplification of DNA

All DNA fragments for cloning cassettes of the pEMG plasmid were amplified using three-step PCR approaches with the proof-reading Phusion® DNA polymerase. Prior to preparation of the reaction mix, primer stock solutions in a concentration of 10 µM and a dNTP mix (dATP, dCTP, dTTP, dGTP) with a concentration of 2 mM were provided. The PCR mix, all stock solutions and especially enzymes, were kept on ice during the entire preparation procedure. The lid heat of the thermocycler was set to 105 °C to prevent evaporation of the PCR reaction. Application of a hot start DNA polymerase type ensured a controlled PCR start at the initial temperature of 98 °C. A Phusion® PCR pipetting instruction and protocol is described in the following:

Table 3.12. Instructions for performing a PCR with Phusion® DNA Polymerase

PCR mix:		Phusion® protocol:	
10.0 µL	5× Phusion® HF Buffer	98 °C	60 sec
5.0 µL	dNTPs [2 mM]		
2.5 µL	forward primer [10 µM]	30 cycles:	
2.5 µL	reverse primer [10 µM]	98 °C	15 sec
1.0 µL	gen. DNA [3 µg μL^{-1}]	55 °C	30 sec
0.5 µL	Phusion® Hot Start II	72 °C	15 sec 1000 nt^{-1}
	DNA polymerase [2 U μL^{-1}]		
28.5 µL	$H_2O^{Mol.Biol.}$	72 °C	10 min
50.0 µL		4 °C	hold

After the PCR run, the quality of the products was tested by gel electrophoresis in an 1 % agarose gel in TAE buffer and stained with the GelRED™ dye to estimate the length of amplified DNA fragments. Agarose gel electrophoresis has been performed as described in detail elsewhere (Mülhardt 2008). Subsequently, the PCR reaction mix was purified with the NucleoSpin® Gel and PCR Clean-up Kit according to the manufacturers manual. During the clean-up process, use was made of the recommended second washing step of the silica membrane. Purified DNA fragments were eluted with $H_2O^{Mol.Biol.}$ (70 °C) in two serial elution steps. Some primer pairs yielded more than one single fragment as PCR product. In these cases, the entire reaction volume was separated on an 1 % agarose gel and the band with the correct fragment length was extracted from the agarose using the NucleoSpin® Gel and PCR Clean-up Kit as described above (3.2.3). Nucleic acid concentrations and purity of these samples were measured with a NanoDrop™ UV-VIS spectrophotometer.

DNA Purification

Before the functional pEMG cloning vector was compiled by DNA assembly, all insert fragments of the cloning cassette were purified and the vector sequence was linearized.

Circular pEMG plasmid DNA was isolated from the host strain *E. coli* DH5$\alpha\lambda$*pir* pEMG. Therefore, the E.Z.N.A.® Plasmid DNA Mini Kit I was used according to the manufacturers manual. Since the pEMG vector is a low-copy plasmid, circular DNA was extracted from 15 mL overnight culture such that recommended volumes of solutions I, II and III were tripled. The optional column equilibration step with 3 M NaOH as well as a second DNA washing step were applied during the process. Plasmid DNA was eluted with $H_2O^{Mol.Biol.}$ (70 °C) in two serial elution steps. Alternatively, larger amounts of plasmid DNA were purified from 100 mL overnight culture. Therefore, the bacterial suspension was centrifuged for 15 min at 4,500×g and 4 °C. Resulting pellets were lyzed in 2 mL alkaline Lysis buffer I (ice-cold), divided into 500 µL aliquots and kept on ice during the entire procedure. Into each aliquot 670 µL of freshly prepared alkaline Lysis buffer II were added, the reaction tubes were carefully inverted 10 times and incubated on ice for 3 min. This step was repeated immediately after with 500 µL of alkaline Lysis buffer III (ice-cold) followed by a centrifugation step of 10 min at 20,800×g and 4 °C. Clear and aqueous supernatants were aliquoted á 600 µL and vortexed together with an equivalent volume of phenol:chloroform:isoamyl alcohol (24:25:1). After centrifugation for 2 min at 12,000×g and RT, the liquid phase was vortexed with 600 µL of chloroform and centrifuged as mentioned before. The following DNA precipitation procedure corresponds to the method described above (3.2.3). Finally, each aliquot of dried DNA pellet was dissolved in 10 µL of $H_2O^{Mol.Biol.}$ or TE buffer and the plasmid DNA was pooled.

Linearization of pEMG plasmids was accomplished by classic DNA cleavage with two independent restriction enzymes. The appropriate combination of restriction endonucleases for each pEMG cloning vector can be obtained from Figure A.1. For this purpose, the Thermo Scientific DoubleDigest Calculator[1] provides all necessary information about the choice of suitable buffer systems, incubation temperatures and enzyme concentrations for the double digest reactions. Equally, the subsequent inactivation of the restriction enzyme activity and the vector dephosphorylation step with FastAP Thermosensitive Alkaline Phosphatase were carried out as specified by the manufacturer. The digestion reaction was checked by agarose gel electrophoresis. The linear vector backbone was purified with the PCR clean-up protocol (3.2.3) and DNA concentrations of all fragments, included in the following step, were measured with the NanoDrop™ device.

[1] https://www.thermofisher.com/de/de/home/brands/thermo-scientific/molecular-biology/thermo-scientific-restriction-modifying-enzymes/restriction-enzymes-thermo-scientific/double-digest-calculator-thermo-scientific.html[Date:28-01-2020,14:20]

DNA Assembly

Finally, this set of multiple DNA fragments was joined together by the Gibson one-step ISO assembly method for overlapping double stranded (ds) DNA sequences (Gibson 2011) to generate a circular, functional pEMG plasmid carrying the cloning cassette for homologous recombination. A protocol for reaction buffer preparation as well as instructions for sufficient DNA amount calculation were obtained from this reference. Initially, the thermocycler block and the lid were preheated to 50 °C and 95 °C respectively, to prevent vaporization of the reaction solution. One aliquot of Gibson Assembly enzyme reaction master mix was kept on ice for each assembly reaction. Calculated volumes of linearized vector DNA, PCR fragments of cloning cassette elements and eventual $H_2O^{Mol.Biol.}$ were pipetted into the lid of the reaction tube containing the enzyme mix. The reaction tube was sealed and shortly spun in a bench-top centrifuge until both solution portions combined at the bottom. Immediately after this step the Gibson Assembly reaction tube was placed in the preheated thermocycler and incubated for 60 min at 50 °C. A following column purification step was not preferred, because very low concentrations of circularized plasmid DNA were further diluted to a high extend and thus impractical for transformation events. Instead, the Gibson Assembly reaction was microdialysed on a hydrophilic mixed cellulose esters membrane filter disk to remove high salt concentrations. Therefore, a Petri dish was filled with 20 mL of $H_2O^{Mol.Biol.}$ and the membrane filter disk was placed carefully on the surface of the liquid using tweezers. The Gibson Assembly reaction was pipetted onto the membrane and incubated for 20 min with the lid on. In this way, the sample volume only increased to a total of 25 – 30 µL.

Preparation of Electrocompetent Cells

Electrocompetent cells were prepared in large batches and stored at -70 °C for a period of up to two years. To gain a total quantity of about 50 aliquots, a 500 mL overnight culture in 2×YT medium with additional antibiotics or supplements in case of need, was prepared. The volume was divided in ten 50 mL reaction tubes and incubated on ice for 30 min to cool down the cell suspension and minimize cellular activities. After that, the cells were centrifuged at 4,500×g and 4 °C for 15 min and the supernatant was discarded. From this time on, it is recommended to continue the washing and resuspension steps

in a cooling chamber or to incessantly keep all reaction tubes in an ice bath and remove the same quickly and only for a short time for repeated mixing rounds. Every reaction tube was filled to the 20 mL mark with ice-cold $H_2O^{Nanopure}$ and resuspended by short vortexing steps. For better handling, the contents of all ten reaction tubes were pooled into four units and kept on ice for 5 min. The cycle of concentrating the cells, washing them in 20 mL ice-cold $H_2O^{Nanopure}$ and cooling them down was repeated two more times. In the last washing step, each of the four cell pellets was resuspended in 400 µL ice-cold sterile 10 % glycerine solution. 50 µL aliquots were frozen immediately in liquid nitrogen and long-term stored at -70 °C.

DNA Transformation

Plasmid DNA was transformed into 50 µL of electrocompetent cells of *E. coli* DH5$\alpha\lambda$*pir* by electroporation. To that end, one aliquot of frozen electrocompetent cells (-70 °C) was thawed on ice for 30 min. 5 µL of desalted Gibson Assembly reaction mixture were mixed with the electrocompetent cells and incubated for 1 min on ice. Subsequently, the electrocompetent cells-plasmid mix was pipetted free of air bubbles into an ice-cold electroporation cuvette and placed in the Eppendorf Eporator®. A voltage of 1700 V was applied and the expected discharge time constant lay between 5.3 and 5.6 seconds. Immediately after electroporation, the cells were absorbed into 1 mL of sterile 2×YT medium and incubated for 1 h at 37 °C on a rotary shaker at 130 rpm. 100 µL of this transformation culture were plated directly on a blue-white selection agar plate containing Kan, IPTG and X-β-Gal. The residual 900 µL were centrifuged at 12,000×g and RT for 20 sec. This bacterial cell pellet was resuspended in 100 µL of medium and plated likewise.

Screening and Validation of Plasmid Constructs

Screening for positive colonies with the pEMG cloning system is a very easy-to-handle procedure. Transformants were plated on blue-white selection agar plates (Kan, IPTG, X-β-Gal), which means that in a first step of selection only cells harbouring a functional pEMG plasmid containing the Kanamycin (Kan) resistance gene were able to

grow. Among these colonies, the ones positive for an inserted cloning cassette within the MCS region of pEMG appeared white, due to a disrupted α*lacZ* region. Basically, the blue-white screening assay makes use of a complementation event between the αLacZ fragment expressed from the pEMG plasmid and the curtailed LacZ gene product expressed by the *lacZ*ΔM15 host strain. The α-complementation process results in an intact β-galactosidase enzyme, whose activity leads to a blue colony staining on agar plates supplemented with IPTG and X-β-Gal (Sambrook and Russell 2001). By implication, non-colored white stained colonies show a lack of functional β-galactosidase and thus implicate a positive fragment insertion event. Those white colonies were separated on a 2×YT+Kan agar plate and grown over night at 37 °C to gain enough bacterial colonies for the subsequent confirmation by colony PCR. Therefore, a small amount of cell material was picked with a sterile pipette tip and resuspended in 50 µL of $H_2O^{Mol.Biol.}$ in a 200 µL reaction tube. These diluted cells were then lysed for 10 min at 95 °C in the thermo cycler to break up the cell membranes and to extract the bacterial DNA. The reaction tubes were centrifuged for 1 min and RT at 12,000×g to receive a clear and debris-free DNA lysate. A *Thermus aquaticus* (*Taq*) PCR pipetting instruction and protocol is described in the following:

Table 3.13. Instructions for performing a PCR with *Taq* DNA Polymerase

PCR mix:		*Taq* protocol:	
2.5 µL	10× PCR Buffer S	95 °C	5 min
2.5 µL	dNTPs [2 mM]		
1.0 µL	forward primer [10 µM]	30 cycles:	
1.0 µL	reverse primer [10 µM]	95 °C	30 sec
1.0 µL	DMSO	55 °C	30 sec
0.1 µL	*Taq* DNA polymerase [5 U μL^{-1}]	72 °C	60 sec 1000 nt^{-1}
10.0 µL	DNA lysate		
6.9 µL	$H_2O^{Mol.Biol.}$	72 °C	10 min
25.0 µL		4 °C	hold

For one thing, the *Taq* colony PCR confirmed the presence of the cloning cassette in the pEMG vector. For another thing, the orientation of the cloning insert was analyzed with a rational choice of PCR primers. A combination of one specific primer from the insert sequence and another pEMG specific primer (Table A.1), binding either up- or downstream of the MCS region, was utilised. Fragment lengths of the colony PCR products were checked in 1 % agarose gels. The insert sequences were validated on purified plasmids with the primers F_pEMG and R_pEMG by Sanger sequencing at GATC Biotech AG (Konstanz, DE). Finally, all completed and validated plasmid-carrying strains were cryo-preserved and long-term stored at -70 °C. In order to do this, 700 µL of an overnight culture in 2×YT medium supplemented with Kan were mixed thoroughly in a cryopreservation tube already containing 300 µL of sterile glycerine.

3.2.4. Scarless Chromosomal Modifications

Seamless modifications of chromosomally encoded genes or parts of gene domains were realized with a recently described method for gene editing by Martínez-García and De Lorenzo 2012. In summary, the work flow of this I-SceI based marker-less mutagenesis protocol started with the construction of the pEMG cloning vector containing a gene replacement fragment of two combined homologous regions (~500 nt) for recombination with the chromosome. This insert was placed within the MCS of pEMG (Table 3.3) and in this way was automatically flanked by two I-SceI recognition sites (Martínez-García and de Lorenzo 2011). Such accurate and sequence validated pEMG+X cloning plasmids were extracted, purified and transformed by electroporation into electrocompetent cells of the host recipient strain - in the case of this study *E. coli* K-12 MG1655 WT. The pEMG mechanism of action is its missing ability of *ori*R6K initiated replication in a *pir* negative genetic background. Thus, colonies surviving on a 2×YT+Kan agar plate have the plasmid sequence, including the antibiotic resistance gene, incorporated into the host chromosome. Homologous recombination between the replacement insert and the *E. coli* genome takes place through the cell-intrinsic *recA*-dependent DNA repair machinery, which produces the so called co-integrates as described in Filutowicz et al. 1986. From those, three colonies were selected and processed for a further electroporation step. Therefore, small batches of electrocompetent cells were prepared from a 10 mL overnight culture in 2×YT+Kan giving a total of two aliquots. These electrocompetent

cells were transformed with 1.0 µL of pACBSR at a concentration of ~100 ng μL^{-1}. After regeneration of the cells, 100 µL and the rest of the transformants were plated on double selection 2×YT+Kan+Cam agar plates and incubated overnight at 37 °C. Again, several colonies were separated on a 2×YT+Kan+Cam master plate. Hence, those cells resistant to both antibiotics were harboring the pEMG plasmid integrated to their chromosome. Additionally, they were equipped with a pACBSR helper plasmids carrying the I-SceI homing endonuclease from *Saccharomyces cerevisiae* (*S. cerevisiae*) as well as the λRed genes under control of the arabinose promoter P_{ara}. For a successful gene replacement event, both, the cleavage activity of I-SceI at its recognition sites and the expression of the λRed genes *gam*, *bet* and *exo*, have to be existent in the cell. First, the homing endonuclease I-SceI cleaves the host DNA and generates double-strand breaks in flanking regions of the gene replacement cassette. Next, the λRed gene products seal those nicks by homologous recombination with the chromosome (Herring et al. 2003). Therefore, 50 µL of an overnight culture in 2×YT+Kan+Cam were inoculated into 5 mL of fresh 2×YT medium containing only Cam to ensure numerous plasmid copies of pACBSR. The test tube culture was grown at 37 °C and 130 rpm until an OD_{600nm} of 0.4 – 0.5 was reached (1.5 – 2.0 h). Gene transcription from the P_{ara} promoter was induced by adding a sterile L-arabinose solution to a final concentration of 0.3 % (v v^{-1}) to the bacterial culture. After 7 h incubation at 37 °C and 130 rpm, 100 µL each of a 10^{-4}, a 10^{-5} and a 10^{-6} dilution were plated on 2×YT+Cam agar plates. The next day, several colonies were separated on a 2×YT+Cam master plate and counter-selected on a 2×YT+Kan agar plate for loss of the pEMG plasmid. Different PCR strategies were run on a set of 16 clones to test for a successful genetic modification event. In cases of gene deletions or gene fragment variations, these fragments were amplified by colony *Taq* PCR (Table 3.13) and positive clones were identified by PCR product lengths. In cases of nucleotide substitutions, PCR products from a Phusion® colony PCR were analyzed by Sanger sequencing to check for positive modifications. Template DNA was received by boiling lysis as described above (3.2.3) and diluted by a factor of 1:50 in the final reaction mix. A Phusion® colony PCR pipetting instruction and protocol is described in the following:

Table 3.14. Instructions for performing a colony PCR with Phusion® DNA Polymerase

PCR mix:		Phusion protocol:	
10.0 µL	5× Phusion® HF Buffer	98 °C	60 sec
2.0 µL	DMSO		
5.0 µL	dNTPs [2 mM]		
2.0 µL	forward primer [10 µM]	30 cycles:	
2.0 µL	reverse primer [10 µM]	98 °C	15 sec
1.0 µL	DNA lysate [1:50]	55 °C	30 sec
0.5 µL	Phusion® Hot Start II	72 °C	15 sec 1000 nt^{-1}
	DNA polymerase [2 U μL^{-1}]		
27.5 µL	$H_2O^{Mol.Biol.}$	72 °C	10 min
50.0 µL		4 °C	hold

Resulting *E. coli* MG1655 mutants were resolved from the pACBSR helper plasmids by repeating the L-arabinose induction step as described above (3.2.4), only with a reduced incubation time of 2 h. Colonies were selected from 2×YT agar plates and tested for the loss of the pACBSR plasmid by counter-selection on 2×YT+Cam. Finally, mutant strains with the desired chromosomal modification were verified by Sanger sequencing (Sanger et al. 1977) of the targeted and flanking genomic loci and cryo-preserved for long-time storage.

3.2.5. Phenotypical Strain Characterization

Glycogen Detection Assay with Iodine

Iodine staining is a very useful and expeditious technique to test different types of organic materials for glycogen contents, since the complex formation capability of glycogen and iodine is well known (Lecker et al. 1997, Little 1957). The purpose of iodine staining in this study was to assess ppGpp concentrations in different chromosomally engineered mutants

of *E. coli* MG1655 by comparing glycogen amounts in the same. The stringent response alarmone is described to play a major role in induction of glycogen synthesizing genes (2.4.1). Therefore, this rapid test facilitated the opportunity to detect and characterize *relA* and *spoT* mutants with an altered ability of ppGpp formation by comparing their glycogen accumulation phenotypes. For the test, overnight grown colonies on 2×YT agar plates were transferred to KM agar plates and likewise incubated at 37 °C. A glass jar containing about 0.2 g iodine was prepared and placed on a hot plate at the temperature of 100 °C. When the solid iodine began to vaporise, the glass lid of the jar was replaced rapidly by the KM agar plate and tightly sealed with Parafilm®. Immediately after an incubation time of 10 sec the resulting colony staining was documented photographically. Iodine vapors are intensely irritating to the respiratory system. Hence, all activities relating to iodine application were performed under a laboratory hood.

Aerobic Shaking Flask Cultivations

For aerobic cultivation of bacterial cultures, sterile 500 mL glass shaking flask (SF) with 3 baffles were used. Additionally, those shaking flasks were equipped with 20 cm long hollow needles, which were attached through the cotton plug and sealed with a luer-lock cap. These extra long stainless steel hollow needles facilitated a fast-sampling possibility by using disposable syringes without removing the cultures from the incubator. The filling volume did not exceed a maximum of 60 mL either complex nor minimal medium per cultivation to ensure high oxygen transfer into the liquid. The medium was inoculated to a starting OD_{600nm} of 0.1 with cells from an overnight preculture grown in the same medium as the main culture. An adequate volume (mostly 5 – 10 mL) of bacterial cells was harvested by centrifugation for 5 min at 4,500×g and 4 °C, washed once with 0.9 % NaCl and pelleted again. Overnight precultures in complex medium were started with a single colony from a 2×YT agar plate, those in minimal medium with 60 µL of a cryo preserved glycerine stock culture. Bacterial strains of *E. coli* were cultivated in triplicates with orbital shaking at 130 rpm and 37 °C.

Stringent Response Induction with SHX

DL-Serine hydroxamate (SHX), a competitive inhibitor of seryl-tRNA synthetase, was used to provoke an artificial intracellular stringent response reaction in exponentially growing cells. For each tested *E. coli* strain, a total of six shaking flask cultures in minimal medium containing 0.5 % glucose was prepared and grown as described above (section 3.2.5). The optical density was followed in intervals of 1 h until an OD_{600nm} of 2 – 3 was reached. Subsequently, stringent response was induced in three shaking flask cultures with a total concentration of 1 mM SHX in the solution and sampling intervals were reduced to 30 mins. In case of the *E. coli* HGT mutant, 4 mM SHX were necessary for stringent response induction. SHX was prepared freshly prior to each use, since it is very unstable for storage in solution. The three remaining cultures were treated as uninduced growth controls and samples were withdrawn every 1 h. 1 mL culture broth was centrifuged at RT for 1 min at 12,000×g and the supernatant was stored at -20 °C for further analysis.

3.2.6. Two-Stage Nitrogen-Limited Batch Cultivations

Overnight precultures of *E. coli* WT and mutant strains were grown in baffled shaking flasks and minimal medium to mid exponential phase and used for inoculation of the bioreactors. This triplex bioreactor system consisted of three parallel double shell glass reactors (HWS Labortechnik, DE) with a working volume (V_R) of 0.2 L each. All bioreactors were equipped with a pitched-blade magnetic stirrer, ceramic sparger, sampling valve, dissolved oxygen (DO) sensor (Mettler-Toledo, CH) and pH electrode (Mettler-Toledo, CH). Main bacterial two-stage batch cultivations were carried out in nitrogen-limited (N-lim) Minimal Medium with varying initial glucose (Glc) concentrations for all different *E. coli* strains, according to their individual consumption behavior. Glucose starting concentrations as well as parameter set points of all cultivations are listed in Table 3.15 and Table 4.3. DO percentage and pH were controlled by constant online measurements and adjusted by increase of agitation speed (N) and volumetric gas flow rate ($\dot{V}_G$) as well as titration with 0.5 M NaOH and 0.5 M H_2SO_4, respectively. Volume fractions of oxygen and carbon dioxide in the off-gas were monitored online with a photoacoustic fermentation monitor

(Innova AirTech Instruments, DK). Foam formation was prevented with 50 µL Struktol™ J 647 (Schill+Seilacher, DE) added prior to cultivation start.

Table 3.15. Parameter set points at two-stage batch cultivation start.

Parameter	Set Point	Unit
$c_{\mathrm{Glc}}{}^{\mathrm{Start}}$	18 – 30	g L^{-1}
$\mathrm{OD}_{600\mathrm{nm}}{}^{\mathrm{Start}}$	0.2	–
T	37	°C
pH	7.0	–
N	200	min^{-1}
$\dot{V}_G$	300	L h^{-1}
DO	$\geq$ 30	%

3.2.7. Analytical Methods

Optical Density

To record bacterial growth during cultivation, the Optical Density at 600 nm ($\mathrm{OD}_{600\mathrm{nm}}$) of the biosuspension was measured in periodical intervals on a GeneQuant® 1300 spectrophotometer. Each value was determined in technical triplicates from 1 mL biosuspension in a semi-micro polystyrene cuvette and 0.9 % NaCl as reference solution. Extinction rates above 0.3 were diluted appropriately in 5 mL graduated flasks with 0.9 % NaCl to stay within the linear scope of the measurement.

Cell Dry Weight

Especially for bioreactor samples, cell dry weight (CDW) formation was followed along the process time to enable calculation of biomass-specific reaction rates. Prior to each

CDW measurement, clean 1.5 mL glass vials were dried for 24 h in a hot air convection drying closet at 110 °C. After transferring these vials into a desiccator (containing silica gel beads as drying agent) for 1 h to cool them down to RT, the tare weight (m_{tare}) of the vials was weighed and served as reference for CDW calculations (Equation 3.1). 500 µL biosuspension from the bioreactor were washed twice in an equivalent volume of deionized water and centrifuged at 6,700×g for 45 sec. In the last step, the cell pellet was resuspended in 500 µL deionized water and transferred into one of the prepared 1.5 mL glass vials. Drying and balancing out the mass (m) of the cell pellet were carried out as described above.

$$\text{CDW} = \frac{m_{drymatter} - m_{\text{tare}}}{V_{biosuspension}} \tag{3.1}$$

A correlation factor (cf) between CDW and $\text{OD}_{600\text{nm}}$ was determined for several strains of *E. coli* MG1655 and thus allowed estimation of biomass values for missing time points where no CDW samples were taken.

$$f = \frac{\text{CDW}}{\text{OD}_{600\text{nm}}} \tag{3.2}$$

Ammonium and Phosphate

Elemental growth supplements such as Ammonium (NH_4^+) and orthophosphate (PO_4^{3-}) were analyzed photometrically with the cuvette test kits LCK303, LCK304, LCK 348 and LCK 349 (Hach, DE). Supernatants of bioreactor samples were processed according to the manufacturers manual at batch cultivation start and immediately after the oxygen online signal indicated the beginning of nitrogen limitation.

Organic Acids, Sugars and Alcohols

Organic compound concentrations in supernatants from shaking flask samples or straight off measurements from bioreactor samples were analyzed based on a UV-method using the Roche Yellow line D-glucose and acetic acid enzymatic tests (R-Biopharm, DE). Manufacturers protocols were applied as prescribed except for one customization. Pipetting vol-

umes of every reaction solution were halved, such that sample applications per kit could be doubled. This means, the total volume of the biochemical reaction fitted in a 1.6 mL PMMA semi-micro cuvette and was measured as specified. Supernatants of bioreactor samples were mainly analyzed by High Performance Liquid Chromatography (HPLC) on an Agilent 1200 series device (Agilent Technologies, US). Sugars, alcohols and a variety of organic acids were separated in a Rezex ROA organic acid H+ (8 %) column (300 mm × 7.8 mm & 8 µm, Phenomenex, DE) protected by a Rezex ROA organic acid H+ (8 %) guard column (50 mm × 7.8 mm, Phenomenex, DE). Analysis was performed for 45 min at 50 °C under isocratic conditions at a constant flow rate of 0.4 mL min^{-1}. 'HPLC elution buffer for organic acids' (5 mM H_2SO_4) was used as mobile phase and sonicated for 15 min previous to HPLC measurement. Organic compounds were detected with a refractive index detector (RID) at 32 °C. From the 5 g L^{-1} organic acids and sugars standard mix (Table 3.7) eight calibration levels between 10 – 1000 mg L^{-1} were diluted in H_2O^{HPLC} and run along with every measurement series.

Precipitation of Phosphate

A high phosphate concentration in the minimal medium is necessary for stabilization of pH over a long batch cultivation period, especially in a small V_R of only 0.2 L. However, such high PO_4^{3-} levels have some negative effects on HPLC column performance, since the salt can precipitate, accumulate and damage the device. In order to prepare samples from the bioreactor, dissolved phosphate was precipitated and removed prior to analysis. Therefore, 1 mL supernatant was mixed successively with 45 µL 4 M NH_3 and 100 µL 1.2 M $MgSO_4$ and incubated for 5 min at RT. The internal standard L-rhamnose was already added to the $MgSO_4$ solution to yield a final concentration of 100 mg L^{-1} and thus to allow for correction of technical variations. After centrifugation at 20,000×g for 5 min, 500 µL of this supernatant were mixed with 500 µL pre-pipetted 0.1 M H_2SO_4 in a fresh 1.5 mL reaction tube and incubated for 15 min at RT. A final centrifugation step at 20,000×g for 15 min resulted in ~900 µL clear and residue-free supernatant that was either directly processed for HPLC or stored at -70 °C.

Nucleotides

Concentrations of adenine and guanine nucleotides, including ppGpp, were analyzed from PCA cell extracts of bioreactor samples (see below) by ion-pair reversed-phase HPLC (RP-HPLC) on an Agilent 1200 series apparatus. Nucleotides were separated on a Supelcosil™ LC 18-T column (150 mm × 4.6 mm & 3 µm, Sigma-Aldrich, US) in combination with a Hypersil™ BDS C18 guard column (10 mm × 4 mm & 5 µm, Thermo Fisher Scientific, US) and detected with a diode array detector (DAD) set at 260 nm and 340 nm. A gradient elution method (with modifications to Cserjan-Puschmann et al. 1999) was performed with a mixture of 'HPLC elution buffer A & B for nucleotides' (Table 3.7) as polar mobile phase with a constant flow rate of 1 mL min^{-1} at 30°C. The gradient program is listed in Table 3.16. For nucleotide quantification, an eight-level calibration series ranging between 0.5 – 100 µM was diluted from a 0.5 mM 'Nucleotides standard mix' (Table 3.7). ppGpp was added only to the calibration levels from 0.5 – 20 µM separately, since intracellular concentrations were not expected to exceed this range. The initial sample of every bioreactor measurement series was spiked with 5 µL of a 100 µM ppGpp solution to precisely identify ppGpp peak throughout all eluents.

Table 3.16. Elution buffer gradient program during HPLC nucleotide analysis.

Profile	Process Time [min]	Buffer A [%]	Buffer B [%]
Start	0	100	0
Initial Isocratic Hold	3.5	100	0
Gradient Times	20	70	30
	22	65	35
	40	40	60
	48	0	100
Purging	55	0	100
Conditioning	60	100	0
Equilibration	67	100	0

Elution Buffer A: 100 mM K_2HPO_4/KH_2PO_4, 4 mM TBAS, pH 6.0
Elution Buffer B: 70 v v^{-1} % Elution Buffer A, 30 v v^{-1} % methanol, pH 7.2

On the basis of analyzed adenine and guanine nucleotide concentrations, the adenylate energy charge (AEC) and equally the guanylate energy charge (GEC) of the cells was calculated according to the following equation (Atkinson and Walton 1967):

$$\mathrm{AEC} = \frac{[\mathrm{ATP}] + 0.5[\mathrm{ADP}]}{[\mathrm{AMP}] + [\mathrm{ADP}] + [\mathrm{ATP}]} \tag{3.3}$$

$$\mathrm{GEC} = \frac{[\mathrm{GTP}] + 0.5[\mathrm{GDP}]}{[\mathrm{GMP}] + [\mathrm{GDP}] + [\mathrm{GTP}]} \tag{3.4}$$

Nucleotide extraction with PCA

Nucleotides were extracted from bioreactor samples with an adapted PCA cell lysis protocol (Theobald et al. 1997) that also allowed for immediate termination of all cellular biocatalytic reactions. 250 µL 35 % (v v^{-1}) PCA were prepared in a 2 mL reaction tube, weighed to maintain a tare weight and pre-cooled overnight to -20°C. With a disposable syringe, 1 mL cell suspension were rapidly withdrawn from the bioreactor, transferred into a pre-cooled PCA reaction tube and kept on ice for the entire procedure. After mixing the samples for 15 min at 4°C on a rotary incubator, all reaction tubes were weighed again to determine the actual volume of the biosuspension. Samples were then neutralized with 250 µL ice-cold 1 M K_2HPO_4 and 185 µL ice-cold 5 M KOH, mixed immediately and centrifuged for 15 min at 20,600 × g and 4°C. Clear and precipitate-free nucleotide extracts were stored at -70°C. Prior to HPLC analysis, the pH of each sample was adjusted to 7.0 ± 0.05 and the extracts were centrifuged at the same conditions.

Biomass Composition

Carbon and nitrogen contents (mmol C g_{CDW}^{-1} and mmol N g_{CDW}^{-1}) in exponentially growing as well as nitrogen-limited *E. coli* cultures were quantitatively determined on a Multi N/C analyzer 2100 S (Analytik Jena, DE) according to a recently published method (Buchholz et al. 2014). In deviation from the described protocol, cells from 2 mL biosuspension were harvested by centrifugation at 20600 × g and 4°C for 2 min. Pellets were washed twice in deionized water and centrifuged again at the same conditions.

Finally, the resulting cell pellets were resuspended in deionized water and transferred into a 5 mL graduated flasks to allow for volume corrections. Based on this, 1:5 and 1:10 dilutions were generated and measured on the N/C analyzer. Calibration of the instrument was realized with dilutions from a 2 g L^{-1} L-phenylalanine standard solution giving a ten-level calibration range of 30 – 1300 mg L^{-1} for total carbon (TC) and 4 – 60 mg L^{-1} for total nitrogen (TN).

3.2.8. Specific Metabolic Rates and Data Analysis

Determination of biomass-specific metabolic rates during constant phases of exponential growth was either performed by linear regression of logarithmic data curses for defined time intervals or calculated from yield coefficients. At conditions of only little growth, e.g. as they apply under nitrogen limitation, biomass-specific metabolic rates were calculated from concentrations (biomass, substrate, product) within a time interval of constant increase or decrease of a compound and the corresponding arithmetic mean value of the biomass. Experimental data sets were initially validated for normal distribution of the data populations with a Shapiro-Wilk normality test at the 0.05 level. Statistical significance of data set mean values was analyzed with a one-way ANOVA least significant difference test at the significance level $\alpha = 0.05$.

Reaction Rates and Yield Coefficients

Bacterial cells have all the attributes to be used as high efficient research strains in a bunch of scientific fields. Growing bacterial cultures for different purposes is often an easy to operate and expeditious task. Liquid suspensions, solid colonies on agar layers or adherent biofilms can be done conveniently since microbes are highly specialized for adapting to a variety of environmental conditions. Practically, bacteria are usually cultured in complex or defined liquid media as biosuspension at adequate conditions. During this process the bacterial cells undergo different specific growth stages (Figure 3.3). A small initial amount of cells is generally inoculated into fresh medium followed by the lag-phase (I) which is characterized by very little or zero growth. Changes in temperature, pH, medium composition, substrate availability, osmolality and so forth demand necessary cellular

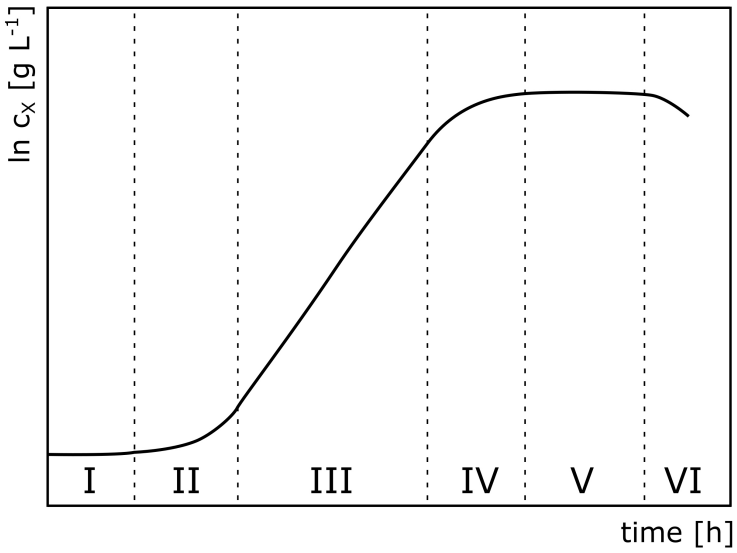

Figure 3.3. Schematic One-Substrate-Growth-Kinetics of a batch cultivation. Typically, microbial batch cultivations start with an initial lag phase (I) with almost zero growth in which cells adapt to their new environment. Followed by a progressively increasing growth rate during the acceleration phase (II) until a constant maximum growth rate is reached in the exponential phase (III). As soon as the substrate becomes limiting, growth rates drop steadily in the deceleration phase (IV). Finally, the microbial culture enters stationary phase (V) due to total substrate depletion followed by declining phase (VI), where cell lysis and cell death lead to a negative growth rate. Graph modified after (Monod 1949).

adjustments on the transcriptional and translational level. In this time, cells adapt to their new environment by modifying gene expression strategies, synthesizing structure elements and consequently adjusting cellular functions towards optimal nutrient uptake and reproduction. Once cellular growth is initiated, the specific growth rate of the culture rises during the acceleration phase (II) and arrives at its maximum value during the ensuing exponential growth phase (III). This maximum growth rate μ_{max} is maintained as long as the carbon and energy supplying substrate is available abundantly. Limitation of one essential nutrient leads to a steady deceleration of the growth rate over a transition period (IV) before subsequently the substrate is depleted and the microbial culture enters stationary phase (V). Now the highest possible biomass concentration is reached since cell lysis and cell division are in balance. Despite shorter nutrient fluctuations during cultivation time, substrate limitation also activates various global cellular stress response systems mainly in this growth phase to overcome environmental changes and adverse conditions. Longer periods of substrate deprivation finally lead to cell lysis, cell death and consequently to a reduction of the biomass concentration in the following declining phase (VI).

A batch-wise fermentation is a closed system, since volumetric alterations due to fluid supply or removal (pH corrections, anti-foam injections, sampling) can be assumed as negligible. Hence, time variant (t) process parameters can be obtained from the mass balance of the biomass:

$$\frac{dm_X}{dt} = \mu \cdot c_X \cdot V_R \tag{3.5}$$

with m_X as amount of biomass (g), c_X as concentration of biomass (g L^{-1}) and V_R as working volume of the bioreactor (L). Considering V_R = constant, as it applies for batch cultivations ($dV_R/dt = 0$), and $m_X = c_X \cdot V_R$, Equation 3.5 for the specific growth rate μ (h^{-1}) simplifies to:

$$\mu = \frac{1}{c_X} \cdot \frac{dc_X}{dt} \tag{3.6}$$

In nutrient excess cultivation environments microorganisms can grow constantly with a maximum specific growth rate μ_{max}. As soon as the availability of one substrate becomes limiting, maximum microbial growth is no longer possible and the specific growth rate μ declines over time (Figure 3.3). According to Monod, bacterial growth with one single limited substrate is defined as:

$$\mu = \mu_{max} \cdot \frac{c_S}{c_S + K_S} \tag{3.7}$$

Therein, μ_{max} is the maximum specific growth rate (h^{-1}), c_S is the limiting substrate concentration (g L^{-1}) and K_S (Monod substrate affinity constant) is the substrate concentration (g L^{-1}) at which $\mu = 1/2\ \mu_{max}$ is reached. For *E. coli* K-12 growing at 37 °C on glucose as the only source of carbon and energy with $\mu_{max} = 0.76$, the K_S constant is published to be 0.0072 g L^{-1} (Dykhuizen 1978, Owens and Legan 1987, Senn et al. 1994, Villadsen et al. 2011). Assuming $c_S >> K_S$ in batch cultivations, Equation 3.7 can be simplified for exponentially growing cultures as follows:

$$\mu = \mu_{max} \tag{3.8}$$

Considering the exponential growth phase, where $\mu = \mu_{max}$ = constant applies, $\ln(c_X/c_{X_0})$ or $\ln(OD_{600nm}/OD_{600nm_0})$ was plotted over time (t) and μ was obtained as slope of the linear regression line. Alternatively, μ was calculated between two defined time points (t_0 and t) with Equation 3.9, resulting from integration of Equation 3.6:

$$c_{X,t} = c_{X,0} \cdot e^{\mu \cdot t} \tag{3.9}$$

Likewise, with given experimental values for μ and maximum c_X, the time point of the nitrogen limitation shift ($t_{N\text{-}lim}$) was estimated with:

$$t_{N-lim} = ln\frac{c_X}{c_{X,0}} \cdot \frac{1}{\mu} \tag{3.10}$$

For the nitrogen-limited microbial cultivation phase μ was calculated by integration of Equation 3.6 for a time interval t_1 to t_2 of a constant increase in biomass concentration resulting in:

$$\mu_{lim} = \frac{c_{X,t2} - c_{X,t1}}{t_2 - t_1} \cdot \frac{1}{\overline{c_X}} \tag{3.11}$$

with $c_{X,t1}$ and $c_{X,t2}$ as biomass concentrations at the given time points t_1 and t_2 as well as the arithmetic mean of the biomass concentration $\overline{c_X}$.

In accordance to the specific growth rate μ other time variant process parameters like substrate (S) consumption and product (P) formation can be obtained from their mass balances in a similar way. First, the substrate mass balance is defined as:

$$\frac{dm_S}{dt} = -q_S \cdot c_X \cdot V_R \tag{3.12}$$

with m_S as amount of substrate (g) and -q_S as biomass specific substrate consumption rate (g_{Glc} g_{CDW}^{-1} h^{-1}). As described above, given the assumptions that V_R is considered to be constant in a closed batch system and $m_S = c_S \cdot V_R$ with c_S being the substrate concentration (g L^{-1}), Equation 3.12 simplifies to:

$$q_S = -\frac{1}{c_X} \cdot \frac{dc_S}{dt} \tag{3.13}$$

All these assumptions are equally valid for the product formation rate q_P ($g_P\ g_{CDW}^{-1}\ h^{-1}$):

$$\frac{dm_P}{dt} = q_P \cdot c_X \cdot V_R \tag{3.14}$$

Likewise, m_P is the amount of product (g) and assuming that $m_P = c_P \cdot V_R$ with c_P being the product concentration ($g\ L^{-1}$), Equation 3.14 simplifies to:

$$q_P = \frac{1}{c_X} \cdot \frac{dc_P}{dt} \tag{3.15}$$

In practice, the biomass-specific rates q_S (from here on indicated as positive value) and q_P for exponentially growing microbial cells were determined by plotting the substrate and product concentration courses (c_S, c_P), respectively, over the corresponding biomass concentrations and calculating the rates as slope of the regression lines. Biomass-specific substrate consumption and product formation rates in the nitrogen-limited cultivation phase were calculated from compound concentration courses at given time points ($c_{S,t}$ and $c_{P,t}$) and the arithmetic mean value of the biomass ($\overline{c_X}$) as follows:

$$q_{S,lim} = \frac{c_{S,t1} - c_{S,t2}}{t_2 - t_1} \cdot \frac{1}{\overline{c_X}} \tag{3.16}$$

$$q_{P,lim} = \frac{c_{P,t2} - c_{P,t1}}{t_2 - t_1} \cdot \frac{1}{\overline{c_X}} \tag{3.17}$$

Specific metabolic rates, as well for exponential as for substrate-limited growth, can be related to each other and thereby reveal characteristic yield coefficients ($Y_{i/j}$) for a particular microbial strain grown at defined conditions. These yield coefficients can be calculated for a range of different specific metabolic rates:

$$Y_{X/S} = \frac{\mu}{q_S} \tag{3.18}$$

$$Y_{P/X} = \frac{q_P}{\mu} \tag{3.19}$$

$$Y_{P/S} = \frac{q_P}{q_S} \tag{3.20}$$

Respiration Rates

Throughout a microbial cultivation process, O_2 is absorbed by the biosuspension in order to maintain aerobic cellular anabolic pathways. At the same time CO_2 is produced by the cells in decarboxylation reactions. For this reason, incoming volumetric gas flow rates ($\dot{V}_G^{in}$) for O_2 and CO_2 are not identical with the outgoing rates ($\dot{V}_G^{out}$). Including nitrogen (N_2) as inert gas gives the possibility to determine all volumetric gas flow rates (L h^{-1}) from substance ratios in the exhaust gas with the inert gas balance:

$$\dot{V}_G^{in} \cdot y_{N_2}^{in} = \dot{V}_G^{out} \cdot y_{N_2}^{out} \tag{3.21}$$

On this basis, the incoming (y^{in}) and outgoing (y^{out}) molar gas fraction (y) only consider oxygen (O_2), carbon dioxide (CO_2) and nitrogen (N_2) to be major constituents of the gas phase:

$$y_{N_2}^{in} = 1 - y_{O_2}^{in} - y_{CO_2}^{in} \tag{3.22}$$

$$y_{N_2}^{out} = 1 - y_{O_2}^{out} - y_{CO_2}^{out} \tag{3.23}$$

Inserting Equations 3.22 and 3.23 into Equation 3.21, gives the outgoing volumetric gas flow rate:

$$\dot{V}_G^{out} = \dot{V}_G^{in} \cdot \left(\frac{1 - y_{O_2}^{in} - y_{CO_2}^{in}}{1 - y_{O_2}^{out} - y_{CO_2}^{out}} \right) \tag{3.24}$$

Therefore, Equation 3.27 applies for the microbial oxygen uptake per reactor volume and time ($Q_{O_2} = OUR$ in mol L^{-1} h^{-1}) having regard to the ideal gas law (Equation 3.25) together with the mass balance of oxygen in the gas phase (Equation 3.26):

$$p \cdot \dot{V}_G^{in} = \dot{n} \cdot R \cdot T \tag{3.25}$$

$$Q_{O_2} = OUR = \frac{\Delta \dot{n}_{O_2}}{V_R} = \frac{\dot{n}_{O_2}^{in} - \dot{n}_{O_2}^{out}}{V_R} \tag{3.26}$$

$$Q_{O_2} = OUR = \frac{p \cdot \dot{V}_G^{in}}{V_R \cdot R \cdot T} \cdot \left(y_{O_2}^{in} - \frac{1 - y_{O_2}^{in} - y_{CO_2}^{in}}{1 - y_{O_2}^{out} - y_{CO_2}^{out}} \cdot y_{O_2}^{out} \right) \tag{3.27}$$

with $\dot{V}_G$ as volumetric gas flow rate (L h^{-1}), p as pressure (Pa), R as universal gas constant (J mol^{-1} K^{-1}), T as temperature (K), V_R as working reactor Volume (L) and $\dot{n}$ as molar amount of a compound (mol).

The carbon dioxide emission rate (CER) (mol L^{-1} h^{-1}) was determined in accordance to the OUR:

$$Q_{CO_2} = CER = \frac{p \cdot \dot{V}_G^{in}}{V_R \cdot R \cdot T} \cdot \left(y_{CO_2}^{out} \cdot \frac{1 - y_{O_2}^{in} - y_{CO_2}^{in}}{1 - y_{O_2}^{out} - y_{CO_2}^{out}} - y_{CO_2}^{in} \right) \tag{3.28}$$

The biomass-specific oxygen uptake rate (q_{O_2}) and the biomass-specific carbon dioxide emission rate (q_{CO_2}) (mol g_{CDW}^{-1} h^{-1}) are defined as follows:

$$-q_{O_2} = \frac{OUR}{c_X} \tag{3.29}$$

$$q_{CO_2} = \frac{CER}{c_X} \tag{3.30}$$

Respiratory rates like OUR and CER of nitrogen-limited microbial cultures were plotted over the process time and q_{O_2} as well as q_{CO_2} were determined from the resulting regression lines:

$$-q_{O_2,lim} = \frac{1}{\overline{c_X} \cdot (t_2 - t_1)} \cdot \int_{t_1}^{t_2} OUR \; dt \tag{3.31}$$

$$q_{CO_2,lim} = \frac{1}{\overline{c_X} \cdot (t_2 - t_1)} \cdot \int_{t_1}^{t_2} CER \; dt \tag{3.32}$$

From the the ratio of carbon dioxide emission rate to oxygen uptake rate, a dimensionless respiratory quotient (RQ) can be calculated as follows:

$$\mathrm{RQ} = \frac{CER}{OUR} \tag{3.33}$$

Maintenance

Microorganisms rely on substrates to perform all necessary metabolic reactions during cell and culture growth. Nevertheless, a growth-inhibited microbial culture still shows minimal substrate consumption in order to keep basic cellular functions active and to cover the minimal cellular energy demand for m_S. Therefore, maintenance demands (g_{Glc} g_{CDW}^{-1} h^{-1}) were calculated using the Pirt's equation (Pirt 1965):

$$q_S = \frac{\mu}{Y_{X/S}^{true}} + m_S \tag{3.34}$$

with $Y_{X/S}^{true}$ being the true yield coefficient of biomass from glucose (g_{CDW} g_{Glc}^{-1}).

4. Results

4.1. Genetically Modified Strains of *E. coli*

Based on the well-known laboratory model strain *Escherichia coli* K-12 MG1655, a set of nine recombinant mutants was generated to investigate the impact of aberrant stringent responses on glucose consumption phenotypes. Following different cloning approaches, ppGpp synthesis and hydrolysis abilities of the cells were modified in order to generate a compilation of various strains with altered ppGpp levels as response upon nutritional stress. To relocate the intracellular carbon distributions, the activity of an actor of the central carbon metabolism was also downregulated to meet an expected increase in glucose consumption rates. All applied genetic deletions, insertions and nucleotide point mutations addressed both stringent response related genes, *relA* and *spoT*, as well as a gene encoding a major protein of the pyruvate (*aceE*) metabolic pathway. Regarding genomic nucleotide substitution mutations, codon usage was considered as crucial factor for expression of functional and active enzymes. For this reason, average relative frequency rates of codon utilization in the *E. coli* host were implied into gene sequence structuring. Such frequency data was derived from established literature (Sharp et al. 1988, Maloy et al. 1996). An overview list of all mutant strains together with a short description of applied genetic adjustments is shown in Table 4.1. Identification of amino acid positions in proteins, which were targets of genetic manipulations, was performed on the basis of predicted protein sequences from the Universal Protein Resource Knowledgebase (UniProtKB) (UniProt Consortium 2015). Corresponding accession numbers of all involved proteins are listed in Table 3.2. The initial methionine at the N-terminus of each peptide sequence was considered as starting point of counting. The following sections include detailed information on chromosomal gene editing and metabolic strain design.

4.1.1. Stringent Response Mutants

Table 4.1. Stringent response mutants derived from the *E. coli* K-12 MG1655 host.

		RelA		SpoT		
Name	Modification	Syn	Hyd	Syn	Hyd	Comment
E. coli K-12 MG1655:						
1. WT	F-, λ-, *ilvG*-, *rfb*-50, *rph*-1	✓	✓	✓	✓	DSM-18039 phenotype
2. Δ*relA*	Deletion of entire *relA* CDS region.	✗	✗	✓	✓	
3. ZERO	ppGpp^0 mutant, deleted *relA* and *spoT* genes.	✗	✗	✗	✗	no growth in standard Minimal Medium.
4. *relA*_RK	Amino acid substitutions E306R & D308K in RelA.	✓	✓	✓	✓	
5. *spoT*_ED	Amino acid substitutions R290E & K292D in SpoT.	✓	✓	✓	✓	^{m}Q287L in RelA synthase domain.
6. SR	*E. coli spoT*_ED with deleted *relA* gene.	✗	✗	✓	✓	
7. HS #13	*spoT* gene encoding ppGpp synthetase sequence from *relA*.	✓	✓	✓	✓	
8. HS #77	*spoT* gene encoding ppGpp synthetase sequence from *relA*.	✓	✓	✓	✓	^{m}L303Q in RelA synthase domain.
9. ACE	Amino acid substitution G267C in AceE.	✓	✓	✓	✓	
10. HGT	*E. coli* SR with amino acid substitution G267C in AceE.	✗	✗	✓	✓	

^{m}: spontaneous amino acid substitution mutation occurring during genomic modification cloning process.

Activities of the two stringent response enzymes RelA and SpoT were engineered with various approaches like knock-out mutations of entire coding DNA sequences, structure variations of catalytic enzyme domains or site-specific amino acid substitution mutations. To test for a minimum metabolic response of cells entering nutritional starvation conditions, genes encoding for ppGpp synthesizing proteins were inactivated. In-frame deletion of the (p)ppGpp-Synthase I (*relA*) CDS resulted in a single knock-out mutant. *E. coli* Δ*relA* was constructed in a first round of cloning, hence it could be used as a basic host strain with impaired ppGpp formation ability for further cloning actions. Since *spoT* is described to have a weak ppGpp-Synthase activity, its CDS was removed easily in a second in-frame deletion to generate the double knock-out mutant *E. coli* ZERO. The characteristic 'relaxed' growth phenotype of this ppGpp^0 strain was observed in cultures transferred from growth in complex nutrient excess broth into amino-acid starvation in synthetic minimal medium (Figure A.3). Although this mutant was available, kinetic parameters were not determined in bioreactor cultivations for this strain due to the lack of growth in the used standard synthetic medium.

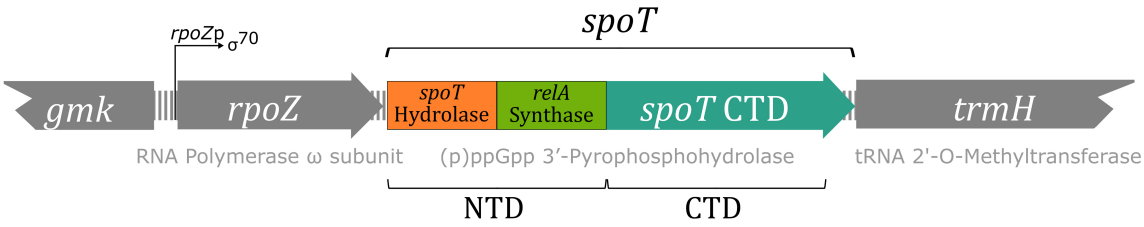

Figure 4.1. Genetic structure of the *E. coli* K-12 MG1655 HS mutant. Construction of a new synthetic *spoT* gene with improved ppGpp synthesis properties. The native genomic sequence of the weak Synthase within the N-terminal domain (NTD) of *spoT* was replaced by a DNA fragment encoding for the strong ppGpp Synthase from RelA (green). Hydrolase activity (orange) of *spoT* and its C-terminal domain (CTD) remain unmodified at the same position within the natural constitution of the *rpoZ-spoT*-trmH-recG* regulon under transcriptional control of the P1 promoter (σ^{70}).

A completely new-to-nature SpoT protein was created from different stringent response protein elements. The coding DNA sequence of the N-terminal *relA* Synthetase domain was amplified and assembled into a new *spoT* gene with its native flanking N-terminal Hydrolase and C-terminal regions. This new structural hybrid SpoT enzyme is expressed naturally in the *rpoZ-spoT*-trmH-recG* regulon background under transcriptional control of the constitutive σ^{70}-dependent P1 promoter *rpoZ*p (Figure 4.1). Hence, the hybrid SpoT protein version is only translated under intracellular conditions of very low ppGpp concentrations and available σ^{70}-factors, as it is the case during exponential growth.

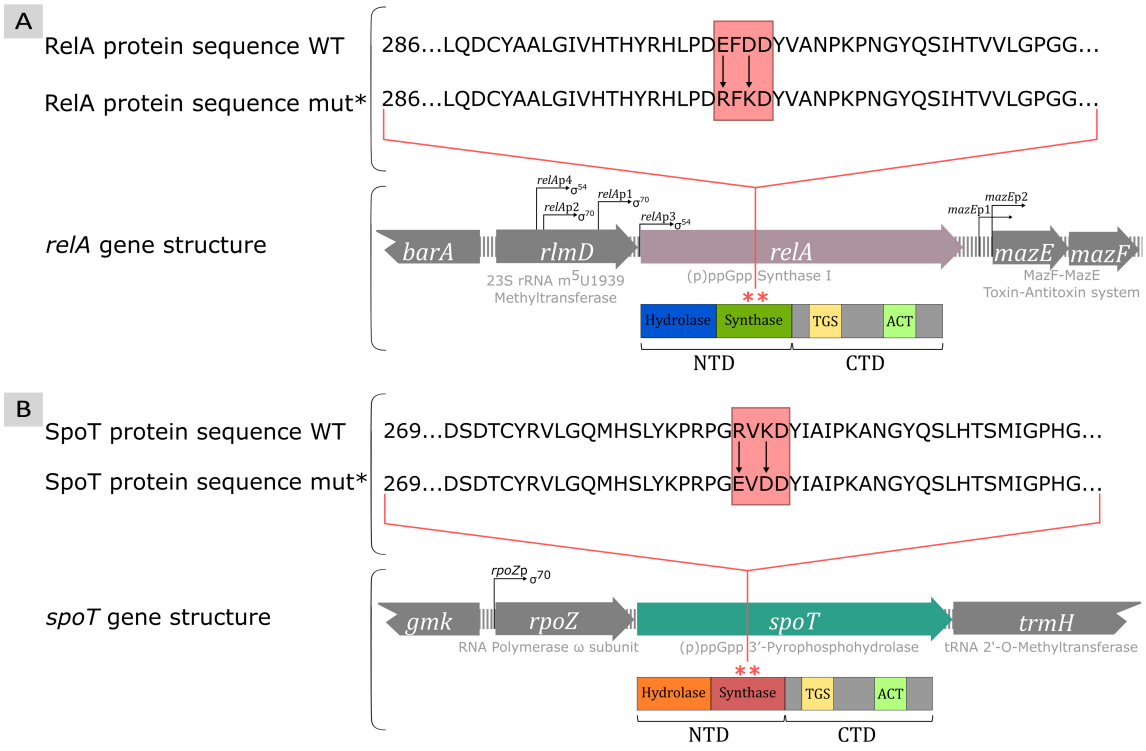

Figure 4.2. Genetic structure of two *E. coli* mutants with modified domains in RSH. A: Amino acid substitutions E306R & D308K within the RelA Synthase ExDD motif result in the *E. coli* K-12 MG1655 *relA*_RK mutant. Transcriptional control of *relA** gene expression is further on realized by the two σ^{70}-dependent promoters P1 and P2 as well as P3 and P4 (σ^{54}). B: The *E. coli* K-12 MG1655 *spoT*_ED mutant was generated by amino acid exchanges at positions R290E and K292D. Gene expression of *spoT** remains in its native genetic context.

Apparently, the ExDD (Glu-x-Asp-Asp) motif in RelA shows different substrate binding affinities compared to the reversely charged RxKD (Arg-x-Lys-Asp) motif in SpoT (Sajish et al. 2007). Thus, corresponding amino acids E306R and D308K were substituted in RelA to generate the mutant *E. coli relA*_RK strain (Figure 4.2 A) which was expected to react with reduced ppGpp levels upon stress. Vice versa, amino acids R290E and K292D were exchanged in the mutant *E. coli spoT*_ED (Figure 4.2 B) to receive a strain with two active ppGpp Synthases. This *spoT*_ED substitution mutation was combined with an *E. coli* Δ*relA* host to result in *E. coli* SR. In this strain, ppGpp formation is still performed by the engineered SpoT version under exponential growth conditions. At transition into nutritional stress, a typical transcriptional upregulation of gene expression is absent due to the native σ^{70}-controlled genetic environment of *spoT* and ppGpp levels are expected to remain at a constant level.

4.1.2. Pyruvate Producing Mutants

During tests of different *E. coli* K-12 MG1655 strains, one microbial culture showed a slow growth phenotype while consuming higher amounts of glucose than the wild-type. Presumably, this characteristic growth deficit was a result of a spontaneously occuring mutation in the *E. coli* chromosome. Consequently, whole genome sequencing of the mutant strain compared to the *Escherichia coli* K-12 substr. MG1655 reference sequence (NCBI-GenBank accession number U00096.3) revealed a single point mutation within the *aceE* gene leading to the specific amino acid substitution G267C in the AceE protein (Pyruvate Dehydrogenase, Decarboxylase component E1).

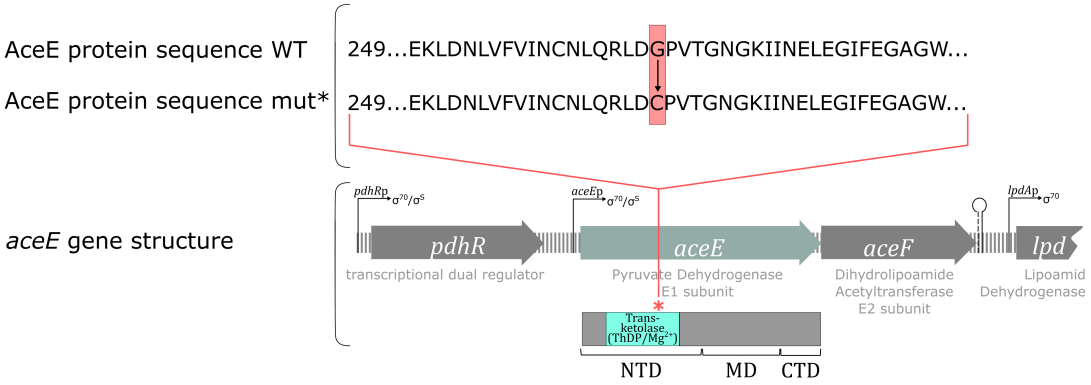

Figure 4.3. Genetic structure of the *E. coli* K-12 MG1655 ACE mutant. Amino acid Glycine at position 267 of the AceE (Pyruvate Dehydrogenase, E1 subunit) protein was exchanged for Cysteine. This substitution mutation was located within the N-terminal catalytic transketolase region (NTD), which is also known for substrate binding of Thiamin diphosphate (ThDP) and Magnesium (Mg^{2+}). Further structure elements of AceE, the middle domain (MD) and the C-terminal domain (CTD), are involved in subunit-subunit interactions.

According to Arjunan et al. 2002, this mutation affects a catalytic Transketolase inside the N-terminal protein domain. The amino acid exchange is located in close proximity to highly conserved polypeptide residues involved in active site interactions and cofactor binding of Thiamin diphosphate (ThDP) and Mg^{2+}. A general structure description of the *E. coli* ACE mutant is displayed in Figure 4.3. Based on the assumptions that first, a substitution mutation in AceE might elevate glucose uptake rates and second, the before mentioned *E. coli* SR mutant reacts with a more balanced stringent response upon nutritional depletion, a high glucose throughput (HGT) and stress stable mutant was constructed. On that level, *E. coli* HGT was developed from a Δ*relA* background host combined with a single point mutation in *aceE* and the corresponding mutations leading

to R290E and K292D in the SpoT protein. The *E. coli* HGT chassis strain has proved to facilitate a conceivably strong intracellular carbon drain towards the synthesis of pyruvate and is already part of a published patent application (Michalowski et al. 2016).

4.2. Using Glycogen Contents for ppGpp Estimation in *E. coli* Mutants

Iodine vapor staining was used as rapid screening method to visualize glycogen contents in a variety of engineered *E. coli* MG1655 mutants. The intensity of colony coloring on solid rich medium agar plates (KM agar) gave a good hint about glycogen accumulation abilities of different mutants which are described to correlate directly with intracellular ppGpp concentrations (Montero et al. 2014). Thus, the iodine vapor staining procedure allowed for estimation of ppGpp amounts in the microbial culture and bacterial colonies with irregular ppGpp contents were distinguished easily.

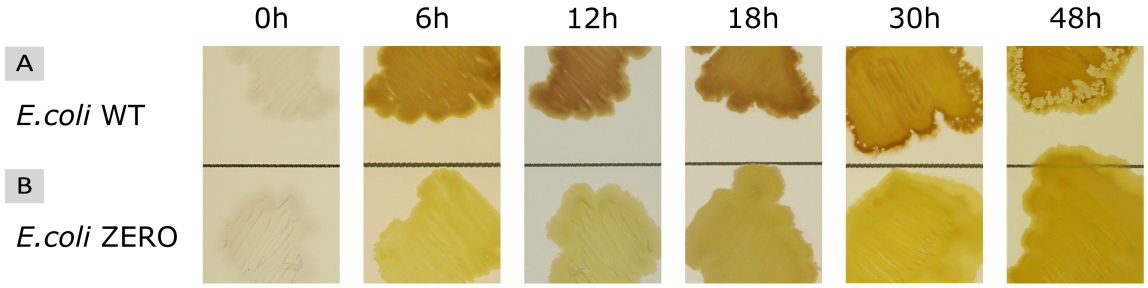

Figure 4.4. Glycogen contents in *E. coli* for ascending growth incubation periods. Cultures of *E. coli* WT and the ppGpp^0 mutant *E. coli* ZERO were streaked on KM agar plates and grown for time periods between 6 h and 48 h at 37 °C. For colony coloring, agar plates were treated with iodine vapors for 10 sec.

The best incubation time for colony growth on solid KM agar plates was determined in a time series between 6 h and 48 h of incubation at 37 °C (Figure 4.4). Glycogen contents for the given time points were analyzed in *E. coli* WT to have a standard reference and compared to *E. coli* ZERO as negative control. The ppGpp deprived, and consequently also glycogen-free, mutant appeared yellow after iodine vapor treatment. Whereas colonies of the *E. coli* WT changed towards a brownish staining.

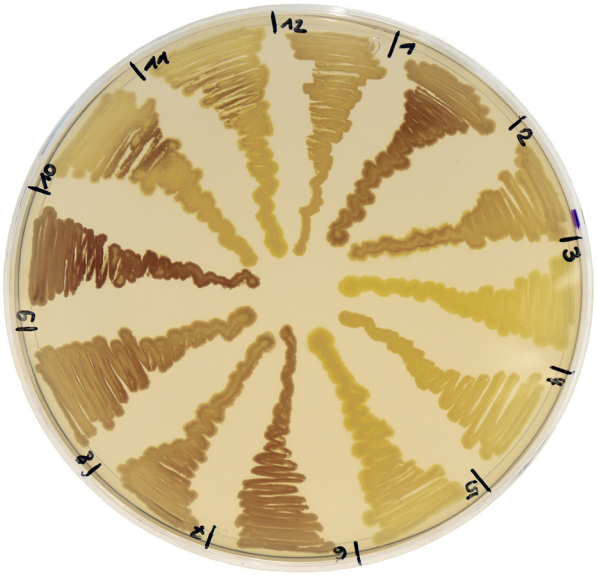

01.	*E. coli* K-12 MG1655	WT
02.	*E. coli* K-12 BW25112	*glgC::kan*
03.	*E. coli* K-12 MG1655	ZERO
04.	*E. coli* K-12 MG1655	HGT
05.	*E. coli* K-12 MG1655	Δ*relA*
06.	*E. coli* K-12 MG1655	*relA*_RK
07.	n.a.	
08.	*E. coli* K-12 MG1655	*spoT*_ED
09.	*E. coli* K-12 MG1655	HS #77
10.	*E. coli* K-12 MG1655	HS #13
11.	*E. coli* K-12 MG1655	SR
12.	*E. coli* K-12 MG1655	ACE

Figure 4.5. Iodine vapor staining of glycogen contents in different *E. coli* mutants. Modified strains of *E. coli* MG1655 were transferred from 2×YT agar onto solid KM agar plates and grown overnight at 37 °C. After exposing the cells to iodine vapors for 10 sec, the colonies obtained a brownish staining that correlated with their intracellular glycogen concentration. *E. coli* K-12 BW25112 *glgC::kan* serves as control strain with reduced glycogen formation due to a missing glucose-1-phosphate Adenylyltransferase.

An overview of glycogen accumulation in all stringent response engineered *E. coli* mutants of this study is shown in Figure 4.5. In direct comparison, different classes of color gradations were observed. As expected, the *E. coli* ZERO mutant (#3) reacted with a yellow staining as result of lacking ppGpp synthesis and therefore inhibition of glycogen formation. Both mutants with deleted (p)ppGpp Synthase I, *E. coli* HGT (#3) and *E. coli* Δ*relA* (#5) indicated low ppGpp levels in the cells by a light brown coloring. Slightly higher stringent alarmone contents were suspected in the mutants *E. coli* HS#13 (#10), *E. coli* SR (#11) and *E. coli* ACE (#12). Interestingly, in *E. coli* HS#77 (#9) the intensity of colony staining was higher than in the *E. coli* WT (#1), such that this mutant seemed to have increased ppGpp synthesis properties. *E. coli* BW25112 *glgC::kan* (#2) was used as control strain with decreased glycogen content, since *glgC* catalyzes the important second step in glycogen biosynthesis from α-D-glucopyranose 1-phosphate and ATP to Adenosine diphosphate (ADP)-α-D-glucose.

4.3. SHX-induced Stringent Response

In advance of bioreactor fermentations, several *E. coli* mutants were cultivated in a shaking flask setup to gain first insights on characteristic growth behaviors and metabolic turnover levels at an exponential and a stringent response related scenarios. For the latter, the amino acid analogue SHX was used to induce an artificial stringent response in unlimited growing cells at nutrient-excess conditions. SHX addition caused an immediate and significant reduction in growth rate of all bacterial cultures as it is illustrated in Figure 4.6 and Figure 4.7. General cultivation progression started with an exponential growth phase in Minimal Medium with all nutrients in abundance. Controlled transition into SHX growth arrest was provoked after an OD_{600nm} of 2–3 was reached. Apparently, this second phase continued for about 1.5 h – 2.5 h, depending on the *E. coli* mutant strain, before the cultures recovered a normal growth and finally proceeded into stationary state at glucose depletion. In essence, this experimental configuration allowed for preliminary determination of biomass-specific glucose consumption rates in exponentially and almost non-growing cultures of all tested mutants, since a high glucose turn-over is a preferable characteristic of the new *E. coli* production platform.

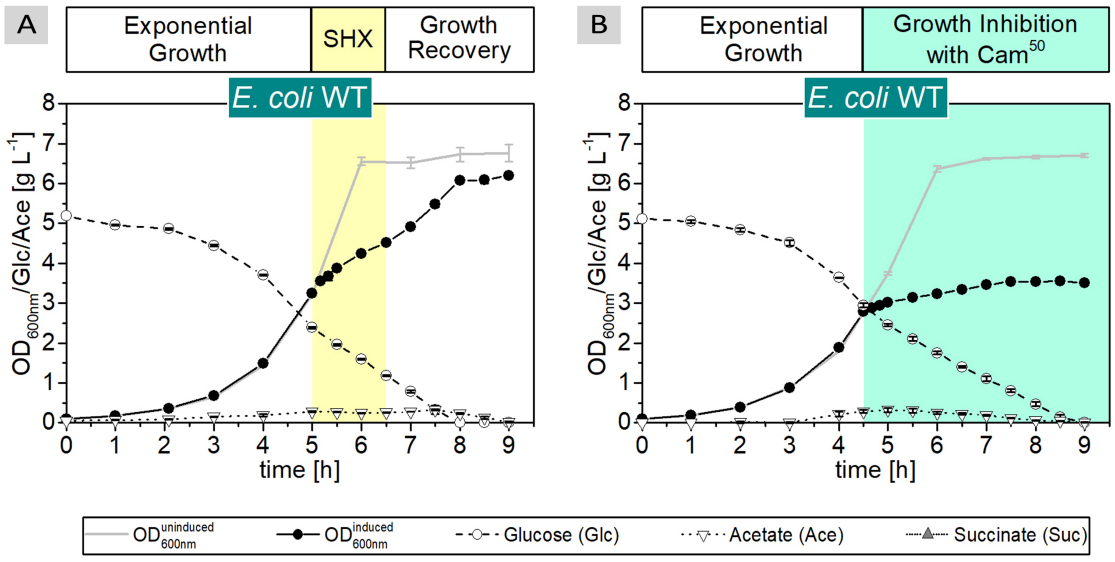

Figure 4.6. *E. coli* WT control with SHX- and Cam^{50}-induced growth arrest. Shaking flask cultivations of the *E. coli* WT and the *E. coli* SUC strains as growth references. The uninduced exponentially growing control groups are displayed as light gray lines in the chart. Growth arrest was induced with 1 mM SHX (yellow) or with Cam (green) at a concentration of 50 µg mL^{-1}. Data represent mean values of biological triplicates with standard deviation.

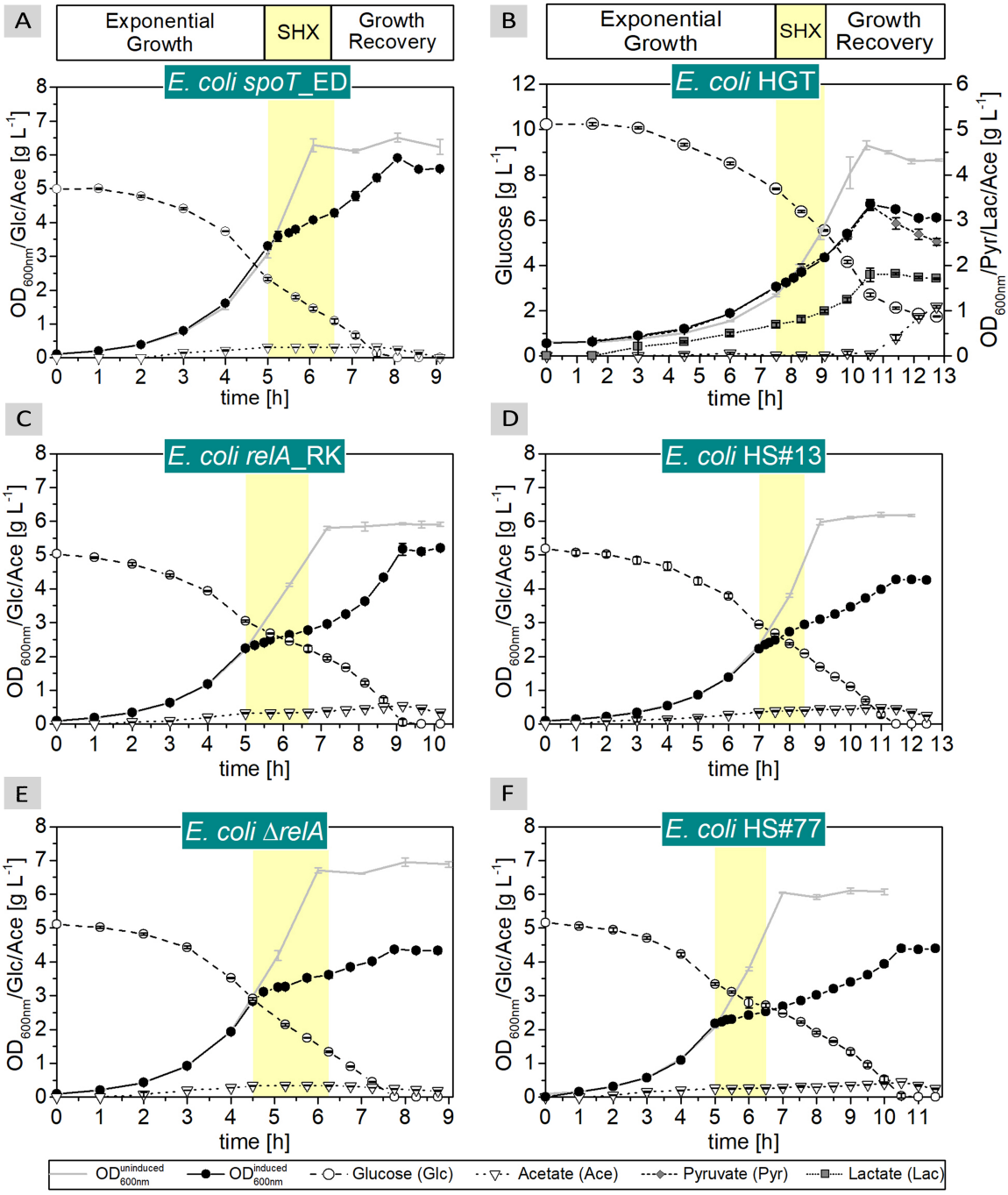

Figure 4.7. *E. coli* mutants in Minimal Medium with SHX-induced growth arrest. Shaking flask cultivations of different *E. coli* stringent response mutants grown in nutrient abundance. The uninduced exponentially growing control groups are displayed as light gray lines in the chart. Growth arrest (yellow) was induced at an OD_{600nm} of 2–3 by addition of SHX to the culture medium in a final concentration of 1 mM (except for *E. coli* HGT, where 4 mM were necessary). Subsequently, the microbial cultures were able to recover exponential growth until they entered stationary phase. Data represent mean values of biological triplicates with standard deviation.

Induction of growth arrest with SHX led to a drastic lowering in growth rate of about 80% for almost all engineered *E. coli* strains within the first 15 minutes. Similarly, biomass-specific glucose uptake rates decreased to one third of the rate measured during exponential growth (Table 4.2). In direct comparison, the mutants *E. coli* HGT, *E. coli* Δ*relA*, *E. coli* HS #13 and *E. coli* HS #77 reacted with a significant increase in glucose consumption upon SHX stress. Interestingly, acetate production in the tested strains entirely stalled upon SHX induction of the culture, but could be resumed afterwards, when the cells recovered their growth. Nevertheless, growth and metabolic turn-over parameters for *E. coli* HGT differ significantly from the residual engineered *E. coli* strains. Even at induction with a four-times elevated SHX concentration, growth rate in *E. coli* HGT was only reduced by about 15% from μ=0.26 h^{-1} to 0.22 h^{-1}. Thus, the limited q_S rate almost resembled the value of 1.74 g_{Glc} g_{CDW} h^{-1} under exponentially growing conditions.

Table 4.2. Growth parameters of different *E. coli* strains in SF cultivations. Comparison of growth rates (μ) and biomass-specific glucose uptake rates (q_S) under exponentially growing and growth inhibited conditions.

	Exponential Phase		SHX/Cam^{50} Limited Phase	
E. coli K-12 MG1655	q_S [g_{Glc} g_{CDW}^{-1} h^{-1}]	μ_{max} [h^{-1}]	q_S [g_{Glc} g_{CDW}^{-1} h^{-1}]	μ_{lim} [h^{-1}]
WT SHX	2.05 ± 0.03	0.73 ± 0.00	0.59 ± 0.03	0.16 ± 0.01
WT Cam^{50}	2.03 ± 0.01	0.75 ± 0.00	0.69 ± 0.01	0.07 ± 0.01
HGT	1.74 ± 0.01	0.26 ± 0.00	1.73 ± 0.05	0.22 ± 0.01
Δ*relA*	1.79 ± 0.04	0.75 ± 0.00	0.68 ± 0.01	0.10 ± 0.01
*relA*_RK	1.91 ± 0.03	0.63 ± 0.00	0.59 ± 0.01	0.13 ± 0.01
*spoT*_ED	1.75 ± 0.02	0.70 ± 0.00	0.58 ± 0.01	0.18 ± 0.01
HS #13	1.40 ± 0.02	0.45 ± 0.00	0.68 ± 0.02	0.13 ± 0.00
HS #77	1.56 ± 0.07	0.62 ± 0.00	0.49 ± 0.04	0.10 ± 0.01

A graphical comparison of glucose uptake rates in engineered *E. coli* mutants under unlimited and SHX-arrested growth conditions is shown in Figure 4.8. While SHX treatment was reversible and directly led to a growth arrest of the culture, Cam^{50} was used as control experiment to perform a total blockade of ribosomal functions. In a final concentration of 50 μg mL^{-1}, chloramphenicol acts as translational inhibitor by blocking the Peptidyl Transferase and preventing protein chain elongation. This data served as reference to evaluate biomass-specific rates from translational arrested cultures (Figure 4.6).

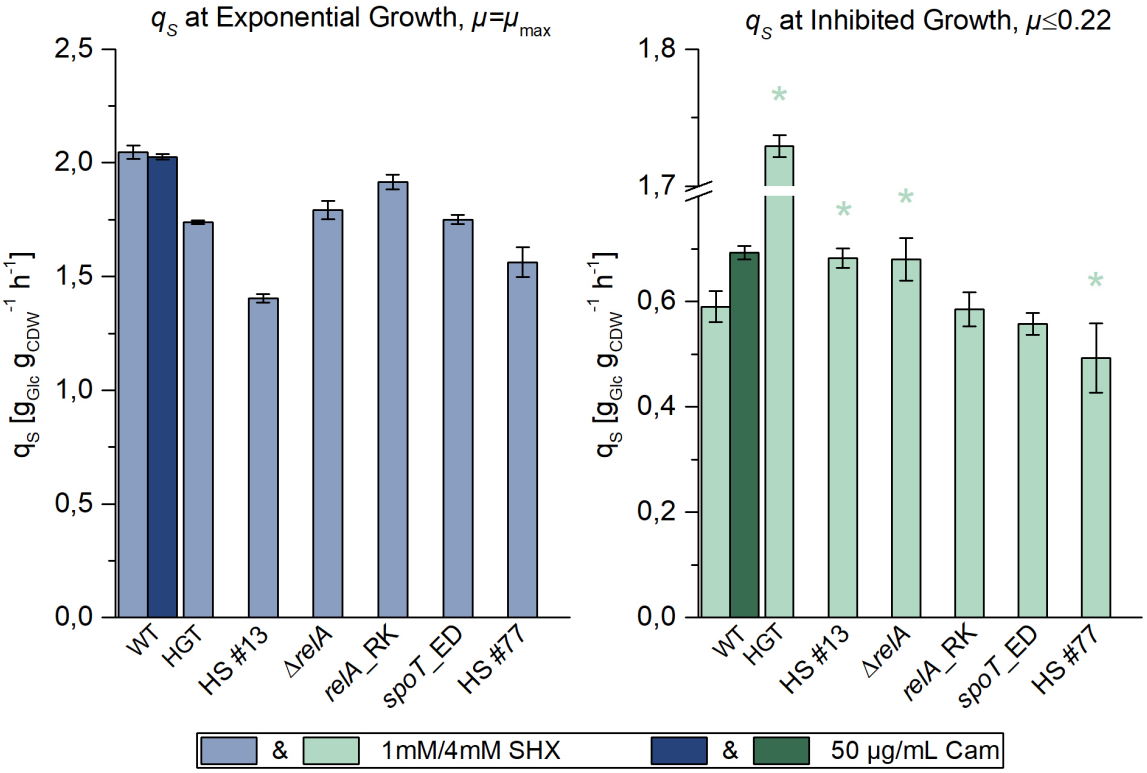

Figure 4.8. Biomass-specific glucose uptake rates for engineered *E. coli* mutants. Comparison of biomass-specific glucose consumption rates q_S in cultures growing exponentially with $\mu=\mu^{max}$ (A) and in cultures under SHX-induced growth arrest with $\mu\leq0.22$ (B). Rates of Cam^{50} growth arrested strains are illustrated as reference. *P=0.05 for significance analysis.

4.4. Bioreactor Cultivations of *E. coli* Stringent Response Mutants

Selective strains from the *E. coli* K-12 MG1655 mutant collection with varying characteristics in their stringent response behavior upon nutritional stress have been subject to a series of screening experiments. For each *E. coli* mutant strain, individual representative growth parameters, substrate and product concentrations as well as intracellular nucleotide levels were investigated in a parallel triplex bioreactor system at optimal and defined growth conditions. In subsequent data analysis, different physiological parameters, stringent response alarmone courses, energy charges and biomass-specific metabolic rates were determined from those experimental data sets.

4.4.1. Two-Stage Batch Fermentations

As process strategy, a batch cultivation scenario that realizes two extremely contrasting applied growth phases in a single fermentation experiment was chosen. Therefore, a synthetic Minimal Medium was composed of all essential nutrients for microbial growth in abundance, except for ammonium, which was supplied as only nitrogen source at a predefined concentration of 40 mM. The two-stage batch cultivations (Figure 4.9) started with a typical exponential maximum growth rate $\mu_{\max}$ and proceeded into a growth-limited phase with $\mu_{\lim}$ immediately upon nitrogen supply exhaustion. This sudden lack of available nitrogen components in the fermentation medium also caused an immediate induction of the stringent response machinery in the cells (Brown et al. 2014b, Simen et al. 2017). In this way, a culture with identical cultivation history was observed to gain insights on physiological parameters and metabolic turn-over rates at exponential growth, transition into reduced nutrient availability and at last starvation conditions. To meet the exact time point of entry into stringent response and starvation, monitoring of the exhaust gases indicated the moment of nitrogen limitation by a reversal progression of O_2 and CO_2 and thus the start of sampling the second phase. Resulting growth parameters for all *E. coli* mutants are listed in Table 4.3.

Table 4.3. Fermentation parameters of *E. coli* two-stage batch cultivations. Parameter list for different *E. coli* mutants cultivated in the triplex bioreactor system. $\mu_{\max}$: exponential growth rate, $\mu_{\lim}$: growth rate under nitrogen limitation, ${c_{Glc}}^{start}$: glucose concentration at fermentation start, $Y_{X/N}$: biomass from nitrogen yield, CDW/OD_{600nm}: biomass to optical density correlation factor. Contents and style modified after Michalowski et al. 2017.

E. coli MG1655	$\mu_{\max}$ [h^{-1}]	$\mu_{\lim}$ [h^{-1}]	${c_{Glc}}^{start}$ [g L^{-1}]	$Y_{X/N}$ [g_{CDW} $g_{NH_4^+}{}^{-1}$]	CDW/ OD_{600nm}
WT	0.72 ± 0.01	0.04 ± 0.01	18.1 ± 0.1	4.94 ± 0.30	0.32
HGT	0.29 ± 0.01	0.00 ± 0.00	26.4 ± 0.4	4.84 ± 0.14	0.36
Δ*relA*	0.77 ± 0.01	0.02 ± 0.00	20.0 ± 0.1	4.98 ± 0.06	0.34
ACE	0.20 ± 0.01	0.01 ± 0.00	30.3 ± 0.2	4.82 ± 0.08	0.38
SR	0.71 ± 0.01	0.01 ± 0.00	26.6 ± 0.2	4.90 ± 0.06	0.35
HS #13	0.47 ± 0.01	0.04 ± 0.01	20.0 ± 0.1	4.58 ± 0.06	0.33
HS #77	0.57 ± 0.01	0.05 ± 0.00	17.8 ± 0.1	4.82 ± 0.05	0.34
*spoT*_ED	0.71 ± 0.01	0.05 ± 0.00	17.8 ± 0.1	4.96 ± 0.05	0.34

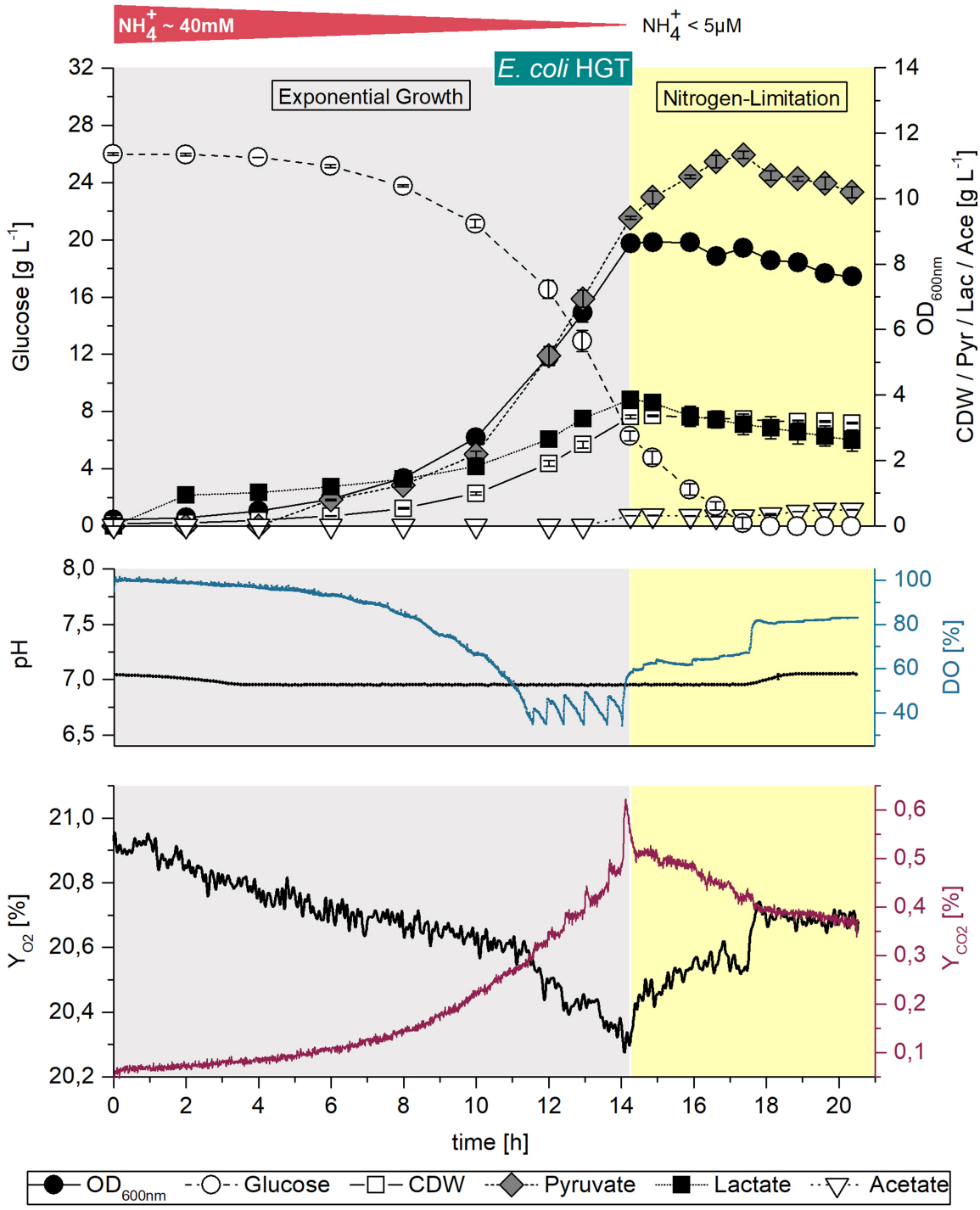

Figure 4.9. Nitrogen-limited two-stage bioreactor cultivation of *E. coli* HGT. A typical two-stage batch cultivation profile in nitrogen-limited Minimal Medium is illustrated exemplary in the upper graph for *E. coli* HGT. The fermentation starts with all nutrients in excess and exponential growth (gray phase) at maximum growth rate until ammonium (40 mM) becomes exhausted and the culture enters the nitrogen-limited cultivation phase (yellow) with almost no growth. Online measurements of pH and DO ratio as well as monitoring of O_2 and CO_2 fractions in the exhaust gas along the process are displayed in the middle and lower graph sections. This graph was modified after Michalowski et al. 2017.

Glucose starting concentrations varied for all different *E. coli* mutants and are listed in the same. Maximum growth rates and such at nitrogen limitation were highly divergent between all compared *E. coli* strains. Especially both mutants carrying the G267C substitution in ACE, *E. coli* ACE and *E. coli* HGT, distinguished themselves from the other strains by very low growth rates of 0.3 h^{-1} and lower, which are however in agreement with published data on PDHC-disruptive strains (Tran et al. 2014). Interestingly, at the terminal stage of exponential growth, when the microbial culture entered nitrogen-limited conditions, all tested strains reached a similar maximum cell dry weight (Table A.2). According to this, the biomass from nitrogen conversion yield $Y_{X/N}$ was in a comparable range of 4.5 – 5.0 $g_{CDW}\ g_{NH_4^+}^{-1}$ in all strains and agreed well with nitrogen yields reported by other groups (Folsom and Carlson 2015). All further corresponding two-stage batch cultivation process graphs are summarized in Figure A.5. It needs to be mentioned, that all microbial fermentations were performed in almost chloride-free minimal cultivation medium in order to control corrosion of the technical equipment. Notably, removal of chloride ions from the cultivation medium had no significant effect on the growth rate of *E. coli* cultures (Figure A.2).

4.4.2. Derived Biomass-Specific Rates

Substrate Consumption and Product Formation

Microbial cultivation studies on determination of growth dynamics and kinetic parameters were progressed under conditions of high glucose abundance as single carbon source. Although initial concentrations (Table 4.3) were not consistent throughout all *E. coli* mutant strains due to their individual demands, these substrate levels never fell below a critical K_S value according to Monod (Eq. 3.7). Thus, biomass-specific glucose consumption rates were maximized at every time point of analysis during cultivation and represent cellular metabolic needs under the correlative batch growth or nitrogen-limited states. Ascertained glucose-based kinetic rates are contrasted in Table 4.4 for the *E. coli* WT strain and seven mutants. During nutrient excess exponential growth, those biomass-specific glucose uptake rates (q_S) were not substantially fluctuant around the WT value of 1.77 $g_{Glc}\ g_{CDW}^{-1}\ h^{-1}$. Nevertheless, biomass from glucose yields ($Y_{X/S}$) of PDHC-activity weakened mutants were significantly lower than in the residual *E. coli*

strains ranging from 0.13 to 0.45 g_{CDW} g_{Glc}^{-1}. This disagreement indicated a carbon drain away from biomass synthesis towards product formation and overflow metabolism. In the nitrogen-limited slowly-growing cultivation phase, the highest glucose consumption rate of 0.59 g_{Glc} g_{CDW}^{-1} h^{-1} was observed for *E. coli* HGT. The unpaired effects of stringent response modifications in the SR mutant and the reduced PDHC-activity of *E. coli* ACE already had elevating influences of about 1.2-fold and 1.4-fold on (q_S) during nitrogen limitation. Eventually, the combination of both genetic manipulations enabled a synergistic increase of glucose consumption in the HGT mutant of more than 2.3-fold compared to the WT and about 1.8-fold as against the other mutants.

Table 4.4. Biomass-specific substrate consumption rates from *E. coli* two-stage batch cultivations. Biomass from glucose yields ($Y_{X/S}$) and biomass-specific glucose (Glc) uptake rates (q_S) in exponentially growing and nitrogen-limited cultures of different *E. coli* mutants. n.d.*: not definable due to lacking biomass formation c_X=0. Contents and style modified after Michalowski et al. 2017.

	Exponential Phase		Nitrogen-Limited Phase		
E. coli MG1655	$Y_{X/S,max}$ [g_{CDW} g_{Glc}^{-1}]	$q_{S,max}$ [g_{Glc} g_{CDW}^{-1} h^{-1}]	$Y_{X/S,lim}$ [g_{CDW} g_{Glc}^{-1}]	$q_{S,lim}$ [g_{Glc} g_{CDW}^{-1} h^{-1}]	$q_{S,lim}$ ratio WT [%]
WT	0.41 ± 0.01	1.77 ± 0.06	0.18 ± 0.03	0.25 ± 0.01	100
HGT	0.17 ± 0.01	1.81 ± 0.09	n.d.*	0.59 ± 0.02	236
Δ*relA*	0.40 ± 0.01	1.93 ± 0.03	0.04 ± 0.01	0.36 ± 0.02	144
SR	0.40 ± 0.01	1.77 ± 0.06	0.04 ± 0.00	0.35 ± 0.02	140
ACE	0.13 ± 0.01	1.51 ± 0.02	0.03 ± 0.01	0.31 ± 0.01	124
HS #13	0.32 ± 0.01	1.47 ± 0.07	0.11 ± 0.03	0.31 ± 0.01	124
HS #77	0.41 ± 0.01	1.38 ± 0.03	0.20 ± 0.00	0.24 ± 0.00	96
*spoT*_ED	0.45 ± 0.00	1.57 ± 0.01	0.23 ± 0.00	0.22 ± 0.01	88

Associated with the above mentioned increased glucose consumption rates of *E. coli* HGT and *E. coli* ACE, both strains appeared to channel high portions of the glucose surplus into a drastic overproduction of pyruvate (Table 4.5). The amino acid substitution mutation G267C within the E1 component of the Pyruvate Dehydrogenase complex in *E. coli* ACE led to a product formation rate of 0.68 g_{Pyr} g_{CDW}^{-1} h^{-1} in the exponential and a rate of 0.18 g_{Pyr} g_{CDW}^{-1} h^{-1} in the subsequent limited growth phase. This corresponded to a final concentration of ~13 g L^{-1} in the culture broth (Figure A.5 C). The combinatorial mutant *E. coli* HGT released a final pyruvate concentration of only ~11.4 g L^{-1}

to the cultivation medium. Anyhow, biomass-specific product synthesis rates (q_P) were 0.84 $g_{\text{pyruvate (Pyr)}}$ g_{CDW}^{-1} h^{-1} and 0.26 g_{Pyr} g_{CDW}^{-1} h^{-1} during exponential and nitrogen-limited growth, respectively. Thus exceeding the ACE mutant by about 24 % and 44 % of productivity. Notably, the *E. coli* WT strain as well as the other five stringent response mutants did not show any detectable pyruvate production throughout the entire fermentation process.

Table 4.5. Biomass-specific product formation rates from *E. coli* two-stage batch cultivations. Product from glucose yields ($Y_{P/S}$) and biomass-specific pyruvate (Pyr) production rates (q_P) in exponentially growing and nitrogen-limited cultures of different *E. coli* mutants. 0.00*: HPLC measurements were below detection limit. Contents and style modified after Michalowski et al. 2017.

	Exponential Phase		Nitrogen-Limited Phase		
E. coli MG1655	$Y_{P/S,max}$ [g_{Pyr} g_{Glc}^{-1}]	$q_{P,max}$ [g_{Pyr} g_{CDW}^{-1} h^{-1}]	$Y_{P/S,lim}$ [g_{Pyr} g_{Glc}^{-1}]	$q_{P,lim}$ [g_{Pyr} g_{CDW}^{-1} h^{-1}]	ratio ACE [%]
WT	0.00*	0.00*	0.00*	0.00*	0
ACE	0.45 ± 0.02	0.68 ± 0.04	0.58 ± 0.06	0.18 ± 0.01	100
HGT	0.49 ± 0.05	0.84 ± 0.04	0.41 ± 0.06	0.26 ± 0.03	144
Δ*relA*	0.00*	0.00*	0.00*	0.00*	0
SR	0.00*	0.00*	0.00*	0.00*	0
HS #13	0.00*	0.00*	0.00*	0.00*	0
HS #77	0.00*	0.00*	0.00*	0.00*	0
*spoT*_ED	0.00*	0.00*	0.00*	0.00*	0

Respiratory Rates

Biomass-specific respiratory rates were determined from O_2 and CO_2 progressions monitored in the exhaust gas throughout the process. By applying the resulting rate of produced CO_2 against consumed O_2, a respiratory quotient (RQ) was calculated with Equation 3.33 for every bacterial cultivation (Figure A.6). RQ values of 1.0 reflect aerobic respiration of the cells by full oxidation of glucose to CO_2 in the central carbon pathway. For *E. coli* WT, a RQ of 1.02 was identified during exponential growth. This value was in good agreement with published values of 1.01 obtained under similar conditions (Andersen and Meyenburg 1980). When intracellular activities slowed down in the

nitrogen limitation phase, respiration rates were reduced by more than 60 %. A slight increase in RQ to 1.16 was observed in non-growing WT cells, which was consistent to marginally elevated RQ values of 1.05 in aerobic glucose-limited chemostat cultivations (Sauer et al. 1999). All other tested *E. coli* mutants showed quite unique and individual respiratory phenotypes (Figure 4.10). It appeared that strains containing a mutation in *aceE* released resembling amounts of CO_2 during exponential growth and nitrogen limitation. Accordingly, RQ values were in a range between 0.39 and 0.99 for those cells. This metabolic stoichiometry of O_2 and CO_2 seemed to be reversed in the mutants *E. coli* SR, Δ*relA* and HS#13 during nitrogen limitation. Constraint abilities of executing a complete stringent response resulted in RQ values of 1.46, 1.38 and 1.45, revealing high CO_2 production rates of the strains. Very prominent oxygen requirement values of the SR mutant in both growth conditions involved enhanced carbon production as well.

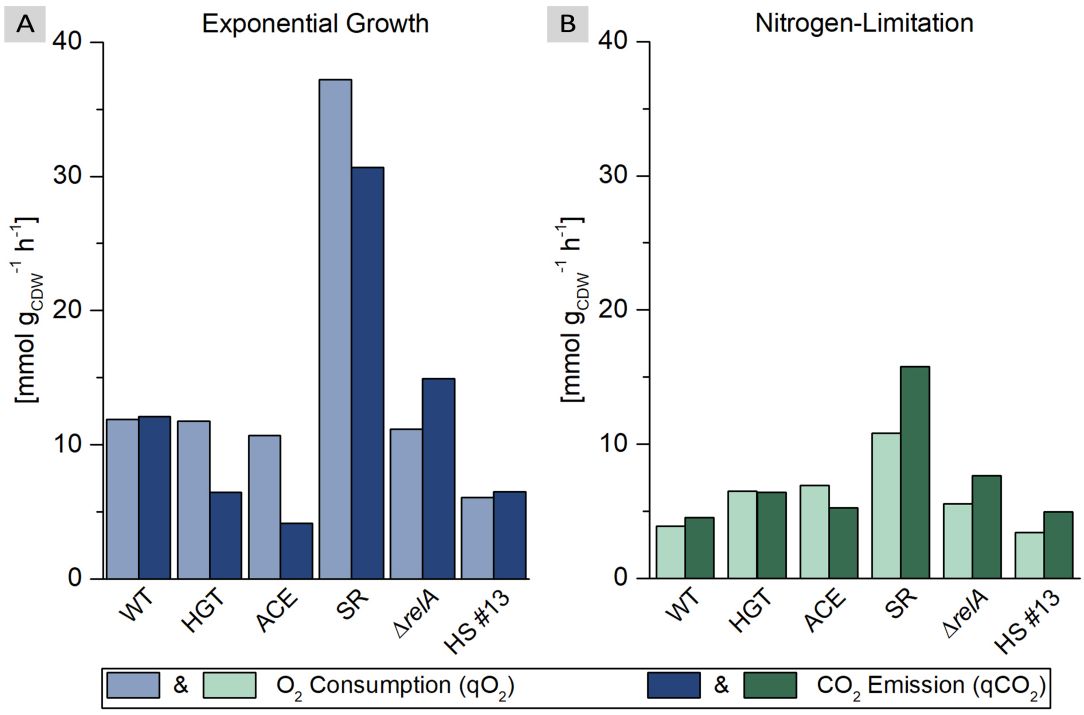

Figure 4.10. Biomass-specific respiratory rates in different *E. coli* mutants. Biomass-specific oxygen consumption (q_{O_2}) and carbon dioxide emission (q_{CO_2}) rates were determined for exponentially growing (A) and nitrogen-limited cultures (B). Graphs modified after Michalowski et al. 2017.

4.4.3. Carbon Balance

A carbon balance was used to compare carbon distributions in *E. coli* WT to five strains with modified stringent response or pyruvate dehydrogenase complex (Figure 4.11). During exponential growth, *E. coli* WT converted all consumed glucose into biomass (48 %), carbon dioxide (44 %) and a small amount of acetate (8 %) - the classical carbon overflow metabolite. In this growth phase, a similar carbon distribution was observed for all non-pyruvate producing mutants. A different carbon ratio pattern was observed for *E. coli* HGT and ACE. Elevated rates of glucose consumption consequently led to a high surplus of total carbon availability, which was entirely channeled into organic acid formation such as pyruvate (49 %), lactate (20 %) and acetate (1.6 %).

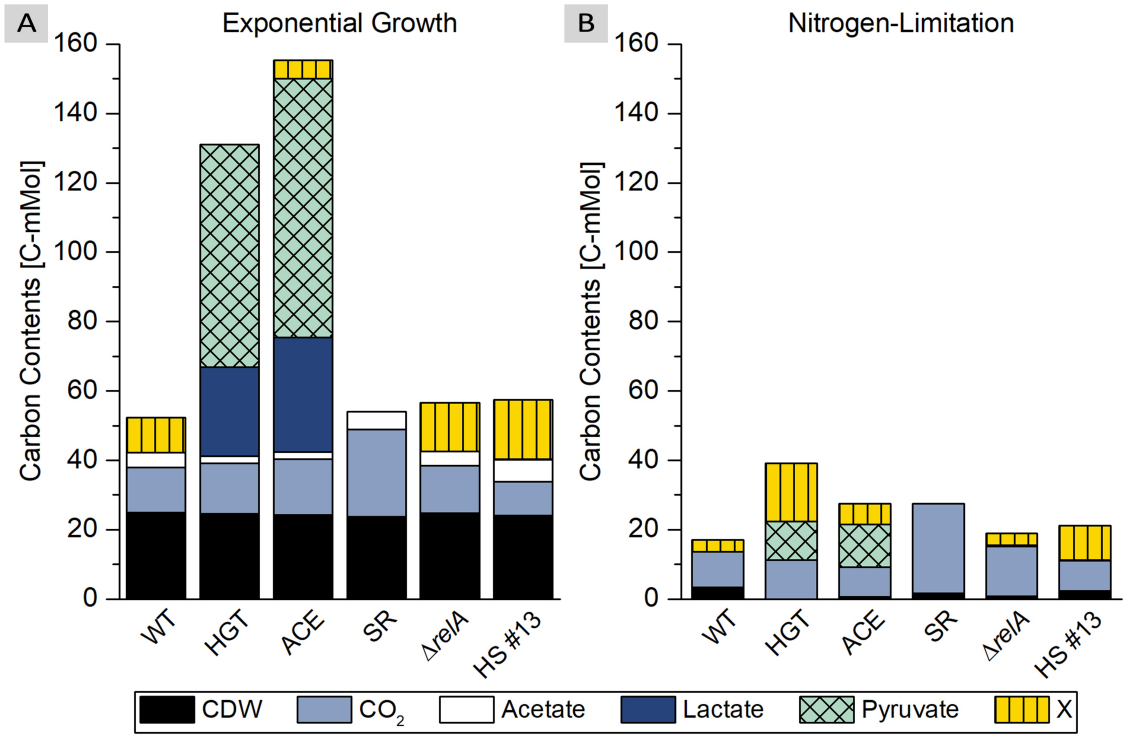

Figure 4.11. Carbon balance of *E. coli* WT and five mutants. Comparison of carbon distributions in various *E. coli* strains during exponential growth and nitrogen-limited growth arrest. Column heights represent the total carbon input in terms of glucose consumption. Allocated products of the carbon metabolism like biomass (CDW), carbon dioxide (CO_2) and organic acids (acetate, lactate, pyruvate) are displayed as proportions of the column height. Unknown organic compounds, that were not identified with the applied methods, are indicated as X-fraction. Graphs modified after Michalowski et al. 2017.

Under conditions of nitrogen limitation, biomass was formed from about 5 % of consumed carbon in *E. coli* Δ*relA* to 11 % in HS#13 and up to 19 % in the WT strain. Residual carbon fractions were compiled of carbon dioxide (76 % in Δ*relA*, 41 % in HS#13, 60 % in WT) and unknown metabolites (19 % in Δ*relA*, 48 % in HS#13, 21 % in WT). *E. coli* SR did not produce any organic acids during nitrogen depletion. 96 % of all consumed glucose molecules were transferred into respiratory reactions and only 6 % were used for biomass formation. The highest calculated glucose uptake rate in *E. coli* HGT was reflected by the highest measured total carbon amount in growth limited bacterial cultures compared in the carbon balance. From about 40 C-mMol of consumed glucose, only 11.3 C-mMol (29 %) were needed for cellular respiration, which was about the same absolute amount of CO_2 as observed in *E. coli* WT. The residual carbon fraction of 28 C-mMol divided into 11.1 C-mMol (28 %) of produced pyruvate and 16.8 C-mMol (43 %) of unknown organic metabolites.

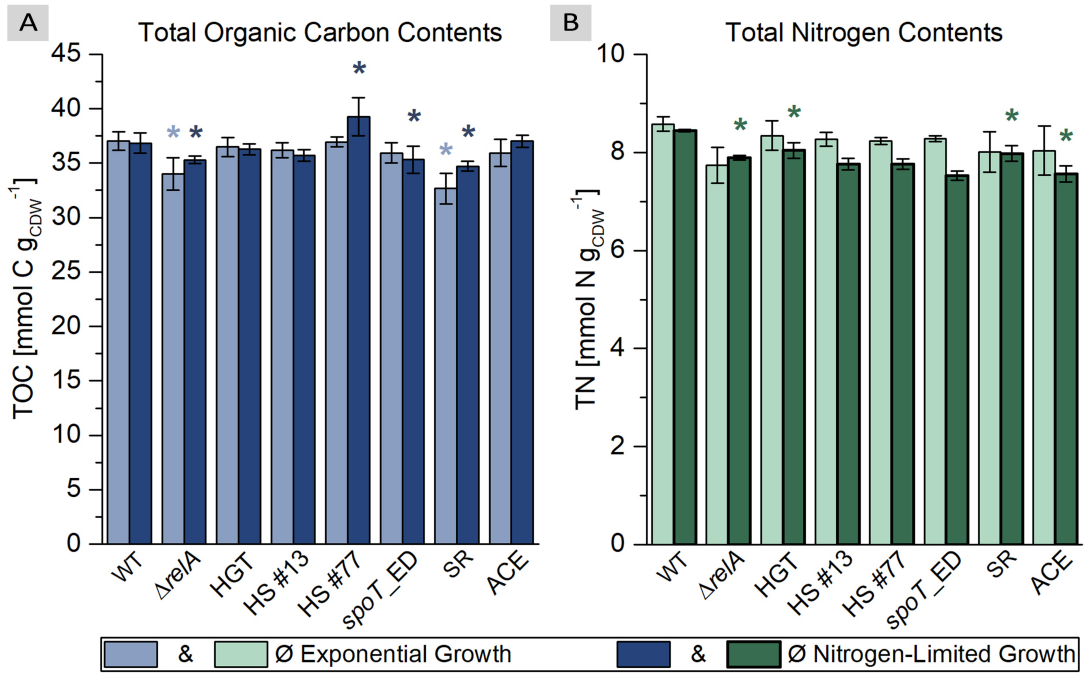

Figure 4.12. Total organic carbon and total nitrogen contents in different *E. coli* mutants. Total organic carbon (A) and total nitrogen (B) contents are compared in the *E. coli* WT and various stringent response and pyruvate producer mutants at exponential growth and after cultivation for 1.5 h under nitrogen-limited conditions. *P=0.05 for significance analysis.

Additionally to the carbon distribution patterns, the bacterial biomass composition was analyzed in the *E. coli* WT and all seven mutant strains (Figure 4.12). Total Organic Carbon (TOC) and also total nitrogen (TN) contents were determined for cells growing at exponential conditions in the mid-log phase and for such growing for 1.5 h under nitrogen limitation. In direct comparison, transition from the nutrient excess exponential growth phase into nutrient depletion conditions had no relevant effect on carbon contents in the cells. A noticeable reducing effect on nitrogen accumulation was only detected for the three mutant strains *E. coli* HS#13, *E. coli* HS#77 and *E. coli spoT*_ED. After entering the nitrogen-limited growth phase, all mutants showed decreased total nitrogen levels in their biomass compared to the WT. Such mutants with a significant difference in their mean TOC or TN values contrasting the WT are marked with an asterisks.

4.4.4. Energy Demand of Stringent Response Mutants

Measurements of nucleotides at defined time points of the process gave relevant insights into energy states of all bacterial cultures during growth and stasis. Those energetic demands of the cells were calculated from adenine and guanine pools according to Equations 3.3 and 3.4, respectively. This so-called adenylate energy charge (AEC) or guanylate energy charge (GEC) reflects the corresponding energetic balance between catabolic and anabolic reactions in a cell at current environmental conditions. Since the main goal was to identify an *E. coli* mutant with a prospective application in large-scale industrial production processes, the progression of energy charges at different nutrient access situations was considered as promising feature. In the following, the sum of all three adenine variants AMP, ADP and ATP will be referred to as AxP. The same applies to all guanine nucleotides, which will be summarized as GxP from here on. Figure 4.13 and the continuation in Figure 4.14 contrasts AEC values and adenine nucleotide compositions in the WT and different mutant strains of *E. coli* along the fermentation processes. Noticeable, summarized adenine concentrations (AxP) adopted three distinct progression states. Either AxP values declined with advancing nitrogen-limited conditions, as in *E. coli* SR and *E. coli* Δ*relA*. According stringent response mutations apparently led to a steady decrease in ATP formation. In contrast to this, the pyruvate producer *E. coli* ACE showed increasing AxP amounts over process time as a result of permanently elevated ATP concentrations together with continuously rising ADP and AMP levels.

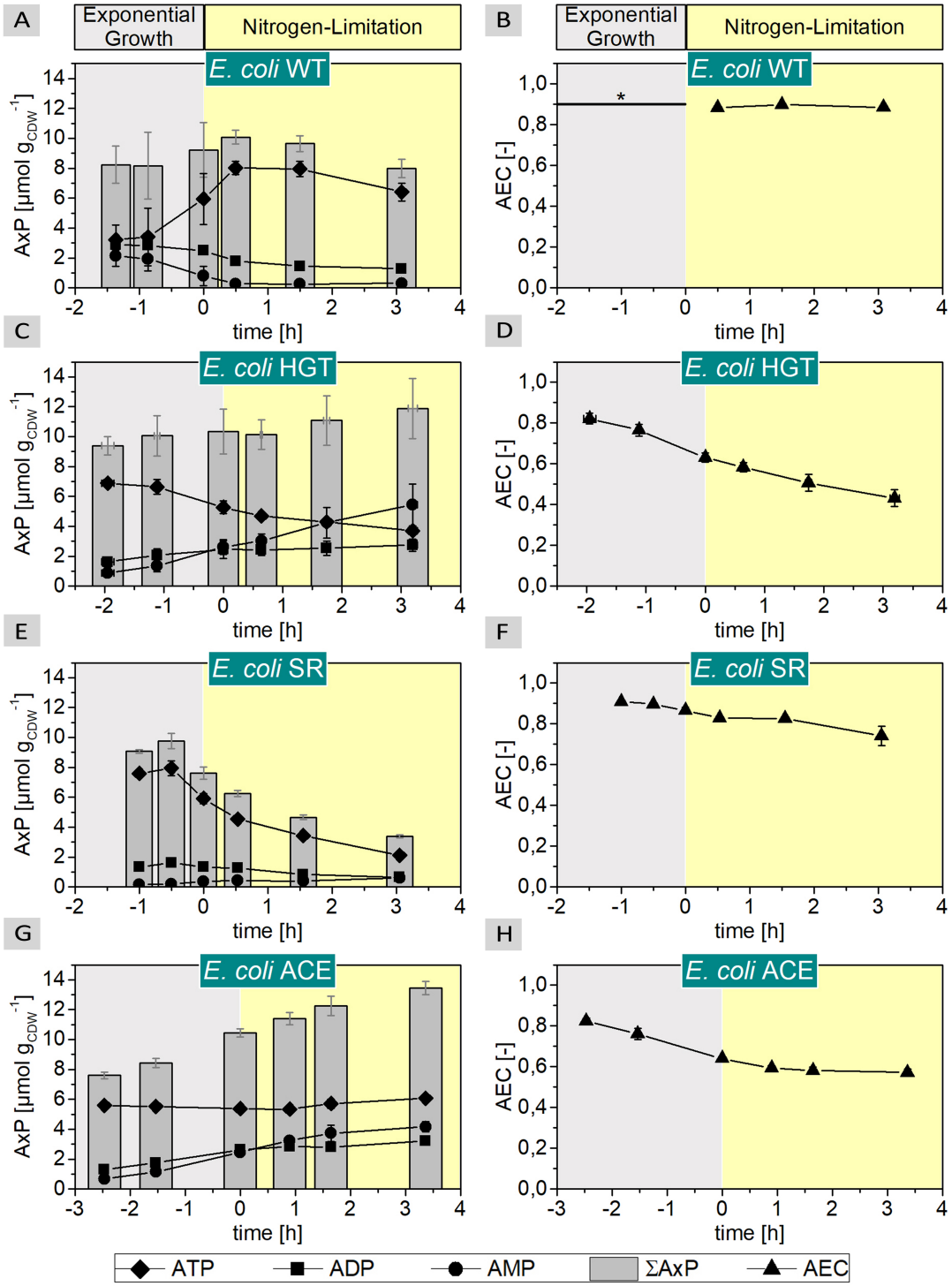

Figure 4.13. Adenine nucleotides and energy profiles of various *E. coli* mutants. Nucleotide pools of AMP, ADP, ATP and calculated AEC values during two-stage batch fermentations (exponential growth in gray and nitrogen-starvation in yellow). Total AxP concentrations (ΣAxP) are indicated as gray bars. All data sets were normalized to the exact time point of entry into nitrogen starvation. *AEC values for the exponentially growing *E. coli* WT strain are taken from a separate growth study (Figure A.4) due to highly error-prone nucleotide measurements in the present data set. Graphs modified after Michalowski et al. 2017.

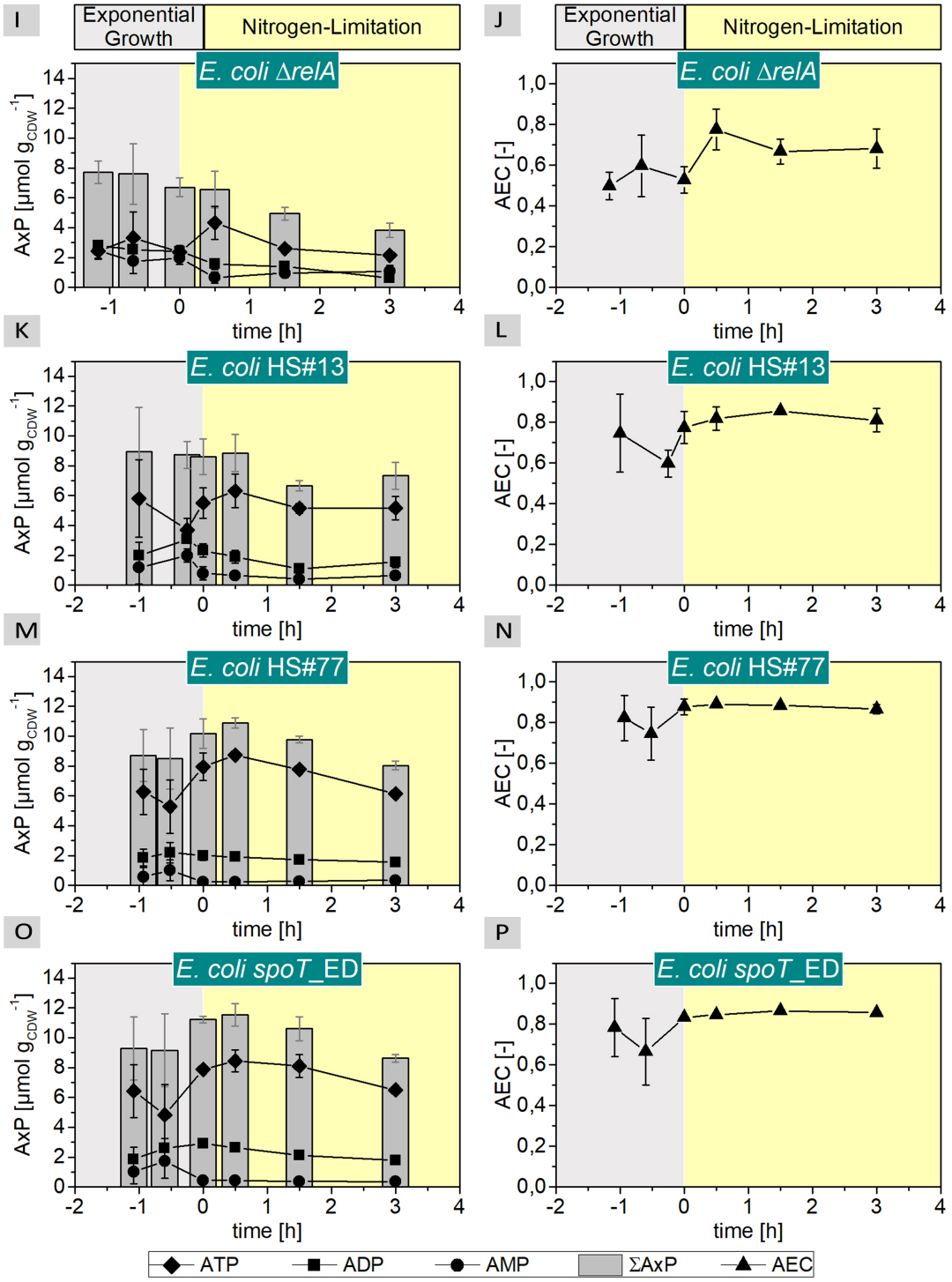

Figure 4.14. Adenine nucleotides and energy profiles of various *E. coli* mutants (continued). Nucleotide pools of AMP, ADP, ATP and calculated AEC values during two-stage batch fermentations (exponential growth in gray and nitrogen-starvation in yellow). Total AxP concentrations (ΣAxP) are indicated as gray bars. All data sets were normalized to the exact time point of entry into nitrogen starvation.

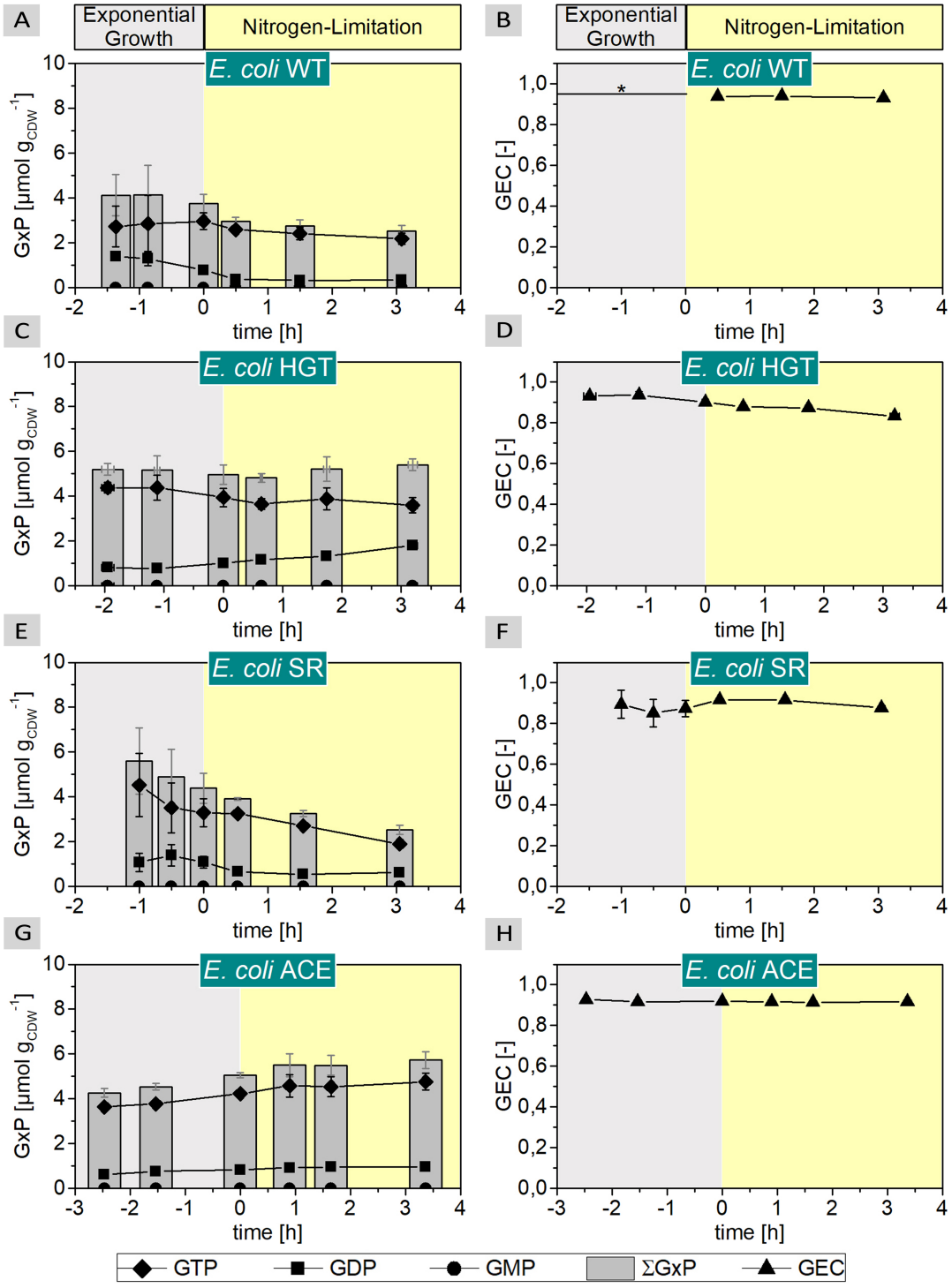

Figure 4.15. Guanine nucleotides and energy profiles of various *E. coli* mutants. Nucleotide pools of GMP, GDP, GTP and calculated GEC values during two-stage batch fermentations (exponential growth in gray and nitrogen-starvation in yellow). Total GxP concentrations (ΣGxP) are indicated as gray bars. All data sets were normalized to the exact time point of entry into nitrogen starvation. *GEC values for the exponentially growing *E. coli* WT strain are taken from a separate growth study (Figure A.4) due to highly error-prone nucleotide measurements in the present data set.

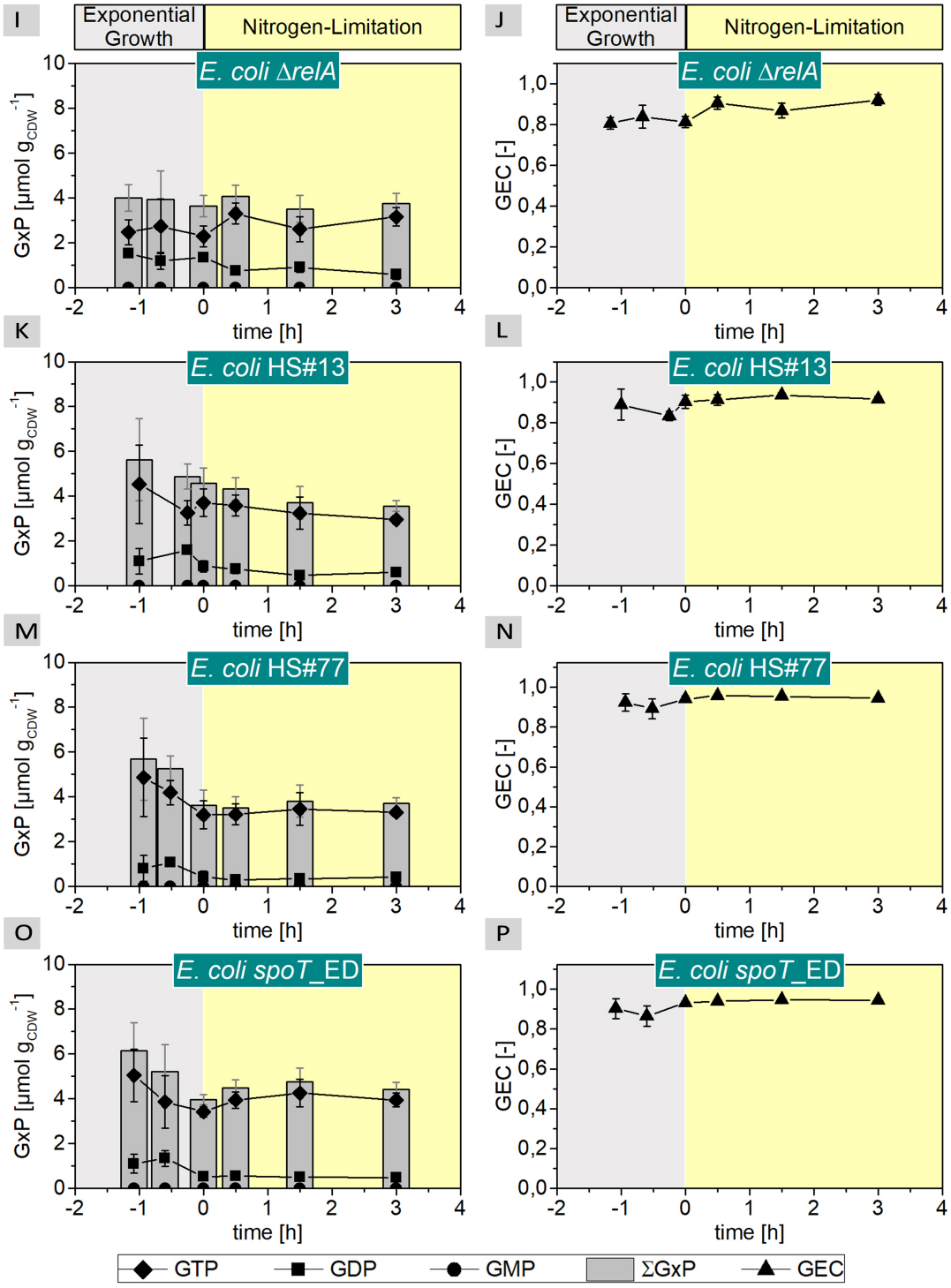

Figure 4.16. Guanine nucleotides and energy profiles of various *E. coli* mutants (continued). Nucleotide pools of GMP, GDP, GTP and calculated GEC values during two-stage batch fermentations (exponential growth in gray and nitrogen-starvation in yellow). Total GxP concentrations (ΣGxP) are indicated as gray bars. All data sets were normalized to the exact time point of entry into nitrogen starvation.

The AxP progression observed for the *E. coli* WT, that kept adenine nucleotides at a constant level over the entire fermentation, was considered as a reference. A similar progression was equally found in all solely *spoT*-modified mutants and interestingly also for *E. coli* HGT. On closer examination, energy charge level progressions revealed that most stringent response mutants were able to maintain a steady AEC value during exponential growth and even during growth arrest. Except for both mutants with restricted activity of the pyruvate dehydrogenase complex, *E. coli* ACE and *E. coli* HGT. In those cases, enhanced formation of ADP and AMP nucleotides paired with reduced ATP synthesis rates were consequently associated with a steadily decreasing adenylate energy charge. Since formation of ppGpp is based on the availability of ATP and GDP/GTP, it was very interesting to compare guanine nucleotide distributions between all mutants. Thereby, high variations in GxP levels were observed during all fermentation processes (Figure 4.15 and Figure 4.16). Strains with a severe ppGpp response, and thus with high guanine nucleotide demands, replied with declining total GxP concentrations during nitrogen stress. Other strains with reduced stringent response activities, showed corresponding steady guanine nucleotide pools at growth and growth arrest. The same applied for GEC values in all tested *E. coli* strains, which remained at a constant high level at both stages of fermentation.

4.4.5. ppGpp Accumulation in Nitrogen-deprived *E. coli* Cultures

Intracellular ppGpp levels were measured in the course of two-stage batch cultivations. As expected, in an exponentially growing *E. coli* WT culture, ppGpp was kept at a low basic level of ~0.3 µmol g_{CDW}^{-1} at first. This level was elevated almost ten-fold to 2.97 µmol g_{CDW}^{-1} in the very moment of nitrogen-deprivation. Other mutants like *E. coli spoT*_ED, *E. coli* HS#13 and HS#77 showed a comparable ppGpp progression, but to a higher and lower maximal value, respectively. Mutants with deficient RelA and PDHC activity presented almost constant ppGpp concentrations near the basic level during growth and limitation. Among these, *E. coli* SR exhibited a ppGpp formation of ~0.8 µmol g_{CDW}^{-1} even under exponential growth conditions. This value was about 3-fold higher than the exponential WT concentration and also the highest non-limited alarmone level measured among all tested *E. coli* mutants.

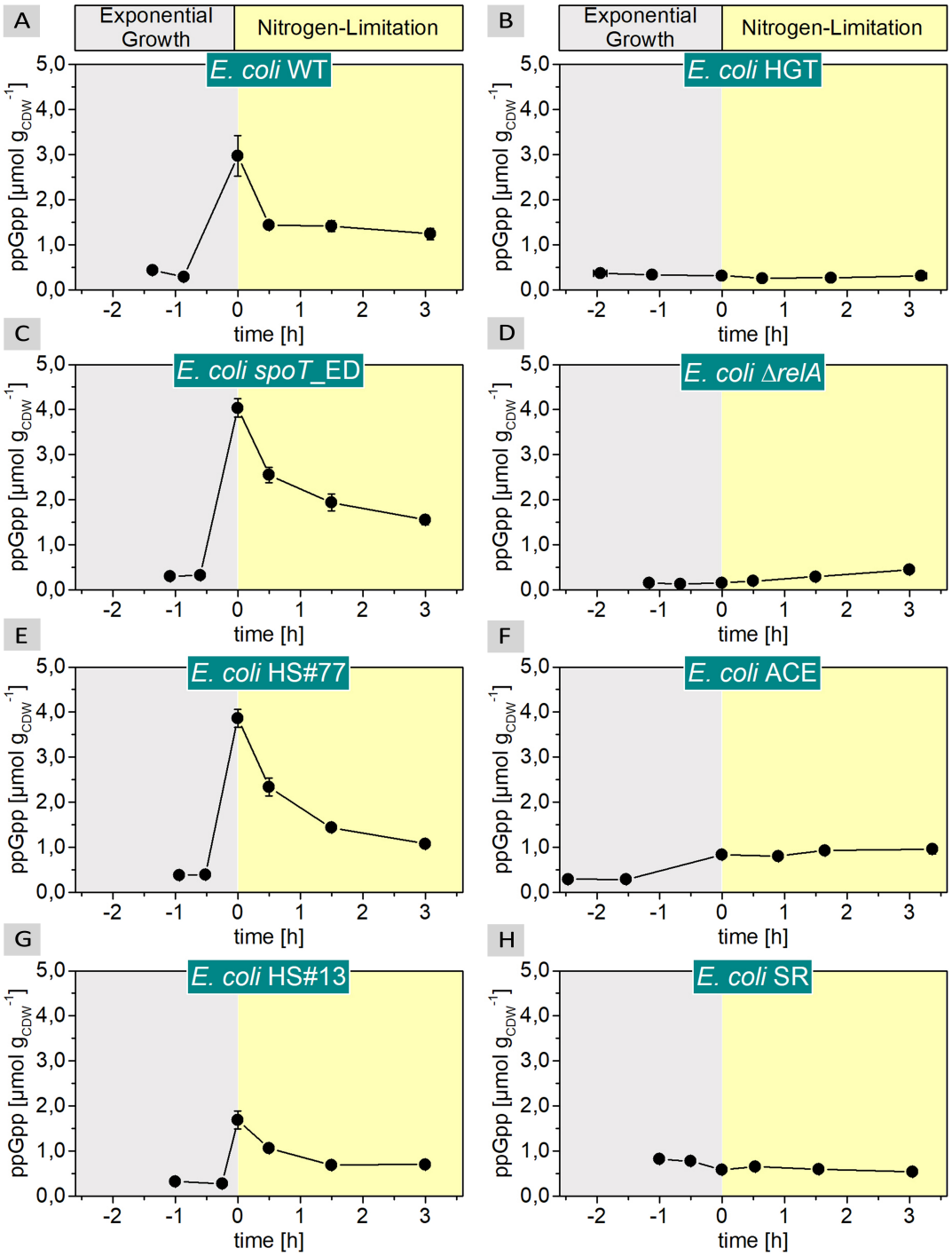

Figure 4.17. Progression of ppGpp in different *E. coli* mutants during two-stage batch fermentations. ppGpp concentrations were measured in exponentially growing cells (gray) and over a period of 3 h after entry into nitrogen limitation (yellow). For better comparison, all data sets were normalized to the time point of nitrogen starvation. Graphs modified after Michalowski et al. 2017.

5. Discussion

5.1. Genetic Modulation of Stringent Response Factors

Among the familiar global regulatory control systems and their attendant second messengers of *E. coli*, the stringent response alarmone ppGpp is indeed a fascinating signaling molecule. Over the last fifty years the secrets of its intracellular actions upon metabolic adjustment for stress survival were revealed piece by piece. Since the catalysts of stringent response induction originate from practically all kinds of unbalanced environmental conditions like nutrition, osmolarity, pH and many others, the importance of this cellular key regulator becomes incontrovertible. Activation of the stringent response brings about a drastic rearrangement of metabolic and transcriptional processes within minutes and simultaneously offers a reversal of the effects following stress-regression over the same period of time. Gene expression modification by ppGpp targets at least one-third of the chromosomal promoter sites during stress and starvation, which emphasizes the suitability of stringent response modulation to gain a profound insight into metabolic adaptations according to nutrient availability (Cashel et al. 1996, Potrykus and Cashel 2008). As one of the main achievements of this study, an assemblage of nine different *E. coli* strains with graduated strength in ppGpp synthesis and hydrolysis properties was generated. This stringent response mutant collection was composed of strains with several mutations affecting the two major enzymes of intracellular ppGpp level regulation, the so-called RelA and SpoT homologues (Figure 5.1). Synthesis of ppGpp is mainly accomplished by the monofunctional RelA protein in a β-γ-diphosphate transfer reaction from ATP to GDP. Whereas the major fraction of ppGpp hydrolysis is attributed to the bifunctional SpoT protein which additionally possess the ability of a weak ppGpp synthesis. Nonetheless, ppGpp degradation is highly preferred as long as nutrients are present in clear abundance.

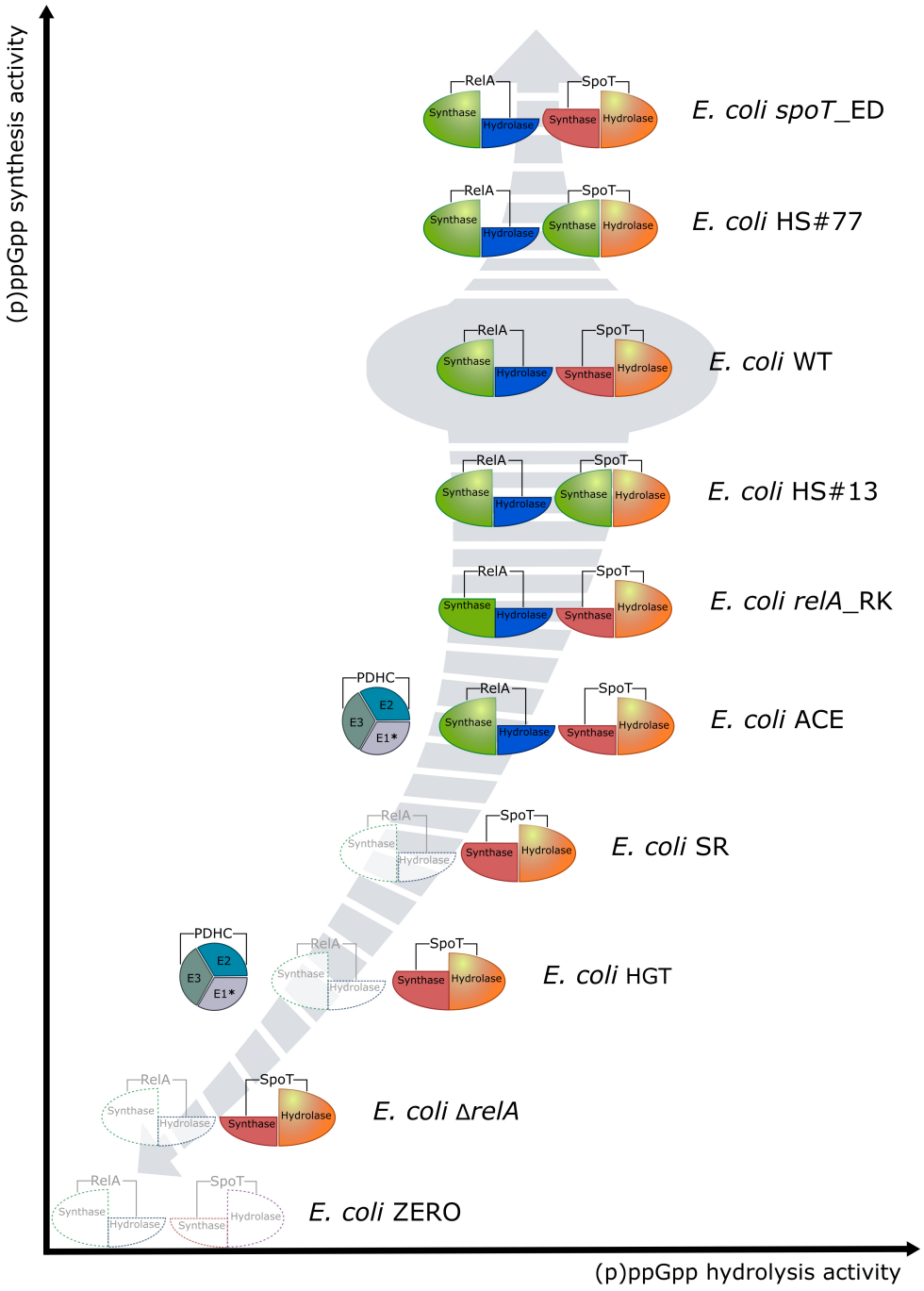

Figure 5.1. Graphical overview of different *E. coli* mutants with variations of the two stringent response enzymes RelA and SpoT. A set of nine *E. coli* mutants is compared graphically based on their theoretical ppGpp synthesis and hydrolysis ability in relation to the *E. coli* WT strain. The two stringent response related enzymes RelA (green & blue) and SpoT (red & orange) are separated into a ppGpp Synthase and a Hydrolase module. Each module size symbolizes the extent of estimated enzymatic activity. The presence of a genetically modified Pyruvate Dehydrogenase complex is displayed by the segmented circle (E1, E2 and E3).

Genetically engineered versions of RelA and SpoT were introduced into the *E. coli* MG1655 host strain in order to create a variation of the catalytical properties of these two enzymes upon their activation. Practically, the focus was on providing different mutants with a deregulated ppGpp homeostasis, especially under starvation conditions. Manipulations of this central switching point of stress-regulation were supposed to result in engineered bacterial strains with uncoupled stringent response from prevalent nutritional realities, at best. By applying various approaches of systematic chromosomal gene modifications, an incremental graduation of the ppGpp formation was realized within the *E. coli* mutant collection. This series of mutants was ranging from an entirely stringent response liberated ppGpp^0 strain (*E. coli* Δ*relA*Δ*spoT*) to novel synthetic gene constructs with enhanced ppGpp synthesis properties (*E. coli* HS, *E. coli spoT*_ED). First evidences of the gradual alarmone levels across the range of *E. coli* mutants were gained by the visualization of intracellular glycogen contents which are directly correlated to the prevalent ppGpp concentration according to Montero et al. 2014. Indeed, this method provided the opportunity to distinguish ppGpp-rich mutants from such with a lower ppGpp content by overnight cultivation prior to the chemical analysis of the actual alarmone concentrations via HPLC. In direct comparison, all individual stringent response variations implied significant color differentiations throughout the mutant collection (Figure 4.5). Mutants with a deletion of *relA* appeared in a very bright shade and thus were in clear contrast to other mutants still harboring a functional *relA* gene. Based on the WT coloring, some mutants like *E. coli relA*_RK and *E. coli* HS #77 indicated higher stress-mediated ppGpp contents which in fact was confirmed by intracellular nucleotide analysis for the latter (Figure 4.17 E). The well-known growth deficits as well as the number of undesirable phenotypes of *E. coli* ppGpp^0 in minimal medium (Xiao et al. 1991, Gentry et al. 1993, Gentry and Cashel 1996, Tedin and Norel 2001) restricted this mutant to the level of a simple control strain for this detection method since its limited application possibilities rather not designated the strain for performance in industrial production processes. Furthermore, this was supported by the fact that a complete lack of ppGpp led to a severely reduced glycolytic flux in *E. coli* during amino acid starvation due to a downshift in gene expression of glycolytic key enzymes (Traxler et al. 2008). The requirement of balanced ppGpp levels in the mutants reinforced the general design strategy of low basic alarmone concentrations during exponential growth to ensure adequate biomass build-up prior to transition into stress and starvation which was correlated with a growth-uncoupled production phase in some mutants. During exponential growth, the bifunctional SpoT enzyme generated an equilibrium of ppGpp synthesis and degradation to maintain a low

basal ppGpp level between 0.2 – 0.4 µmol g_{CDW}^{-1} in all tested *E. coli* mutants, except *E. coli* SR, which basal level was at a value of ~0.8 µmol g_{CDW}^{-1} (Figure 4.17). The average logarithmic growth ppGpp concentration of approximately 0.3 µmol g_{CDW}^{-1} was in good agreement with reported values of *E. coli* cultivations in carbon-excess batch conditions (Hardiman et al. 2007, Marisch et al. 2013, Löffler et al. 2016). Constant maximum basal levels of exclusively SpoT-mediated ppGpp synthesis were primarily implemented by a knock-out deletion of the *relA* gene which encodes the (p)ppGpp-Synthase I enzyme, the main intracellular source of ppGpp formation. The lack of the coding *relA* DNA sequence was realized in the mutants *E. coli* Δ*relA*, *E. coli* SR and *E. coli* HGT with different genetic *spoT* backgrounds. All three modified strains showed a characteristic steady ppGpp level that remained unchanged even at the onset of the external starvation signal (Figure 4.17 B, D, H). Whereas in *E. coli* Δ*relA* the *spoT* genetic locus corresponded to the WT situation, in both other *relA* deleted mutants a special catalytic motif within the Synthase domain of SpoT was engineered towards an improved ppGpp formation. This approach was based on the high structural similarity of the RelA and SpoT protein sequences. Although both enzymes perform quite contradictory roles in balancing ppGpp concentrations at different nutritional conditions, they share a common architecture of their general protein structure including all main catalytic and regulatory domains (Figure 2.9). As described earlier (section 2.3.1), the difference between a high or low ppGpp formation activity was predefined by a short catalytic motif of only four amino acids in the central Synthase domain. Within the N-terminus of both proteins, the ExDD/RxKD motif was responsible for the substrate affinity of the catalytic site and thus determined the resulting ppGpp levels from RelA and SpoT activities, respectively (Sajish et al. 2007). Following a motif reversal strategy of the highly conserved amino acids Arg-x-Lys-Asp (RxKD) in the native structure of the bifunctional SpoT protein to the Glu-x-Asp-Asp (ExDD) sequence of the monofunctional RelA, an alteration of the ppGpp formation ability was possible in general (Sajish et al. 2009). The amino acid substitutions R290E and K292D in SpoT were supposed to provoke an elevated ppGpp synthesis and a second active Synthase in the *E. coli* SR (Δ*relA* *spoT*[ExDD]) and the *E. coli* *spoT*_ED mutants, respectively. Apparently, basal ppGpp levels in the standalone *E. coli* *spoT*_ED strain as well as in the *E. coli* HGT mutant were at a comparable range to the WT reference in the logarithmic growth phase (Figure 4.17 B, C). In contrast, the Δ*relA* mutation in combination with a *spoT* motif charge reversal in the *E. coli* SR mutant seemed to have an increasing effect on the ppGpp level since the alarmone concentration was elevated by a factor of 2.5-fold during logarithmic growth (Figure 4.17 H).

Since the natural inducer of the SpoT-mediated stringent response was not tested within this study, no predication on ppGpp stimulation during one of the corresponding starvation conditions could be made. The same applied for the two mutants *E. coli* HS #13 and #77. Within the given boundaries of these investigations, no significant variation of basal ppGpp levels to the WT were observed during exponential growth of both strains (Figure 4.17 E, G), although an adequate carbon- or phosphate-starved environment could have offered answers to the stress response of these strains, this content was not in the focus of the experiments. Nevertheless, the generation of the *E. coli* HS mutants provided some fairly interesting insights into the tight regulation of the optimum and maximum admissive ppGpp levels in the bacterial cells. In contrast to the previous *spoT* modifications, the *E. coli* HS approach was based on the idea to extend the catalytic ppGpp synthesis repertoire of the cell by replacing the complete N-terminal Synthase domain within the *spoT* gene with the native *relA* element to create a novel synthetic SpoT protein construct. In this way, the rather weak SpoT Synthase activity should have been modulated to remain its bifunctional structure though with improved ppGpp formation properties. Although this synthetic construct did presumably not contribute to a higher exponential basal alarmone level, the substitution of an entire catalytic domain in the *spoT* gene was possible in principle. All above-mentioned genetic attempts to reduce ppGpp concentrations rather proceeded without any observed unusual features during the process. However, different intentions to elevate the alarmone level with modifications of *spoT* encouraged the occurrence of spontaneous *relA* suppressor mutations as in the cases of *E. coli* HS #77 as well as in *E. coli spoT*_ED (Table 4.1). This led to the assumptions that first, the synthetic SpoT hybrid protein most likely was expressed in the cells since a functional ppGpp Hydrolase must be present during growth due to the described lethal phenotype of Δ*spoT* mutants (Gentry and Cashel 1996). And second, possibly the synthetic SpoT Synthase possessed an improved ppGpp formation compared to the weak natural domain version because suppressor mutants were reported to arise whenever the intracellular alarmone balance was shifted upwards. For instance, the generation of *spoT* null mutants (Δ*spoT*) in *relA*$^+$ cells provoked non-inactivating mutations within the *relA* gene locus which finally resulted in ppGpp contents of up to 85% of the WT synthesis. Many of these mutations (His219 to Glu351) affected amino acid substitutions in the central Synthase domain of RelA in close proximity to the ExDD/RxKD motif (Montero et al. 2014). The two *relA* suppressor mutations in *E. coli* HS #77 and *E. coli spoT*_ED were equally located in the same domain segment (Gln287 and Leu303).

5.2. Nitrogen-Starvation is a Trigger for Stringent Response

Bacterial batch cultivations were designed to transit from a nutrient abundant growth scenario into a sudden nitrogen famine situation due to a predefined ammonium concentration in the minimal medium. Such a nitrogen limitation not only led to the observed nutrient depletion-mediated growth arrest of the cultures. Likewise, an intracellular increase in ppGpp concentrations and thus an upregulation of stringent response were observed for the *E. coli* WT strain and such mutants with functional *relA* gene in the absence of nitrogen (discussed in section 5.1). A correlation between nitrogen stress regulation and direct initiation of transcription at the *relA* promoter region was described recently. The group reported how the master regulator of nitrogen stress, NtrC, facilitated the coupling of the σ^{54}-dependent transcriptional rearrangements with the ppGpp-mediated stringent response (Brown et al. 2014a;b). Primarily, limited availability of nitrogen was sensed as declining glutamine concentration which activated a variety of Ntr stress response processes at the transcriptional level. Many of these NtrC/σ^{54}-dependent gene expressions involved members of the transport systems for nitrogen-containing compounds. The new understanding for the NtrC regulon actions in *E. coli* led to the conclusion that the cellular strategy against nitrogen starvation was a scavenging response in the first place (Zimmer et al. 2000). With the integration of this defense mechanism and stringent response the opportunity emerged to leverage the remaining N-resources and to adapt the intracellular nitrogen metabolism to a minimum need. By directly interacting with two newly described upstream promoter sites of *relA*, the sigma factor σ^{54} recruited RNAP and activated transcription of *relA* during nitrogen starvation which caused a significant increase in the RelA pool for ppGpp synthesis (Brown 2019). With regard to stringent response coordination, transcription at the *spoT* gene locus was downregulated in an antagonistic manner to *relA* upregulation upon nitrogen depletion (Villadsen and Michelsen 1977, Brown et al. 2014a;b). The principles of this regulatory activities were confirmed to a certain extent by another very recent study. The NtrC-dependent transcriptional response of ammonia-starved *E. coli* cells was researched at a short-term as well as at a long-term view. Ammonia limitation initiated the σ^{54}-based nitrogen stress response and simultaneously an intracellular stringent response within the time span of only 30 – 70 sec. Apparently, this short time interval was sufficient to elicit an increase of the ppGpp level to 2.0 µmol g_{CDW}^{-1} and induce σ^{S}-mediated control of gene expression. However, the

described short-term response did not include a transcriptional increase of the *relA* RNA levels (Simen et al. 2017). Thus, ppGpp accumulation was feasible due to alternative signal inducers like amino acid starvation and uncharged tRNAs which caused ppGpp formation at the ribosomes that intensified RelA Synthase activity by positive allosteric feedback loops (Shyp et al. 2012). Moreover, high amounts of de novo synthesized RelA protein might not even be necessary for a profound increase of the ppGpp level. Intracellular ratios of one RelA protein per 200 ribosomes were reported to be sufficient for a stringent response that reflected the range of a respective stress reaction upon uncharged tRNA binding (Wendrich et al. 2002).

In the present study, ppGpp accumulation was monitored during exponential growth and within few minutes after an optical signal indicated the start of nitrogen limitation and subsequent stringent response activation. As displayed in the lower graph segment of Figure 4.9, the reversal progression of the O_2 consumption and the CO_2 production output signals announced the exact time point of nitrogen deprivation. The measured ppGpp level increase of the *E. coli* WT to 3.0 µmol g_{CDW}^{-1} upon starvation (Figure 5.2) agreed very well with the reported data of Simen et al. 2017. Based on these findings, seven

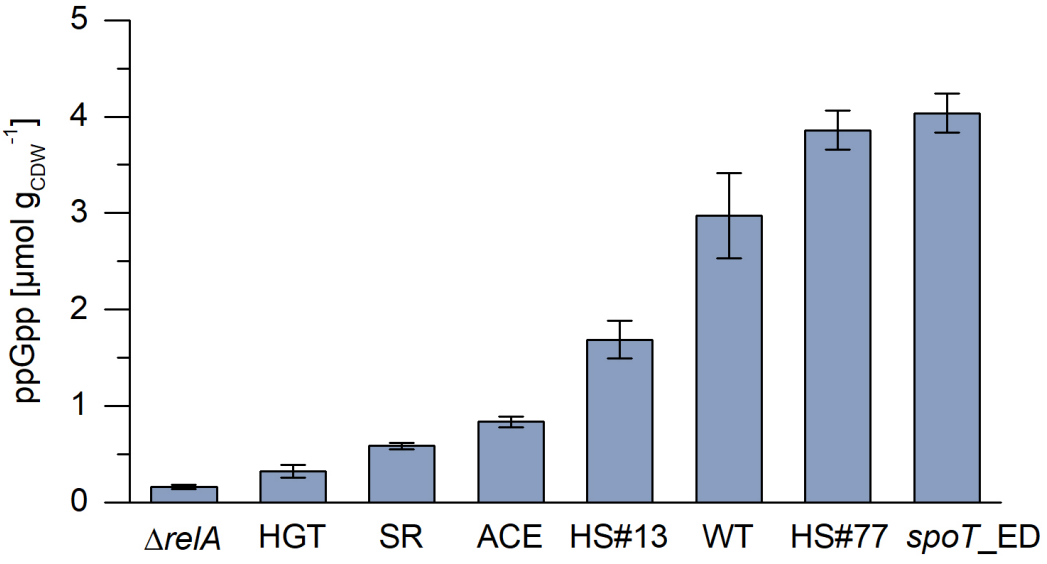

Figure 5.2. Maximum ppGpp levels in *E. coli* stringent response mutants at entry into nitrogen limitation. Comparison of stringent response alarmone concentrations at the exact time point of nitrogen limitation and thus transition into nutrient starvation.

strains of the *E. coli* stringent response mutant collection and the WT were evaluated in terms of their individual performance in growth and stress behavior at transition from nutrient excess to nitrogen-deprived conditions (Figure A.5 and Figure 4.9). In essence, the observed unique ppGpp phenotypes (Figure 4.17) reflected the individual contributions of various genetic manipulations of both stringent response elements as well as of pyruvate overexpression on alarmone accumulation in the mutants. An array of the maximum ppGpp concentrations, which were obtained immediately after nitrogen stress initiation, revealed an ascending order of stringent response performance in the examined mutants (Figure 5.2). As expected, nitrogen stress-stimulated ppGpp formation was absent in *relA* deleted mutants like *E. coli* Δ*relA*, *E. coli* HGT and *E. coli* SR. Consequently, the Δ*relA* and HGT strains yielded the lowest alarmone concentrations of 0.16 µmol g_{CDW}^{-1} and 0.26 µmol g_{CDW}^{-1}, respectively, from their corresponding SpoT Synthase activity during exponential growth. Nevertheless, *E. coli* HGT showed an alarmone phenotype of very special interest. All ppGpp dynamics in the mutant were diminished, which was characterized by a constant low alarmone level during growth and starvation. Even the small alarmone accumulation at the late stationary phase as in *E. coli* Δ*relA* was not observed in *E. coli* HGT after three hours (Figure 4.17 B, D). Apparently, in both mutants the SpoT Synthase was not activated by nitrogen-deprived conditions in the minimal medium such that with a lacking RelA enzyme stress-induced ppGpp levels resembled those of the preceded exponential phase. The absence of ppGpp formation in nitrogen-starved cultures of *relA*-lacking *E. coli* complies to the very recent results of D. R. Brown who reported an inevitable need of the stress regulator NtrC and the RelA enzyme for nitrogen-mediated stringent response and persister cell induction. Particularly in the described scenario, binding of RNAP to promoter sites related to ppGpp degradation, as in the case of *spoT*, was negatively affected by nitrogen limitation such that SpoT-driven ppGpp synthesis as well as further degradation were excluded and the alarmone maintained its basal level (Brown 2019). A comparable ppGpp phenotype was observed in *E. coli* SR which shared a common *relA* and *spoT* constitution with HGT. The mutants were characterized by the combination of a *relA* deletion with the ExDD motif reversal within SpoT. In summary, these results indicated a great potential for uncoupling stringent response from external stress signals by relieving the cells from the major ppGpp source, RelA. Intriguingly, the stand-alone mutant *E. coli* ACE, carrying a single amino acid substitution within the PDHC, showed similar decreased starvation-mediated ppGpp formation at twice the value of the basal range, despite a seamless genetic structure of both stringent response genes. Possibly, the low-functional E1 subunit (*aceE*) of the Pyruvate Dehydrogenase

complex affected the intracellular RpoS stability in a similar way as the described effects of an inactivated *aceE* gene. An *E. coli* Δ*aceE* mutant responded with increased levels of σ^S (RpoS) in the exponential phase due to higher translation, decreased degradation and elevated stabilizing of σ^S by the anti-adaptor proteins IraP and IraD (Battesti et al. 2015). Usually, the level of σ^S expression was found to be undetectable during exponential growth in the *E. coli* MG1655 WT strain (Dong et al. 2008). Thus, one feasible explanation for the missing typical escalating signal up-shift of ppGpp in *E. coli* ACE could have been the slightly elevated alarmone concentration during growth combined with a σ^S availability that might have reduced σ^{70}-dependent *relA* transcription due to sigma factor competition (Jishage et al. 2002, Nyström 2004). Several modifications affecting the bifunctional stringent response enzyme SpoT resulted in *E. coli* mutants with gradually higher ppGpp levels compared to the WT. *E. coli spoT*_ED and *E. coli* HS #77 yielded maximum ppGpp concentrations of 3.86 µmol g_{CDW}^{-1} and 4.04 µmol g_{CDW}^{-1}, respectively. The short-termed ppGpp increase directly after nitrogen-depletion was followed by a rapid adjustment of a constant stationary phase alarmone level at 1.44 µmol g_{CDW}^{-1} within the time span of 30 min in the WT. Both SpoT mutants with a potentially upregulated Synthase activity equilibrated their corresponding ppGpp levels to a similar constant value in a time span that took six times longer than the WT degradation process.

5.3. Metabolic Properties of Stringent Response Mutants

The central question behind this study was whether an unbalanced stringent response would implicate advantageous properties to an *E. coli* culture upon environmental stress conditions in terms of an enhanced carbon uptake capacity. This means, the incrementally increasing ppGpp formation properties of the stringent response mutant collection (section 5.1) were applied to investigate to what extent the internal stress signal processing could be uncoupled from a starvation-induced response. At best the metabolic turnover rates, especially for carbon, would be independent from external nutritional realities such that growth-like cellular activities could be maintained in late process phases and unwanted stress regulation could be minimized to conserve intracellular resources and energy. The goal was to identify one mutant strain with a deregulated ppGpp sys-

tem that was characterized by novel properties compared to the *E. coli* WT like a higher stress tolerance towards nutritional fluctuations and a higher level substrate uptake rate even during limited cultivations. To gain first insights into stringent response initiated stress behavior and glucose consumption of the mutants, an inducible and highly effective growth interference of an exponentially growing bacterial culture was accomplished with the amino acid analogue SHX. This competitive inhibitor of seryl-tRNA Synthetase is known to cause an accumulation of uncharged tRNAs at the ribosomes which usually resulted in an impermanent inhibition of translation and triggered an artificial RelA-mediated stringent response in growing cells at nutrient-excess conditions (Tosa and Pizer 1971). Within the scope of this study, SHX was supplemented to exponentially growing cultures of the *E. coli* mutants and biomass-specific glucose consumption was determined for the growth and the limited phases (Figure 4.7). The expected drastic growth repression was observed 15 min after SHX treatment which corresponded well to other reported SHX-induced stringent control investigations (Nowicki et al. 2014). Apparently, after 30 min of induction a rapid and extensive reprogramming of transcription was activated in SHX treated *E. coli* cells. The expression of central metabolic pathways, flagellar synthesis and glucose-specific PTS enzymes were downregulated in the *E. coli* MG1655 WT and a *relA* mutant (Durfee et al. 2008). Across the engineered *E. coli* variants of this study, all strains except *E. coli* HGT reacted with a significant reduction of their initial growth rate upon SHX addition in the range between 70 – 85 %. Consequently, biomass-specific glucose uptake rates (q_S) declined as a result of decreased growth rates in the range of 50 – 70 % (Table 4.2). Compared to the WT, a significantly increased q_S value was determined for the mutants *E. coli* HS #13, *E. coli* Δ*relA* and *E. coli* HGT (Figure 4.8). However, the q_S value of the chloramphenicol treated WT culture was already elevated above the SHX level due to total ribosome blocking. By taking this value into account as basis for significance analysis, solely *E. coli* HGT remained as appropriate candidate with enhanced glucose consumption out of the mutant collection. In fact, the HGT strain acquired an exceptional position within the mutant bank since it took a four-times higher inhibitor concentration of SHX than in all other tested cultures to obtain a small but noticeable cellular reaction of growth arrest. Thus, the growth rate and the glucose uptake rate of HGT were almost identical during exponential growth and induced stringent response. Possible explanations could have been a strongly delayed metabolic and translational slow-down in *E. coli* HGT caused by its low maximum growth rate or a conceivable emancipation of the mutant from RelA-mediated stringent response. Most certainly, further investigations of all mutants were essential to evaluate the impact of a

naturally induced stringent response on the metabolic glucose turnover at conditions of a functional translation apparatus.

The application of nitrogen starvation was considered an appropriate strategy to characterize growth phenotypes, cellular kinetics, stress behavior and partially product formation of these cells under realistic stringent response conditions. As mentioned above, nitrogen-deprived cells of *E. coli* were competent to directly induce a stringent response as consequence of the NtrC-based nitrogen stress reaction (section 5.2). Thus, the external stress signal did not interfere with general intracellular functions which were not primarily affected by the stress activator itself. In this way, the cultures ran slowly from a nutrient-excess into a nitrogen-limited and finally into a nitrogen-depleted growth phase while glucose was available in abundance throughout all process stages. The limitation of a non-carbon nutrient promoted the advantage to be able to refer to a fully active carbon metabolism that could feed into product synthesis, energy supply and intermediate provisioning especially during the growth-uncoupled phase (Shaikh et al. 2009, Rühl et al. 2012). The chosen bioreactor cultivations were designed to provide information about glycolytic rates in growing and stress-inhibited cells as well as to resemble production-like conditions as they would be realized in industrial cultivations. Hence, a biomass formation process stage would be followed by a growth arrest stage for product formation. Often these fermentation scenarios were performed to circumvent possible technical restrictions in terms of mixing capacities, oxygen transfer and heat exchange to ensure e.g. the high nutritional demand of the microbial culture was satisfied and oxygen assimilation rates during the process were manageable (Takors 2012). Practically, the exact time point of nitrogen limitation divided this two-stage fermentation process into an initial maximum growth phase and a following stationary phase which was characterized by highly reduced bacterial metabolic rates. Specific glucose consumption rates of the tested strains were likewise determined at their maximum level during exponential growth and at their growth-uncoupled level in the resting cell state. Since glucose was available in high excess during nitrogen depletion, the second stage consumption rates were solely dependent on the cellular demand for limited growth, product synthesis, survival and maintenance. Other studies, allowing for a completely active stringent response, reported a frequent transcriptional on/off switching of regulatory programs when the *E. coli* cultures were facing repeated fluctuations in ammonia supply. These dynamic conditions caused a rapid accumulation of ppGpp during a time span of only 70 sec followed by the activation of a large number of genes involved in amino acid transport and metabolism,

protein degradation and catabolic pathways as well as the downregulation of translation, nucleotide synthesis, cell motility and replication. Apparently, within the course of increasing ammonia starvation that was part of the experimental setup, the σ^N-regulated gene expression of metabolic pathways was described to be amplified in an equal measure (Simen et al. 2017). An interrelated scale-down study simulated the scenario of *E. coli* cultures fluctuating between different nutritional gradients as these can be a result of limited mixing under large-scale conditions. They confirmed the previous findings that intracellular alarmone levels increased within seconds upon substrate limitation and a tactical regulatory response of the cells coincidentally induced an overexpression of gene transcription related to the σ^S regulon. The energetic costs of the initiated regulatory activities in terms of transcription and translation demanded a growth-uncoupled ATP increase of ~40 – 50 % for cell maintenance. Thus, a list of top energy-consuming genes was proposed with the recommendation to selectively reduce these energy impasses in future metabolic engineering approaches towards robust bacterial large-scale producer strains. This list included genes for biosynthesis of flagella and filament structure proteins, glutamine ABC transporters and PTS permeases, chaperones and the two enzymes Acetyl-CoA Synthetase (AMP-forming) and Malate dehydrogenase (Löffler et al. 2016). To prepare the bacterial cells for prolonged starvation conditions, a different strategy was targeted in the present study. Alternating cellular stress states as consequences of nutrient gradients in the microbial environment were approached at the level of stringent response regulation. A special focus was on the role of the stringent response alarmone ppGpp which was modified in order to find a balanced genetic *relA* and *spoT* structure that supported an elevated glucose uptake rate in starved and growth-arrested *E. coli* cells. Down to the present day, quite contrasting attempts to interfere with stringent response for the purpose of product synthesis enhancement in *E. coli* were shown. By elevating the intracellular *relA* transcription units on a recombinant plasmid, ppGpp synthesis was specifically induced and alarmone levels increased accordingly. With this amplified stringent response reaction the amino acid synthesis of L-Lysine and L-glutamate was highly stimulated in an *E. coli* overproducer strain. Nevertheless, deletion of *relA* within the chromosome of the overproducer resulted in the opposing effect which was accompanied by poorly growing cells and significantly lower amino acid accumulation in rich medium cultivations (Imaizumi et al. 2006). Many other genetic approaches from the past concentrated on bacterial producers with a *relA* deleted genetic background (*relA*$^-$). For instance, heterologous protein synthesis (Dedhia et al. 1997, Harcum and Bentley 1999) and equally expression of the recombinant model protein GFP (Carneiro et al. 2011)

were substantially improved when the cells were only dependent on the SpoT-mediated stringent response at conditions of nutrient deprivation and minimal cell growth.

The direct comparison of individual cellular kinetics of the stringent response mutants within this study was performed with metabolic turnover rates obtained from two-stage bioreactor fermentations at logarithmic growth and in a subsequent period of growth-arrest. Although the process setup had to be adjusted due to highly varying maximum growth rates of the different *E. coli* mutants (Table 4.3) which demanded distinct settings for the initial glucose concentrations, process times and sampling intervals, the resulting maximum cell dry weight from 40 mM ammonium was almost identical in all strains based on a CDW variance of < 1.5 % (Table A.2). Accordingly to these values, the biomass conversion from nitrogen $Y_{X/N}$ yielded a similar narrow and uniform distribution of the data with a comparable variance of < 2.5 % (Table 4.3). Both pyruvate producers *E. coli* ACE and *E. coli* HGT carry the G267C amino acid substitution mutation in their E1 subunit of the Pyruvate Dehydrogenase complex. Naturally, among all members of the mutant selection these two strains were the only ones that showed a significant pyruvate formation during the predefined aerobic cultivation conditions at growth and stasis as long as glucose was present in the medium. The single position exchange of glycine to cysteine in the AceE protein apparently led to product synthesis of pyruvate from glucose and drastically reduced the exponential growth rate of the culture by 60 – 70 % compared to the WT. This decrease in culture growth by more than a half agrees well with growth rates of either *aceE* defective mutants or pyruvate producers reported by other groups (Causey et al. 2004, Tran et al. 2014). Intriguingly, the minor interference with the AceE protein structure had a large effect on pyruvate synthesis and resulted in maximum values of 11 – 13 g L^{-1} in entirely aerobic fermentations. Similar product from substrate yields in the range of $Y_{P/S} = 0.41 - 0.56$ g_{Pyr} g_{Glc}^{-1}, compared to 0.45 and 0.49 g_{Pyr} g_{Glc}^{-1} in *E. coli* ACE and *E. coli* HGT respectively, were obtained in batch and fed-batch cultivations of *E. coli* mutants containing mainly disrupted genes of pyruvate consumption like *adhE*, *ldhA*, *poxB*, *ppc* and *aceEF* (Tomar et al. 2003, Akita et al. 2016). At the level of industrial relevant pyruvate production rates, a great additional expenditure in metabolic engineering of the microbial strains was necessary in a wide range of approaches from the past (reviewed in Maleki and Eiteman 2017). High performance *E. coli* producers yielded pyruvate from glucose ratios up to 0.75 g_{Pyr} g_{Glc}^{-1} and produced final pyruvate concentrations of 65 g L^{-1}. However, a further set of genetic manipulations which led to diminished growth rates, ATP supply and CO_2 formation as well as eliminated fermen-

tative pathways was necessary to generate such elaborate overproducers. In this context, glycolytic flux was reported to be elevated by more than 50% as a consequence of pyruvate production and artificial ATP reduction (Causey et al. 2004). In accordance to these findings Δ*aceEF* mutants of *E. coli* were equally described to display increased glucose uptake rates in nitrogen limited chemostat cultivations (Zhu et al. 2008). At a comparable growth rate of 0.15 h^{-1}, *E. coli* ACE and *E. coli* HGT from this study, would theoretically exhibit an 1.4-fold higher q_S value than the reported rate of 0.85 g_{Glc} g_{CDW}^{-1} h^{-1} (Figure 5.3). Non-growing and nitrogen starved cultures of the other *E. coli* mutant collection members showed varying glucose consumption rates. Whereas glucose uptake matched very well in *relA* disrupted mutants (Δ*relA* and SR), q_S values in *spoT* modified strains (HS #13, HS #77 and *spoT*_ED) diverged by 15 % (Table 4.4). Notably, the declining nitrogen concentrations in the two-stage processes affected the nitrogen metabolism and the central carbon metabolism at the same time as already published by Kumar and Shimizu in 2010. In culture conditions of constantly high glucose concentrations and gradually lowered nitrogen levels, the C/N ratio increased proportionally and transcription of the dual regulator CRP decreased. This resulted in an upregulation of genes of the PTS^{sugar} system like *ptsG* and *ptsH* as well as glycolysis like *pfkA* and *pykF*. Consequently, suppression of the CRP regulator increased the cell-specific glucose turnover rate by 170 % compared to N-rich conditions (Kumar and Shimizu 2010). Highly elevated glucose consumption was likewise proposed to be an effect of a deleted PTS in *E. coli* whereby glucose uptake was performed through the Galactose Permease transporter and intracellular conversion was accomplished by Phosphoglucose Isomerase and Pyruvate Kinase (Flores et al. 2002). Within the scope of this study, the carbon surplus during nitrogen limited stationary growth in mutants with elevated glucose consumption was determined to be directed into carbon dioxide, organic acid synthesis and product formation as it was the case for *aceE*-defective mutants (Figure 4.11). Respiratory rates of both *aceE* mutants were comparable during the two process stages. Reduced CO_2 formation indicated that pyruvate decarboxylation was slowed down due to reduced PDHC activity and this condition limited the TCA and fatty acid synthesis in turn (Battesti et al. 2015). Interestingly, *E. coli* SR showed a very unique respiratory phenotype since almost 90 % of the consumed carbon in the nitrogen-depleted culture were converted into CO_2 which implied an inactive bypass of glucose into fermentative pathways. This metabolic feature was supported by the highest requirements for oxygen paired with the highest carbon dioxide formation among the *E. coli* strains (Figure 4.10). From this respiratory behavior one can speculate that oxidative phosphorylation and the TCA were strongly activated

which would explain the high O_2 uptake and CO_2 release. However, the sum of adenosine and guanosine nucleotides respectively was decreasing in the course of the two-stage process (Figures 4.13 and 4.15) although the ppGpp concentration remained constant in *E. coli* SR (Figure 4.17). Possibly, a futile cycle of ppGpp synthesis and degradation was generated by the SR mutant because ATP, GDP and GTP residue levels were declining simultaneously. The metabolic background of this special energetic phenotype would certainly need more dedicated investigations to highlight the expected catalytic enhancement of the modified SpoT enzyme. The intracellular energy level with respect to the adenylate and guanylate energy charges was of special interest in search of an *E. coli* mutant with the potential of robust metabolic performance in prospective industrial applications. Observations of the guanosine nucleotide pools in the mutants (except *E. coli* SR) revealed a high similarity in the overall nucleotide residue levels, the progressions of ΣGxP pool sizes and steady values for the GEC of ≥ 0.8 at different growth conditions (Figures 4.15 and 4.16). A comparable progress was reported for typical shake flask batch cultivations during growth and subsequently induced acute amino acid starvation. The relative ratios of what they called the guanosine and adenosine housekeeping nucleotides maintained at stable individual quotients in the exponential, the stationary as well as in the transition phase in between (Varik et al. 2017). Thus, these results indicated constant energy charge levels at different growth rates for an *E. coli* WT strain which was also in good accordance with the present adenylate energy charge progression in *E. coli* MG1655 (Figure 4.13). The sudden deprivation of the bacterial culture for nitrogen had widely distinct effects on the further composition of the adenosine nucleotide pools with process time. AEC values in the WT strain and in *spoT* modified mutants proceeded at rather constant levels of ≥ 0.8 with advancing nitrogen limitation time, suggesting the importance of a functional RelA activity in the cells to maintain an equilibrated energy metabolism especially during starvation. Such steady energy charges were equally observed in different glucose-limited continuous cultivations of *E. coli*. Transfer of the culture from growth with 0.2 h^{-1} into a temporary glucose shortage caused a decrease in AEC to about 0.7 in 30 sec (Löffler et al. 2016). This fast downshift of the energy charge was likewise reported in cultivations that were reduced in their growth rate settings from 0.23 h^{-1} to 0.07 h^{-1}. Within minutes, the decline in AEC was reversed and finally reached a new steady-state value that was even closer to the maximum value of 1.0 than with the higher growth rate before (Weber et al. 2005b). Those mutants disrupted for the ppGpp Synthase I (*E. coli* SR) and additionally those deficient for a high rate pyruvate conversion (*E. coli* HGT and *E. coli* ACE) adopted steadily decreasing AEC progressions which was surprising because the decline already

started at exponential growth. A similar continuous dropping of the adenylate energy charge down to a low energy status of 0.5 was caused by the application of a constantly increasing phosphate limitation of an *E. coli* L-Tryptophan overproducer. Severely restricted phosphate availability reduced the cellular energy charge and thus decoupled the ATP Synthase activity and eventually induced an increase of growth independent glucose consumption (Schuhmacher et al. 2014). The general mechanism of increased ATP formation rates that were fueled by elevated substrate-level phosphorylation in glycolysis due to limited proton motive force were extensively described in the past. Corresponding approaches included e.g. the deletion of the F_0F_1 ATP Synthase complex (Causey et al. 2003, Noda et al. 2006), the extension of the genetic background with additional ATPase activity (Koebmann et al. 2002) and the artificial enforcement of the cell for ATP wasting (Boecker et al. 2019). With regard to the mutant strains, *E. coli* ACE showed an elevated glycolytic flux at comparable growth rates to the WT , however, an active stringent response control most likely rearranged transcriptional regulation and prepared the cells for survival such that the ATP surplus was accompanied by accumulation of ADP and AMP. The increasing ATP shortage with proceeding limitation time in *E. coli* SR and *E. coli* HGT had rather contradictory effects on the carbon metabolism in the cells. While the SR mutant was not able to compensate for its higher ATP demand by elevated glucose consumption this was true for *E. coli* HGT due to evidently increased glucose uptake rates that were probably controlled by the ATP demand. Apparently, the entirely balanced stringent response in HGT contributed to a more severe decline of the energy level than the stand-alone ACE mutant. The enormously high AMP concentrations after three hours of nitrogen limitation were solely observed in strains with defective Pyruvate Dehydrogenase complex. One possible explanation was an activated pyruvate to PEP conversion by the PEP Synthetase (*ppsA*). The reaction per pyruvate required the hydrolysis of one ATP molecule and released one molecule AMP together with PP_i (Figure 2.14). Although this enzymatic supply with PEP could have channeled into the TCA by additional activity of PEP Carboxylase (*ppc*) to form oxaloacetate, evidence for this branch reaction to bypass the PDHC was not provided by this study.

5.3.1. The Unique Characteristics of *E. coli* HGT

Indeed, *E. coli* HGT had a very special position in many ways among all engineered mutants within this study. By carrying the single amino acid exchange mutation [G267C] in the E1 subunit of the Pyruvate Dehydrogenase complex, HGT was one of the two pyruvate producing strains. The consolidation of the *aceE* gene modification with the genetic background of *E. coli* SR, namely the lack of an encoded ppGpp Synthase I (Δ*relA*) in combination with the Synthase activated SpoT ExDD motif (*spoT*_ED), conferred some interesting abilities to HGT in terms of metabolic turnover and stress regulation. In particular, nitrogen limitation did neither trigger the major RelA-dependent increase of the stringent response alarmone as it was expected from a *relA*$^-$ strain. Nor was an alarmone elevation observed after a certain time delay which could have been ascribed to SpoT-dependent ppGpp synthesis (Figure 4.17). Since nitrogen depletion was not described to stimulate the stringent response directly, induction of ppGpp synthesis at the level of secondary stimuli as for instance multiple amino acid deprivation was feasible (Murray and Bremer 1996). The predefined cultivation conditions and the process settings, however, did not allow for insights into such regulatory scenarios and the ppGpp pool maintained a constant low level during all process stages. Comparison of all three *relA*-disrupted mutants created the impression of an arithmetically averaged ppGpp profile of HGT in between Δ*relA* and SR. Although the elevated basal ppGpp levels of SR (0.8 µmol g_{CDW}^{-1}) were not reached by HGT, the activity of the engineered SpoT ExDD version apparently increased the balanced ppGpp synthesis to hydrolysis ratio by a factor of 1.6-fold compared to Δ*relA* (Figure 5.2). The integration of a deregulated stringent response with a disturbed flow of pathway intermediates in the central carbon metabolism eventually generated a strain that distinguished itself from the others by the highest observed glucose consumption in non-growing cells. Furthermore it provided this carbon surplus for product formation (Figure 5.3). On the basis of this 'Pirt-like' correlation, the capability of all different *E. coli* strains to adsorb and turnover glucose as sole carbon source at two extremely divergent growth conditions was illustrated. Biomass-specific glucose consumption rates (q_S) were plotted against their corresponding specific high growth rates (μ) in a nutrient excess environment and at diminishing low rates at nitrogen depletion, respectively. The intercept with the y-axis of those interpolations gave a hint towards the possible maintenance ranges for the set of mutants. In general, maintenance demand of a cell is considered as the amount of carbon required to cover energy supply for a minimum

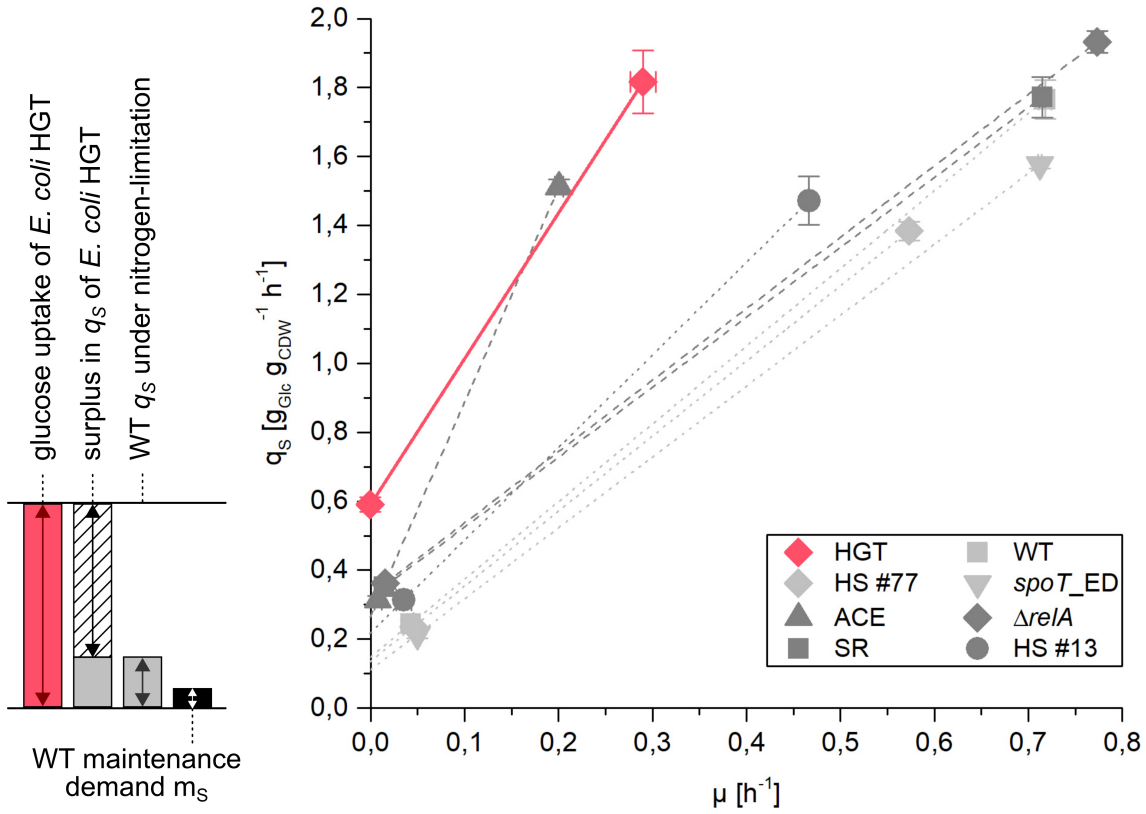

Figure 5.3. Bacterial growth plotted against glucose consumption in a 'Pirt-like' diagram. Maximum and minimum values of growth parameters (μ) and substrate uptake rates (q_S) in exponentially growing and almost resting cells were correlated in a Pirt-like manner. The individual values for cellular maintenance (m_S) are the interpolated glucose consumption rates at $\mu = 0$ h^{-1}. The depicted minimum maintenance demand of carbon-limited *E. coli* WT ($m_S =$ 0.057 g_{Glc} g_{CDW}^{-1} h^{-1}) was obtained from the literature (Villadsen et al. 2011). All data points represent calculated mean values of at least three parallel cultivation experiments in the triplex reactor system. Graph modified after Michalowski et al. 2017.

of intracellular activities as it is usually the case in resting cells. Within the range of the present study, those particular m_S values showed enormous variations (Table A.3). Depending on their estimated m_S, all mutants besides HGT were separated into a medium requirement (dark gray) and a low requirement (light gray) group, respectively. The obtained *E. coli* WT data indicated a minimum q_S value of 0.14 g_{Glc} g_{CDW}^{-1} h^{-1} at growth arrest caused by the present nitrogen-limited conditions. Similar amounts of glucose demand for maintenance purposes were reported for phosphate or nitrogen starved *E. coli* cultures by others (Hua et al. 2004, Kumar and Shimizu 2010, Chubukov and Sauer 2014, Schuhmacher et al. 2014). Distinctly lower values of m_S = 0.024 – 0.057 g_{Glc} g_{CDW}^{-1} h^{-1} were determined for carbon-limited, non-growing bacterial cultures in the past (Taymaz-

Nikerel et al. 2010, Villadsen et al. 2011). In a resting cellular state, characterized by no detectable growth, *E. coli* HGT demonstrated the highest substrate uptake rate of $q_S = 0.59$ g_{Glc} g_{CDW}^{-1} h^{-1} among all compared strains. Even at its maximum growth of $\mu_{max} = 0.29$ h^{-1}, which was less than halve the WT max. growth rate, *E. coli* HGT consumed glucose at a WT comparable level. The carbon balance together with the monitored respiratory O_2 uptake and CO_2 emission rates revealed the probable directions of the carbon surplus in the HGT cells (Figures 4.10 and 4.11). At exponential growth, biomass and carbon dioxide amounts were almost identical to the WT turnover such that all excess glucose was fueled into the products lactate (20 %) and pyruvate (49 %). During nitrogen limitation 29 % of the total carbon was released as CO_2 from decarboxylation reactions. The residual 71 % thereby remained for synthesis of pyruvate (28 %) and unknown organic compounds (43 %) since no biomass was formed. Apparently, the elevated glucose consumption in the resting cells was triggered by a strongly elevated ATP demand (Figure 4.13) such that the carbon surplus could be redirected into product formation instead of increased cell maintenance activities to maximize cell-specific productivity. Such scenarios have already been described for anaerobic glucose-limited chemostat cultures of *S. cerevisiae* at growth rates ≤ 0.001 h^{-1} (Boender et al. 2009). Thus, *E. coli* HGT builds a suitable basic platform for a promising future chassis strain. According to its interesting range of attractive metabolic features, it holds a great potential for applications in industrial large-scale processes. However, the underlying mechanisms involving the actual stringent response signal cascade upon nutritional or physiological stress as well as the pathway activities for continuous pyruvate synthesis in HGT are not yet completely understood and still need further investigations.

5.4. Conclusion and Perspectives

The major goal of this study was to investigate the effects of disconnecting the intracellular stringent response reaction of a microbial cell from the prevailing nutritional circumstances in the environment. The development of an *Escherichia coli* platform strain, which was mainly characterized by an uncoupled stress signaling network upon nitrogen starvation, was targeted. For this purpose, a mutant collection based on the *E. coli* K-12 MG1655 host strain with variable abilities due to a synthetically rearranged stringent response system was provided. The focus was on selecting one bacterial clone with new-to-nature properties like a higher stress tolerance in situations of e.g. reduced amino acid availability, as it can be caused by nitrogen depletion, and improved metabolic fluxes in non-growing cells. Such an industrially-relevant production platform was expected to show carbon requirements which were independent from the growth conditions of the culture. In other words, the biomass-specific glucose uptake rates were targeted to be significantly increased compared to the regular *E. coli* WT behavior especially at very low growth rates or even in resting cells. The potential of this high level substrate uptake could then in turn be redirected into enhanced product synthesis in nutrient limited environments. With *E. coli* HGT one such platform strain candidate was found that met the basic requirements for a potential future industrial chassis. In the HGT strain, a balanced alarmone concentration relieved the cells from the typical ppGpp boost at stringent response induction as a result of *relA* gene deletion and *spoT* modification. The consolidation of this stress response features with a pyruvate producing central metabolism (mutant *aceE* gene) finally generated a strain that directed the elevated carbon drain into product formation at nitrogen limitation. At its maximum growth rate of 0.3 h^{-1}, *E. coli* HGT consumed glucose already with a rate of 1.8 g_{Glc} g_{CDW}^{-1} h^{-1} that was equal to the WT consumption at greatly higher growth rates of 0.6 – 0.8 h^{-1}. The decreased growth rate of HGT extended the process time of the initial biomass formation phase for about nine hours, however, its high q_S of 0.6 g_{Glc} g_{CDW}^{-1} h^{-1} exceeded the WT value by a factor of four-fold in the subsequent growth-arrested phase. Thus, the advantages of the carbon surplus for production should outweigh the prolonged biomass expansion. At nitrogen limitation, 28 % of the carbon surplus was directly converted to pyruvate. Another 43 % were available for synthesis of unknown organic acids or similar compounds. The carbon balance revealed the true benefits of HGT, because carbon dioxide formation was almost identical to the WT strain at limitation, all residual glucose could possibly be likewise converted to

a carbon-based product after additional metabolic engineering of central pathways would be established in HGT. Accordingly, oxygen uptake rates were highly comparable to the WT at growth and limitation such that *E. coli* HGT could be easily taken into consideration for a prospective novel basic production chassis. Based on the gained respiratory phenotype, the oxygen demand of HGT would most likely not interfere with technical constraints of current large-scale applications as these are designed to supply bacterial cultivations at higher growth rates than the maximum of HGT. In times of fast-paced developments and enhancements in the fields of metabolic engineering and synthetic biology it probably is an easier task to modify a microorganism of choice to comply with the needs of an industrial bioproducer than several decades ago. However, since sophisticated molecular biology tools are available and constantly emerge, the portfolio of engineered microbial functions expanded to heterologous expression of difficult-to-express proteins (Kim et al. 2020), reduced-genome cell factories with enhanced production characteristics (Chi et al. 2019) as well as different bacterial species (Calero and Nikel 2018). A recent study reported the development of an *E. coli* chassis that was based on a very similar basic idea as stated here. In correspondence to this present work, the researchers aimed at a growth-decoupled product formation during a nitrogen-limited stationary phase with a characteristically active metabolism. A global metabolic pathway was modified in an *E. coli* host strain to an extend that nitrogen-limited cells performed four-fold increased metabolic rates at stationary conditions. Overexpression of the PtsI enzyme, which is part of the glucose uptake machinery, or alternatively the galactose permease GalP and glucokinase Glk in a Δ*ptsI* background resulted for both constructs in a q_S value of 0.44 g_{Glc} g_{CDW}^{-1} h^{-1} (Chubukov et al. 2017). Interestingly, the nitrogen-depleted WT consumption was in a very close range to the one described here ($q_S = 0.14$ g_{Glc} g_{CDW}^{-1} h^{-1}). The PtsI overexpressing mutant similarly showed a four-times elevated glucose uptake rate than WT cells, whereas a direct comparison of actual limited q_S values revealed that *E. coli* HGT consumed the glucose molecules at an almost 30 % higher rate in a resting state. On the contrary, the induced PtsI overexpression maintained the adenylate energy charge at a similar level to exponentially growing cells at limited conditions (Chubukov et al. 2017).

In summary, these outstanding findings of Chubukov et al. prove the general suitability of *E. coli* HGT as basic chassis that has a high potential to meet the wide array of challenges in industrial processes. The key properties of *E. coli* HGT, in particular the combination of a decoupled stringent response with low growth rates and high glycolytic turnover,

comply well with the intention of other research groups to seek platform producer strains that are equipped with highly profitable genetic and metabolic features. Nevertheless, the genetic robustness of the *aceE* modification and the HGT strain performance still need to be tested under various stress conditions to verify strain stability and culture homogeneity. Thus, I would like to encourage future researches in the field of bacterial metabolic engineering to proceed with the here presented platform strain *E. coli* HGT to further explore the benefits of its balanced stringent response to produce other carbon- or nitrogen-based compounds. As an example, the precursor accumulation of pyruvate could be used as substrate for subsequent metabolic conversion routes to amino acid or terpenoids production pathways as well as to organic acid formation of lactate, acetate and many others. A strong intracellular carbon-drain would facilitate the metabolic flux direction towards the synthesis of an intermediate of the central carbon metabolism. The genetic background of the non-pyruvate producer *E. coli* SR could be consolidated with a succinate producer strain like the one generated in the course of this study (section A.4.3) or of course alternatively with other reported genetic combinations that lead to succinate overproduction (Lin et al. 2005, Meng et al. 2016).

6. Author Contribution

This chapter summarizes my (Annette Margarete Kahlig, née Michalowski) contribution to the manuscript that was already published in a peer-reviewed international journal. The contents of the manuscript are provided in the chapter 'Publication' in section B.1.

Manuscript:

Michalowski, A., Siemann-Herzberg, M., and Takors, R. (2017). *Escherichia coli* HGT: Engineered for high glucose throughput even under slowly growing or resting conditions. Metabolic Engineering, 40:93–103.

Annette Kahlig, née Michalowski (A. M.) designed the study, established the mutant *Escherichia coli* strain collection and carried out all experiments. A. M. performed the data analysis and interpretation as well as the preparation of the manuscript.

References

Agashe, D. (2017). The road not taken: Could stress-specific mutations lead to different evolutionary paths? *PLoS Biol.*, 15(6):e2002862.

Akita, H., Nakashima, N., and Hoshino, T. (2016). Pyruvate production using engineered Escherichia coli. *AMB Express*, 6(94):1–8.

Alföldi, L., Stent, G. S., and Clowes, R. C. (1962). The chromosomal site of the RNA control (RC) locus in Escherichia coli. *J Mol Biol.*, 5(3):348–355.

Amato, S., Orman, M., and Brynildsen, M. (2013). Metabolic Control of Persister Formation in Escherichia coli. *Mol Cell*, 50(4):475–487.

Andersen, K. B. and Meyenburg, K. V. (1980). Are growth rates of Escherichia coli in batch cultures limited by respiration? *J Bacteriol.*, 144(1):114–123.

Angelides, K. J., Akiyama, S. K., and Hammes, G. G. (1979). Subunit stoichiometry and molecular weight of the pyruvate dehydrogenase multienzyme complex from Escherichia coli. *Proc. Natl. Acad. Sci. USA*, 76(7):3279–3283.

Antranikian, G. (2006). *Angewandte Mikrobiologie*. Springer-Verlag GmbH, Heidelberg, Berlin - Germany, 1 edition.

Aravind, L. and Koonin, E. V. (1998). The HD domain defines a new superfamily of metal-dependent phosphohydrolases. *Trends Biochem Sci.*, 23(12):469–472.

Arjunan, P., Nemeria, N., Brunskill, A., Chandrasekhar, K., Sax, M., Yan, Y., Jordan, F.,

Guest, J. R., and Furey, W. (2002). Structure of the Pyruvate Dehydrogenase Multienzyme Complex E1 Component from Escherichia coli at 1.85 Å Resolution. *Biochemistry*, 41:5213–5221.

Atkinson, D. E. and Walton, G. M. (1965). Kinetics of Regulatory Enzymes: Escherichia coli Phosphofructokinase. *J Biol Chem.*, 240(2):757–763.

Atkinson, D. E. and Walton, G. M. (1967). Adenosine triphosphate conservation in metabolic regulation. Rat liver citrate cleavage enzyme. *J Biol Chem.*, 242(13):3239–3241.

Atkinson, G. C. and Hauryliuk, V. (2012). Evolution and Function of the RelA/SpoT Homologue (RSH) Proteins. *eLS. John Wiley & Sons, Ltd: Chichester.*, DOI:10.1002/9780470015902.a0023959.

Atkinson, G. C., Tenson, T., and Hauryliuk, V. (2011). The RelA/SpoT Homolog (RSH) superfamily: Distribution and functional evolution of ppgpp synthetases and hydrolases across the tree of life. *PLoS ONE*, 6(8):e23479.

Baba, T., Ara, T., Hasegawa, M., Takai, Y., Okumura, Y., Baba, M., Datsenko, K. A., Tomita, M., Wanner, B. L., and Mori, H. (2006). Construction of Escherichia coli K-12 in-frame, single-gene knockout mutants: the Keio collection. *Mol Syst Biol.*, 2:2006 0008.

Babul, J. (1978). Phosphofructokinases from Escherichia coli. Purification and characterization of the nonallosteric isozyme. *J Biol Chem.*, 253(12):4350–4355.

Baker, C. S., Morozov, I., Suzuki, K., Romeo, T., and Babitzke, P. (2002). CsrA regulates glycogen biosynthesis by preventing translation of glgC in Escherichia coli. *Mol Microbiol.*, 44(6):1599–1610.

Barker, M. M., Gaal, T., and Gourse, R. L. (2001a). Mechanism of regulation of transcription initiation by ppGpp. II. Models for positive control based on properties of RNAP mutants and competition for RNAP. *J Mol Biol.*, 305(4):689–702.

Barker, M. M., Gaal, T., Josaitis, C. A., and Gourse, R. L. (2001b). Mechanism of regulation of transcription initiation by ppGpp. I. Effects of ppGpp on transcription initiation in vivo and in vitro. *J Mol Biol.*, 305(4):673–688.

Basan, M., Hui, S., Okano, H., Zhang, Z., Shen, Y., Williamson, J., and Hwa, T. (2015). Overflow metabolism in Escherichia coli results from efficient proteome allocation. *Nature*, 528:99–104.

Bates, D. L., Danson, M. J., Hale, G., Hooper, E. A., and Perham, R. N. (1977). Self-assembly and catalytic activity of the pyruvate dehydrogenase multienzyme complex of Escherichia coli. *Nature*, 268(5618):313–316.

Battesti, A. and Bouveret, E. (2006). Acyl carrier protein/SpoT interaction, the switch linking SpoT-dependent stress response to fatty acid metabolism. *Mol Microbiol.*, 62(4):1048–1063.

Battesti, A., Majdalani, N., and Gottesman, S. (2011). The RpoS-Mediated General Stress Response in Escherichia coli. *Annu Rev Microbiol.*, 65:189–213.

Battesti, A., Majdalani, N., and Gottesman, S. (2015). Stress sigma factor RpoS degradation and translation are sensitive to the state of central metabolism. *Proc Natl Acad Sci USA*, 112(16):5159–5164.

Bennison, D. J., Irving, S. E., and Corrigan, R. M. (2019). The Impact of the Stringent Response on TRAFAC GTPases and Prokaryotic Ribosome Assembly. *Cells*, 8(1313):1–24.

Berg, J. M., Tymoczko, J. L., and Stryer, L. (2003). *Biochemie*. Spektrum Akademischer Verlag GmbH Heidelberg, Berlin - Germany, 5 edition.

Bilder, P., Lightle, S., Bainbridge, G., Ohren, J., Finzel, B., Sun, F., Holley, S., Al-Kassim, L., Spessard, C., Melnick, M., Newcomer, M., and Waldrop, G. L. (2006). The Structure of the Carboxyltransferase Component of Acetyl-CoA Carboxylase Reveals a Zinc-Binding Motif Unique to the Bacterial Enzyme. *Biochemistry*, 45(6):1712–1722.

BioCyc Database Collection (2020). GDP/GTP pyrophosphokinase in Escherichia coli K-12 substr. MG1655 [https://biocyc.org/gene?orgid=ECOLI&id=EG10835#tab=TU]. *SRI International*, Date: 28-01-2020(14:20).

Bjedov, I., Tenaillon, O., Gérard, B., Souza, V., Denamur, E., Radman, M., Taddei, F., and Matic, I. (2003). Stress-Induced Mutagenesis in Bacteria. *Science*, 300(5624):1404–1409.

Blangy, D., Buc, H., and Monod, J. (1968). Kinetics of the allosteric interactions of phosphofructokinase from Escherichia coli. *J Mol Biol.*, 31(1):13–35.

Bledig, S. A., Ramseier, T. M., and Saier, M. H. (1996). FruR mediates catabolite activation of pyruvate kinase (pykF) gene expression in Escherichia coli. *J Bacteriol.*, 178(1):280–283.

Bley Folly, B., Ortega, A. D., Hubmann, G., Bonsing-Vedelaar, S., Wijma, H. J., van der Meulen, P., Milias-Argeitis, A., and Heinemann, M. (2018). Assessment of the interaction between the flux-signaling metabolite fructose-1,6-bisphosphate and the bacterial transcription factors CggR and Cra. *Mol Microbiol.*, 109(3):278–290.

Boecker, S., Zahoor, A., Schramm, T., Link, H., and Klamt, S. (2019). Broadening the Scope of Enforced ATP Wasting as a Tool for Metabolic Engineering in Escherichia coli. *Biotechnol J.*, 14(9):1800438.

Boender, L. G. M., De Hulster, E. A. F., van Maris, A. J. A., Daran-Lapujade, P. A. S., and Pronk, J. T. (2009). Quantitative Physiology of Saccharomyces cerevisiae at Near-Zero Specific Growth Rates. *Appl Environ Microbiol.*, 75(17):5607–5614.

Bokinsky, G., Baidoo, E. E., Akella, S., Burd, H., Weaver, D., Alonso-Gutierrez, J., García-Martín, H., Lee, T. S., and Keasling, J. D. (2013). HipA-triggered growth arrest and beta-lactam tolerance in Escherichia coli are mediated by RelA-dependent ppGpp synthesis. *J Bacteriol.*, 195(14):3173–3182.

Boos, W. and Shuman, H. (1998). Maltose/Maltodextrin System of Escherichia coli: Transport, Metabolism, and Regulation. *Microbiol Mol Biol Rev.*, 62(1):204–229.

Botsford, J. L. and Harman, J. G. (1992). Cyclic AMP in Prokaryotes. *Microbiol Rev.*, 56(1):100–122.

Bougdour, A. and Gottesman, S. (2007). ppGpp regulation of RpoS degradation via anti-adaptor protein IraP. *Proc Natl Acad Sci USA*, 104(31):12896–12901.

Brauer, M. J., Yuan, J., Bennett, B. D., Lu, W., Kimball, E., Botstein, D., and Rabinowitz, J. D. (2006). Conservation of the metabolomic response to starvation across two divergent microbes. *Proc Natl Acad Sci USA*, 103(51):19302–19307.

Britton, R. A. (2009). Role of GTPases in Bacterial Ribosome Assembly. *Annu Rev Microbiol.*, 63(1):155–176.

Brown, D. R. (2019). Nitrogen starvation induces persister cell formation in Escherichia coli. *J Bacteriol.*, 201(3):e00622–18.

Brown, D. R., Barton, G., Pan, Z., Buck, M., and Wigneshweraraj, S. (2014a). Combinatorial stress responses: direct coupling of two major stress responses in Escherichia coli. *Microb Cell*, 1(9):315–317.

Brown, D. R., Barton, G., Pan, Z., Buck, M., and Wigneshweraraj, S. (2014b). Nitrogen stress response and stringent response are coupled in Escherichia coli. *Nat Commun.*, 5(May):4115.

Buchholz, J., Graf, M., Blombach, B., and Takors, R. (2014). Improving the carbon balance of fermentations by total carbon analyses. *Biochem Eng J.*, 90:162–169.

Burgess, R. R. (1971). RNA Polymerase. *Annu Rev Biochem.*, 40(1):711–740.

Burgess, R. R. and Anthony, L. (2001). How sigma docks to RNA polymerase and what sigma does. *Curr Opin Microbiol.*, 4(2):126–131.

Burgess, R. R., Travers, A. A., Dunn, J. J., and Bautz, E. K. (1969). Factor stimulating transcription by RNA polymerase. *Nature*, 221(5175):43–46.

Busby, S. and Ebright, R. H. (1999). Transcription activation by catabolite activator protein (CAP). *J Mol Biol.*, 293:199–213.

Bylund, F., Collet, E., Enfors, S.-O., and Larsson, G. (1998). Substrate gradient formation in the large-scale bioreactor lowers cell yield and increases by-product formation. *Bioprocess Engineering*, 18:171–180.

Calero, P. and Nikel, P. I. (2018). Chasing bacterial chassis for metabolic engineering: a perspective review from classical to non-traditional microorganisms. *Microb Biotechnol.*, 12:98–124.

Carneiro, S., Villas-Bôas, S. G., Ferreira, E. C., and Rocha, I. (2011). Metabolic footprint analysis of recombinant Escherichia coli strains during fed-batch fermentations. *Mol Biosyst.*, 7(3):899–910.

Cases, I., Velázquez, F., and de Lorenzo, V. (2007). The ancestral role of the phosphoenolpyruvate-carbohydrate phosphotransferase system (PTS) as exposed by comparative genomics. *Res Microbiol.*, 158(8-9):666–670.

Cashel, M. and Gallant, J. (1969). Two compounds implicated in the function of the RC gene of Escherichia coli. *Nature*, 221(5183):838–841.

Cashel, M., Gentry, D. R., Hernandez, V. J., and Vinella, D. (1996). The Stringent Response. In Neidhardt, F. C., editor, *Escherichia coli and Salmonella: Cellular and Molecular Biology.*, volume 2, page 2898. American Society for Microbiology.

Causey, T. B., Shanmugam, K. T., Yomano, L. P., and Ingram, L. O. (2004). Engineering Escherichia coli for efficient conversion of glucose to pyruvate. *Proc Natl Acad Sci USA*, 101(8):2235–40.

Causey, T. B., Zhou, S., Shanmugam, K. T., and Ingram, L. O. (2003). Engineering the metabolism of Escherichia coli W3110 for the conversion of sugar to redox-neutral and oxidized products: homoacetate production. *Proc Natl Acad Sci USA*, 100(3):825–832.

Cavanagh, A. T., Chandrangsu, P., and Wassarman, K. M. (2010). 6S RNA regulation of relA alters ppGpp levels in early stationary phase. *Microbiology*, 156(Pt 12):3791–3800.

Chatterji, D., Fujita, N., and Ishihama, A. (1998). The mediator for stringent control, ppGpp, binds to the beta-subunit of Escherichia coli RNA polymerase. *Genes Cells*, 3(5):279–287.

Chatterji, D. and Ojha, A. K. (2001). Revisiting the stringent response, ppGpp and starvation signaling. *Curr Opin Microbiol.*, 4(2):160–165.

Chavarría, M. and de Lorenzo, V. (2018). The imbroglio of the physiological Cra effector clarified at last. *Mol Microbiol.*, 109(3):273–277.

Chavarría, M., Santiago, C., Platero, R., Krell, T., Casasnovas, J. M., and de Lorenzo, V. (2011). Fructose 1-Phosphate Is the Preferred Effector of the Metabolic Regulator Cra of Pseudomonas putida. *J Biol Chem.*, 286(11):9351–9359.

Chi, H., Wang, X., Shao, Y., Qin, Y., Deng, Z., Wang, L., and Chen, S. (2019). Engineering and modification of microbial chassis for systems and synthetic biology. *Synth Syst Biotechnol.*, 4(1):25–33.

Chmiel, H. (2011). *Bioprozesstechnik*. Spektrum Akademischer Verlag Heidelberg, Heidelberg - Germany, 3 edition.

Chubukov, V., Desmarais, J. J., Wang, G., Chan, L. J. G., Ek Baidoo, E., Petzold, C. J., Keasling, J. D., and Mukhopadhyay, A. (2017). Engineering glucose metabolism of Escherichia coli under nitrogen starvation. *NPJ Syst Biol Appl.*, 3:1–7.

Chubukov, V. and Sauer, U. (2014). Environmental Dependence of Stationary-Phase Metabolism in Bacillus subtilis and Escherichia coli. *Appl Environ Microbiol.*, 80(9):2901–2909.

Cortay, J. C., Bleicher, F., Duclos, B., Cenatiempo, Y., Gautier, C., Prato, J. L., and Cozzone, A. J. (1989). Utilization of acetate in Escherichia coli: structural organization and differential expression of the ace operon. *Biochimie*, 71(9-10):1043–1049.

Cozzone, A. J. and El-Mansi, M. (2006). Control of isocitrate dehydrogenase catalytic activity by protein phosphorylation in Escherichia coli. *J Mol Microbiol Biotechnol.*, 9(3-4):132–146.

Crater, J. S. and Lievense, J. C. (2018). Scale-up of industrial microbial processes. *FEMS Microbiology Letters*, 365(13).

Cserjan-Puschmann, M., Kramer, W., Duerrschmid, E., Striedner, G., and Bayer, K. (1999). Metabolic approaches for the optimisation of recombinant fermentation processes. *Appl Microbiol Biotechnol.*, 53(1):43–50.

Csörgő, B., Nyerges, Á., Pósfai, G., and Fehér, T. (2016). System-level genome editing in microbes. *Curr Opin Microbiol.*, 33:113–122.

Dalebroux, Z. D. and Swanson, M. S. (2012). ppGpp: magic beyond RNA polymerase. *Nat Rev Microbiol.*, 10(3):203–212.

Datsenko, K. A. and Wanner, B. L. (2000). One-step inactivation of chromosomal genes in Escherichia coli K-12 using PCR products. *Proc Natl Acad Sci USA*, 97(12):6640–6645.

Death, A. and Ferenci, T. (1994). Between Feast and Famine: Endogenous Inducer Synthesis in the Adaptation of Escherichia coli to Growth with Limiting Carbohydrates. *J Bacteriol.*, 176(16):5101–5107.

Dedhia, N., Richins, R., Mesina, A., and Chen, W. (1997). Improvement in recombinant protein production in ppGpp-deficient Escherichia coli. *Biotechnol Bioeng.*, 53(4):379–386.

Deutscher, J., Francke, C., and Postma, P. W. (2006). How Phosphotransferase System-Related Protein Phosphorylation Regulates Carbohydrate Metabolism in Bacteria. *Microbiol Mol Biol Rev.*, 70(4):939–1031.

Dietzler, D. N., Leckie, M. P., and Lais, C. J. (1973). Rates of glycogen synthesis and the cellular levels of ATP and FDP during exponential growth and the nitrogen-limited

stationary phase of Escherichia coli W4597 (K). *Arch Biochem Biophys.*, 156(2):684–693.

Dix, D. B. and Thompson, R. C. (1986). Elongation factor Tu-guanosine 3'-diphosphate 5'-diphosphate complex increases the fidelity of proofreading in protein biosynthesis: Mechanism for reducing translational errors introduced by amino acid starvation. *Proc Natl Acad Sci USA*, 83:2027–2031.

Dong, T., Kirchhof, M. G., and Schellhorn, H. E. (2008). RpoS regulation of gene expression during exponential growth of Escherichia coli K12. *Mol Genet Genomics*, 279(3):267–277.

Durfee, T., Hansen, A. M., Zhi, H., Blattner, F. R., and Jin, D. J. (2008). Transcription profiling of the stringent response in Escherichia coli. *J Bacteriol.*, 190(3):1084–1096.

Dykhuizen, D. (1978). Selection for Tryptophan Auxotrophs of Escherichia coli in Glucose-Limited Chemostats as a Test of the Energy Conservation Hypothesis of Evolution. *Evolution*, 32:125–150.

Edwards, A. N., Patterson-Fortin, L. M., Vakulskas, C. A., Mercante, J. W., Potrykus, K., Vinella, D., Camacho, M. I., Fields, J. A., Thompson, S. A., Georgellis, D., Cashel, M., Babitzke, P., and Romeo, T. (2011). Circuitry linking the Csr and stringent response global regulatory systems. *Mol Microbiol.*, 80(6):1561–1580.

Egli, T. (2015). Microbial growth and physiology: A call for better craftsmanship. *Front Microbiol.*, 6:1–12.

Elf, J. and Ehrenberg, M. (2005). Near-critical behavior of aminoacyl-tRNA pools in E. coli at rate-limiting supply of amino acids. *Biophys J.*, 88(1):132–146.

Enfors, S.-O., Jahic, M., Rozkov, A., Xu, B., Hecker, M., Jürgen, B., Krüger, E., Schweder, T., Hamer, G., O'Beirne, D., Noisommit-Rizzi, N., Reuss, M., Boone, L., Hewitt, C., McFarlane, C., Nienow, A., Kovacs, T., Trägårdh, C., Fuchs, L., Revstedt, J., Friberg, P., Hjertager, B., Blomsten, G., Skogman, H., Hjort, S., Hoeks, F., Lin, H.-Y., Neubauer, P., van der Lans, R., Luyben, K., Vrabel, P., and Manelius, Å. (2001).

Physiological responses to mixing in large scale bioreactors. *J Biotechnol.*, 85(2):175–185.

English, B. P., Hauryliuk, V., Sanamrad, A., Tankov, S., Dekker, N. H., and Elf, J. (2011). Single-molecule investigations of the stringent response machinery in living bacterial cells. *Proc Natl Acad Sci USA*, 108(31):E365–73.

Ereky, K. (1919). *Biotechnologie der Fleisch-, Fett-, und Milcherzeugung im landwirtschaftlichen Grossbetriebe: für naturwissenschaftlich gebildete Landwirte verfasst.* P. Parey, Berlin.

Ferenci, T. (2001). Hungry bacteria - Definition and properties of a nutritional state. *Environ Microbiol.*, 3(10):605–611.

Filutowicz, M., McEachern, M. J., and Helinski, D. R. (1986). Positive and negative roles of an initiator protein at an origin of replication. *Proc Natl Acad Sci USA*, 83(24):9645–9.

Flores, N., Escalante, A., Anda de, R., Báez-Viveros, J., Merino, E., Franco, B., Georgellis, D., Gosset, G., and Bolívar, F. (2008). New Insights into the Role of Sigma Factor RpoS as Revealed in Escherichia coli Strains Lacking the strain including most glycolytic genes. *J Mol Microbiol Biotechnol.*, 14:176–192.

Flores, S., Gosset, G., Flores, N., De Graaf, A. A., and Bolívar, F. (2002). Analysis of Carbon Metabolism in Escherichia coli Strains with an Inactive Phosphotransferase System by ^{13}C Labeling and NMR Spectroscopy. *Metab Eng.*, 4:124–137.

Folsom, J. P. and Carlson, R. P. (2015). Physiological, biomass elemental composition and proteomic analyses of Escherichia coli ammoniumlimited chemostat growth, and comparison with iron- and glucose-limited chemostat growth. *Microbiology*, 161(8):1659–1670.

Förster, A. H. and Gescher, J. (2014). Metabolic Engineering of Escherichia coli for Production of Mixed-Acid Fermentation End Products. *Front Bioeng Biotechnol.*, 2(16):1–12.

Foster, P. L. (2007). Stress-Induced Mutagenesis in Bacteria. *Crit Rev Biochem Mol Biol.*, 42(5):373–397.

Freundlieb, S. and Boos, W. (1986). Alpha-amylase of Escherichia coli, mapping and cloning of the structural gene, malS, and identification of its product as a periplasmic protein. *J Biol Chem.*, 261(6):2946–2953.

Frick, D. N. and Richardson, C. C. (2001). DNA Primases. *Annu Rev Biochem.*, 70(1):39–80.

Fuchs, R. P., Fujii, S., and Wagner, J. (2004). Properties and Functions of Escherichia coli: Pol IV and Pol V. *Adv Protein Chem.*, 69:229–264.

Fuhrer, T., Fischer, E., and Sauer, U. (2005). Experimental identification and quantification of glucose metabolism in seven bacterial species. *Society*, 187(5):1581–1590.

Gallant, J., Irr, J., and Cashel, M. (1971). The Mechanism of Amino Acid Control of Guanylate and Adenylate Biosynthesis. *J Biol Chem.*, 246(18):5812–5816.

Gentry, D. R. and Cashel, M. (1996). Mutational analysis of the Escherichia coli spoT gene identifies distinct but overlapping regions involved in ppGpp synthesis and degradation. *Mol Microbiol.*, 19(6):1373–1384.

Gentry, D. R., Hernandez, V. J., Nguyen, L. H., Jensen, D. B., and Cashel, M. (1993). Synthesis of the stationary-phase sigma factor σ^{S} is positively regulated by ppGpp. *J Bacteriol.*, 175(24):7982–7989.

Gerdes, K. and Maisonneuve, E. (2012). Bacterial Persistence and Toxin-Antitoxin Loci. *Annu Rev Microbiol.*, 66:103–123.

Germain, E., Castro-Roa, D., Zenkin, N., and Gerdes, K. (2013). Molecular mechanism of bacterial persistence by HipA. *Mol Cell*, 52(2):248–254.

Gibson, D. G. (2011). Enzymatic assembly of overlapping DNA fragments. *Methods Enzym.*, 498:349–361.

Görke, B. and Stülke, J. (2008). Carbon catabolite repression in bacteria: Many ways to make the most out of nutrients. *Nat Rev Microbiol.*, 6(8):613–624.

Gourse, R. L., Chen, A. Y., Gopalkrishnan, S., Sanchez-Vazquez, P., Myers, A., and Ross, W. (2018). Transcriptional Responses to ppGpp and DksA. *Annu Rev Microbiol.*, 72:163–184.

Govons, S., Vinopal, R., Ingraham, J., and Preiss, J. (1969). Isolation of Mutants of Escherichia coli B Altered in Their Ability to Synthesize Glycogen. *J Bacteriol.*, 97(2):970–972.

Groat, R. G., Schultz, J. E., Zychlinsky, E., Bockman, A., and Matin, A. (1986). Starvation Proteins in Escherichia coli: Kinetics of Synthesis and Role in Starvation Survival. *J Bacteriol.*, 168(2):486–493.

Gropp, M., Strausz, Y., Gross, M., and Glaser, G. (2001). Regulation of Escherichia coli RelA requires oligomerization of the C-terminal domain. *J Bacteriol.*, 183(2):570–579.

Gruber, T. M. and Gross, C. A. (2003). Multiple Sigma Subunits and the Partitioning of Bacterial Transcription Space. *Annu Rev Microbiol.*, 57(1):441–466.

Hädicke, O., Bettenbrock, K., and Klamt, S. (2015). Enforced ATP futile cycling increases specific productivity and yield of anaerobic lactate production in Escherichia coli. *Biotechnol Bioeng.*, 112(10):2195–2199.

Hansen, S., Vulić, M., Jungki, M., Yen, T.-J., Schumacher, M. A., Brennan, R. G., and Lewis, K. (2012). Regulation of the Escherichia coli HipBA Toxin-Antitoxin System by Proteolysis. *PLoS One*, 7(6):e39185.

Hara, K. Y. and Kondo, A. (2015). ATP regulation in bioproduction. *Microb Cell Fact.*, 14:198.

Harcum, S. W. and Bentley, W. E. (1999). Heat-Shock and Stringent Responses Have Overlapping Protease Activity in Escherichia coli. *Appl Biochem Biotechnol.*, 80:23–37.

Hardiman, T., Lemuth, K., Keller, M. A., Reuss, M., and Siemann-Herzberg, M. (2007). Topology of the global regulatory network of carbon limitation in Escherichia coli. *J Biotechnol.*, 132(4):359–374.

Harshman, R. B. and Yamazaki, H. (1971). Formation of ppGpp in a relaxed and stringent strain of Escherichia coli during diauxie lag. *Biochemistry*, 10(21):3980–3982.

Haseltine, W. A. and Block, R. (1973). Synthesis of guanosine tetra- and pentaphosphate requires the presence of a codon-specific, uncharged transfer ribonucleic acid in the acceptor site of ribosomes. *Proc Natl Acad Sci USA*, 70(5):1564–1568.

Hauryliuk, V., Atkinson, G. C., Murakami, K. S., Tenson, T., and Gerdes, K. (2015). Recent functional insights into the role of (p)ppGpp in bacterial physiology. *Nat Rev Microbiol.*, 13(5):298–309.

Heath, R. J., Jackowski, S., and Rock, C. . (1994). Guanosine Tetraphosphate Inhibition of Fatty Acid and Phospholipid Synthesis in Escherichia coli Is Relieved by Overexpression of Glycerol-3-phosphate Acyltransferase (plsB)*. *J Biol Chem.*, 269(42):26584–26590.

Helling, R. B. (1994). Why does Escherichia coli have two primary pathways for synthesis of glutamate? *J Bacteriol.*, 176(15):4664–4668.

Helling, R. B. (1998). Pathway choice in glutamate synthesis in Escherichia coli. *J Bacteriol.*, 180(17):4571–4575.

Herbert, D. (1958). Some principles of continuous culture. In *Recent Progress in Microbiology, VII Intern. Congr. for Microbiology*, pages 381–396. Tunevall, G, Stockholm.

Herring, C. D., Glasner, J. D., and Blattner, F. R. (2003). Gene replacement without selection: Regulated suppression of amber mutations in Escherichia coli. *Gene*, 311(1-2):153–163.

Hinkle, D. C. and Chamberlin, M. J. (1972). Studies of the binding of Escherichia coli RNA polymerase to DNA. I. The role of sigma subunit in site selection. *J Mol Biol.*, 70(2):157–185.

Hofmann, N., Wurm, R., and Wagner, R. (2011). The E. coli anti-sigma factor Rsd: studies on the specificity and regulation of its expression. *PLoS One*, 6(5):e19235.

Hofmeyr, J.-H. S. and Cornish-Bowden, A. (2000). Regulating the cellular economy of supply and demand. *FEBS Letters*, 476(1-2):47–51.

Hogema, B. M., Arents, J. C., Bader, R., Eijkemans, K., Yoshida, H., Takahashi, H., Aiba, H., and Postma, P. W. (1998). Inducer exclusion in Escherichia coli by non-PTS substrates: the role of the PEP to pyruvate ratio in determining the phosphorylation state of enzyme IIAGlc. *Mol Microbiol.*, 30(3):487–498.

Holm, A. K., Blank, L. M., Oldiges, M., Schmid, A., Solem, C., Jensen, P. R., and Vemuri, G. N. (2010). Metabolic and transcriptional response to cofactor perturbations in Escherichia coli. *J Biol Chem.*, 285(23):17498–17506.

Holme, T. and Palmstierna, H. (1956). Changes in glycogen and nitrogen-containing compounds in Escherichia coli B during growth in deficient media II. Phosphorus and sulphur starvation. *Acta Chem Scand.*, 10:1553–1556.

Holms, H. (1996). Flux analysis and control of the central metabolic pathways in Escherichia coli. *FEMS Microbiol Rev.*, 19:85–116.

Hua, Q., Yang, C., Oshima, T., Mori, H., and Shimizu, K. (2004). Analysis of Gene Expression in Escherichia coli in Response to Changes of Growth-Limiting Nutrient in Chemostat Cultures. *Appl Environ Microbiol.*, 70(4):2354–2366.

Hunt, T. P. and Magasanik, B. (1985). Transcription of glnA by purified Escherichia coli components: Core RNA polymerase and the products of glnF, glnG, and glnL. *Proc Natl Acad Sci USA*, 82(24):8453–8457.

Hunter, I. S. and Kornberg, H. L. (1979). Glucose Transport of Escherichia coli Growing in Glucose-Limited Continuous Culture. *Biochem J.*, 178(1):97–101.

Ilag, L. L., Westblade, L. F., Deshayes, C., Kolb, A., Busby, S. J. W., and Robinson,

C. V. (2004). Mass Spectrometry of Escherichia coli RNA Polymerase: Interactions of the Core Enzyme with σ^{70} and Rsd Protein. *Structure*, 12:269–275.

Imaizumi, A., Kojima, H., and Matsui, K. (2006). The effect of intracellular ppGpp levels on glutamate and lysine overproduction in Escherichia coli. *J Biotechnol.*, 125(3):328–337.

Ingledew, W. J. and Poole, R. K. (1984). The Respiratory Chains of Escherichia coli. *Microbiol Rev.*, 48(3):222–271.

Irving, S. E. and Corrigan, R. M. (2018). Triggering the stringent response: Signals responsible for activating (p)ppGpp synthesis in bacteria. *Microbiology*, 164(3):268–276.

Izui, K., Taguchi, M., Morikawa, M., and Katsuki, H. (1981). Regulation of Escherichia coli Phosphoenolpyruvate Carboxylase by Multiple Effectors In Vivo . II. Kinetic Studies with a Reaction System Containing Physiological Concentrations of Ligands. *J Biochem.*, 90(5):1321–1331.

Jain, V., Saleem-Batcha, R., China, A., and Chatterji, D. (2006). Molecular dissection of the mycobacterial stringent response protein Rel. *Protein Sci.*, 15(6):1449–1464.

Jinek, M., Chylinski, K., Fonfara, I., Hauer, M., Doudna, J. A., and Charpentier, E. (2012). A Programmable Dual-RNA–Guided DNA Endonuclease in Adaptive Bacterial Immunity. *Science*, 337(August):816–822.

Jishage, M., Kvint, K., Shingler, V., and Nyström, T. (2002). Regulation of sigma factor competition by the alarmone ppGpp. *Genes Dev.*, 16(10):1260–1270.

Junker, B. H. (2004). Scale-up methodologies for Escherichia coli and yeast fermentation processes. *J Biosci Bioeng.*, 97(6):347–364.

Kameshita, I., Tokushige, M., and Katsuki, H. (1978). Phosphoenolpyruvate carboxylase of Escherichia coli: Essential arginyl residues for catalytic and regulatory functions. *J Biol Chem.*, 84(4):795–803.

Kang, P. J. and Craig, E. A. (1990). Identification and characterization of a new Escherichia coli gene that is a dosage-dependent suppressor of a dnaK deletion mutation. *J Bacteriol.*, 172(4):2055–2064.

Kanjee, U., Ogata, K., and Houry, W. A. (2012). Direct binding targets of the stringent response alarmone (p)ppGpp. *Mol Microbiol.*, 85(6):1029–1043.

Keck, J. L., Roche, D. D., Lynch, A. S., and Berger, J. M. (2000). Structure of the RNA polymerase domain of E. coli primase. *Science*, 287(5462):2482–2486.

Kim, D., Kwon, Y.-K., and Cho, K.-H. (2007). Coupled positive and negative feedback circuits form an essential building block of cellular signaling pathways. *BioEssays*, 29(1):85–90.

Kim, K., Choe, D., Lee, D. H., and Cho, B. K. (2020). Engineering biology to construct microbial chassis for the production of difficult-to-express proteins. *Int J Mol Sci.*, 21(990):1–25.

Koch, A. L. (1971). The Adaptive Responses of Escherichia coli to a Feast and Famine Existence. *Adv Microb Physiol.*, 6:147–217.

Koebmann, B. J., Westerhoff, H. V., Snoep, J. L., Nilsson, D., and Jensen, P. R. (2002). The glycolytic flux in Escherichia coli is controlled by the demand for ATP. *J Bacteriol.*, 184(14):3909–3916.

Korch, S. B., Henderson, T. A., and Hill, T. M. (2003). Characterization of the hipA7 allele of Escherichia coli and evidence that high persistence is governed by (p)ppGpp synthesis. *Mol Microbiol.*, 50(4):1199–1213.

Kornberg, H. and Malcovati, M. (1973). Control in situ of the pyruvate kinase activity of Escherichia coli. *FEBS Letters*, 32(2):257–259.

Koschorreck, M. (2005). Microorganisms in Their Natural Environment. In J. H. Lehr and Keeley, J., editors, *Water Encyclopedia*, pages 309–313. John Wiley & Sons, Inc., Hoboken, NJ, USA.

Kumar, R. and Shimizu, K. (2010). Metabolic regulation of Escherichia coli and its gdhA, glnL, gltB, D mutants under different carbon and nitrogen limitations in the continuous culture. *Microb Cell Fact.*, 9(8):1–17.

Kuschel, M., Siebler, F., and Takors, R. (2017). Lagrangian Trajectories to Predict the Formation of Population Heterogeneity in Large-Scale Bioreactors. *Bioengineering*, 4(27):1–13.

Lange, R., Fischer, D., and Hengge-Aronis, R. (1995). Identification of Transcriptional Start Sites and the Role of ppGpp in the Expression of rpoS, the Structural Gene for the σ^s Subunit of RNA Polymerase in Escherichia coli. *J Bacteriol.*, 177(16):4676–4680.

Langheinrich, C. and Nienow, A. W. (1999). Control of pH in large-scale, free suspension animal cell bioreactors: Alkali addition and pH excursions. *Biotechnol Bioeng.*, 66(3):171–179.

LaPorte, D. C., Walsh, K., and Koshland, D. E. (1984). The Branch Point Effect: Ultrasensitivity and subsensitivity to metabolic control. *J Biol Chem.*, 259(22):14068–14075.

Lecker, D. N., Kumari, S., and Khan, A. (1997). Iodine binding capacity and iodine binding energy of glycogen. *Journal of Polymer Science Part A -Polymer Chemistry*, 35(8):1409–1412.

Lee, S. Y. and Kim, H. U. (2015). Systems strategies for developing industrial microbial strains. *Nat Biotechnol.*, 33(10):1061–72.

Lehman, I. R., Bessman, M. J., Simms, E. S., and Kornberg, A. (1958). Enzymatic Synthesis of Deoxyribonucleic Acid. I. Preparation of substrates and partial purification of an enzyme from Escherichia coli. *J Biol Chem.*, 233:163–170.

Leipe, D. D., Wolf, Y. I., Koonin, E. V., and Aravind, L. (2002). Classification and evolution of P-loop GTPases and related ATPases. *J Mol Biol.*, 317(1):41–72.

Lemuth, K., Hardiman, T., Winter, S., Pfeiffer, D., Keller, M. A., Lange, S., Reuss, M., Schmid, R. D., and Siemann-Herzberg, M. (2008). Global transcription and metabolic

flux analysis of Escherichia coli in glucose-limited fed-batch cultivations. *Appl Environ Microbiol.*, 74(22):7002–7015.

Lengeler, J. W., Drews, G., and Schlegel, H. G. (1999). *Biology of the Prokaryotes*. Georg Thieme Verlag, Stuttgart (Germany).

Lin, C. Y., Awano, N., Masuda, H., Park, J. H., and Inouye, M. (2013). Transcriptional repressor HipB regulates the multiple promoters in Escherichia coli. *J Mol Microbiol Biotechnol.*, 23(6):440–447.

Lin, H., Bennett, G. N., and San, K. Y. (2005). Metabolic engineering of aerobic succinate production systems in Escherichia coli to improve process productivity and achieve the maximum theoretical succinate yield. *Metab Eng.*, 7(2):116–127.

Link, A. J., Phillips, D., and Church, G. M. (1997). Methods for generating precise deletions and insertions in the genome of wild-type Escherichia coli: application to open reading frame characterization. *J Bacteriol.*, 179(20):6228–6237.

Little, R. R. (1957). Permanent Staining with Iodine Vapor. *Stain Technology*, 32(1):7–9.

Liu, M. Y., Yang, H., and Romeo, T. (1995). The Product of the Pleiotropic Escherichia coli Gene csrA Modulates Glycogen Biosynthesis via Effects on mRNA Stability. *J Bacteriol.*, 177(10):2663–2672.

Lobry, J. R., Flandrois, J. P., Carret, G., and Pave, A. (1992). Monod's bacterial growth model revisited. *Bull Math Biol.*, 54(1):117–122.

Löffler, M., Simen, J. D., Jäger, G., Schäferhoff, K., Freund, A., and Takors, R. (2016). Engineering E. coli for large-scale production – Strategies considering ATP expenses and transcriptional responses. *Metab Eng.*, 38:73–85.

Löffler, M., Simen, J. D., Müller, J., Jäger, G., Laghrami, S., Schäferhoff, K., Freund, A., and Takors, R. (2017). Switching between nitrogen and glucose limitation: Unraveling transcriptional dynamics in Escherichia coli. *J Biotechnol.*, 258:2–12.

Maciąg, M., Kochanowska, M., Łyżeń, R., Węgrzyn, G., and Szalewska-Pałasz, A. (2010). ppGpp inhibits the activity of Escherichia coli DnaG primase. *Plasmid*, 63(1):61–67.

Magasanik, B. (1993). The regulation of nitrogen utilization in enteric bacteria. *J Cell Biochem.*, 51(1):34–40.

Magnusson, L. U., Farewell, A., and Nyström, T. (2005). ppGpp: a global regulator in Escherichia coli. *Trends Microbiol.*, 13(5):236–242.

Magnusson, L. U., Gummesson, B., Joksimović, P., Farewell, A., and Nyström, T. (2007). Identical, independent, and opposing roles of ppGpp and DksA in Escherichia coli. *J Bacteriol.*, 189(14):5193–5202.

Maharjan, R. P. and Ferenci, T. (2017). A shifting mutational landscape in 6 nutritional states: Stress-induced mutagenesis as a series of distinct stress input-mutation output relationships. *PLoS Biology*, 15(6):e2001477.

Maisonneuve, E., Castro-Camargo, M., and Gerdes, K. (2013). (p)ppGpp Controls Bacterial Persistence by Stochastic Induction of Toxin-Antitoxin Activity. *Cell*, 154(5):1140–1150.

Malan, T., Kolb, A., Buc, H., and McClure, W. R. (1984). Mechanism of CRP-cAMP Activation of lac Operon Transcription Initiation Activation of the P1 Promoter. *J Mol Biol.*, 180:881–909.

Maleki, N. and Eiteman, M. A. (2017). Recent progress in the microbial production of pyruvic acid. *Fermentation*, 3(1):1–17.

Maloy, S. R., Stewart, V. J., and Taylor, R. K. (1996). *Genetic Analysis of Pathogenic Bacteria: A Laboratory Manual*. Cold Spring Harbor Laboratory Press, NY.

Mandel, M. J. and Silhavy, T. J. (2005). Starvation for different nutrients in Escherichia coli results in differential modulation of RpoS levels and stability. *J Bacteriol.*, 187(2):434–442.

Mao, X. J., Huo, Y. X., Buck, M., Kolb, A., and Wang, Y. P. (2007). Interplay between CRP-cAMP and PII-Ntr systems forms novel regulatory network between carbon metabolism and nitrogen assimilation in Escherichia coli. *Nucleic Acids Res.*, 35(5):1432–1440.

Marisch, K., Bayer, K., Cserjan-Puschmann, M., Luchner, M., and Striedner, G. (2013). Evaluation of three industrial Escherichia coli strains in fed-batch cultivations during high-level SOD protein production. *Microb Cell Fact.*, 12(58):1–11.

Markus, M., Plesser, T., Boiteux, A., Hess, B., and Malcovatit, M. (1980). Analysis of progress curves: Rate Law of Pyruvate Kinase Type I from Eschericha coli. *Biochem J.*, 189:421–433.

Martínez-García, E. and de Lorenzo, V. (2011). Engineering multiple genomic deletions in Gram-negative bacteria: Analysis of the multi-resistant antibiotic profile of Pseudomonas putida KT2440. *Environ Microbiol.*, 13(10):2702–2716.

Martínez-García, E. and De Lorenzo, V. (2012). Transposon-based and plasmid-based genetic tools for editing genomes of gram-negative bacteria. *Methods Mol Biol.*, 813:267–283.

Maurizi, M. R. and Rasulova, F. (2002). Degradation of L-glutamate dehydrogenase from Escherichia coli: Allosteric regulation of enzyme stability. *Arch Biochem Biophys.*, 397(2):206–216.

Mayer, C. and Boos, W. (2005). Hexose/Pentose and Hexitol/Pentitol Metabolism. *EcoSal Plus*, 1(2).

Mechold, U., Potrykus, K., Murphy, H., Murakami, K. S., and Cashel, M. (2013). Differential regulation by ppGpp versus pppGpp in Escherichia coli. *Nucleic Acids Res.*, 41(12):6175–6189.

Meek, T. D. and Villafranca, J. J. (1980). Kinetic Mechanism of Escherichia coli Glutamine Synthetase. *Biochemistry*, 19(24):5513–5519.

Meng, J., Wang, B., Liu, D., Chen, T., Wang, Z., and Zhao, X. (2016). High-yield anaerobic succinate production by strategically regulating multiple metabolic pathways based on stoichiometric maximum in Escherichia coli. *Microb Cell Fact.*, 15(141):1–13.

Merlie, J. P. and Pizer, L. I. (1973). Regulation of Phospholipid Synthesis in Escherichia coli by Guanosine Tetraphosphate. *J Bacteriol.*, 116(1):355–366.

Merrick, M. J. and Edwards, R. A. (1995). Nitrogen control in bacteria. *Microbiol Rev.*, 59(4):604–622.

Metzger, S., Dror, I. B., Aizenman, E., Schreiber, G., Toone, M., Friesen, J. D., Cashel, M., and Glaser, G. (1988). The nucleotide sequence and characterization of the relA gene of Escherichia coli. *J Biol Chem.*, 263(30):15699–15704.

Michalowski, A., Siemann-Herzberg, M., and Takors, R. (2016). Bacterial strain and method for high throughput of sugar in the microbial conversion into biosynthetic products. *Patent Application*, Eur. Union/WO Patent(EP 3239291 A1/WO2017186327 A1).

Michalowski, A., Siemann-Herzberg, M., and Takors, R. (2017). Escherichia coli HGT: Engineered for high glucose throughput even under slowly growing or resting conditions. *Metab Eng.*, 40:93–103.

Milon, P., Tischenko, E., Tomšic, J., Caserta, E., Folkers, G., La Teana, A., Rodnina, M. V., Pon, C. L., Boelens, R., and Gualerzi, C. O. (2006). The nucleotide-binding site of bacterial translation initiation factor 2 (IF2) as a metabolic sensor. *Proc Natl Acad Sci USA*, 103(38):13962–13967.

Mitkevich, V. A., Ermakov, A., Kulikova, A. A., Tankov, S., Shyp, V., Soosaar, A., Tenson, T., Makarov, A. A., Ehrenberg, M., and Hauryliuk, V. (2010). Thermodynamic characterization of ppGpp binding to EF-G or IF2 and of initiator tRNA binding to free IF2 in the presence of GDP, GTP, or ppGpp. *J Mol Biol.*, 402:838–846.

Mittenhuber, G. (2001). Comparative genomics and evolution of genes encoding bacterial

(p)ppGpp synthetases/hydrolases (the Rel, RelA and SpoT proteins). *J Mol Microbiol Biotechnol.*, 3(4):585–600.

Moats, W. A. (1971). Kinetics of Thermal Death of Bacteria. *J Bacteriol.*, 105(1):165–171.

Monod, J. (1942). *Recherches sur la croissance des cultures bacteriennes.* Hermann, Paris.

Monod, J. (1949). The Growth of Bacterial Cultures. *Annu Rev Microbiol.*, 3:371–394.

Montero, M., Rahimpour, M., Viale, A. M., Almagro, G., Eydallin, G., Sevilla, A., Cánovas, M., Bernal, C., Lozano, A. B., Muñoz, F. J., Baroja-Fernández, E., Bahaji, A., Mori, H., Codoñer, F. M., and Pozueta-Romero, J. (2014). Systematic Production of Inactivating and Non- Inactivating Suppressor Mutations at the relA Locus That Compensate the Detrimental Effects of Complete spoT Loss and Affect Glycogen Content in Escherichia coli. *PLoS One*, 9(9):e106938.

Morán-Zorzano, M. T., Viale, A. M., Muñoz, F. J., Alonso-Casajús, N., Eydallín, G. G., Zugasti, B., Baroja-Fernández, E., and Pozueta-Romero, J. (2007). Escherichia coli AspP activity is enhanced by macromolecular crowding and by both glucose-1,6-bisphosphate and nucleotide-sugars. *FEBS Letters*, 581(5):1035–1040.

Moreno-Bruna, B., Baroja-Fernández, E., Muñoz, F. J., Bastarrica-Berasategui, A., Zandueta-Criado, A., Rodríguez-López, M., Lasa, I., Akazawa, T., and Pozueta-Romero, J. (2001). Adenosine diphosphate sugar pyrophosphatase prevents glycogen biosynthesis in Escherichia coli. *PNAS*, 98(14):8128–8132.

Mülhardt, C. (2008). *Der Experimentator: Molekularbiologie / Genomics.* Spektrum Akademischer Verlag, Heidelberg - Germany, 6 edition.

Müller, S., Harms, H., and Bley, T. (2010). Origin and analysis of microbial population heterogeneity in bioprocesses. *Curr Opin Biotechnol.*, 21:100–113.

Muñoz, M. E. and Ponce, E. (2003). Pyruvate kinase: Current status of regulatory and functional properties. *Comparative Biochemistry and Physiology Part B: Biochemistry and Molecular Biology*, 135(2):197–218.

Murray, K. D. and Bremer, H. (1996). Control of spoT-dependent ppGpp synthesis and degradation in Escherichia coli. *J Mol Biol.*, 259(1):41–57.

Nakagawa, A., Oshima, T., and Mori, H. (2006). Identification and characterization of a second, inducible promoter of relA in Escherichia coli. *Genes Genet Syst.*, 81(5):299–310.

Neidhardt, F. C., Curtiss, R. I., Ingraham, J. L., Lin, E. C. C., Low, K. B., Magasanik, B., Reznikoff, W. S., Riley, M., Schaechter, M., and Umbarger, H. E. (1996). *Escherichia coli and Salmonella: Cellular and Molecular Biology.* ASM Press, Washington, D.C., 2 edition.

Neubauer, P., Cruz, N., Glauche, F., Junne, S., Knepper, A., and Raven, M. (2013). Consistent development of bioprocesses from microliter cultures to the industrial scale. *Eng Life Sci.*, 13:224–238.

Ninfa, A. J., Jiang, P., Atkinson, M. R., and Peliska, J. A. (2001). Integration of antagonistic signals in the regulation of nitrogen assimilation in Escherichia coli. *Curr Top Cell Regul.*, 36(C):31–75.

Noda, S., Takezawa, Y., Mizutani, T., Asakura, T., Nishiumi, E., Onoe, K., Wada, M., Tomita, F., Matsushita, K., and Yokota, A. (2006). Alterations of Cellular Physiology in Escherichia coli in Response to Oxidative Phosphorylation Impaired by Defective F_1-ATPase. *J Bacteriol.*, 188(19):6869–6876.

Notley, L. and Ferenci, T. (1995). Differential expression of mal genes under cAMP and endogenous inducer control in nutrient-stressed Escherichia coli. *Mol Microbiol.*, 16(1):121–129.

Notley, L. and Ferenci, T. (1996). Induction of RpoS-Dependent Functions in Glucose-Limited Continuous Culture: What Level of Nutrient Limitation Induces the Stationary Phase of Escherichia coli? *J Bacteriol.*, 178(5):1465–1468.

Notley-Mcrobb, L., Death, A., and Ferenci, T. (1997). The relationship between external glucose concentration and cAMP levels inside Escherichia coli: implications for

models of phosphotransferase-mediated regulation of adenylate cyclase. *Microbiology*, 143:1909–1918.

Notley-Mcrobb, L., King, T., and Ferenci, T. (2002). rpoS Mutations and Loss of General Stress Resistance in Escherichia coli Populations as a Consequence of Conflict between Competing Stress Responses. *J Bacteriol.*, 184(3):806–811.

Nowicki, D., Maciąg-Dorszyńska, M., Kobiela, W., Herman-Antosiewicz, A., Węgrzyn, A., Szalewska-Pałasz, A., and Węgrzyn, G. (2014). Phenethyl isothiocyanate inhibits Shiga toxin production in enterohemorrhagic Escherichia coli by stringent response induction. *Antimicrob Agents Chemother.*, 58(4):2304–2315.

Nyström, T. (2004). Growth versus maintenance: a trade-off dictated by RNA polymerase availability and sigma factor competition? *Mol Microbiol.*, 54(4):855–862.

OECD (1999). Modern Biotechnology and the OECD [Date:28-01-2020,14:47] (http://www.oecd.org/science/emerging-tech/1890904.pdf). pages 1–8.

Onyeaka, H., Nienow, A. W., and Hewitt, C. J. (2003). Further Studies Related to the Scale-up of High Cell Density Escherichia coli Fed-Batch Fermentations: The Additional Effect of a Changing Microenvironment When Using Aqueous Ammonia to Control pH. *Biotechnol Bioeng.*, 84(4):474–484.

Owens, J. and Legan, J. (1987). Determination of the Monod substrate saturation constant for microbial growth. *FEMS Microbiol Rev.*, 46:419–432.

Paget, M. S. (2015). Bacterial sigma factors and anti-sigma factors: Structure, function and distribution. *Biomolecules*, 5(3):1245–1265.

Pao, C. C. and Dyes, B. T. (1981). Effect of unusual guanosine nucleotides on the activities of some Escherichia coli cellular enzymes. *Biochim Biophys Acta*, 677(3-4):358–362.

Papenfort, K., Pfeiffer, V., Lucchini, S., Sonawane, A., Hinton, J. C., and Vogel, J. (2008). Systematic deletion of Salmonella small RNA genes identifies CyaR, a conserved CRP-dependent riboregulator of OmpX synthesis. *Mol Microbiol.*, 68(4):890–906.

Pastan, I. and Adhya, S. (1976). Cyclic Adenosine 5'-Monophosphate in Escherichia coli. *Bacteriol Rev.*, 40(3):527–551.

Patnaik, R., Roof, W. D., Young, R. F., and Liao, J. C. (1992). Stimulation of Glucose Catabolism in Escherichia coli by a Potential Futile Cycle. *J Bacteriol.*, 174(23):7527–7532.

Paul, B. J., Barker, M. M., Ross, W., Schneider, D. A., Webb, C., Foster, J. W., and Gourse, R. L. (2004). DksA: A Critical Component of the Transcription Initiation Machinery that Potentiates the Regulation of rRNA Promoters by ppGpp and the Initiating NTP. *Cell*, 118:311–322.

Paul, B. J., Berkmen, M. B., and Gourse, R. L. (2005). DksA potentiates direct activation of amino acid promoters by ppGpp. *Proc Natl Acad Sci USA*, 102(22):7823–7828.

Peled, O. N., Salvadori, A., Peled, U. N., and Kidby, D. K. (1977). Death of Microbial Cells: Rate Constant Calculations. *J Bacteriol.*, 129(3):1648–1650.

Phaiboun, A., Zhang, Y., Park, B., and Kim, M. (2015). Survival Kinetics of Starving Bacteria Is Biphasic and Density-Dependent. *PLoS Comput Biol.*, 11(4):e1004198.

Piper, S. E., Mitchell, J. E., Lee, D. J., and Busby, S. J. (2009). A global view of Escherichia coli Rsd protein and its interactions. *Mol Biosyst.*, 5(12):1943–1947.

Pirt, S. (1965). The maintenance energy of bacteria in growing cultures. *Proc R Soc Lond B Biol Sci.*, 163(991):224–231.

Polakis, S. E., Guchhait, R. B., and Lake, M. D. (1973). Stringent Control of Fatty Acid Synthesis in Escherichia coli. *J Biol Chem.*, 248(22):7957–7966.

Polayes, D. A., Rice, P. W., Garner, M. M., and Dahlberg, J. E. (1988). Cyclic AMP - Cyclic AMP Receptor Protein as a Repressor of Transcription of the spf Gene of Escherichia coli. *J Bacteriol.*, 170(7):3110–3114.

Postma, P. W., Lengeler, J. W., and Jacobson, G. R. (1993). Phosphoenolpyru-

vate:Carbohydrate Phosphotransferase Systems of Bacteria. *Microbiol Rev.*, 57(3):543–594.

Potrykus, K. and Cashel, M. (2008). (p)ppGpp: still magical? *Annu Rev Microbiol.*, 62:35–51.

Potrykus, K., Murphy, H., Philippe, N., and Cashel, M. (2011). ppGpp is the major source of growth rate control in E. coli. *Environ Microbiol.*, 13(3):563–575.

Preiss, J. (1984). Bacterial Glycogen Synthesis and its Regulation. *Annu Rev Microbiol.*, 38(1):419–458.

Preiss, J. (2014). Glycogen: Biosynthesis and Regulation. *EcoSal Plus 2014*, 6(1).

Radman, M. (1975). SOS Repair Hypothesis: Phenomenology of an Inducible DNA Repair Which is Accompanied by Mutagenesis. In Hanawalt P.C., S. R. e., editor, *Molecular Mechanisms for Repair of DNA. Basic Life Sciences.*, pages 355–367. Springer US, Boston, MA.

Raha, M., Kawagishi, I., Müller, V., Kihara, M., and Macnab, R. M. (1992). Escherichia coli produces a cytoplasmic α-amylase, AmyA. *J Bacteriol.*, 174(20):6644–6652.

Rahman, M., Hasan, M. R., Oba, T., and Shimizu, K. (2006). Effect of rpoS gene knockout on the metabolism of Escherichia coli during exponential growth phase and early stationary phase based on gene expressions, enzyme activities and intracellular metabolite concentrations. *Biotechnol Bioeng.*, 94(3):585–595.

Ramseier, T. (1996). Cra and the control of carbon flux via metabolic pathways. *Res Microbiol.*, 147(6-7):489–493.

Ramseier, T. M., Bledig, S., Michotey, V., Feghali, R., and Saier, M. H. (1995). The global regulatory protein FruR modulates the direction of carbon flow in Escherichia coli. *Mol Microbiol.*, 16(6):1157–1169.

Reeves, R. E. and Sols, A. (1973). Regulation of Escherichia coli phosphofructokinase in situ. *Biochem Biophys Res Commun.*, 50(2):459–466.

Reitzer, L. (2003). Nitrogen assimilation and global regulation in Escherichia coli. *Annu Rev Microbiol.*, 57:155–176.

Reitzer, L. (2004). Biosynthesis of Glutamate, Aspartate, Asparagine, L-Alanine, and D-Alanine. *EcoSal Plus 2004*, 1(1).

Reitzer, L. and Schneider, B. L. (2001). Metabolic context and possible physiological themes of σ^{54}-dependent genes in Escherichia coli. *Microbiol Mol Biol Rev.*, 65(3):422–444.

Reitzer, L. J. (1996). Sources of nitrogen and their utilization. In Neidhardt, F. C., Curtiss, R. I., Ingraham, J. L., Lin, E. C. C., Low, K. B., Magasanik, B., Reznikoff, W. S., Riley, M., Schaechter, M., and Umbarger, H. E., editors, *Escherichia coli and Salmonella: Cellular and Molecular Biology.*, pages 380–390. ASM Press, Washington, DC.

Rojas, A. M., Ehrenberg, M., Andersson, S. G., and Kurland, C. G. (1984). ppGpp inhibition of elongation factors Tu, G and Ts during polypeptide synthesis. *Mol Gen Genet.*, 197(1):36–45.

Romeo, T. and Babitzke, P. (2018). Global regulation by CsrA and its RNA antagonists. *Microbiol Spectr.*, 6(2):1–24.

Romeo, T., Black, J., and Preiss, J. (1990). Genetic regulation of glycogen biosynthesis in Escherichia coli: In vivo effects of the catabolite repression and stringent response systems in glg gene expression. *Curr Microbiol.*, 21(2):131–137.

Romeo, T., Gong, M., Mu Ya Liu, and Brun-Zinkernagel, A. M. (1993). Identification and molecular characterization of csrA, a pleiotropic gene from Escherichia coli that affects glycogen biosynthesis, gluconeogenesis, cell size, and surface properties. *J Bacteriol.*, 175(15):4744–4755.

Romeo, T. and Snoep, J. L. (2005). Glycolysis and Flux Control. *EcoSal Plus*, 1(2).

Ronneau, S. and Hallez, R. (2019). Make and break the alarmone: regulation of (p)ppGpp synthetase/hydrolase enzymes in bacteria. *FEMS Microbiol Rev.*, 009:389–400.

Ross, W., Sanchez-Vazquez, P., Chen, A. Y., Lee, J.-H., Burgos, H. L., and Gourse, R. L. (2016). ppGpp Binding to a Site at the RNAP-DksA Interface Accounts for Its Dramatic Effects on Transcription Initiation during the Stringent Response. *Mol Cell*, 62(6):811–823.

Ross, W., Vrentas, C. E., Sanchez-Vazquez, P., Gaal, T., and Gourse, R. L. (2013). The Magic Spot: A ppGpp Binding Site on E. coli RNA Polymerase Responsible for Regulation of Transcription Initiation. *Mol Cell*, 50(3):420–429.

Rühl, M., Le Coq, D., Aymerich, S., and Sauer, U. (2012). ^{13}C-flux Analysis Reveals NADPH-balancing Transhydrogenation Cycles in Stationary Phase of Nitrogen-starving Bacillus subtilis. *J Biol Chem.*, 287(33):27959–27970.

Sahm, H., Antranikian, G., Stahmann, K. P., and Takors, R. (2014). *Industrielle Mikrobiologie*. Springer Berlin Heidelberg.

Saier, M. H. and Ramseier, T. M. (1996). The Catabolite Repressor/Activator (Cra) Protein of Enteric Bacteria. *J Bacteriol.*, 178(12):3411–3417.

Sajish, M., Kalayil, S., Verma, S. K., Nandicoori, V. K., and Prakash, B. (2009). The significance of EXDD and RXKD motif conservation in Rel proteins. *J Biol Chem*, 284(14):9115–9123.

Sajish, M., Tiwari, D., Rananaware, D., Nandicoori, V. K., and Prakash, B. (2007). A charge reversal differentiates (p)ppGpp synthesis by monofunctional and bifunctional Rel proteins. *J Biol Chem.*, 282(48):34977–34983.

Sakamoto, N., Kotre, A. M., and Savageau, M. A. (1975). Glutamate Dehydrogenase from Escherichia coli: Purification and Properties. *J Bacteriol.*, 124(2):775–783.

Sambrook, J. and Russell, D. W. (2001). *Molecular Cloning: A Laboratory Manual*. Cold Spring Harbour Laboratory Press, New York, 3 edition.

Sanchez-Vazquez, P., Dewey, C. N., Kitten, N., Ross, W., and Gourse, R. L. (2019). Genome-wide effects on Escherichia coli transcription from ppGpp binding to its two sites on RNA polymerase. *Proc Natl Acad Sci USA*, 116(17):8310–8319.

Sanger, F., Nicklen, S., and Coulson, A. R. (1977). DNA sequencing with chain-terminating inhibitors. *Proc Natl Acad Sci USA*, 74(12):5463–5467.

Sarubbi, E., Rudd, K. E., and Cashel, M. (1988). Basal ppGpp level adjustment shown by new spoT mutants affect steady state growth rates and rrnA ribosomal promoter regulation in Escherichia coli. *Mol Gen Genet.*, 213(2-3):214–222.

Sauer, U. and Eikmanns, B. J. (2005). The PEP-pyruvate-oxaloacetate node as the switch point for carbon flux distribution in bacteria. *FEMS Microbiol Rev.*, 29(4):765–794.

Sauer, U., Lasko, D. R., Fiaux, J., Hochuli, M., Glaser, R., Szyperski, T., Wüthrich, K., and Bailey, J. E. (1999). Metabolic flux ratio analysis of genetic and environmental modulations of Escherichia coli central carbon metabolism. *J Bacteriol.*, 181(21):6679–6688.

Schuhmacher, T., Löffler, M., Hurler, T., and Takors, R. (2014). Phosphate limited fed-batch processes: Impact on carbon usage and energy metabolism in Escherichia coli. *J Biotechnol.*, 190:96–104.

Schumacher, M. A., Piro, K. M., Xu, W., Hansen, S., Lewis, K., and Brennan, R. G. (2009). Molecular Mechanisms of HipA Mediated Multidrug Tolerance and its Neutralization by HipB. *Science*, 323(5912):396–401.

Semkiv, M. V., Dmytruk, K. V., Abbas, C. A., and Sibirny, A. A. (2016). Activation of futile cycles as an approach to increase ethanol yield during glucose fermentation in Saccharomyces cerevisiae. *Bioengineered*, 7(2):106–111.

Senn, H., Lendenmann, U., Snozzi, M., Hamer, G., and Egli, T. (1994). The growth of

Escherichia coli in glucose-limited chemostat cultures: a re-examination of the kinetics. *Biochim Biophys Acta*, 1201(3):424–436.

Shaikh, A. S., Tang, Y. J., Mukhopadhyay, A., Martín, G., Gin, J., Benke, P. I., and Keasling, J. D. (2009). Study of Stationary Phase Metabolism Via Isotopomer Analysis of Amino Acids from an Isolated Protein. *Biotechnol Prog.*, 26:52–56.

Sharkey, M. A. and Engel, P. C. (2008). Apparent negative co-operativity and substrate inhibition in overexpressed glutamate dehydrogenase from Escherichia coli. *FEMS Microbiology Letters*, 281(2):132–139.

Sharma, U. K. and Chatterji, D. (2010). Transcriptional switching in Escherichia coli during stress and starvation by modulation of σ^{70} activity. *FEMS Microbiol Rev*, 34(5):646–657.

Sharp, P. M., Cowe, E., Higgins, D. G., Shields, D. C., Wolfe, K. H., and Wright, F. (1988). Codon usage patterns in Escherichia coli, Bacillus subtilis, Saccharomyces cerevisiae, Schizosaccharomyces pombe, Drosophila melanogaster and Homo sapiens; a review of the considerable within-species diversity. *Nucleic Acids Res.*, 16(17):8207–8211.

Shimizu, K. (2013). Regulation Systems of Bacteria such as Escherichia coli in Response to Nutrient Limitation and Environmental Stresses. *Metabolites*, 4(1):1–35.

Shyp, V., Tankov, S., Ermakov, A., Kudrin, P., English, B. P., Ehrenberg, M., Tenson, T., Elf, J., and Hauryliuk, V. (2012). Positive allosteric feedback regulation of the stringent response enzyme RelA by its product. *EMBO Rep.*, 13(9):835–839.

Simen, J. D., Löffler, M., Jäger, G., Schäferhoff, K., Freund, A., Matthes, J., Müller, J., Takors, R., Feuer, R., von Wulffen, J., Lischke, J., Ederer, M., Knies, D., Kunz, S., Sawodny, O., Riess, O., Sprenger, G., Trachtmann, N., Nieß, A., and Broicher, A. (2017). Transcriptional response of Escherichia coli to ammonia and glucose fluctuations. *Microb Biotechnol.*, 10(4):858–872.

Song, H., Parsons, M. R., Rowsell, S., Leonard, G., and Phillips, S. E. (1999). Crystal

structure of intact elongation factor EF-Tu from Escherichia coli in GDP conformation at 2.05 Å resolution. *J Mol Biol.*, 285(3):1245–1256.

Spira, B., Silberstein, N., and Yagil, E. (1995). Guanosine 3',5'-Bispyrophosphate (ppGpp) Synthesis in Cells of Escherichia coli Starved for P_i. *J Bacteriol.*, 177(14):4053–4058.

Sprinzl, M. (1994). Elongation factor Tu: a regulatory GTPase with an integrated effector. *Trends Biochem Sci.*, 19(6):245–250.

Steinsiek, S. and Bettenbrock, K. (2012). Glucose Transport in Escherichia coli Mutant Strains with Defects in Sugar Transport Systems. *J. Bacteriol.*, 194(21):5897–5908.

Stülke, J. and Hillen, W. (1999). Carbon catabolite repression in bacteria. *Curr Opin Microbiol.*, 2(2):195–201.

Swim, H. E. and Krampitz, L. O. (1954). Acetic acid oxidation by Escherichia coli: evidence for the occurrence of a tricarboxylic acid cycle. *J Bacteriol.*, 67(4):419–425.

Taguchi, M., Izui, K., and Katsuki, H. (1980). Augmentation of Glycogen Synthesis under Stringent Control in Escherichia coli. *J Biochem.*, 88:379–387.

Takors, R. (2012). Scale-up of microbial processes: Impacts, tools and open questions. *J Biotechnol.*, 160:3–9.

Takors, R. (2016). Editorial: How can we ensure the successful transfer from lab- to large-scale production? *Eng Life Sci.*, 16:587.

Takors, R. and de Lorenzo, V. (2016). Editorial overview: Microbial systems biology: systems biology prepares the ground for successful synthetic biology. *Curr Opin Microbiol.*, 33:viii–x.

Taymaz-Nikerel, H., Borujeni, A. E., Verheijen, P. J. T., Heijnen, J. J., and van Gulik, W. M. (2010). Genome-derived minimal metabolic models for Escherichia coli MG1655

with estimated in vivo respiratory ATP stoichiometry. *Biotechnol Bioeng.*, 107(2):369–381.

Tedin, K. and Norel, F. (2001). Comparison of ΔrelA strains of Escherichia coli and Salmonella enterica serovar typhimurium suggests a role for ppGpp in attenuation regulation of branched-chain amino acid biosynthesis. *J Bacteriol.*, 183(21):6184–6196.

Tenaillon, O., Denamur, E., and Matic, I. (2004). Evolutionary significance of stress-induced mutagenesis in bacteria. *Trends Microbiol.*, 12(6):264–270.

Terada, K. and Izui, K. (1991). Site-directed mutagenesis of the conserved histidine residue of phosphoenolpyruvate carboxylase: His 138 is essential for the second partial reaction. *Eur J Biochem.*, 202(3):797–803.

Theobald, U., Mailinger, W., Baltes, M., Rizzi, M., and Reuss, M. (1997). In vivo analysis of metabolic dynamics in Saccharomyces cerevisiae : I. Experimental observations. *Biotechnol Bioeng.*, 55(2):305–316.

Tippin, B., Pham, P., and Goodman, M. F. (2004). Error-prone replication for better or worse. *Trends Microbiol.*, 12(6):288–295.

Tomar, A., Eiteman, M. A., and Altman, E. (2003). The effect of acetate pathway mutations on the production of pyruvate in Escherichia coli. *Appl Microbiol Biotechnol.*, 62:76–82.

Tosa, T. and Pizer, L. I. (1971). Effect of serine hydroxamate on the growth of Escherichia coli. *J Bacteriol.*, 106(3):966–971.

Toulokhonov, I. I., Shulgina, I., and Hernandez, V. J. (2001). Binding of the transcription effector ppGpp to Escherichia coli RNA polymerase is allosteric, modular, and occurs near the N terminus of the β'-subunit. *J Biol Chem.*, 276(2):1220–1225.

Tozawa, Y. and Nomura, Y. (2011). Signalling by the global regulatory molecule ppGpp in bacteria and chloroplasts of land plants. *Plant Biol (Stuttg)*, 13(5):699–709.

Tran, K. T., Maeda, T., and Wood, T. K. (2014). Metabolic engineering of Escherichia coli to enhance hydrogen production from glycerol. *Appl Microbiol Biotechnol.*, 98(10):4757–4770.

Traxler, M. F., Summers, S. M., Nguyen, H. T., Zacharia, V. M., Hightower, G. A., Smith, J. T., and Conway, T. (2008). The global, ppGpp-mediated stringent response to amino acid starvation in Escherichia coli. *Mol Microbiol.*, 68(5):1128–1148.

Traxler, M. F., Zacharia, V. M., Marquardt, S., Summers, S. M., Nguyen, H. T., Stark, S. E., and Conway, T. (2011). Discretely calibrated regulatory loops controlled by ppGpp partition gene induction across the 'feast to famine' gradient in Escherichia coli. *Mol Microbiol.*, 79(4):830–845.

UniProt Consortium (2015). UniProt: a hub for protein information. *Nucleic Acids Res.*, 43(Database issue):D204–D212.

United Nations (1992). Convention on Biological Diversity [Date:28-01-2020,14:50] (https://www.cbd.int/doc/legal/cbd-en.pdf). pages 1–30.

Van Der Biezen, E. A., Sun, J., Coleman, M. J., Bibb, M. J., and Jones, J. D. G. (2000). Arabidopsis RelA/SpoT homologs implicate (p)ppGpp in plant signaling. *Proc Natl Acad Sci USA.*, 97(7):3747–3752.

Van Heeswijk, W. C., Westerhoff, H. V., and Boogerd, F. C. (2013). Nitrogen Assimilation in Escherichia coli: Putting Molecular Data into a Systems Perspective. *Microbiol Mol Biol Rev.*, 77(4):628–695.

Varik, V., Alves Oliveira, R. S., Hauryliuk, V., and Tenson, T. (2017). HPLC-based quantification of bacterial housekeeping nucleotides and alarmone messengers ppGpp and pppGpp. *Sci Rep.*, 7(11022):1–12.

Veronese, F. M., Boccu, E., and Conventi, L. (1975). Glutamate dehydrogenase from Escherichia coli: Induction, purification and properties of the enzyme. *Biochim Biophys Acta*, 377(2):217–228.

Verstraeten, N., Fauvart, M., Versées, W., and Michiels, J. (2011). The Universally Conserved Prokaryotic GTPases. *Microbiol Mol Biol Rev.*, 75(3):507–542.

Villadsen, I. S. and Michelsen, O. (1977). Regulation of PRPP and nucleoside tri and tetraphosphate pools in Escherichia coli under conditions of nitrogen starvation. *J Bacteriol.*, 130(1):136–143.

Villadsen, J., Nielsen, J., and Lidén, G. (2011). *Bioreaction Engineering Principles*. Springer US, Boston, MA, 3 edition.

Vinella, D., Albrecht, C., Cashel, M., and D'Ari, R. (2005). Iron limitation induces SpoT-dependent accumulation of ppGpp in Escherichia coli. *Mol Microbiol.*, 56(4):958–970.

Wassarman, K. M. and Storz, G. (2000). 6S RNA Regulates E. coli RNA Polymerase Activity. *Cell*, 101:613–623.

Weber, H., Polen, T., Heuveling, J., Wendisch, V. F., and Hengge, R. (2005a). Genome-wide analysis of the general stress response network in Escherichia coli: σ^S-dependent genes, promoters, and sigma factor selectivity. *J Bacteriol*, 187(5):1591–1603.

Weber, J., Kayser, A., and Rinas, U. (2005b). Metabolic flux analysis of Escherichia coli in glucose-limited continuous culture. II. Dynamic response to famine and feast, activation of the methylglyoxal pathway and oscillatory behaviour. *Microbiology*, 151(3):707–716.

Weichart, D., Querfurth, N., Dreger, M., and Hengge-Aronis, R. (2003). Global Role for ClpP-Containing Proteases in Stationary-Phase Adaptation of Escherichia coli. *J Bacteriol.*, 185(1):115–125.

Wendrich, T. M., Blaha, G., Wilson, D. N., Marahiel, M. A., and Nierhaus, K. H. (2002). Dissection of the Mechanism for the Stringent Factor RelA. *Mol Cell*, 10(4):779–788.

Wigneshweraraj, S., Bose, D., Burrows, P. C., Joly, N., Schumacher, J., Rappas, M., Pape, T., Zhang, X., Stockley, P., Severinov, K., and Buck, M. (2008). Modus operandi of the bacterial RNA polymerase containing the σ^{54} promoter-specificity factor. *Mol Microbiol.*, 68(3):538–546.

Wilson, W. A., Roach, P. J., Montero, M., Baroja-Fernández, E., Muñoz, F. J., Eydallin, G., Viale, A. M., and Pozueta-Romero, J. (2010). Regulation of glycogen metabolism in yeast and bacteria. *FEMS Microbiol Rev.*, 34:952–985.

Wolfe, A. J. (2015). Glycolysis for Microbiome Generation. *Microbiol Spectr.*, 3(3):MBP–0014–2014.

Xiao, H., Kalman, M., Ikehara, K., Zemel, S., Glaser, G., and Cashel, M. (1991). Residual guanosine 3',5'-bispyrophosphate synthetic activity of relA null mutants can be eliminated by spoT null mutations. *J Biol Chem.*, 266(9):5980–5990.

Yang, H., Liu, M. Y., and Romeo, T. (1996). Coordinate Genetic Regulation of Glycogen Catabolism and Biosynthesis in Escherichia coli via the CsrA Gene Product. *J Bacteriol.*, 178(4):1012–1017.

Yang, X. and Ishiguro, E. E. (2001). Dimerization of the RelA protein of Escherichia coli. *Biochem Cell Biol.*, 79(6):729–736.

Zhang, Y., Zborníková, E., Rejman, D., and Gerdes, K. (2018). Novel (p)ppGpp Binding and Metabolizing Proteins of Escherichia coli. *mBio*, 9(2):1–20.

Zhao, K., Liu, M., and Burgess, R. R. (2010). Promoter and regulon analysis of nitrogen assimilation factor, σ^{54}, reveal alternative strategy for E. coli MG1655 flagellar biosynthesis. *Nucleic Acids Res.*, 38(4):1273–1283.

Zhou, J., Lancaster, L., Donohue, J. P., and Noller, H. F. (2019). Spontaneous ribosomal translocation of mRNA and tRNAs into a chimeric hybrid state. *Proc Natl Acad Sci USA.*, 116(16):7813–7818.

Zhou, Y. N. and Jin, D. J. (1998). The rpoB mutants destabilizing initiation complexes at stringently controlled promoters behave like "stringent" RNA polymerases in Escherichia coli. *Proc Natl Acad Sci USA*, 95(6):2908–2913.

Zhu, Y., Eiteman, M. A., Altman, R., and Altman, E. (2008). High Glycolytic Flux

Improves Pyruvate Production by a Metabolically Engineered Escherichia coli Strain. *Appl Environ Microbiol.*, 74(21):6649–6655.

Zimmer, D. P., Soupene, E., Lee, H. L., Wendisch, V. F., Khodursky, A. B., Peter, B. J., Bender, R. A., and Kustu, S. (2000). Nitrogen regulatory protein C-controlled genes of Escherichia coli: Scavenging as a defense against nitrogen limitation. *Proc Natl Acad Sci USA*, 97(26):14674–14679.

Zuo, Y., Wang, Y., and Steitz, T. A. (2013). Molecular Cell The Mechanism of E. coli RNA Polymerase Regulation by ppGpp Is Suggested by the Structure of their Complex. *Mol Cell*, 50(3):430–436.

A. Supporting Information

A.1. Gene and Amino Acid Sequences

RelA: (p)ppGpp synthase I/ATP:GTP 3'-pyrophosphotransferase

Protein sequence (744 aa) of RelA:

```
MVAVRSAHINKAGEFDPEKWIASLGITSQKSCECLAETWAYCLQQTQGHPDASLLLWRGVEMVEILSTLSMDIDTL
RAALLFPLADANVVSEDVLRESVGKSVVNLIHGVRDMAAIRQLKATHTDSVSSEQVDNVRRMLLAMVDDFRCVVIK
LAERIAHLREVKDAPEDERVLAAKECTNIYAPLANRLGIGQLKWELEDYCFRYLHPTEYKRIAKLLHERRLDREHY
IEEFVGHLRAEMKAEGVKAEVYGRPKHIYSIWRKMQKKNLAFDELFDVRAVRIVAERLQDCYAALGIVHTHYRHLP
DEFDDYVANPKPNGYQSIHTVVLGPGGKTVEIQIRTKQMHEDAELGVAAHWKYKEGAAAGGARSGHEDRIAWLRKL
IAWQEEMADSGEMLDEVRSQVFDDRVYVFTPKGDVVDLPAGSTPLDFAYHIHSDVGHRCIGAKIGGRIVPFTYQLQ
MGDQIEIITQKQPNPSRDWLNPNLGYVTTSRGRSKIHAWFRKQDRDKNILAGRQILDDELEHLGISLKEAEKHLLP
RYNFNDVDELLAAIGGGDIRLNQMVNFLQSQFNKPSAEEQDAAALKQLQQKSYTPQNRSKDNGRVVVEGVGNLMHH
IARCCQPIPGDEIVGFITQGRGISVHRADCEQLAELRSHAPERIVDAVWGESYSAGYSLVVRVVANDRSGLLRDIT
TILANEKVNVLGVASRSDTKQQLATIDMTIEIYNLQVLGRVLGKLNQVPDVIDARRLHGS
```

DNA sequence (2235 nt) of the *relA* open reading frame (ORF):

```
ATGGTTGCGG TAAGAAGTGC ACATATCAAT AAGGCTGGTG AATTTGATCC GGAAAAATGG ATCGCAAGTC
TGGGTATTAC CAGCCAGAAG TCGTGTGAGT GCTTAGCCGA AACCTGGGCG TATTGTCTGC AACAGACGCA
GGGGCATCCG GATGCCAGTC TGTTATTGTG GCGTGGTGTT GAGATGGTGG AGATCCTCTC GACATTAAGT
ATGGACATTG ACACGCTGCG GGCGGCGCTG CTTTTCCCTC TGGCGGATGC CAACGTAGTC AGCGAAGATG
TGCTGCGTGA GAGCGTCGGT AAGTCGGTCG TTAACCTTAT TCACGGCGTG CGTGATATGG CGGCGATCCG
CCAGCTGAAA GCGACGCACA CTGATTCTGT TTCCTCCGAA CAGGTCGATA ACGTTCGCCG GATGTTATTG
GCGATGGTCG ATGATTTTCG CTGCGTAGTC ATCAAACTGG CGGAGCGTAT TGCTCATCTG CGCGAAGTAA
AAGATGCGCC GGAAGATGAA CGTGTACTGG CGGCAAAAGA GTGTACCAAC ATCTACGCAC CGCTGGCTAA
CCGTCTCGGA ATCGGACAAC TGAAATGGGA ACTGGAAGAT TACTGCTTCC GTTACCTCCA TCCAACCGAA
TACAAACGAA TTGCCAAACT GCTGCATGAA CGGCGTCTCG ACCGCGAACA CTACATCGAA GAGTTCGTTG
GTCATCTGCG CGCTGAGATG AAAGCTGAAG GCGTTAAAGC GGAAGTGTAT GGTCGTCCGA AACACATCTA
```

```
CAGCATCTGG CGTAAAATGC AGAAAAAGAA CCTCGCCTTT GATGAGCTGT TTGATGTGCG TGCGGTACGT
ATTGTCGCCG AGCGTTTACA GGATTGCTAT GCCGCACTGG GGATAGTGCA CACTCACTAT CGCCACCTGC
CGGATGAGTT TGACGATTAC GTCGCTAACC CGAAACCAAA CGGTTATCAG TCTATTCATA CCGTGGTTCT
GGGGCCGGGT GGAAAAACCG TTGAGATCCA AATCCGCACC AAACAGATGC ATGAAGATGC AGAGTTGGGT
GTTGCTGCGC ACTGGAAATA TAAAGAGGGC GCGGCTGCTG GCGGCGCACG TTCGGGACAT GAAGACCGGA
TTGCCTGGCT GCGTAAACTG ATTGCGTGGC AGGAAGAGAT GGCTGATTCC GGCGAAATGC TCGACGAAGT
ACGTAGTCAG GTCTTTGACG ACCGGGTGTA CGTCTTTACG CCGAAAGGTG ATGTCGTTGA TTTGCCTGCG
GGATCAACGC CGCTGGACTT CGCTTACCAC ATCCACAGTG ATGTCGGACA CCGCTGCATC GGGGCAAAAA
TTGGCGGGCG CATTGTGCCG TTCACCTACC AGCTGCAGAT GGGCGACCAG ATTGAAATTA TCACCCAGAA
ACAGCCGAAC CCCAGCCGTG ACTGGTTAAA CCCAAACCTC GGTTACGTCA CAACCAGCCG TGGGCGTTCG
AAAATTCACG CCTGGTTCCG TAAACAGGAC CGTGACAAAA ACATTCTGGC TGGGCGGCAA ATCCTTGACG
ACGAGCTGGA ACATCTGGGG ATCAGCCTGA AAGAAGCAGA AAAACATCTG CTGCCGCGTT ACAACTTCAA
TGATGTCGAC GAGTTGCTGG CGGCGATTGG TGGCGGGGAT ATCCGTCTCA ATCAGATGGT GAACTTCCTG
CAATCGCAAT TTAATAAGCC GAGTGCCGAA GAGCAGGACG CCGCCGCGCT GAAGCAACTT CAGCAAAAAA
GCTACACGCC GCAAAACCGC AGTAAAGATA ACGGTCGCGT GGTAGTCGAA GGTGTTGGCA ACCTGATGCA
CCACATCGCG CGCTGCTGCC AGCCGATTCC TGGAGATGAG ATTGTCGGCT TCATTACCCA GGGGCGCGGT
ATTTCAGTAC ACCGCGCCGA TTGCGAACAA CTGGCGGAAC TGCGCTCCCA TGCGCCAGAA CGCATTGTTG
ACGCGGTATG GGGTGAGAGC TACTCCGCCG GATATTCGCT GGTGGTCCGC GTGGTAGCTA ATGATCGTAG
TGGGTTGTTA CGTGATATCA CGACCATTCT CGCCAACGAG AAGGTGAACG TGCTTGGCGT TGCCAGCCGT
AGCGACACCA AACAGCAACT GGCGACCATC GACATGACCA TTGAGATTTA CAACCTGCAA GTGCTGGGGC
GCGTGCTGGG TAAACTCAAC CAGGTGCCGG ATGTTATCGA CGCGCGTCGG TTGCACGGGA GTTAG
```

SpoT: (p)ppGpp synthase II/(p)ppGpp 3'-pyrophosphohydrolase

Protein sequence (702 aa) of SpoT:

```
MYLFESLNQLIQTYLPEDQIKRLRQAYLVARDAHEGQTRSSGEPYITHPVAVACILAEMKLDYETLMAALLHDVIE
DTPATYQDMEQLFGKSVAELVEGVSKLDKLKFRDKKEAQAENFRKMIMAMVQDIRVILIKLADRTHNMRTLGSLRP
DKRRRIARETLEIYSPLAHRLGIHHIKTELEELGFEALYPNRYRVIKEVVKAARGNRKEMIQKILSEIEGRLQEAG
IPCRVSGREKHLYSIYCKMVLKEQRFHSIMDIYAFRVIVNDSDTCYRVLGQMHSLYKPRPGRVKDYIAIPKANGYQ
SLHTSMIGPHGVPVEVQIRTEDMDQMAEMGVAAHWAYKEHGETSTTAQIRAQRWMQSLLELQQSAGSSFEFIESVK
SDLFPDEIYVFTPEGRIVELPAGATPVDFAYAVHTDIGHACVGARVDRQPYPLSQPLTSGQTVEIITAPGARPNAA
WLNFVVSSKARAKIRQLLKNLKRDDSVSLGRRLLNHALGGSRKLNEIPQENIQRELDRMKLATLDDLLAEIGLGNA
MSVVVAKNLQHGDASIPPATQSHGHLPIKGADGVLITFAKCCRPIPGDPIIAHVSPGKGLVIHHESCRNIRGYQKE
PEKFMAVEWDKETAQEFITEIKVEMFNHQGALANLTAAINTTTSNIQSLNTEEKDGRVYSAFIRLTARDRVHLANI
MRKIRVMPDVIKVTRNRN
```

DNA sequence (2109 nt) of the *spoT* open reading frame (ORF):

```
TTGTATCTGT TTGAAAGCCT GAATCAACTG ATTCAAACCT ACCTGCCGGA AGACCAAATC AAGCGTCTGC
GGCAGGCGTA TCTCGTTGCA CGTGATGCTC ACGAGGGGCA AACACGTTCA AGCGGTGAAC CCTATATCAC
GCACCCGGTA GCGGTTGCCT GCATTCTGGC CGAGATGAAA CTCGACTATG AAACGCTGAT GGCGGCGCTG
CTGCATGACG TGATTGAAGA TACTCCCGCC ACCTACCAGG ATATGGAACA GCTTTTTGGT AAAAGCGTCG
```

CCGAGCTGGT AGAGGGGGTG TCGAAACTTG ATAAACTCAA GTTCCGCGAT AAGAAAGAGG CGCAGGCCGA
AAACTTTCGC AAGATGATTA TGGCGATGGT GCAGGATATC CGCGTCATCC TCATCAAACT TGCCGACCGT
ACCCACAACA TGCGCACGCT GGGCTCACTT CGCCCGGACA AACGTCGCCG CATCGCCCGT GAAACTCTCG
AAATTTATAG CCCGCTGGCG CACCGTTTAG GTATCCACCA CATTAAAACC GAACTCGAAG AGCTGGGTTT
TGAGGCGCTG TATCCCAACC GTTATCGCGT AATCAAAGAA GTGGTGAAAG CCGCGCGCGG CAACCGTAAA
GAGATGATCC AGAAGATTCT TTCTGAAATC GAAGGGCGTT TGCAGGAAGC GGGAATACCG TGCCGCGTCA
GTGGTCGCGA GAAGCATCTT TATTCGATTT ACTGCAAAAT GGTGCTCAAA GAGCAGCGTT TTCACTCGAT
CATGGACATC TACGCTTTCC GCGTGATCGT CAATGATTCT GACACCTGTT ATCGCGTGCT GGGCCAGATG
CACAGCCTGT ACAAGCCGCG TCCGGGCCGC GTGAAAGACT ATATCGCCAT TCCAAAAGCG AACGGCTATC
AGTCTTTGCA CACCTCGATG ATCGGCCCGC ACGGTGTGCC GGTTGAGGTC CAGATCCGTA CCGAAGATAT
GGACCAGATG GCGGAGATGG GTGTTGCCGC GCACTGGGCT TATAAAGAGC ACGGCGAAAC CAGTACTACC
GCACAAATCC GCGCCCAGCG CTGGATGCAA AGCCTGCTGG AGCTGCAACA GAGCGCCGGT AGTTCGTTTG
AATTTATCGA GAGCGTTAAA TCCGATCTCT TCCCGGATGA GATTTACGTT TTCACACCGG AAGGGCGCAT
TGTCGAGCTG CCTGCCGGTG CAACGCCCGT CGACTTCGCT TATGCAGTGC ATACCGATAT CGGTCATGCC
TGCGTGGGCG CACGCGTTGA CCGCCAGCCT TACCCGCTGT CGCAGCCGCT TACCAGCGGT CAAACCGTTG
AAATCATTAC CGCTCCGGGC GCTCGCCCGA ATGCCGCTTG GCTGAACTTT GTCGTTAGCT CGAAAGCGCG
CGCCAAAATT CGTCAGTTGC TGAAAAACCT CAAGCGTGAT GATTCTGTAA GCCTGGGCCG TCGTCTGCTC
AACCATGCTT TGGGTGGTAG CCGTAAGCTG AATGAAATCC CGCAGGAAAA TATTCAGCGC GAGCTGGATC
GCATGAAGCT GGCAACGCTT GACGATCTGC TGGCAGAAAT CGGACTTGGT AACGCAATGA GCGTGGTGGT
CGCGAAAAAT CTGCAACATG GGGACGCCTC CATTCCACCG GCAACCCAAA GCCACGGACA TCTGCCCATT
AAAGGTGCCG ATGGCGTGCT GATCACCTTT GCGAAATGCT GCCGCCCTAT TCCTGGCGAC CCGATTATCG
CCCACGTCAG CCCCGGTAAA GGTCTGGTGA TCCACCATGA ATCCTGCCGT AATATCCGTG GCTACCAGAA
AGAGCCAGAG AAGTTTATGG CTGTGGAATG GGATAAAGAG ACGGCGCAGG AGTTCATCAC CGAAATCAAG
GTGGAGATGT TCAATCATCA GGGTGCGCTG GCAAACCTGA CGGCGGCAAT TAACACCACG ACTTCGAATA
TTCAAAGTTT GAATACGGAA GAGAAAGATG GTCGCGTCTA CAGCGCCTTT ATTCGTCTGA CCGCTCGTGA
CCGTGTGCAT CTGGCGAATA TCATGCGCAA AATCCGCGTG ATGCCAGACG TGATTAAAGT CACCCGAAAC
CGAAATTAA

AceE: Pyruvate dehydrogenase, decarboxylase component E1

Protein sequence (887 aa) of AceE - subunit E1:

MSERFPNDVDPIETRDWLQAIESVIREEGVERAQYLIDQLLAEARKGGVNVAAGTGISNYINTIPVEEQPEYPGNL
ELERRIRSAIRWNAIMTVLRASKKDLELGGHMASFQSSATIYDVCFNHFFRARNEQDGGDLVYFQGHISPGVYARA
FLEGRLTQEQLDNFRQEVHGNGLSSYPHPKLMPEFWQFPTVSMGLGPIGAIYQAKFLKYLEHRGLKDTSKQTVYAF
LGDGEMDEPESKGAITIATREKLDNLVFVINCNLQRLDGPVTGNGKIINELEGIFEGAGWNVIKVMWGSRWDELLR
KDTSGKLIQLMNETVDGDYQTFKSKDGAYVREHFFGKYPETAALVADWTDEQIWALNRGGHDPKKIYAAFKKAQET
KGKATVILAHTIKGYGMGDAAEGKNIAHQVKKMNMDGVRHIRDRFNVPVSDADIEKLPYITFPEGSEEHTYLHAQR
QKLHGYLPSRQPNFTEKLELPSLQDFGALLEEQSKEISTTIAFVRALNVMLKNKSIKDRLVPIIADEARTFGMEGL
FRQIGIYSPNGQQYTPQDREQVAYYKEDEKGQILQEGINELGAGCSWLAAATSYSTNNLPMIPFYIYYSMFGFQRI
GDLCWAAGDQQARGFLIGGTSGRTTLNGEGLQHEDGHSHIQSLTIPNCISYDPAYAYEVAVIMHDGLERMYGEKQE
NVYYYITTLNENYHMPAMPEGAEEGIRKGIYKLETIEGSKGKVQLLGSGSILRHVREAAEILAKDYGVGSDVYSVT
SFTELARDGQDCERWNMLHPLETPRVPYIAQVMNDAPAVASTDYMKLFAEQVRTYVPADDYRVLGTDGFGRSDSRE
NLRHHFEVDASYVVVAALGELAKRGEIDKKVVADAIAKFNIDADKVNPRLA

DNA sequence (2664 nt) of the *aceE* open reading frame (ORF):

```
ATGTCAGAAC GTTTCCCAAA TGACGTGGAT CCGATCGAAA CTCGCGACTG GCTCCAGGCG ATCGAATCGG
TCATCCGTGA AGAAGGTGTT GAGCGTGCTC AGTATCTGAT CGACCAACTG CTTGCTGAAG CCCGCAAAGG
CGGTGTAAAC GTAGCCGCAG GCACAGGTAT CAGCAACTAC ATCAACACCA TCCCCGTTGA AGAACAACCG
GAGTATCCGG GTAATCTGGA ACTGGAACGC CGTATTCGTT CAGCTATCCG CTGGAACGCC ATCATGACGG
TGCTGCGTGC GTCGAAAAAA GACCTCGAAC TGGGCGGCCA TATGGCGTCC TTCCAGTCTT CCGCAACCAT
TTATGATGTG TGCTTTAACC ACTTCTTCCG TGCACGCAAC GAGCAGGATG GCGGCGACCT GGTTTACTTC
CAGGGCCACA TCTCCCCGGG CGTGTACGCT CGTGCTTTCC TGGAAGGTCG TCTGACTCAG GAGCAGCTGG
ATAACTTCCG TCAGGAAGTT CACGGCAATG GCCTCTCTTC CTATCCGCAC CCGAAACTGA TGCCGGAATT
CTGGCAGTTC CCGACCGTAT CTATGGGTCT GGGTCCGATT GGTGCTATTT ACCAGGCTAA ATTCCTGAAA
TATCTGGAAC ACCGTGGCCT GAAAGATACC TCTAAACAAA CCGTTTACGC GTTCCTCGGT GACGGTGAAA
TGGACGAACC GGAATCCAAA GGTGCGATCA CCATCGCTAC CCGTGAAAAA CTGGATAACC TGGTCTTCGT
TATCAACTGT AACCTGCAGC GTCTTGACGG CCCGGTCACC GGTAACGGCA AGATCATCAA CGAACTGGAA
GGCATCTTCG AAGGTGCTGG CTGGAACGTG ATCAAAGTGA TGTGGGGTAG CCGTTGGGAT GAACTGCTGC
GTAAGGATAC CAGCGGTAAA CTGATCCAGC TGATGAACGA AACCGTTGAC GGCGACTACC AGACCTTCAA
ATCGAAAGAT GGTGCGTACG TTCGTGAACA CTTCTTCGGT AAATATCCTG AAACCGCAGC ACTGGTTGCA
GACTGGACTG ACGAGCAGAT CTGGGCACTG AACCGTGGTG GTCACGATCC GAAGAAAATC TACGCTGCAT
TCAAGAAAGC GCAGGAAACC AAAGGCAAAG CGACAGTAAT CCTTGCTCAT ACCATTAAAG GTTACGGCAT
GGGCGACGCG GCTGAAGGTA AAAACATCGC GCACCAGGTT AAGAAAATGA ACATGGACGG TGTGCGTCAT
ATCCGCGACC GTTTCAATGT GCCGGTGTCT GATGCAGATA TCGAAAAACT GCCGTACATC ACCTTCCCGG
AAGGTTCTGA AGAGCATACC TATCTGCACG CTCAGCGTCA GAAACTGCAC GGTTATCTGC CAAGCCGTCA
GCCGAACTTC ACCGAGAAGC TTGAGCTGCC GAGCCTGCAA GACTTCGGCG CGCTGTTGGA AGAGCAGAGC
AAAGAGATCT CTACCACTAT CGCTTTCGTT CGTGCTCTGA ACGTGATGCT GAAGAACAAG TCGATCAAAG
ATCGTCTGGT ACCGATCATC GCCGACGAAG CGCGTACTTT CGGTATGGAA GGTCTGTTCC GTCAGATTGG
TATTTACAGC CCGAACGGTC AGCAGTACAC CCCGCAGGAC CGCGAGCAGG TTGCTTACTA TAAAGAAGAC
GAGAAAGGTC AGATTCTGCA GGAAGGGATC AACGAGCTGG GCGCAGGTTG TTCCTGGCTG GCAGCGGCGA
CCTCTTACAG CACCAACAAT CTGCCGATGA TCCCGTTCTA CATCTATTAC TCGATGTTCG GCTTCCAGCG
TATTGGCGAT CTGTGCTGGG CGGCTGGCGA CCAGCAAGCG CGTGGCTTCC TGATCGGCGG TACTTCCGGT
CGTACCACCC TGAACGGCGA AGGTCTGCAG CACGAAGATG GTCACAGCCA CATTCAGTCG CTGACTATCC
CGAACTGTAT CTCTTACGAC CCGGCTTACG CTTACGAAGT TGCTGTCATC ATGCATGACG GTCTGGAGCG
TATGTACGGT GAAAAACAAG AGAACGTTTA CTACTACATC ACTACGCTGA ACGAAAACTA CCACATGCCG
GCAATGCCGG AAGGTGCTGA GGAAGGTATC CGTAAAGGTA TCTACAAACT CGAAACTATT GAAGGTAGCA
AAGGTAAAGT TCAGCTGCTC GGCTCCGGTT CTATCCTGCG TCACGTCCGT GAAGCAGCTG AGATCCTGGC
GAAAGATTAC GGCGTAGGTT CTGACGTTTA TAGCGTGACC TCCTTCACCG AGCTGGCGCG TGATGGTCAG
GATTGTGAAC GCTGGAACAT GCTGCACCCG CTGGAAACTC CGCGCGTTCC GTATATCGCT CAGGTGATGA
ACGACGCTCC GGCAGTGGCA TCTACCGACT ATATGAAACT GTTCGCTGAG CAGGTCCGTA CTTACGTACC
GGCTGACGAC TACCGCGTAC TGGGTACTGA TGGCTTCGGT CGTTCCGACA GCCGTGAGAA CCTGCGTCAC
CACTTCGAAG TTGATGCTTC TTATGTCGTG GTTGCGGCGC TGGGCGAACT GGCTAAACGT GGCGAAATCG
ATAAGAAAGT GGTTGCTGAC GCAATCGCCA AATTCAACAT CGATGCAGAT AAAGTTAACC CGCGTCTGGC
GTAA
```

A.2. Oligonucleotides

Table A.1. List of oligonucleotides for sequencing or molecular cloning purposes.

oligo name	sequence 5' → 3'	length [nt]	T_a [°C]	GC [%]	5'-extension	function
pEMG:						
pEMG_F	GGCAGCAGCTGAACCAACTC	20	55	60		fwd primer for pEMG MCS seq
pEMG_R	AATGCAGCTGGCACGACAGG	20	58	60		rev primer for pEMG MCS seq
F_Kan	ACGATTCCGAAGCCCAAC	18	52	55		fwd primer for kan^R seq on pEMG
R_Kan	TTGGGAAGCCCTGCAAAG	18	53	55		rev primer for kan^R seq on pEMG
relA:						
F_rlmD	CGTGCGTTGGAATGGCTG	18	56	61		fwd primer for *relA* sequencing, binds in upstream region
F_rlmD_2	GCTAAGTTCGGCAGATCG	18	48	55		fwd primer for *relA* sequencing, binds in upstream region
F_relA	GTATGGACATTGACACGC	18	43	50		fwd primer for *relA* sequencing, binds in *relA* 5'-coding DNA sequence (CDS)
R_relA	CGCAGTTCCGCCAGTTGTTC	20	58	60		rev primer for *relA* sequencing, binds in *relA* 3'-CDS

Table A.1 List of oligonucleotides for sequencing or molecular cloning purposes (continued).

oligo name	sequence 5' → 3'	length [nt]	T_a [°C]	GC [%]	5'-extension	function
R_mazG	GCGCTGCATAATAGTGAG	18	44	50		rev primer for *relA* sequencing, binds in downstream region
R_mazF	GGAACACACAGACACATAC	19	39	47		rev primer for *relA* sequencing, binds in downstream region
F_rlmD_3	GCACTCGCCCGATTAATG	18	51	55		fwd primer for *relA* sequencing, binds at -900 nt upstream
R_mazG_2	AACACCACCTGGAATAGC	18	44	50		rev primer for double *relA* sequencing, binds in downstream region
R_relA_ -RBS	TCCTCTCCTTTAGGGAC	17	40	52		rev primer for *relA* sequencing, binds in ribosome binding site (RBS) of *relA*
F_relA_2	GTGAACTTCCTGCAATCG	18	46	50		fwd primer for *relA* sequencing, binds in *relA* 5'-CDS
R_relA_2	GGTTGGATGGAGGTAACG	18	47	55		rev primer for *relA* sequencing, binds in *relA* 3'-CDS
relA_TS1F	GGAATTCTGGATGTGCAACC-TGAAG	25	54	48	EcoRI	fwd primer TS1 for *relA* deletion/reintegration
relA_TS1R	CCTCTCCTTTAGGGACCAGA-CCTGCCGAAATCGGCAAATC	40	78	55	20 nt overlap with relA_TS2F	rev primer TS1 for *relA* deletion
relA_TS2F	TCTGGTCCCTAAAGGAGAGG-GCCGAAATTTGCTCGTATC	39	55	51	20 nt overlap with relA_TS1R	fwd primer TS2 for *relA* deletion

Table A.1 List of oligonucleotides for sequencing or molecular cloning purposes (continued).

oligo name	sequence 5' → 3'	length [nt]	T_a [°C]	GC [%]	5'-extension	function
relA_TS2R	GCTCTAGAACAACTTCGAAC-GGATATCC	28	53	53	XbaI	rev primer TS2 for *relA* deletion/ reintegration
relA_RK_-TS1F	GGAATTCTATTGGCGATGGT-CGATG	25	52	48	EcoRI	fwd primer TS1 for *relA* amino acid substitution
relA_RK_-TS1R	AGCGACGTAATCTTTAAAGC-GATCCGGCAGGTGG	34	74	52	E306R & D308K	rev primer TS1 for *relA* amino acid substitution
relA_RK_-TS2F	GCCACCTGCCGGATCGCTTT-AAAGATTACGTCGC	34	75	55	complementary to relA_RK_TS1R	fwd primer TS2 for *relA* amino acid substitution
relA_RK_-TS2R	CGGGATCCTCAATCTGGTCG-CCCATC	26	55	61	BamHI	rev primer TS2 for *relA* amino acid substitution
F_relA(wt)	AGTATAGGGATAACAGGGTA-ATCTGAATTCCTGGATGTGC-AACCTGAAG	49	61	42	24 nt overlap with pEMG+EcoRI	fwd primer for *relA*(wt) reintegration into Δ*relA* strains [Gib]
R_relA(wt)	AGAAGCTTGCATGCCTGCAG-GTCGACACAACTTCGAACGG-ATATCC	46	52	52	20 nt overlap with pEMG+SalI	rev primer for *relA*(wt) reintegration into Δ*relA* strains [Gib]
spoT:						
F_gmk	GTGAGGCCATTGAGCAAG	18	48	55		fwd primer *spoT* sequencing, binds in upstream region

Table A.1 List of oligonucleotides for sequencing or molecular cloning purposes (continued).

oligo name	sequence 5' → 3'	length [nt]	T_a [°C]	GC [%]	5'-extension	function
F_rpoZ	TTGTTGGCAGACTGAACC	18	46	50		fwd primer *spoT* sequencing, binds in upstream region
F_spoT	CTCAAGTTCCGCGATAAG	18	46	50		fwd primer *spoT* sequencing, binds in *spoT* 5'-CDS
R_spoT	CGCAGATGCGTGCATAAC	18	51	55		rev primer *spoT* sequencing, binds in *spoT* 3'-CDS
R_recG	TAGATCCTGCACGGTATG	18	43	50		rev primer *spoT* sequencing, binds in downstream region
R_recG_2	ACTAAGTGCTGCGCCAAC	18	49	55		rev primer *spoT* sequencing, binds in downstream region
F_spoT_C-term_2	CAAAGCCACGGACATCTG	18	49	55		fwd primer *spoT* sequencing, binds in *spoT* 3'-CDS
spoT_TS1F	TCCCCCCGGGGCAGAAATGA-GCCATTACG	29	52	62	XmaI	fwd primer TS1 for *spoT* deletion
spoT_TS1R	GGGCGACCCGCTTTGTGATT-AACGACGACCTTCAGCAATA	40	79	52	20 nt overlap with spoT_TS2F	rev primer TS1 for *spoT* deletion
spoT_TS2F	AATCACAAAGCGGGTCGCCC-TGTTTTATGAACCCAACACG	40	51	50	20 nt overlap with spoT_TS1R	fwd primer TS2 for *spoT* deletion
spoT_TS2R	TTCCGCGGCCGCTATGGCCG-ACGTCGACCAACAGGCGTTG-TTGCTC	46	55	65	SalI	rev primer TS2 for *spoT* deletion

Table A.1 List of oligonucleotides for sequencing or molecular cloning purposes (continued).

oligo name	sequence 5' → 3'	length [nt]	T_a [°C]	GC [%]	5'-extension	function
spoT_ED_ -TS1F	GGAATTCATCCGCGTCATCC-TCATC	25	55	52	EcoRI	fwd primer TS1 for *spoT* amino acid substitution
spoT_ED_ -TS1R	ATGGCGATATAGTCATCCAC-TTCGCCCGGACGCG	34	77	58	R290E & K292D	rev primer TS1 for *spoT* amino acid substitution
spoT_ED_ -TS2F	CGCGTCCGGGCGAAGTGGAT-GACTATATCGCCAT	34	77	58	complementary to spoT_ED_TS1R	fwd primer TS2 for *spoT* amino acid substitution
spoT_ED_ -TS2R	CGGGATCCTTCAGCCAAGCG-GCATTC	26	57	61	BamHI	rev primer TS2 for *spoT* amino acid substitution
F_spoT_ -Hyd	ACGGCCAGTATAGGGATAAC-AGGGTAATCTGAATTCATGT-ATCTGTTTGAAAGCCTG	57	50	42	36 nt overlap with pEMG+EcoRI	fwd primer fragment 1 for (p)ppGpp synthetase domain swap in *spoT* $^{\text{Gib}}$
R_spoT_ -Hyd	TTACGCCAGATGCTGTAGAT-GTGTTTCGGACGACCACTGA-CGCGGCACGG	50	66	58	30 nt overlap with relA (p)ppGpp synthetase domain	rev primer fragment 1 for (p)ppGpp synthetase domain swap in *spoT* $^{\text{Gib}}$
F_relA_ -swap	TCCGAAACACATCTACAGC	19	45	47		fwd primer fragment 2 for (p)ppGpp synthetase domain swap in *spoT* $^{\text{Gib}}$
R_relA_ -swap	GATTTGTGCGGTAGTACTGG-TTTCGCCGTGCTCTTTATAT-TTCCAGTGC	49	78	46	30 nt overlap with *spoT* C-terminal domain	rev primer fragment 2 for (p)ppGpp synthetase domain swap in *spoT* $^{\text{Gib}}$

Table A.1 List of oligonucleotides for sequencing or molecular cloning purposes (continued).

oligo name	sequence 5' → 3'	length [nt]	T_a [°C]	GC [%]	5'-extension	function
F_spoT_C-term	CACGGCGAAACCAGTACTAC	20	50	55		fwd primer fragment 3 for (p)ppGpp synthetase domain swap in *spoT* [Gib]
R_spoT_C-term	AAGCTTGCATGCCTGCAGGT-CGACTCTAGAGGATCCTTAA-TTTCGGTTTCGGGTG	55	51	50	36 nt overhang with pEMG+BamHI	rev primer fragment 3 for (p)ppGpp synthetase domain swap in *spoT* [Gib]
aceE:						
F_pdhR	GCCATCTGGCCTTTATCG	18	50	55		fwd primer *aceE* sequencing, binds in upstream region
F_aceE_1	TTCCGTCAGGAAGTTCAC	18	45	50		fwd primer *aceE* sequencing, binds in *aceE* 5'-CDS
F_aceE_2	TCTGTTCCGTCAGATTGG	18	46	50		fwd primer *aceE* sequencing, binds in *aceE* central region
R_aceF_2	AGTTACGGCTCAGGTTCG	18	47	55		rev primer *aceE* sequencing, binds in downstream region
R_aceF_ -down	CACCCAGAAATCCATAGG	18	44	50		rev primer *aceE* sequencing, binds in downstream region
aceE_TS1F	CAGTATAGGGATAACAGGGT-AATCTGAATTCTCCGGGTAA-TCTGGAACTG	50	54	44	25 nt overlap with pEMG+EcoRI	fwd primer TS1 for *aceE* amino acid substitution [Gib]

Table A.1 List of oligonucleotides for sequencing or molecular cloning purposes (continued).

oligo name	sequence 5' → 3'	length [nt]	T_a [°C]	GC [%]	5'-extension	function
aceE_TS2R	TGTTATCCCTAGAAGCTTGC-ATGCCTGCAGGTCGACGACG-GCTTGGCAGATAACC	55	56	54	30 nt overlap with pEMG+SalI	rev primer TS2 for *aceE* amino acid substitution [Gib]
aceE_mut_-TS1_R	TTACCGGTGACCGGGCAGTC-AAGACGCTGCA	31	77	61	G267C & 31 nt overlap with aceE_mut_TS2_F	rev primer TS1 for *aceE* amino acid substitution [Gib]
aceE_mut_-TS2_F	TGCAGCGTCTTGACTGCCCG-GTCACCGGTAA	31	77	61	G267C & 31 nt overlap with aceE_mut_TS1_R	fwd primer TS2 for *aceE* amino acid substitution [Gib]
aceE_WT_-TS1_R	TTACCGGTGACCGGGCCGTC-AAGACGCTGCA	31	79	64	C267G & 31 nt overlap with aceE_WT_TS2_F	rev primer TS1 for *aceE* amino acid substitution [Gib]
aceE_WT_-TS2_F	TGCAGCGTCTTGACGGCCCG-GTCACCGGTAA	31	79	64	C267G & 31 nt overlap with aceE_WT_TS1_R	fwd primer TS2 for *aceE* amino acid substitution [Gib]
iclR & sdhAB:						
F_metH	AGAACACCGGCAACGTAG	18	48	55		fwd primer *iclR* sequencing, binds in upstream region
F_iclR	AGACTGTCATGGTCGCAC	18	45	55		fwd primer *iclR* sequencing, binds in binds in *iclR* 5'-CDS

Table A.1 List of oligonucleotides for sequencing or molecular cloning purposes (continued).

oligo name	sequence 5' → 3'	length [nt]	T_a [°C]	GC [%]	5'-extension	function
R_iclR	AAGTCAGCGCATTCCACC	18	51	55		rev primer *iclR* sequencing, binds in binds in *iclR* 3'-CDS
R_arpA	GAGTGTCTGAGCGTTGAG	18	42	55		rev primer *iclR* sequencing, binds in downstream region
R_arpA_2	AACCAACGCCAAAGTCTG	18	48	50		rev primer *iclR* sequencing, binds in downstream region
F_sdhC_2	AATCTGGACCTACAGACC	18	40	50		fwd primer *sdhAB* sequencing, binds in upstream region
F_sdhC	CTTACCGCTCTGGCGTATC	19	50	57		fwd primer *sdhAB* sequencing, binds in upstream region
F_sdhA	CGGAAGCGATTCTGGAAC	18	50	55		fwd primer *sdhAB* sequencing, binds in *sdhA* 5'-CDS
R_sdhB	GCTGTCAGTCTCGGTATC	18	41	55		rev primer *sdhAB* sequencing, binds in *sdhB* 3'-CDS
R_sucA	GAAGCGGTATGCGTTAATG	19	48	47		rev primer *sdhAB* sequencing, binds in downstream region
R_sucA_2	ATGAACCGACGTTGAAGG	18	48	50		rev primer *sdhAB* sequencing, binds in downstream region
iclR_TS1F	TCCCCCCGGGATCATGGTGC-CCATACCG	28	56	67	XmaI	fwd primer TS1 for *iclR* deletion

Table A.1 List of oligonucleotides for sequencing or molecular cloning purposes (continued).

oligo name	sequence 5' → 3'	length [nt]	T_a [°C]	GC [%]	5'-extension	function
iclR_TS1R	GCCAACCTGACGCACGAAAC-CCTGCTGTTGCATCGTGGT	39	82	58	20 nt overlap with iclR_TS2F	rev primer TS1 for *iclR* deletion
iclR_TS2F	GTTTCGTGCGTCAGGTTGGC-CTTTTTCTGGCGGGCAGAGG	40	56	60	20 nt overlap with iclR_TS1R	fwd primer TS2 for *iclR* deletion
iclR_TS2R	TTCCGCGGCCGCTATGGCCG-ACGTCGACGGCAATGGTTTG-AGTAAG	46	56	60	SalI	rev primer TS2 for *iclR* deletion
sdhAB_-TS1F	GGAATTCTTACCGCTCTGGC-GTATC	25	55	52	EcoRI	fwd primer TS1 for *sdhAB* deletion
sdhAB_-TS1R	CACACACCCCACACCACAAC-GAATCCATAAATCACGTAAA	40	75	45	20 nt overlap with sdhAB_TS2F	rev primer TS1 for *sdhAB* deletion
sdhAB_-TS2F	GTTGTGGTGTGGGGTGTGT-GACCGTAGGCCTGATAAGACG	40	56	57	20 nt overlap with sdhAB_TS1R	fwd primer TS2 for *sdhAB* deletion
sdhAB_-TS2R	CGGGATCCAACGTGAAGCGT-CTTTCG	26	56	57	BamHI	rev primer TS2 for *sdhAB* deletion

GC: Guanine-Cytosine content

seq: oligonucleotide for sequencing purposes

T_a: annealing temperature for those nt of an oligonucleotide involved in base pairing

Gib: oligonucleotide used in a Gibson Cloning one-step ISO DNA assembly reaction

A.3. Cloning plasmids

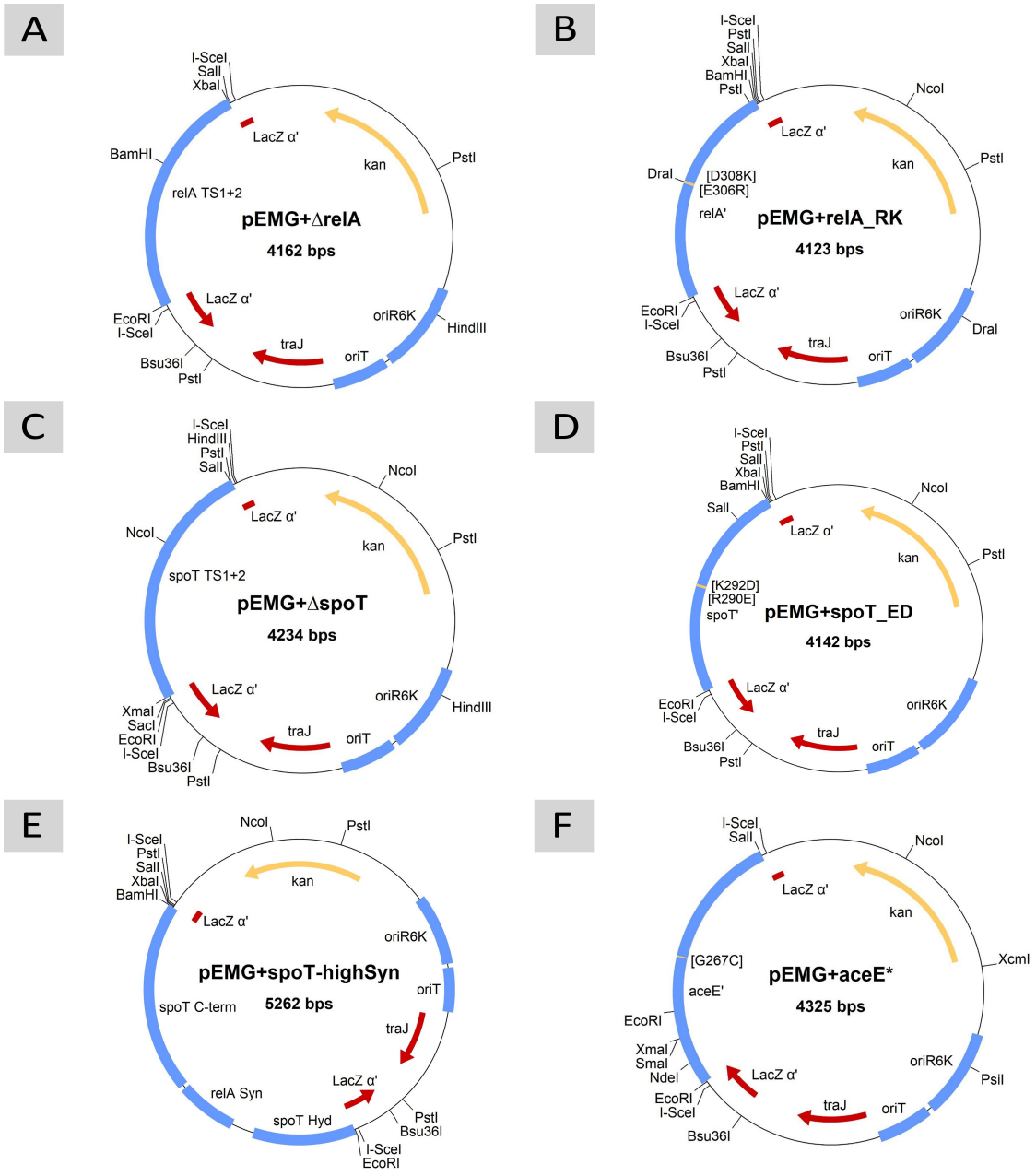

Figure A.1. Vector maps of all pEMG cloning plasmid variants used for chromosomal modifications. A-B: Variants of the pEMG vector with *relA*: ppGpp synthase I. C-E: Vector variants containing fragments of *spoT*: ppGpp 3'-pyrophosphohydrolase and synthase II. F: pEMG vector variant with a mutant *aceE* version: Pyruvate dehydrogenase. *ori*R6K: origin of replication; Kan: kanamycin resistance gene; *ori*T: origin of transfer; *traJ*: conjugal mobility; *lacZ*α: fragment of β-D-galactosidase including the MCS; TS1+2: target sequences, C-term: C-terminus; Syn: synthase region; Hyd: hydrolase region.

A.4. Figures and Data of Bacterial Cultivations

A.4.1. Shaking Flask Cultivations of *E. coli*

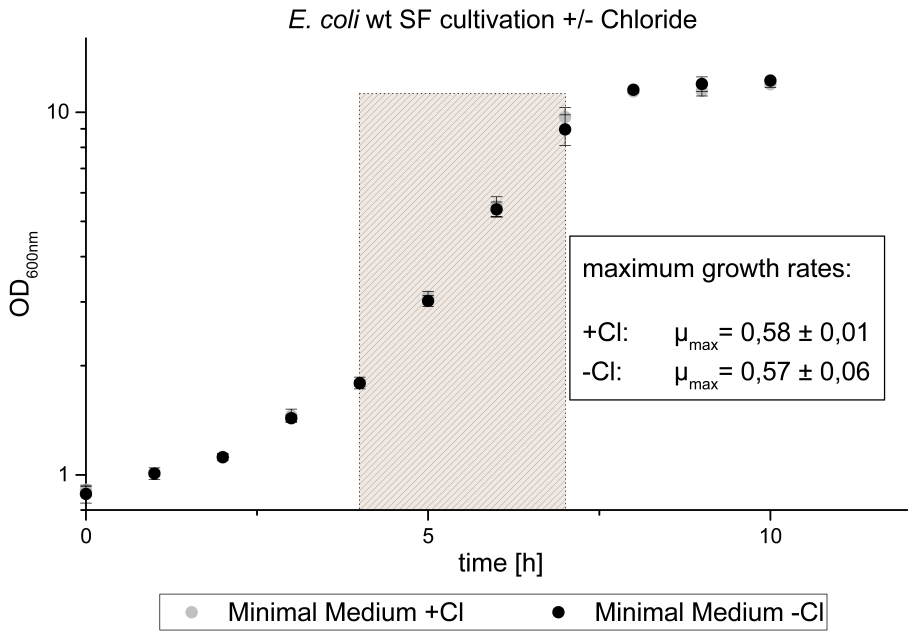

Figure A.2. Comparison of *E. coli* WT growth with and w/o Chloride. *E. coli* K-12 MG1655 WT growth curves in Minimal Medium for bacterial growth as described in Table 3.6 (-Cl, black circles) and supplemented with 20 mM chloride (+Cl, gray circles) are displayed. The SF cultivations were performed at 37 °C and 130 rpm on a bench top orbital shaker. Data points derive from mean value calculations and determination of standard deviations of three individual SF cultivations each.

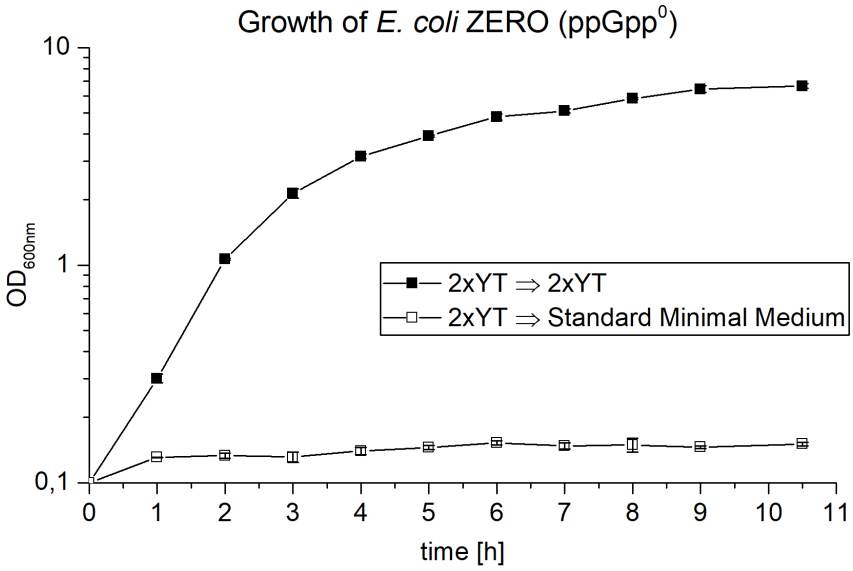

Figure A.3. Growth of *E. coli* ZERO in Complex and Minimal Medium. An overnight culture of *E. coli* ZERO was grown at 37 °C and 130 rpm on an orbital shaker. Cells were washed in 0.9% NaCl solution and transferred into 500 mL baffled shaking flasks containing 60 mL fresh 2×YT (Complex) or Standard Minimal Medium and grown under the same conditions. While the ppGpp^0 mutant was unable to grow upon transfer into Minimal Medium, growth in Complex Medium followed a rather linear than exponential course. Data represent mean values with standard deviations, n=3.

A.4.2. Bioreactor Cultivations of *E. coli*

Table A.2. Maximum CDW from 40 mM NH_4^+ as limiting nutritional factor.

E. coli MG1655	CDW [g L^{-1}]
WT	3.38 ± 0.03
HGT	3.27 ± 0.07
Δ*relA*	3.26 ± 0.04
ACE	3.31 ± 0.04
SR	3.23 ± 0.02
HS #13	3.27 ± 0.07
HS #77	3.36 ± 0.03
*spoT*_ED	3.24 ± 0.01

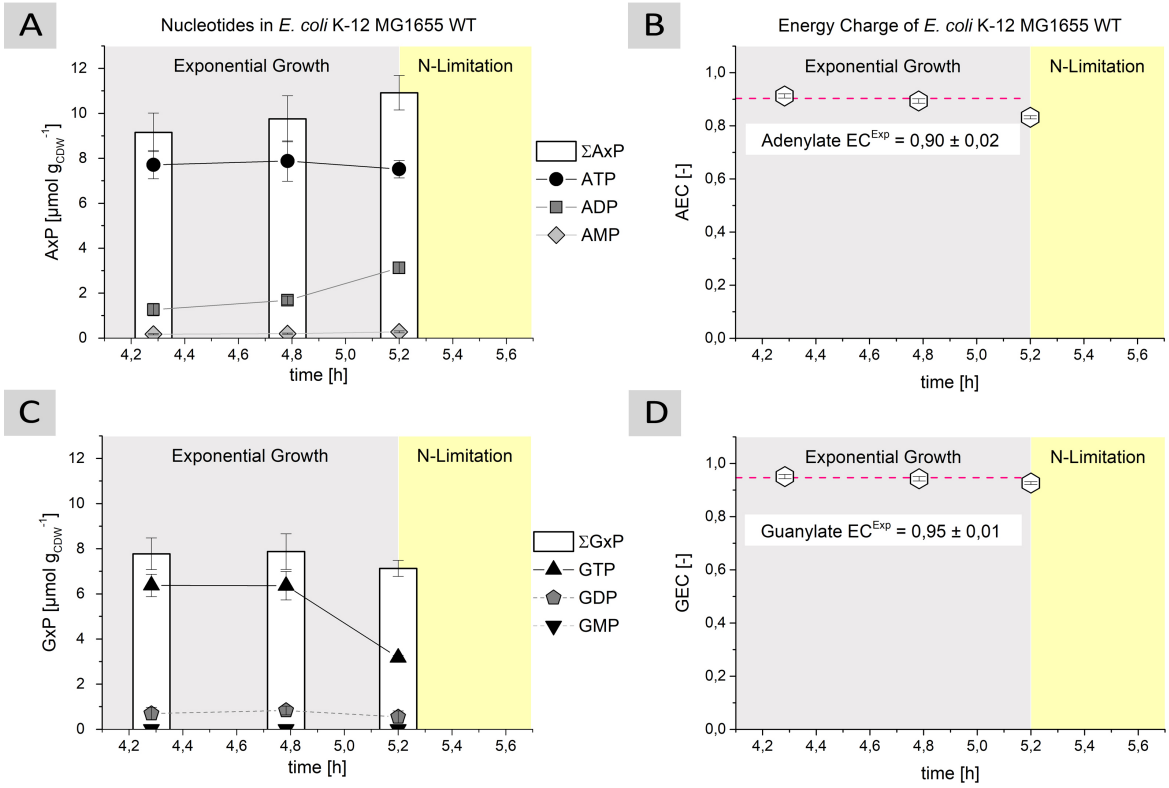

Figure A.4. Nucleotide levels and energy charge in *E. coli* K-12 MG1655 WT during exponential growth. A&C: Adenylate and guanylate nucleotide concentrations are shown for *E. coli* K-12 MG1655. Cells are exponentially growing in a pH, temperature and O_2 controlled bioreactor system. The third time point was measured at transition from nutrient surplus into nitrogen limitation (N-Limitation). B&D: The calculated adenylate energy charge (AEC) and guanylate energy charge (GEC) values are shown for each time point. Also a mean energy charge value and the standard deviation are indicated, calculated from the first two exponential growth data points.

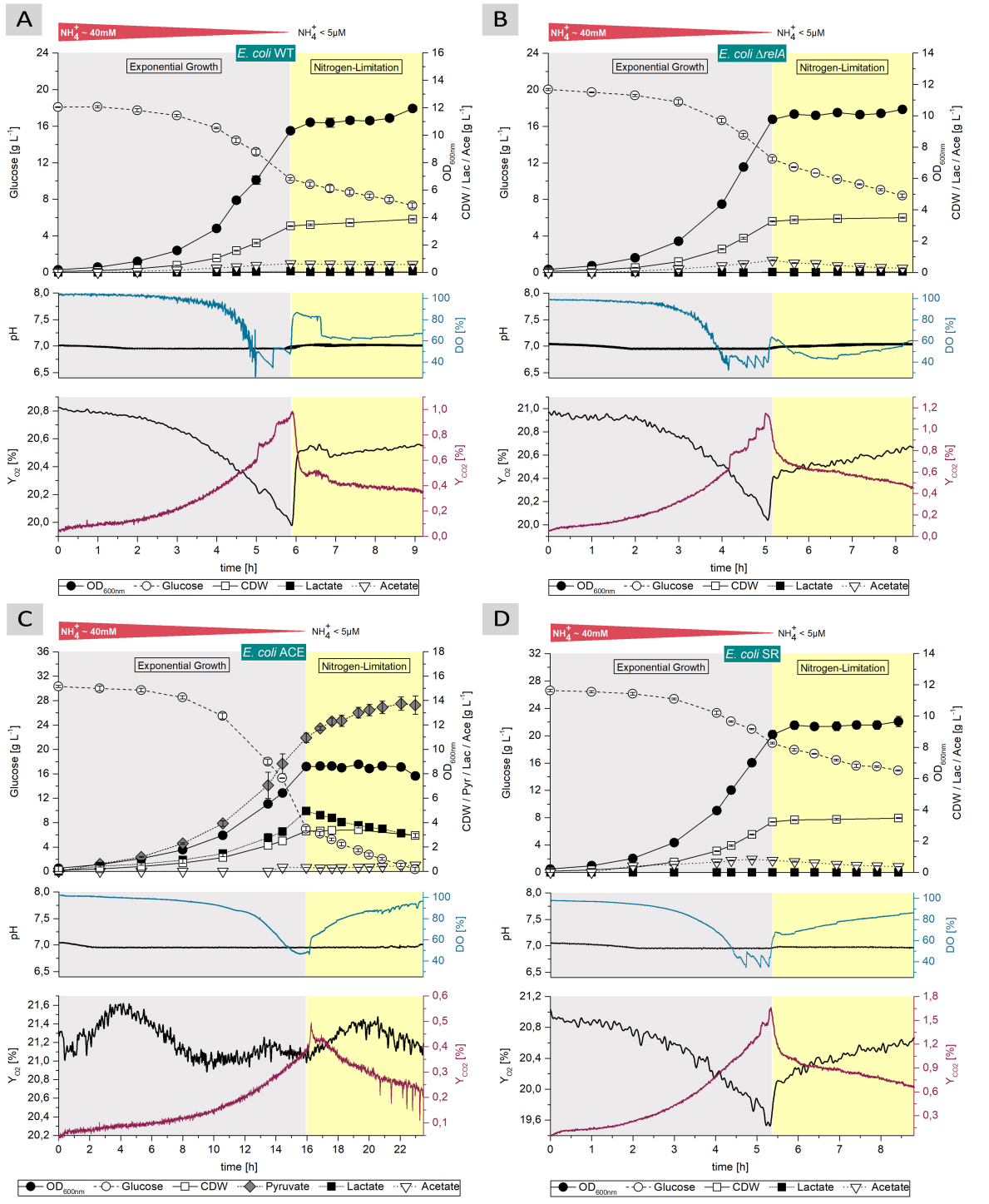

Figure A.5. Nitrogen-limited two-stage bioreactor cultivations. Parallelized microbial cultivations in the triplex bioreactor system are described for different mutant strains of *E. coli* MG1655 and the WT in minimal medium at 37 °C. Bacterial growth curves, glucose consumption and formation of various organic acids were measured for all individual process times to ensure sufficient sampling intervals as well during exponential growth (gray) as for the Nitrogen-limited phase (yellow). Controlled pH and DO ratio progressions are displayed in each middle graph sections. Where available, lower graph sections show the monitoring of O_2 and CO_2 percentage shares in the exhaust gas along the process.

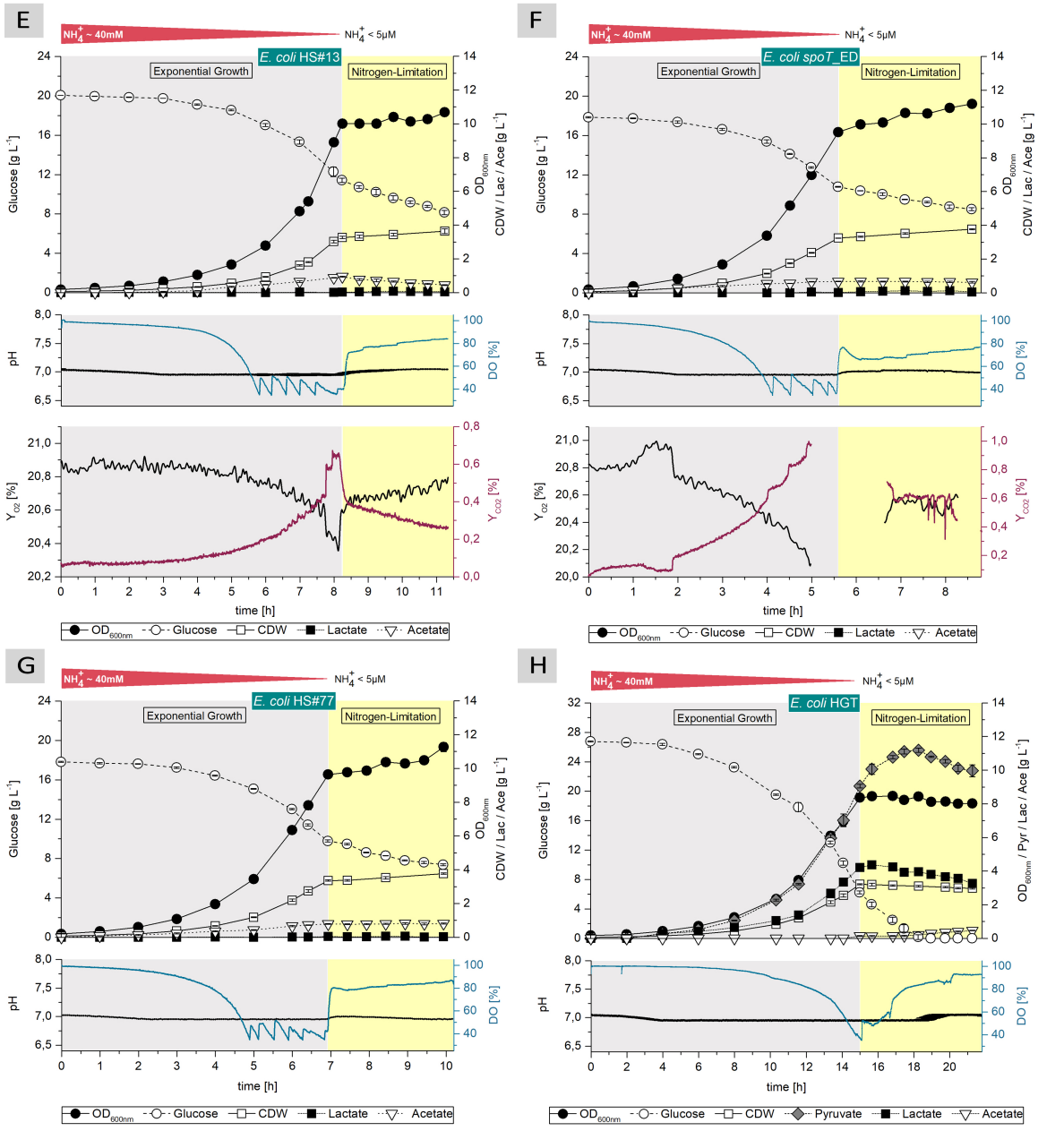

Figure A.5 Nitrogen-limited two-stage bioreactor cultivations (continued). Parallelized microbial cultivations in the triplex bioreactor system are described for different mutant strains of *E. coli* MG1655 and the WT in minimal medium at 37 °C. Bacterial growth curves, glucose consumption and formation of various organic acids were measured for all individual process times to ensure sufficient sampling intervals as well during exponential growth (gray) as for the Nitrogen-limited phase (yellow). Controlled pH and DO ratio progressions are displayed in each middle graph sections. Where available, lower graph sections show the monitoring of O_2 and CO_2 percentage shares in the exhaust gas along the process.

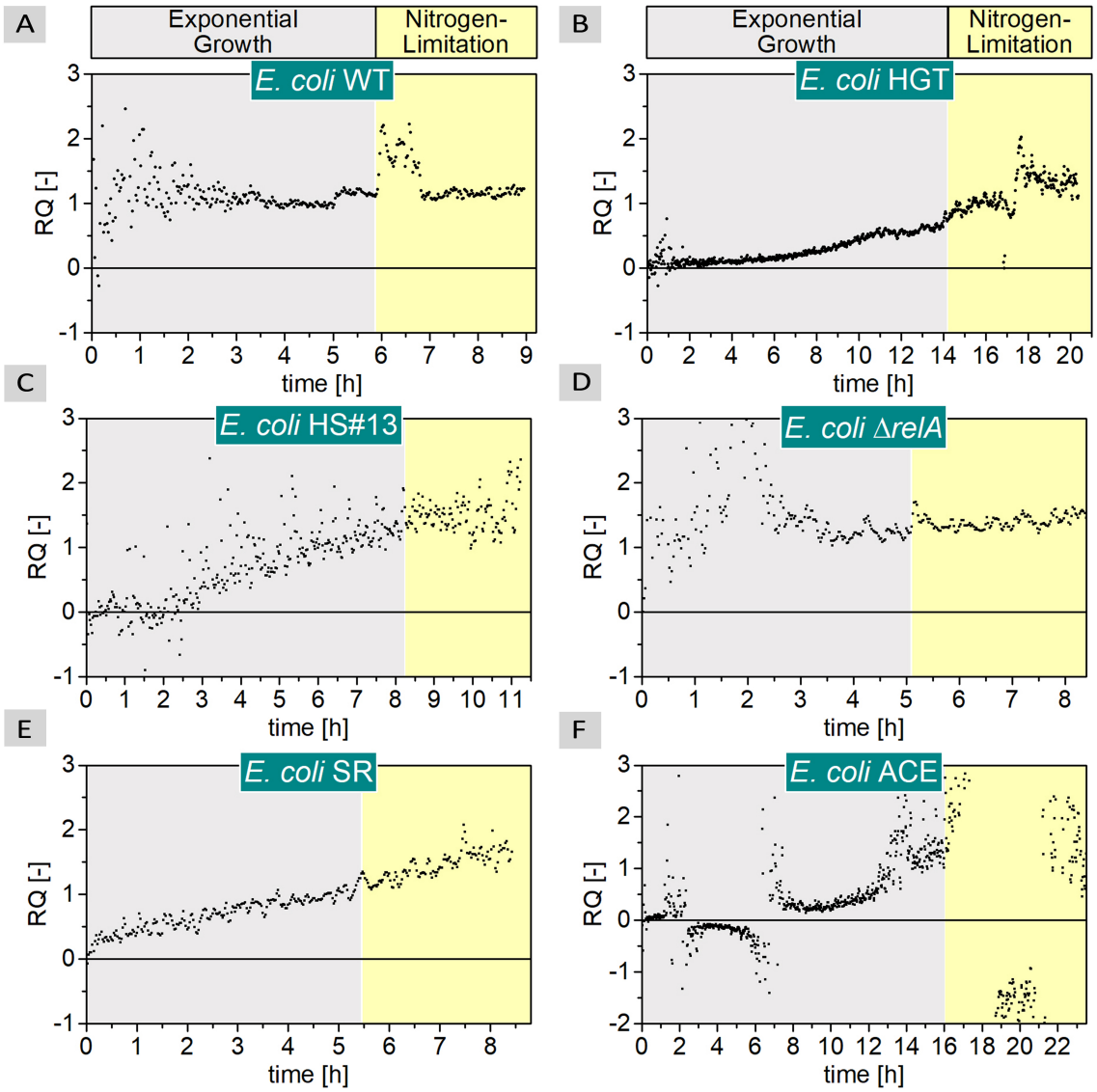

Figure A.6. Respiratory quotients of various *E. coli* MG1655 mutants strains. The respiratory quotient (RQ) values for different *E. coli* mutants were calculated from carbon and oxygen ratios in the exhaust gas analysis and plotted against process time. Unlimited growth phases with nutrient excess conditions are highlighted in gray. Whereas, nitrogen-limited fermentation phases are marked with a yellow background color.

Table A.3. Estimation of maintenance demands from 'Pirt-like' diagram. Glucose consumption for cell maintenance of *E. coli* WT and another seven mutant strains estimated from interception with y-axis (Figure 5.3).

E. coli MG1655	estimated m_S demand [g_{Glc} g_{CDW}^{-1} h^{-1}]
WT	0.14
HGT	0.59
Δ*relA*	0.33
SR	0.32
ACE	0.27
HS #13	0.22
HS #77	0.13
*spoT*_ED	0.11

A.4.3. Aerobic Succinate Producing Mutant

E. coli MG1655 SUC was constructed with the help of two cloning plasmids (Figure A.7) as a second potential representative for a C-source-dependent microbial chassis. This aerobic succinate producer is genetically based on three in frame deletions of genes related to proteins of the TCA cycle and the glyoxylate shunt (Figure A.8).

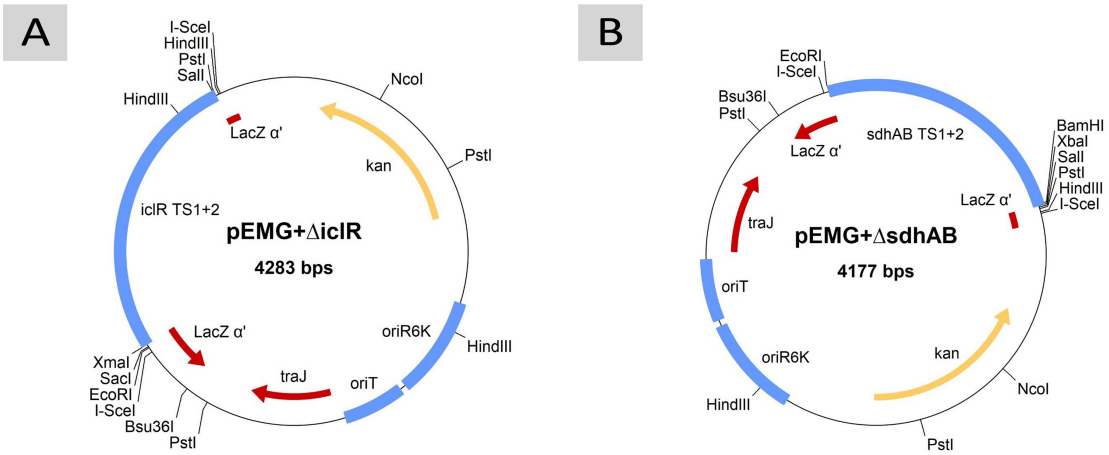

Figure A.7. Vector maps of pEMG cloning plasmids used for generation of *E. coli* SUC. A-B: Variants of the pEMG vector with *iclR*: Isocitrate lyase Regulator and *sdhAB*: Succinate dehydrogenase subunits. *ori*R6K: origin of replication; Kan: kanamycin resistance gene; *ori*T: origin of transfer; *traJ*: conjugal mobility; *lacZ*α: fragment of β-D-galactosidase including the MCS; TS1+2: target sequences.

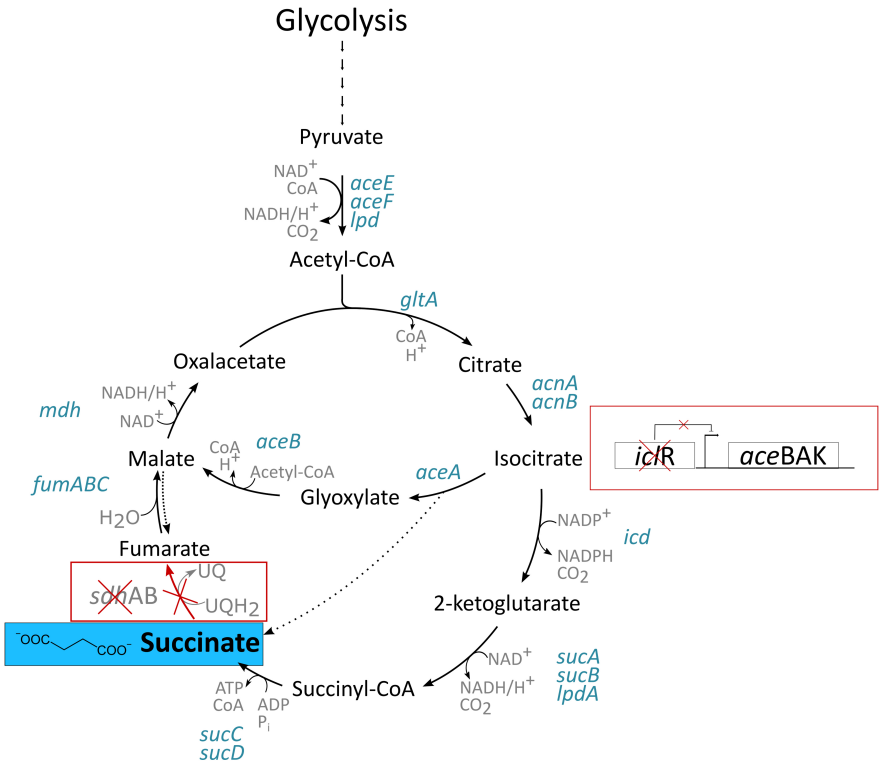

Figure A.8. Metabolic pathway for aerobic succinate production with *E. coli* SUC. Regulatory scheme of the Tricarboxylic Acid Cycle (TCA) with an open glyoxylate shunt. Deletion of the *iclR* gene results in a permanently active glyoxylate bypass, giving two ways of succinate production. Loss of the conversion step from succinate to fumarate leads to succinate accumulation and transport. Genes involved in the TCA cycle: *gltA* (Citrate Synthase); acnAB (Aconitate Hydratases); *icd* (Isocitrate Dehydrogenase); *sucAB*/*lpdA* (2-keto-Glutarate Dehydrogenase complex); *sucCD* (Succinyl-CoA Synthetase); *fumABC* (Fumarases); *mdh* (Malate Dehydrogenase). Genes of the glyoxylate shunt: *aceA* (Isocitrate Lyase); *aceB* (Malate Synthase A).

In a first cloning round, a fragment of the 3'-region in the transcriptional repressor *iclR*, regulator of the *aceBAK* operon, was removed from the chromosome leaving the intrinsic *metH* P2 promoter intact. This led to a complete absence and inactivation of the Isocitrate Lyase regulator protein IclR. Hence, the glyoxylate bypass is permanently open and unregulated, even in the presence of glucose as main C-source. Succinate is now converted regularly from succinyl-CoA via Succinyl-CoA Synthetase (*sucCD*) and from isocitrate by Isocitrate Lyase (*aceA*). The second step in metabolic engineering of the succinate producer included additional deletions of the two hydrophilic subunits SdhA and SdhB (*sdhAB*) from the prokaryotic succinate-ubiquinone oxidoreductase (SQR) complex (Lin et al. 2005). Metabolic loss of these two Succinate Dehydrogenase enzymes termi-

nates formation of fumarate from succinate and promotes succinate accumulation and transport. Growth parameters and succinate formation performance of *E. coli* SUC are described in Figure A.9 and Table A.4.

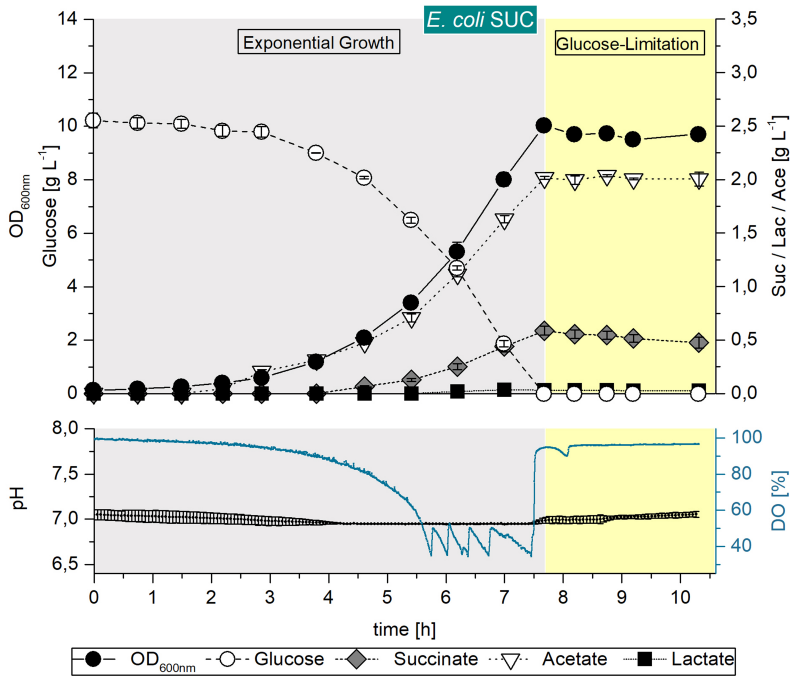

Figure A.9. Aerobic cultivation of *E. coli* SUC in the triplex bioreactor system. The microbial culture was inoculated from an overnight growing preculture and grown under aerobic batch conditions in Minimal Medium at 37 °C. Glucose was supplemented in an initial concentration of 10 g L^{-1} as only carbon source. Optical Density as well as glucose and organic acid concentrations were measured at several time points during exponential growth (yellow) and right after glucose depletion. Data represent mean values with standard deviations, n=3.

Table A.4. Yields and biomass-specific rates for *E. coli* SUC. Maximum growth rate μ_{max}, biomass from substrate yield $Y_{X/S}$, biomass-specific glucose consumption q_S, succinate from substrate yield $Y_{P/S}$, biomass-specific succinate production q_P.

μ_{max} [h^{-1}]	$Y_{X/S}$ [g_{CDW} g_{Glc}^{-1}]	$Y_{P/S}$ [g_P g_{Glc}^{-1}]	q_S [g_{Glc} g_{CDW}^{-1} h^{-1}]	q_P [g_P g_{CDW}^{-1} h^{-1}]
0.67 ± 0.02	0.31 ± 0.01	0.07 ± 0.00	2.16 ± 0.02	0.09 ± 0.00

B. Publication

B.1. Manuscript

The following article was published in *Metabolic Engineering* 40: 93-103 in 2017.

Escherichia coli HGT: Engineered for high glucose throughput even under slowly growing or resting conditions

Annette Michalowski, Martin Siemann-Herzberg, Ralf Takors∗

University of Stuttgart, Institute of Biochemical Engineering, Allmandring 31, 70569, Stuttgart, Germany

∗Corresponding author: takors@ibvt.uni-stuttgart.de

Keywords: High glucose uptake, Stringent response, ppGpp, Nitrogen-limitation, *Escherichia coli*

A B S T R A C T

Aerobic production-scale processes are constrained by the technical limitations of maximum oxygen transfer and heat removal. Consequently, microbial activity is often controlled via limited nutrient feeding to maintain it within technical operability. Here, we present an alternative approach based on a newly engineered *Escherichia coli* strain. This *E. coli* HGT (high glucose throughput) strain was engineered by modulating the stringent response regulation program and decreasing the activity of pyruvate dehydrogenase. The strain offers about three-fold higher rates of cell-specific glucose uptake under nitrogen-limitation (0.6 g_{Glc} g_{CDW}^{-1} h^{-1}) compared to that of wild type, with a maximum glucose

uptake rate of about 1.8 g_{Glc} g_{CDW}^{-1} h^{-1} already at a 0.3 h^{-1} specific growth rate. The surplus of imported glucose is almost completely available via pyruvate and is used to fuel pyruvate and lactate formation. Thus, *E. coli* HGT represents a novel chassis as a host for pyruvate-derived products.

1. Introduction

Aerobic industrial production processes using microbes are predominantly run in fed-batch mode to achieve the highest product titers, substrate conversion yields and product purity. After the exponential phase of biomass formation, such processes typically need to induce low microbial activities to meet the technical limitations in maximum oxygen transfer (often in the range of 150–180 mmol L^{-1} h^{-1}) and heat removal (Takors, 2012). As an easy-to-implement measure, operators in industrial plants often introduce carbon (glucose)-limiting feeds, which in turn also reduce product formation rates.

If process engineers were asked to list the characteristics of ideal producers, they would prefer strains that show high product conversion rates, even if they are limited in growth and oxygen uptake. In other words, cell-specific productivity and conversion yield should be high in non-growing (resting) or slowly growing cells.

Studying *Escherichia coli*, Chubukov and Sauer (2014) have shown that the limitation of nitrogen, phosphate, sulfur or magnesium yields different glucose conversion rates for non-growing cells, for example achieving biomass-specific glucose uptake rates of 0.083 and 0.162 g_{Glc} g_{CDW}^{-1} h^{-1} for the limitation of nitrogen and phosphate, respectively. In comparison, a documented value of maintenance for *E. coli* is only 0.057 g_{Glc} g_{CDW}^{-1} h^{-1} (Nielsen et al., 2003) derived from glucose-limited conditions and some authors have even detected lower values about 0.024 g_{Glc} g_{CDW}^{-1} h^{-1} (Taymaz-Nikerel et al., 2010). Indeed, proper phosphate-limitation may be a useful tool for industrial applications to install nutrient limitations without limiting elements of the target molecules, but it has inherent drawbacks that could severely hamper large-scale productions (Schuhmacher et al., 2014). The question therefore arises as to whether *E. coli* strains can be specifically engineered to create a chassis for high glucose uptake even under non- or slowly-growing conditions.

Studies on pyruvate production by Zhu et al. (2008) have shown that reducing the activity of AceE (E1 component of pyruvate dehydrogenase complex, PDHC) is essentially beneficial for achieving high glucose uptake rates. Accordingly, likewise strains may serve as a starting point of strain engineering for providing enhanced amounts of pyruvate for downstream products. However, strain performance in large-scale is often

hampered by regulation programs that are induced under such heterogeneous conditions. Recent studies by Löffler et al. (2016) revealed that stringent response plays a key role in large-scale fermentations, because related regulation programs are frequently switched on and off when circulating cells face heterogeneities in a production vessel. The stringent response is very complex (Fig.1); activating and repressing different segments of microbial metabolism at the same time and closely networking with cAMP- and Cra-mediated control regimes (Hardiman et al., 2007; Johansson et al., 2000; Lemuth et al., 2008). GTP pyrophosphokinase is encoded by the *relA* gene and plays a dominant role, as it is responsible for production of the stringent response alarmone (p)ppGpp (from here on referred to as ppGpp).

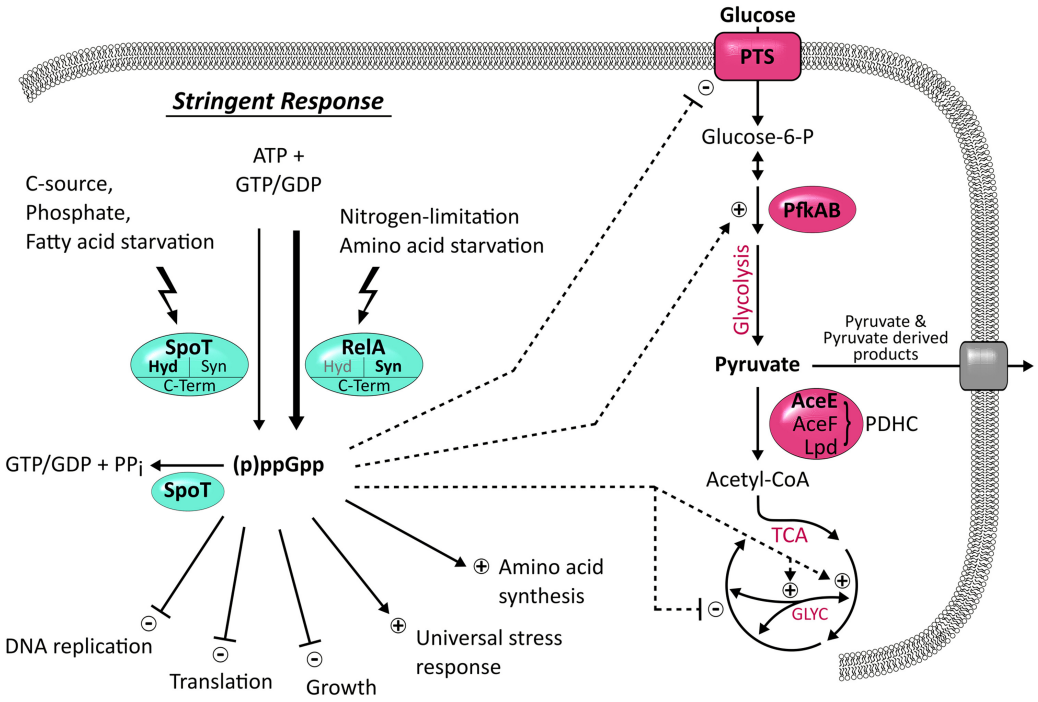

Fig. 1. Stringent response in *Escherichia coli*.

Nutritional depletion conditions in the environment are sensed by the two major factors of stringent response: RelA and SpoT. Intracellular signaling occurs via the alarmone (p)ppGpp, which is catalyzed from ATP and GTP or GDP, respectively. Activity of RelA is initiated at nitrogen-based stress conditions (Brown et al., 2014) and amino acid starvation (Haseltine and Block, 1973). SpoT is activated e.g. upon phosphate (Bougdour and Gottesman, 2007), carbon (Gentry and Cashel, 1996) or fatty acid starvation (Battesti and Bouveret, 2006). The two proteins share high structural similarity within their conserved N- and C-terminal (C-Term) domains, although the monofunctional RelA pro-

tein exerts only (p)ppGpp synthase activity, while SpoT has both abilities of (p)ppGpp synthesis (Syn) and hydrolysis (Hyd). Elevated (p)ppGpp levels have activating (plus symbol) or inhibitory (minus symbol) regulatory effects on various cellular mechanisms. Transcription profiling studies (Durfee et al., 2008; Traxler et al., 2008) suggest possible effects of (p)ppGpp on different sites of the central carbon metabolism (indicated with dashed arrows), like the PTS (phosphotransferase system), glycolysis (PfkAB: phosphofructokinase), TCA (tricarboxylic acid) cycle and GLYC (glyoxylate cycle).

Consequently, changing fundamental glucose uptake kinetics is a challenging goal that requires the careful modulation of regulatory signals, such that glucose uptake of *E. coli* is increased to provide a surplus for product formation that native regulatory programs would prevent. The present study demonstrates the engineering and kinetic characterization of *E. coli* HGT (high glucose throughput) as a novel chassis for exploiting additional glucose uptake to fuel product formation even under non- or slow-growth conditions.

2. Material and methods

2.1 Strains and plasmids

The laboratory wild type strain *Escherichia coli* MG1655 (Leibniz Institute DSMZ-German Collection of Microorganisms and Cell Cultures; #DSM-18039) was used in all experiments. This host strain and its derivatives as well as all plasmids and oligonucleotides used in this study are listed in Table 1. For cloning purposes, strains were grown either on tryptone-yeast extract (2×TY (Sambrook and Russell, 2001)) agar plates or in 5 mL 2×TY in glass reaction tubes, supplemented with the appropriate antibiotic at 50 µg mL^{-1}.

2.2 Scarless genome modifications

Chromosomal modifications of genes, without leaving any marker sequences in the genome, were accomplished by combining the pEMG and pACBSR genetic systems. The donor plasmid constructs (pEMG) were designed using classical cloning methods, as described in the deletion/replacement system protocol (Martínez-García and de Lorenzo, 2012) for pEMG+Δ*relA* and pEMG+*spoT*$^{[R290E;K292D]}$. Another pEMG plasmid construct, pEMG+*aceE*$^{[G267C]}$ was cloned using the Gibson one-step ISO assembly method (Gibson, 2011). Plasmid DNA was transfected into cells via electroporation. First, the pEMG

donor plasmid was delivered into host cells. Due to a missing *pir* gene in the *E. coli* MG1655 hosts, *ori*R6K is unable to replicate, and thus the pEMG plasmid sequences were integrated into the host chromosome (Filutowicz et al., 1986). These co-integrates were resolved by introducing the pACBSR plasmid and inducing transcription of I-SceI and the λ Red genes with L-arabinose. The homing endonuclease, I-SceI, cuts the donor plasmid and generates double-strand breaks in flanking regions of the desired mutations. Products of the λ Red genes subsequently seal these linear fragments by homologous recombination with the chromosome (Herring et al., 2003). Plasmid sequences and genetic modifications were verified by Sanger sequencing (GATC, Konstanz, Germany). Amino acid positions in proteins of *E. coli* MG1655 derive from predicted protein sequences from the Universal Protein Resource Knowledgebase (UniProt Consortium, 2015). Both amino acid positions in SpoT, which were targets of genetic manipulation, were identified based on the UniProtKB entry with accession number P0AG25. The G267C amino acid substitution in AceE occurred spontaneously in *E. coli* tests causing a growth phenotype that encouraged further sequencing and engineering in *E. coli* HGT. This position in AceE was determined based on the UniProtKB entry P0AFG8. For each sequence, Met-1 was considered as first amino acid and starting point of the counting method.

2.3 Fermentation and growth conditions

Precultures of all four fermenter strains (Table 1) were grown aerobically in minimal medium at 37 °C on a rotary shaker at 130 rpm (Infors HT, Bottmingen, Switzerland). From glycerol stock seed cultures, 50 µL of *E. coli* MG1655 wild type (*E. coli* WT) and the stringent response mutant *E. coli* Δ*relA spoT*[R290E;K292D] (*E. coli* SR) or 100 µL of *E. coli aceE*[G267C] (*E. coli* ACE) and *E. coli aceE*[G267C] Δ*relA spoT*[R290E;K292D] (*E. coli* HGT) were inoculated into 60 mL of minimal medium in 500 mL baffled shaking flasks. Minimal medium consisted of: 0.5 % (w/v) α-D(+)-glucose, 9.84 g L^{-1} $NaH_2PO_4 \cdot 2H_2O$, 4.69 g L^{-1} K_2HPO_4, 1.32 g L^{-1} $(NH_4)_2HPO_4$, 2.68 g L^{-1} $(NH_4)_2SO_4$, 0.88 g L^{-1} Na_2SO_4, 14.7 mg L^{-1} $CaCl_2 \cdot 2H_2O$, 246.5 mg L^{-1} $MgSO_4 \cdot 7H_2O$, 10.1 mg L^{-1} Thiamine HCl, 1:2000 vol. Trace Element Solution (TES: 16.7 g L^{-1} $FeCl_3 \cdot 6H_2O$, 20.1 g L^{-1} Na_2EDTA, 0.18 g L^{-1} $ZnSO_4 \cdot 7H_2O$, 0.10 g L^{-1} $MnSO_4 \cdot H_2O$, 0.16 g L^{-1} $CuSO_4 \cdot 5H_2O$, 0.18 g L^{-1} $CoCl_2 \cdot 6H_2O$). Bacterial precultures were grown to an $OD_{600\ nm}$ of 5, such that 8 mL cell suspension per bioreactor could be used to achieve a starting $OD_{600\ nm}$ of 0.2. Batch fermentations were carried out in triplicates for each *E. coli* mutant in a parallel triplex glass bioreactor system (HWS Labortechnik, Mainz, Germany) with a working

Table 1
Bacterial strains, plasmids and oligonucleotides.

Strain/Plasmid/Primer	Genotype/Sequence (5'-3')	Reference/Purpose
Cloning strain		
E. coli DH5α*λpir*	*supE44*, Δ*lac*U169(Φ80lacZΔM15), *rec*A1, *end*A1, *hsdR*17, *thi*-1, *gyrA*96, *relA*1, λpir phage lysogen	Martínez-García and de Lorenzo (2011)
Fermentation strains		
E. coli MG1655:		
1. WT	*E. coli* wild type strain MG1655: F-, λ-, *ilvG*-, *rfb*-50, *rph*-1	DSM-18039
2. Δ*relA*	*E. coli* WT with deleted *relA* gene (ppGpp synthase I)	Current study
3. ACE	*E. coli* WT with G267C aa substitution in the *aceE* gene (E1p of the pyruvate dehydrogenase complex)	
4. SR	*E. coli* Δ*relA* with two aa substitutions R290E & K292D in the *spoT* gene (ppGpp hydrolase and ppGpp synthase II)	Current study
5. HGT	*E. coli* SR with additional G267C aa substitution in *aceE*	Current study
Plasmids		
pEMG	Km^R, *ori*R6K, *lacZ*αflanked by two I-SceI sites	Martínez-García and de Lorenzo (2011)
pACBSR	Cm^R, p15A*ori*, P_{ara}BAD controlling I-SceI and λRed genes	Herring et al. (2003)
pEMG+Δ*relA*	pEMG with TS1 & TS2 for deletion of *relA*	Current study
pEMG+*spoT*$^{[R290E;K292D]}$	pEMG with 990 bp of *spoT* incl. substitutions R290E&K292D	Current study
pEMG+*aceE*$^{[G267C]}$	pEMG with 1184 bp of *aceE* incl. substitution G267C	Current study
Primer		
pEMG_F	GGCAGCAGCTGAACCAACTC	fwd pEMG sequencing
pEMG_R	AATGCAGCTGGCACGACAGG	rev pEMG sequencing
relA_TS1F	G**GAATTC**TGGATGTGCAACCTGAAG	fwd TS1 relA, EcoRI
relA_TS1R	CCTCTCCTTTAGGGACC-AGACCTGCCGAAATCGGCAAATC	rev TS1 relA
relA_TS2F	TCTGGTCCCTAAAGGAGAGG-GCCGAAATTTGCTCGTATC	fwd TS2 relA
relA_TS2R(3)	GC**TCTAGA**ACAACTTCGAACGGATATCC	rev TS2 relA, XbaI
spoT_ED_TS1F	G**GAATTC**ATCCGCGTCATCCTCATC	fwd TS1 *spoT*$^{[R290E;K292D]}$, EcoRI
spoT_ED_TS1R	ATGGCGATATAGTC*ATC*CAC*TTC*GCCCGGACGCG	rev TS1 *spoT*$^{[R290E;K292D]}$
spoT_ED_TS2F	CGCGTCCGGGC*GAA*GTG*GAT*GACTATATCGCCAT	fwd TS2 *spoT*$^{[R290E;K292D]}$
spoT_ED_TS2R(2)	CG**GGATCC**TTCAGCCAAGCGGCATTC	rev TS2 *spoT*$^{[R290E;K292D]}$, BamHI
aceE_TS1F	CAGTATAGGGATAACAGGGTAATCTGAATTC-TCCGGGTAATCTGGAACTG	fwd TS1 *aceE*$^{[G267C]}$, pEMG overlap
aceE_mut_TS1R	TTACCGGTGACCGG*GCA*GTCAAGACGCTGCA	rev TS1 *aceE*$^{[G267C]}$
aceE_mut_TS2F	TGCAGCGTCTTGAC*TGC*CCGGTCACCGGTAA	fwd TS2 *aceE*$^{[G267C]}$
aceE_TS2R	TGTTATCCCTAGAAGCTTGCATGCCTGCAGGTCGAC-GACGGCTTGGCAGATAACC	rev TS2 *aceE*$^{[G267C]}$, pEMG overlap

aa: amino acid, Km^R: kanamycin resistance, Cm^R: chloramphenicol resistance, TS: targeting sequence, *ori*R6K: replication dependent on λpir, p15A*ori*: origin of replication, P_{ara}BAD:L-arabinose inducible promoter, restriction enzyme sites are highlighted, overlapping regions are underlined, nucleotide exchange sequences are shown in italics.

volume of 250 mL. The composition of the nitrogen-reduced batch minimal medium was equal to the preculture minimal medium, except for the addition of $(NH_4)_2SO_4$, which was supplied at only 1.27 g L^{-1}. Initial glucose starting concentrations varied for all different *E. coli* mutants and are listed in Table 2. Standard sensor equipment was used to record pH and pO_2 (Mettler-Toledo GmbH, Albstadt, Germany). The temperature was kept constant at 37 °C, pH was maintained at 7.0 and the dissolved oxygen concentration was

kept ≥30 % by constant online measurements and adjustment of agitation speed and gas flow rate. The pH value was automatically regulated by addition of 0.5 M NaOH or 0.5 M H_2SO_4, as required. To prevent foam formation in the reactors, 50 µL Struktol™J 647 (Schill+Seilacher, Hamburg, Germany) was added prior to start of cultivation.

2.4 Biomass-specific rates

During exponential growth, all biomass-specific rates were either obtained directly from linear regression of the logarithmic $OD_{600\ nm}$ plots or calculated from specific growth rates and the yield coefficients. Under nitrogen-limited conditions, biomass-specific rates were calculated as the slope from the approximated linear fit for each investigated period divided by the arithmetic mean of the biomass concentration. This gives biomass-specific glucose consumption rates q_S, biomass-specific growth rates µ, biomass-specific product synthesis rates q_{Pyr} and biomass-specific respiratory rates qO2 and qCO2. Data was analyzed with a one-way ANOVA for statistical significance.

2.5 Analytics

Biomass formation was followed by measurement of $OD_{600\ nm}$ on a GeneQuant™ spectrophotometer (Fisher Scientific, MA, USA). For selected time points, cell dry weight (CDW) was determined by drying double-washed cell pellets from 0.5 mL cell suspension at 110 °C for 24 h. Correlations between $OD_{600\ nm}$ and CDW revealed a factor of 0.3 for all tested mutants. In this way, biomass values could be calculated for the missing time points with the equation $CDW = OD_{600\ nm} \times 0.3$, where no CDW samples were taken. Ammonium concentration in the supernatant was analyzed using test kits LCK303 and LCK304 (Hach Lange, Duesseldorf, Germany) at the start and immediately after the oxygen signal shifted upwards, which indicated the beginning of nitrogen-limitation.

Organic compounds and sugars from the supernatant were separated by high-pressure liquid chromatography (HPLC) in a Rezex ROA organic acid H+(8 %) column (300 mm × 7.8 mm, 8 µm Phenomenex, Aschaffenburg, Germany) on an Agilent 1200 series device (Agilent Technologies GmbH, Waldbronn, Germany), equipped with a refractive index detector (32 °C). The main column was protected by a Rezex ROA organic acid H+(8 %) guard column (50 mm × 7.8 mm). Different organic components in the samples were separated in the column for 45 min at 50 °C under isocratic conditions at a constant flow rate of 0.4 mL min^{-1}. The mobile phase consisted of a 5 mM H_2SO_4 solution, which

was sonicated for 15 min. Prior to HPLC, the dissolved phosphate in a 1 mL sample volume was precipitated by adding 45 µL 4 M NH_3 and 100 µL 1.2 M $MgSO_4$ followed by mixing and incubating for 5 min. The $MgSO_4$ solution was supplemented with 2.29 g L^{-1} L-rhamnose, which served as internal standard with a final concentration of 100 mg L^{-1} to allow correction of the quantified data for technical variation. All steps of this procedure were carried out at room temperature. After incubation, samples were centrifuged at 20,000×g for 5 min. A 500 µL aliquot of the supernatant was then added to 500 µL of 0.1 M H_2SO_4, thoroughly mixed, incubated for 15 min and again centrifuged at 20,000×g for 15 min. The clear and residue-free supernatant was either stored at -20 °C, or directly processed for HPLC.

Nucleotides such as ppGpp, ATP, ADP and AMP were analyzed by ion-pair reversed-phase HPLC (RP-HPLC) on an Agilent 1200 series apparatus. The measuring procedure was similar to published methods (Cserjan-Puschmann et al., 1999), with some modifications. Samples were withdrawn from the bioreactor with a disposable syringe, about 1,000 µL fermentation broth was rapidly transferred into 250 µL pre-cooled (-20 °C) 35 % $HClO_4$ and mixed immediately on a rotary shaker for 15 min at 4 °C. This lysed the cells and stopped all biochemical reactions immediately. All reaction tubes were weighed before and after sample addition to obtain the actual volume of extracted fermentation broth. After incubation, samples were neutralized on ice with 250 µL ice-cold 1 M K_2HPO_4 and 185 µL ice-cold 5 M KOH. To maintain a clear supernatant, samples were mixed immediately and all solid cellular residues as well as precipitated $KClO_4$ were removed by centrifugation at 22,000×g for 15 min at 4 °C. The resulting nucleotide extracts were stored at -70 °C until RP-HPLC measurement. Before injection into the HPLC system, the pH of each sample was adjusted to 7.0 ± 0.05 and the solution was centrifuged again at the above conditions. Separation and quantification of nucleotides was performed using a Supelcosil™ LC 18-T column (250 mm × 4.6 mm, 3 µm Supelco Inc., Bellefonte, PA, USA) protected by a Hypersil™ BDS C18 guard column. The mobile phase consisted of two separate eluents. Buffer A was composed of 100 mM K_2HPO_4/KH_2PO_4 and 4 mM tetrabutylammonium sulfate at pH 6.0. Buffer B contained 70 vol% Buffer A adjusted to pH 7.2 and 30 vol% CH_3OH. Both solvents were pumped at a constant flow rate of 1 mL min^{-1} at 30 °C with the following gradient program: 100 % Buffer A for the first 3.5 min, incrementing to 100 % Buffer B during the next 40 min, 100 % Buffer B plateau for 7.5 min, shifting to 100 % Buffer A within 5 min and finally a plateau of 100 % Buffer A for the last 10 min. Nucleotides were detected using a diode array detector set at 260 nm and 340 nm. Adenylate energy charges (AEC) were calculated according to

previous methods (Atkinson and Walton, 1967):

$$AEC = \frac{[ATP] + 0.5[ADP]}{[AMP] + [ADP] + [ATP]} \quad (1)$$

3. Results

3.1 Construction of E. coli *mutants*

Independent studies from other groups have shown that varying ppGpp concentrations upon transition into nutritional stress can have contradictory effects on the outcome of product synthesis rates. Amplified ppGpp levels have been shown to intensify the overproduction of metabolites derived from central metabolism (Imaizumi et al., 2006). In contrast, ppGpp-deficient strains showed improved recombinant protein formation (Dedhia et al., 1997). More recent results point to putatively elevated glucose consumption during nutrient deprivation, along with enhanced biosynthesis of recombinant green fluorescent protein (GFP) in strains performing attenuated ppGpp synthesis (Carneiro et al., 2011).

To investigate glucose uptake phenotypes of different mutants of *E. coli* MG1655, strains with reduced stringent response, partly in combination with impaired pyruvate conversion activity, were constructed. On the basis of the Δ*relA* (GTP pyrophosphokinase or ppGpp synthase I) host, two additional point-mutations were introduced into *spoT*, the gene encoding for ppGpp 3'-pyrophosphohydrolase and ppGpp synthase II, to generate *E. coli* SR (stringent response). Accordingly, these two amino acid exchanges Arg290Glu [R290E] and Lys292Asp [K292D] inside the synthase domain cause a charge reversal in the catalytic site and lead to different substrate binding affinities (Sajish et al., 2007). Additionally, a single point mutation leading to the amino acid exchange Gly267Cys [G267C] in AceE (E1p component of the PDH complex) was inserted into the *E. coli* SR host to investigate interactions between glucose uptake and changing AceE activity. The site-specific single amino acid substitution is located in close proximity to the thiamine- and Mg^{2+}-binding sites within the N-terminal domain of the AceE protein. These actions resulted in the high glucose throughput mutant *E. coli* HGT, which is part of patent filing activities (Michalowski et al., 2016).

3.2 Highest glucose uptake and pyruvate formation rates were observed for E. coli *HGT*

Two-phase batch fermentations were performed to investigate cellular kinetics during exponential growth and subsequent slow-growth or resting periods. This fermentation scenario resembles production conditions and also induces a stringent response (Brown et al., 2014), thus defining the consequence of engineered ppGpp levels on strain performance. The synthetic fermentation medium contained all essential nutrients in excess, excluding ammonium, which was provided as the sole nitrogen source at a predefined concentration of 40 mM. Cells grew exponentially with a maximum specific growth rate (phase I) until nitrogen was exhausted and cultivation proceeded to the non-growing phase (Fig. 2).

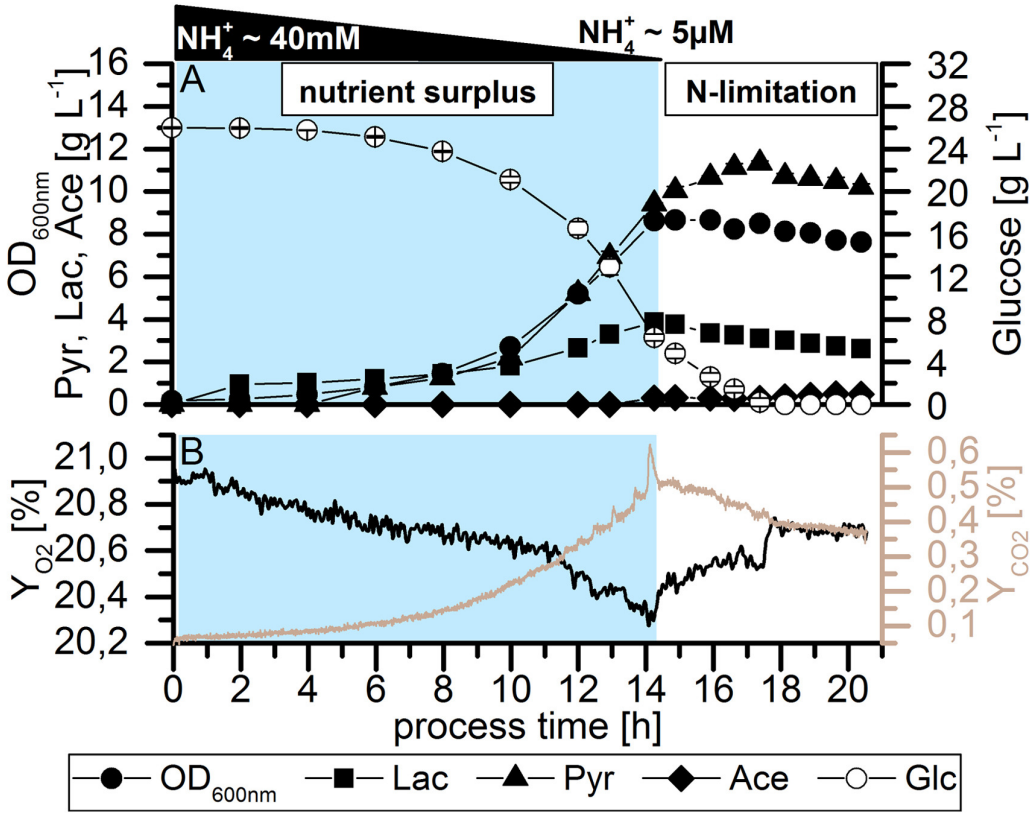

Fig. 2. Two-phase batch fermentation of *E. coli* HGT.

A: Profile of a two-phase batch cultivation in minimal medium supplemented with 40 mM ammonium using *E. coli* HGT fermentation as an example. The process phase of nitrogen availability (nutrient surplus - shaded in light blue) was followed by a nitrogen-limited growth phase (N-limitation). Offline measurements of optical density ($OD_{600\ nm}$),

glucose consumption (Glc) and the formation of pyruvate (Pyr), lactate (Lac) and acetate (Ace) were taken. Values represent arithmetic mean with standard deviation of three parallel cultivation experiments. B: Online monitoring of oxygen (Y_{O2}) and carbon dioxide (Y_{CO2}) fractions in the exhaust gas throughout the fermentation process.

Monitoring of oxygen (O_2) and carbon dioxide (CO_2) in the exhaust gas indicated nitrogen depletion at t=14.27 h, which coincided with the start of sampling during phase II. Table 2 gives an overview of the observed kinetics. Although specific growth rates and process time vary between pyruvate producers and non-producers, maximum cell dry weight (CDW^{max}) was similar for all strains, indicating a similar nitrogen-to-biomass conversion yield ($Y_{X/N}$). Low specific growth rates of *aceE*[G267C]-containing mutants are in agreement with published data for PDHC-disruptive mutations (Tran et al., 2014).

Table 2
Fermentation parameters.

E. coli MG1655	μ^{max} [h^{-1}]	CDW^{max} on NH_4^+ [g L^{-1}]	$Y_{X/N}$ [g_{CDW} $g_{NH4+}{}^{-1}$]	time at N-lim [h]	c_{Glc} start [g L^{-1}]	c_{Glc} at N-lim [g L^{-1}]
WT	0.72±0.01	3.38±0.03	4.94±0.03	5.87	18.08±0.04	10.22±0.14
ACE	0.20±0.01	3.31±0.04	4.82±0.08	15.97	30.33±0.19	7.01±0.37
SR	0.71±0.01	3.23±0.02	4.90±0.06	5.38	26.62±0.19	18.92±0.13
HGT[a]	0.29±0.01	3.27±0.07	4.84±0.14	14.27/15.00	26.38±0.37	6.33±0.21

μ^{max}: maximum specific growth rate during exponential growth, CDW^{max}: maximum cell dry weight generated from 40 mM NH_4^+, $Y_{X/N}$: biomass from nitrogen yield, c_{Glc} start: glucose concentration at fermentation start, values represent arithmetic mean with standard deviation of three parallel experiments.
[a] Values were calculated from 2 biological replicates, each with 3 parallel fermentations.

Table 3
Biomass-specific product formation rates (q_P) and pyruvate from glucose yields ($Y_{P/S}$) during exponential growth and N-limitation of both pyruvate producer *E. coli* MG1655 strains.

	exponential phase		N-limited phase		
E. coli MG1655	$Y_{P/S}$ [g_{Pyr} $g_{Glc^{-1}}$]	q_P [g_{Pyr} $g_{CDW}{}^{-1}$ h^{-1}]	$Y_{P/S}$ [g_{Pyr} $g_{Glc^{-1}}$]	q_P [g_{Pyr} $g_{CDW}{}^{-1}$ h^{-1}]	fold increase in q_P to ACE
WT	0.00∗	0.00∗	0.00∗	0.00∗	0.00
ACE	0.45±0.02	0.68±0.04	0.58±0.06	0.18±0.01	1.00
SR	0.00∗	0.00∗	0.00∗	0.00∗	0.00
HGT[a]	0.49±0.05	0.84±0.04	0.41±0.06	0.26±0.03	1.44

0.00∗: measurement was below detection limit, $Y_{P/S}$: product from substrate yield, q_P: biomass-specific pyruvate production rate, values represent arithmetic mean with standard deviation of three parallel experiments.
[a] Values were calculated from 2 biological replicates, each with 3 parallel fermentations.

The single G267C amino acid exchange within E1p of PDHC led to a drastic overproduction of pyruvate, which was associated with increased glucose consumption in the *E. coli* ACE mutants compared to *E. coli* WT and the stringent response mutant. *E. coli* ACE accumulated 13 g L^{-1} and *E. coli* HGT 11.4 g L^{-1} of pyruvate over a process time of 19 h and 17 h, respectively. Average biomass-specific productivity was 0.68 g_{Pyr} g_{CDW}^{-1} h^{-1} for *E. coli* ACE and 0.84 g_{Pyr} g_{CDW}^{-1} h^{-1} for *E. coli* HGT during exponential growth. The values decreased during nitrogen-limitation, reaching production rates of 0.18 g_{Pyr} g_{CDW}^{-1} h^{-1} for *E. coli* ACE and 0.26 g_{Pyr} g_{CDW}^{-1} h^{-1} for *E. coli* HGT (Table 3).

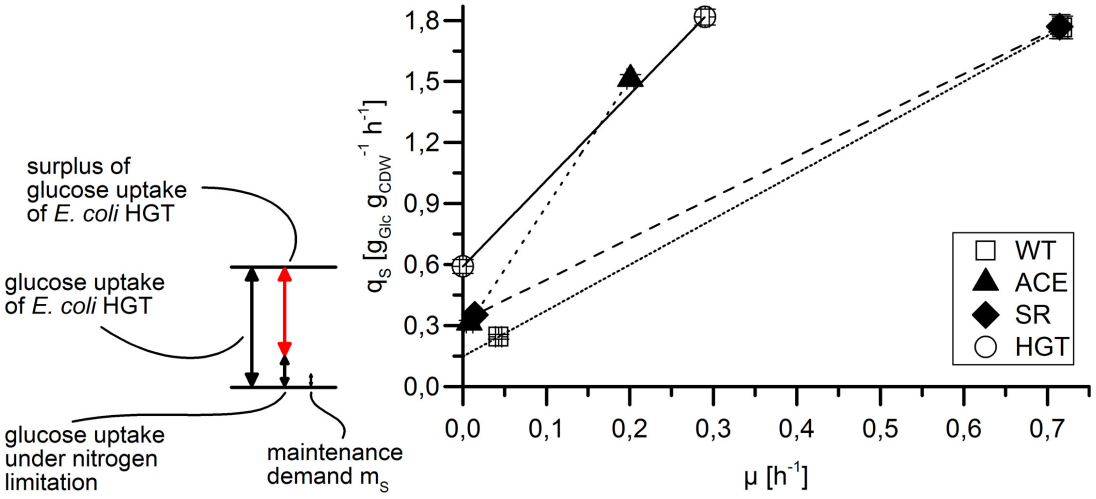

Fig. 3. Pirt-like correlation between biomass-specific glucose uptake and growth.

Notably, *E. coli* WT and *E. coli* SR did not show any pyruvate production. The highest pyruvate synthesis rate of *E. coli* HGT reflects the highest cell-specific glucose consumption rate (Table 4). Glucose uptake rates (q_S) of *E. coli* HGT exceeded *E. coli* WT values by more than 2.3-fold and were about 1.8-fold the level of the other mutants. The differences of growth and substrate uptake kinetics are summarized in the ' Pirt-like'diagram of Fig. 3. *E. coli* HGT showed highest substrate uptake rates under non-growing conditions and maximum uptake for cell growth of 0.3 h^{-1}. The latter was also found to be the maximum specific growth rate of *E. coli* HGT.

Maximum and minimum glucose uptake rates (q_S), calculated from exponentially growing and growth-arrested bacterial cultures in two-phase batch fermentations, plotted against their corresponding specific growth rates (μ). Point of intersection with the y-axis is considered the minimum glucose consumption to cover the energy demand for cell

maintenance (m_S). From the literature, a q_S value of 0.057 g_{Glc} g_{CDW}^{-1} h^{-1} was obtained for carbon-limited, non-growing bacterial cultures (maintenance demand m_S) of *E. coli* (Nielsen et al., 2003). Interpolation of the *E. coli* WT data results in a minimum q_S value of 0.14 g_{Glc} g_{CDW}^{-1} h^{-1} for glucose uptake under nitrogen-limited conditions. Values represent arithmetic mean with standard deviation of three and six (*E. coli* HGT) parallel cultivation experiments.

Table 4
Biomass-specific glucose uptake rates (q_S) and biomass from glucose yields ($Y_{X/S}$) during exponential growth and N-limitation of all four *E. coli* MG1655 strains.

	exponential phase		N-limited phase		
E. coli MG1655	$Y_{X/S}$ [g_{CDW} g_{Glc}^{-1}]	q_S [g_{Glc} g_{CDW}^{-1} h^{-1}]	$Y_{X/S}$ [g_{CDW} g_{Glc}^{-1}]	q_S [g_{Glc} g_{CDW}^{-1} h^{-1}]	fold increase in q_S to WT
WT	0.41±0.01	1.77±0.06	0.18±0.026	0.25±0.01	1.00
ACE	0.13±0.01	1.51±0.02	0.03±0.012	0.31±0.01	1.24
SR	0.40±0.01	1.77±0.06	0.04±0.005	0.35±0.02	1.40
HGT[a]	0.17±0.01	1.81±0.09	n.d.*	0.59±0.02	2.36

n.d.*: not defined, because biomass formation was c_X=0, $Y_{X/S}$: biomass from substrate yield, q_S: biomass-specific glucose consumption rate, values represent arithmetic mean with standard deviation of three parallel experiments.
[a] Values were calculated from 2 biological replicates, each with 3 parallel fermentations. Differences in q_S (N-limited) were found to be significant applying the ANOVA F-test with reference to *E. coli* WT. All values were significant among each other for a P value < 0.01, except for *E. coli* SR to *E. coli* ACE.

3.3 E. coli *HGT shows a unique ppGpp phenotype*

Gram-negative bacteria possess one monofunctional RelA/SpoT Homologue (RSH) protein for major ppGpp synthesis and one bifunctional RSH protein that performs only reduced synthesis, but drives hydrolysis of ppGpp with high affinity (Mittenhuber, 2001). The engineered set of *E. coli* mutants in the present study was used to investigate the individual contributions of these genes on ppGpp formation (Fig. 4).

Measurements of the stringent response alarmone ppGpp at 30-45 min intervals over 3 h prior to and after entry into the nitrogen-limitation phase. The *E. coli* WT strain was compared to the mutants *E. coli* ACE, *E. coli* SR and *E. coli* HGT. Data sets for all cultivated strains were normalized to the exact time point of nitrogen-limitation. Values represent arithmetic mean with standard deviation of three and six (*E. coli* HGT) parallel cultivation experiments and two technical replicates for each sample from the bioreactor.

The *E. coli* WT culture exhibited (the expected) amplification of ppGpp formation, shifting the alarmone concentration from 0.3 to 3 µmol g_{CDW}^{-1} and reflecting the tran-

sition from nitrogen saturation to depletion. Nitrogen-limitation induced only a slight shift in ppGpp pools to 0.7/0.8 µmol g_{CDW}^{-1} in the pyruvate producer *E. coli* ACE and the *E. coli* SR strain. The combination of stringent response deregulation and pyruvate overexpression in the *E. coli* HGT strain diminished any dynamics in ppGpp synthesis, which was indicated by the constant low level of ppGpp.

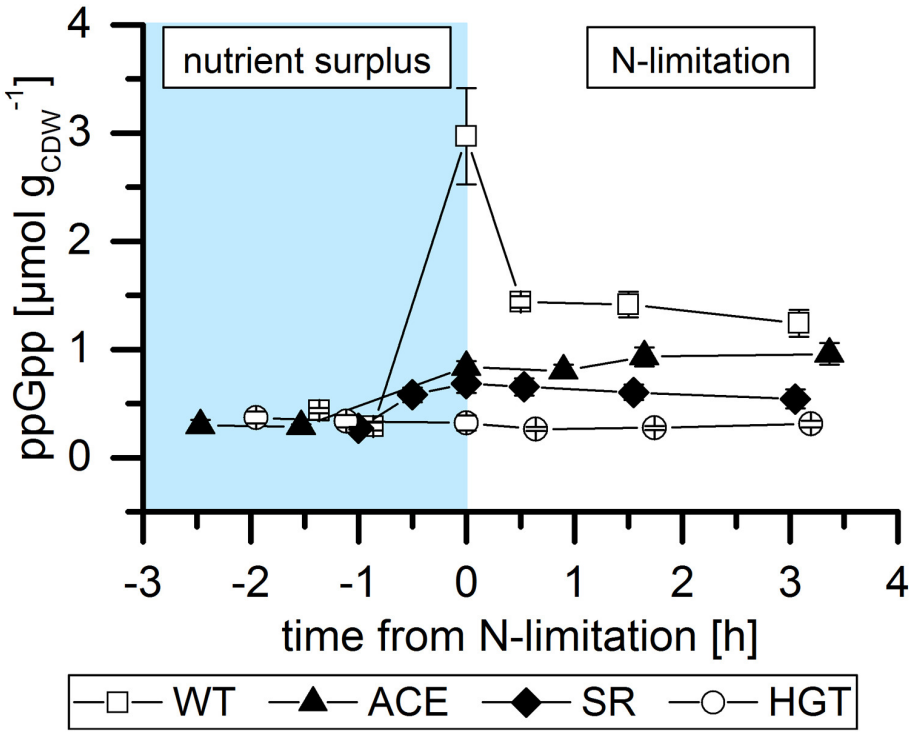

Fig. 4. ppGpp concentrations at different time points during two-phase batch fermentations.

3.4 Carbon balance reveals that a surplus glucose uptake is available for organic acid formation

To investigate the fate of surplus glucose uptake, *E. coli* WT was compared to HGT under exponential growth and N-limited conditions (Fig. 5).

Detailed composition of carbon distribution in two *E. coli* strains for the process phases of exponential growth (A) and nitrogen depletion (B). Column height represents glucose consumption as total carbon input for each fermentation phase. Absolute carbon amounts of allocated products, biomass (CDW), carbon dioxide (CO_2) and unknown compounds

are demonstrated as proportions of the column height. X indicates unknown carbon mass of organic compounds that were not determined by the applied measurements.

E. coli WT produced biomass (48 %), carbon dioxide and other compounds (52 %) including small amounts of acetate and classical overflow metabolites, during the exponential growth phase. Interestingly, *E. coli* HGT produced almost identical amounts of biomass and carbon dioxide under exponential growth. The glucose uptake surplus is fueled completely to organic acids such as pyruvate (49 %), lactate (20 %) and acetate (1.6 %). Under N-limitation, *E. coli* WT cells still formed biomass from about 20 % of the consumed carbon. All residual C-molecules were converted to carbon dioxide in respiratory reactions (60 %) and to unknown metabolites X (20 %). No biomass formation was observed for *E. coli* HGT during nitrogen depletion. Compared to *E. coli* WT, *E. coli* HGT showed a strongly enhanced glucose uptake during N-limitation but produced the same amount of carbon dioxide as the WT, which resulted in only 29 % of total carbon. Consequently, 71 % of the carbon was fueled in organic components, of which 28 % was identified as pyruvate.

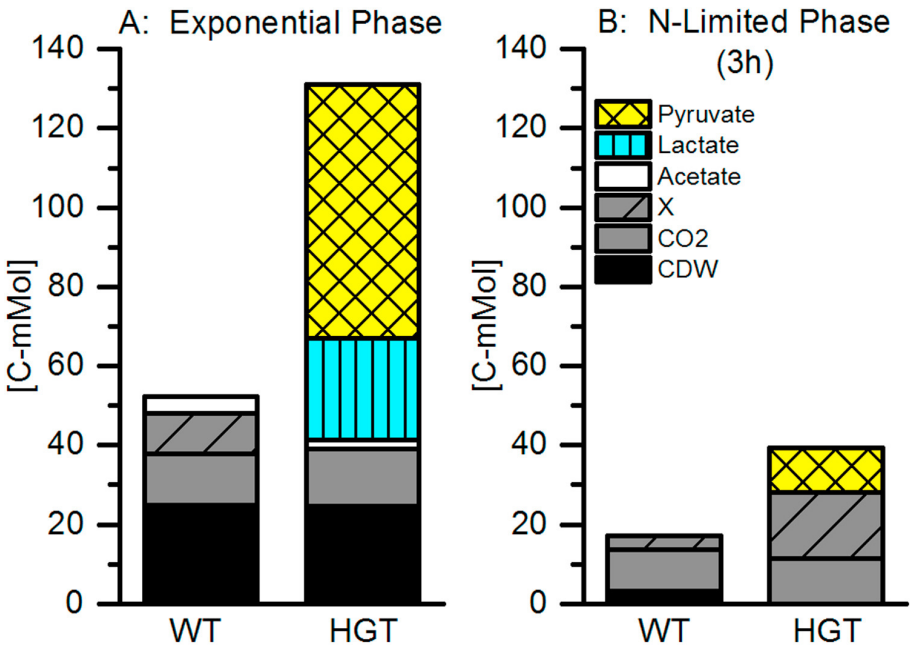

Fig. 5. Carbon balance of *E. coli* WT compared to *E. coli* HGT.

3.5 Individual respiratory phenotypes for the mutants

The respiratory quotient (RQ) of *E. coli* WT, which is the ratio of carbon dioxide emission rate to oxygen uptake rate, was found to be close to 1 during both fermentation phases (Fig. 6).

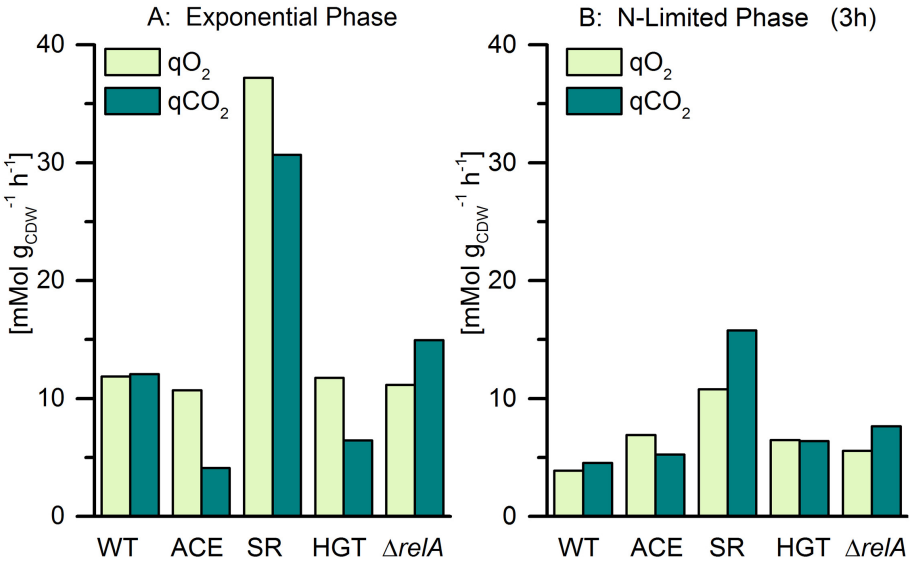

Fig. 6. Biomass-specific respiratory rates.

Oxygen consumption (qO2) and carbon dioxide emission (qCO2) rates for the *E. coli* WT strain and different mutants. A: Respiratory rates during exponential growth. B: Respiratory rates during the first 3 h of nitrogen-limitation.

An RQ value of 1.02 for exponential growth was in agreement with the RQ value of 1.05 obtained for aerobic glucose-limited chemostat *E. coli* WT cultures (Sauer et al., 1999). Respiration rates were reduced by about 60 % when cell growth slowed down due to nitrogen-limitation and a slight increase in RQ to 1.16 was observed. Strains containing the *aceE* mutation showed almost unchanged qCO_2 values (4-5.5 mmol g_{CDW}^{-1} h^{-1}) during exponential growth and nitrogen-limitation. Consequently, RQs ranged between 0.4 and 1. Equilibrated ratios were found during nitrogen-limitation. The stand-alone Δ*relA* mutation showed a different phenotype. The lack of active ppGpp synthase I resulted in RQ values of 1.34 (exponential) and 1.38 (N-limited), revealing a relAtively high carbon dioxide production. Interestingly, qO_2 values for *E. coli* HGT (comprising the *aceE* mutation) were similar to *E. coli* WT, whereas *E. coli* SR mutants showed severely enhanced oxygen requirements. Accordingly, the respiratory phenotype of *E. coli* HGT resembled a combination of the individual SR and ACE phenotypes.

3.6 Energy levels and adenylate energy charge

The energetic condition of cells is reflected by the adenylate energy charge (AEC), which is calculated from intracellular adenylate pool concentrations (1) and represents the energetic balance between catabolic and anabolic functions. A direct comparison of exponential growth and nitrogen-limited growth arrest is of special interest for strains with a prospective application in large-scale industrial fermentations. Comparison of energy levels in *E. coli* WT and mutant strains illustrated high variation in AEC values and adenine nucleotide compositions during the fermentation process (Fig. 7).

A-D: Concentration of adenosine triphosphate (ATP), adenosine diphosphate (ADP) and adenosine monophosphate (AMP) in an environment of nutrient excess (exponential phase is shaded in light blue) and during nutrient starvation (nitrogen-limitation). The total adenine nucleotide concentration (ΣAxP) for each sampling point is indicated as a dark grey bar. Data sets for all cultivated strains were normalized to the exact time point of nitrogen-limitation (t=0). Values represent arithmetic mean with standard deviation of three and six (*E. coli* HGT) parallel cultivation experiments and two technical replicates for each sample from the bioreactor. E-H: Adenylate energy charge (AEC) calculated for *E. coli* WT and the three mutants *E. coli* ACE, *E. coli* SR and *E. coli* HGT. An AEC value could not be calculated from available data for an exponentially growing *E. coli* WT culture due to highly error-prone nucleotide measurements. Instead, the horizontal line (∗) represents an AEC value of 0.9-0.94 in *E. coli* during aerobic, exponential growth in various media from a previous report (Franzen and Binkley, 1961).

From here on, the sum of all three adenine nucleotides AMP, ADP and ATP will be referred to as AxP. This concentration was kept at a constant level over the entire fermentation process for *E. coli* WT and *E. coli* HGT mutant strains. The pyruvate producer *E. coli* ACE and the stringent response mutant *E. coli* SR showed divergent patterns, since the AxP amount was either increasing or decreasing with time. Nevertheless, these cells were able to maintain a steady AEC value, even during growth arrest. ATP concentration in the *E. coli* ACE mutant was constantly high, in contrast to ADP and AMP levels, which were steadily rising. In the *E. coli* SR mutant, the stringent response mutation apparently led to a steady decrease in overall AxP levels, caused by a continuous decline in ATP concentration. The combined effects of the stringent response mutation and a defect in central carbon metabolism caused a combination of both distinct AxP phenotypes, leading to the AxP pattern in the triple *E. coli* HGT mutant.

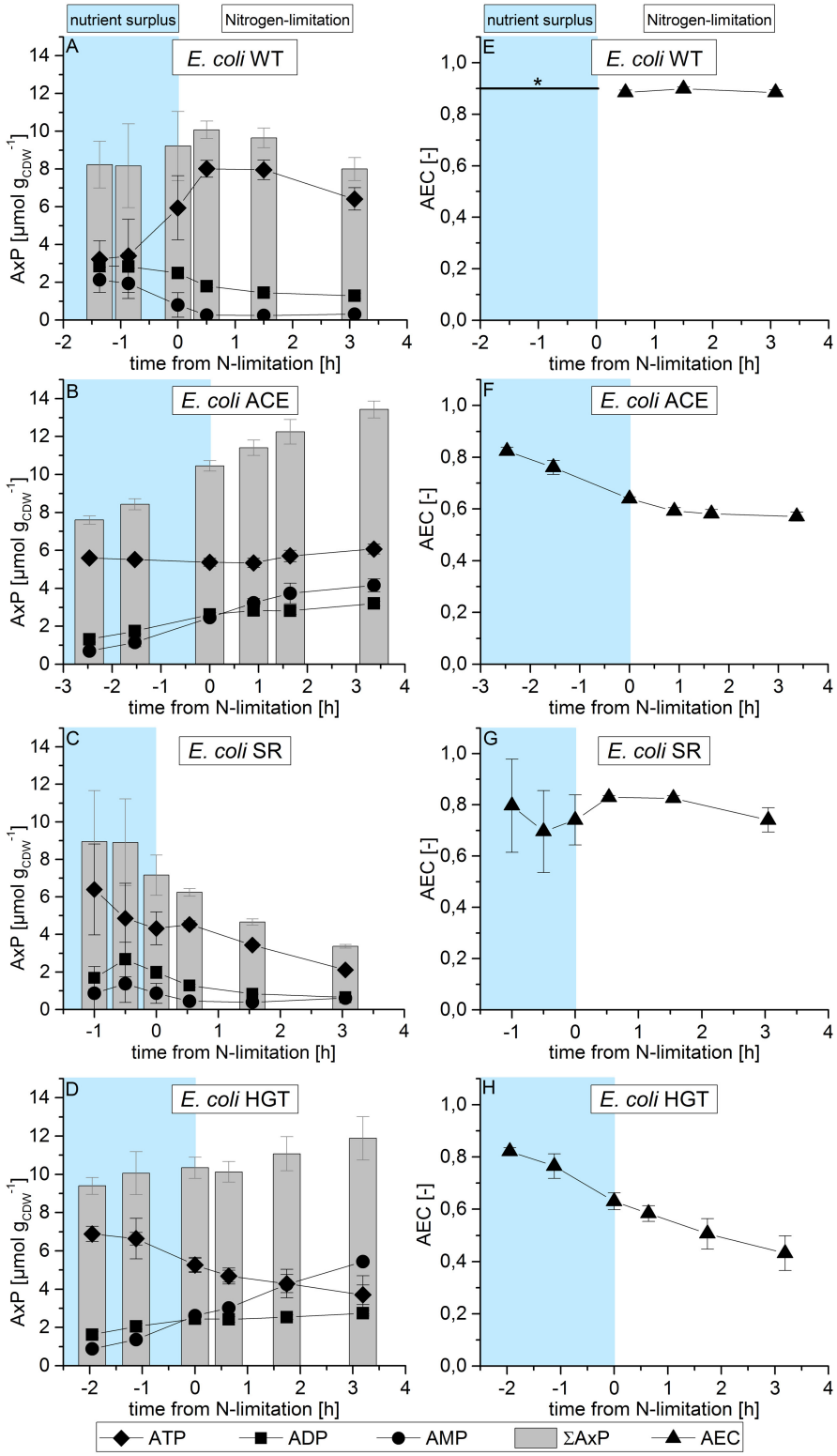

Fig. 7. Energy profiles of different *E. coli* strains during two-phase batch fermentations.

4. Discussion

4.1 Modulation of stringent response is very sensitive with respect to strain stability and performance

Stringent response plays a key role in the regulatory portfolio of *E. coli*. In conjunction with cAMP and Cra, stringent response is a crucial tool for adapting metabolic activity to the availability of carbon- and nitrogen-containing substrates (Hardiman et al., 2007; Sauer et al., 1999). Scale-down studies by Löffler et al. (2016) showed that stringent response-mediated transcriptional control is frequently switched on and off when cells are fluctuating in large-scale bioreactors experiencing typical substrate gradients. Consequently, ATP demands increase to fulfill the transcriptional and translational regulatory programs that were initiated.

Due to the central role of stringent response, modulating this to engineer cellular performance was the focus of the present study. In essence, ppGpp levels, the alarmone of stringent response, can be altered such that glucose uptake rates will be maximized for slow-growing or even resting cells. The choice of this growth phenotype was motivated by large-scale production conditions, when cellular activity is typically reduced in order to overcome the technical constraints of maximum oxygen transfer and heat removal (Takors, 2012).

However, a metabolic engineering strategy for altering ppGpp levels has not been identified and contradicting examples exist in the literature. Imaizumi et al. (2006) successfully increased L-lysine and L-glutamate formation in *E. coli* by amplifying *relA*, i.e. ppGpp synthesis. Although elevated ppGpp levels appear to stimulate amino acid synthesis, its intracellular concentration has to be regulated at its upper limit by an active ppGpp hydrolase, since deletion of the *spoT* gene is lethal in a $relA^+$ background (Gentry and Cashel, 1996). On the contrary, a completely disrupted stringent response ($\Delta relA$ and $\Delta spoT$) yields $ppGpp^0$ strains that show a range of undesirable phenotypic features such as multiple amino acid requirements for growth on minimal medium (Tedin and Norel, 2001), defects in cell division and cell separation and an inability for stable survival in the stationary phase (Gentry et al., 1993; Xiao et al., 1991). Bacterial cells that completely lack ppGpp show a severe transcriptional downshift in glycolytic genes such as glucose permease, phosphoglucose isomerase and pyruvate dehydrogenase that drastically diminishes glycolytic flux (Traxler et al., 2008). Deletion of the *relA* gene,

expressing only one stringent response regulating protein has been shown to increase the expression of heterologous proteins in a *relA* deficient strain (Harcum and Bentley, 1999).

Our metabolic design strategy followed the basic idea of keeping ppGpp levels so low that the beneficial effects could be exploited, while at the same time preventing the unwanted extreme phenotypes of $ppGpp^0$ strains. Complementary studies using *relA* amplified strains have been conducted but did not yield desirable phenotypes (Table A1). As such, *E. coli* HGT comprises a deletion of *relA* to suppress the main ppGpp synthesis and modulation of *spoT* by integrating the ExDD motif. Thus, the modified SpoT is expected to bind GDP, GTP and ATP like WT RelA (Sajish et al., 2007).

Several studies highlight variations in glucose consumption based on mutations of genes involved in central metabolic pathways. One such approach targeted the phosphotransferase system of *E. coli* and uncovered a higher glycolytic flux through phosphoglucose isomerase and pyruvate kinases, although elevated glucose consumption could not be observed directly (Flores et al., 2002). It has been reported that AceE mutants instead show increased glucose uptake rates (Zhu et al., 2008), therefore, this approach was also taken into consideration in the present metabolic engineering study. As such, the *aceE*[G267C] mutation, which affects the E1 protein component of the pyruvate dehydrogenase complex, was integrated. This caused ppGpp pools to remain at the same low level during nitrogen-limitation, as was observed during the exponential growth. Apparently, stringent response was not induced via high ppGpp levels in *E. coli* HGT, although the native trigger was set by the cultivation conditions. Interestingly, ppGpp levels of all other constructs increased during nitrogen-limitation in *E. coli* WT, showing a (predicted) strong response to nitrogen-limitation. The *E. coli* SR mutant also showed a three-fold elevation in ppGpp levels due to residual mutant SpoT synthase activity. Notably, ppGpp levels in *E. coli* SR were significantly lower than those in *E. coli* WT, but still higher than those in *E. coli* HGT. The interaction with the *aceE* mutation appears to support the yielded metabolic engineering goal. However, the underlying mechanisms are not yet completely understood.

4.2 E. coli *HGT shows the highest glucose uptake rates and offers a surplus for product formation*

One of the key properties of *E. coli* HGT is its ability to consume high amounts of glucose, even when cells are in a growth-arrested state. The Pirt-like correlations between glucose consumption (q_S) and growth (μ) obtained from the two-phase batch

fermentations are depicted in Fig. 3. During N-limited cultivation, bacterial growth is minimized or undetectable ($\mu^{min,\ lim}$=0-0.043 h^{-1}). According to Brown et al. (2014), nitrogen exhaustion immediately activates intracellular regulatory mechanisms, such as stringent response and the global nitrogen-regulated stress response (Ntr). Cells subsist on storage compounds or even foster glucose uptake. We found the q_S for resting cells (called m_S) to be 0.14 g_{Glc} g_{CDW}^{-1} h^{-1}, which is in good agreement with other studies (Chubukov and Sauer, 2014; Hua et al., 2004; Kumar and Shimizu, 2010). Similar phenomena have been observed for phosphate- or nitrogen-limitation (Chubukov and Sauer, 2014; Schuhmacher et al., 2014). Taymaz-Nikerel et al. (2010) indicate the glucose demand for non-growing carbon-limited cultures of *E. coli* to be 0.024 g_{Glc} g_{CDW}^{-1} h^{-1}. Fig. 3 shows that the *E. coli* ACE mutant also alleviated glucose uptake. However, only the combination of *aceE* modulation with an engineered stringent response in *E. coli* HGT achieved maximum glucose uptake rates. Interestingly, glucose uptake rates were increased not only for resting cells but also for slowly-growing cells. Specifically, the q_S value of exponentially-growing *E. coli* WT was already achieved by *E. coli* HGT growing at 0.3 h^{-1}.

Fig. 5 shows that the surplus of glucose is fueled in organic acids (pyruvate and lactate). Accordingly, increased glucose uptake rates do not mirror putatively increased cellular maintenance demands and in fact, carbon should be available for redirecting fluxes to other pathways and products of interest.

E. coli HGT shows very similar oxygen uptake kinetics compared to *E. coli* WT (Fig. 6). This is important because it means that increased glucose uptake rates are not proportional to oxygen needs. Consequently, resting *E. coli* HGT may be used with alleviated glucose uptake rates on an industrial scale without compromising the technical constraints of oxygen transfer and cooling.

All *aceE* mutants showed reduced carbon dioxide formation compared to *E. coli* WT. Apparently, *aceE*[G267C] causes reduced decarboxylation activity of pyruvate to acetyl-CoA, which in turn limits the TCA cycle and fatty acid synthesis (Battesti et al., 2015). Because ATP generation via the respiratory chain is also reduced, increased glycolytic activity of *aceE* mutants is likely controlled by ATP demand. Similar observations have been demonstrated in Δ*atpFH* strains (Causey et al., 2003) and in mutants with additional ATPase activity that lowered their [ATP]/[ADP] ratio (Koebmann et al., 2002). Such scenarios are also in agreement with the previous findings of (Atkinson and Walton, 1967).

5. Conclusion

E. coli HGT strain was engineered as a novel chassis that offers about three-fold higher cell-specific glucose uptake rates (0.6 g_{Glc} g_{CDW}^{-1} h^{-1}) under nitrogen-limited conditions compared to that of *E. coli* WT. Maximum glucose uptake rates of about 1.8 g_{Glc} g_{CDW}^{-1} h^{-1} were achieved with cells growing at only 0.3 h^{-1}. Accordingly, *E. coli* HGT achieves approximately 40 % of the maximum specific growth rate of *E. coli* WT, which may extend the initial phase of biomass formation in large-scale production processes. However, productivity benefits of the subsequent production phase should compensate the growth phenotype. Notably, oxygen demands did not increase proportionally. Instead, oxygen needs were comparable to *E. coli* WT, which makes the *E. coli* HGT strain applicable to large-scale cultivations. Surplus glucose is predominantly used to fuel organic acid synthesis, indicating high pyruvate availability. This property should be exploitable for products that specifically require pyruvate as a precursor. Some examples include terpenoids produced via the methylerythritol 4-phosphate (MEP) pathway, intermediates or derivatives of the valine or isoleucine pathways and organic acids such as lactate and pyruvate. In summary, *E. coli* HGT has the potential to be a novel high productivity chassis for metabolic engineering applications.

Acknowledgments

Special thanks to Michael Kraml and Ulrike Hillemann for their technical support during fermentation processes, sampling procedures and strain constructions. We thank Mira Lenfers-Lücker for her help with HPLC measurements. We are also grateful for the collaboration with Belén Calles, Esteban Martínez and Sofia Fraile (CSIC, CNB, University of Madrid) for providing the pEMG and pACBSR plasmids and appreciate their support with the I-SceI method. The authors would like to thank the European Union for funding these studies as part of the 'ST-Flow'project (Grant no.: 289326) in the framework 7 program KBBE.2011.3.6-03.

Appendix A

(See Table A1).

Table A1
relA amplified strains for stringent response modulation and their phenotypes.

E. coli MG1655	genomic modification	comment	μ^{max} [h^{-1}]	$q_S{}^{exp}$ [g_{Glc} $g_{CDW}{}^{-1}$ h^{-1}]	$q_S{}^{lim}$ [g_{Glc} $g_{CDW}{}^{-1}$ h^{-1}]	$ppGpp^{lim}$ [µmol $g_{CDW}{}^{-1}$]
*spoT*Syn↑#13	*spoT* with *relA* synthase sequence		0.47	1.47±0.07	0.31±0.01	1.69-0.71
*spoT*Syn↑#77	*spoT* with *relA* synthase sequence	^{m}L303Q in RelA	0.57	1.38±0.03	0.24±0.00	3.86-1.08
double *relA*	chromosomal duplication of *relA* gene		0.71	1.72±0.08	0.26±0.02	1.93-1.34
spoT[R290E, K292D]	*spoT* with R290E & K292D substitutions	^{m}Q287L in RelA	0.71	1.57±0.01	0.22±0.01	4.04-1.56

exp: rates calculated from exponential growth, lim: rates and values obtained from cultivation under N-limited conditions, q_S: biomass-specific glucose consumption rate, CDW: cell dry weight, Glc: glucose, ^{m}: spontaneous mutation, R: arginine, E: glutamate, K: lysine, D: aspartate, L: leucine, Q: glutamine.

References

Atkinson, D.E., Walton, G.M., 1967. Adenosine triphosphate conservation in metabolic regulation. Rat liver citrate cleavage enzyme. J. Biol. Chem. 242, 3239-3241.

Battesti, A., Bouveret, E., 2006. Acyl carrier protein/SpoT interaction, the switch linking SpoT-dependent stress response to fatty acid metabolism. Mol. Microbiol. 62, 1048-1063. http://dx.doi.org/10.1111/j.1365-2958.2006.05442.x.

Battesti, A., Majdalani, N., Gottesman, S., 2015. Stress sigma factor RpoS degradation and translation are sensitive to the state of central metabolism. Proc. Natl. Acad. Sci. USA. 112, 5159-5164. doi: http://dx.doi.org/10.1073/pnas.1504639112.

Bougdour, A., Gottesman, S., 2007. ppGpp regulation of RpoS degradation via anti-adaptor protein IraP. Proc. Natl. Acad. Sci. USA 104, 12896-12901. http://dx.doi.org/10.1073/pnas.0705561104.

Brown, D.R., Barton, G., Pan, Z., Buck, M., Wigneshweraraj, S., 2014. Nitrogen stress response and stringent response are coupled in Escherichia coli. Nat. Commun. 5, 4115. http://dx.doi.org/10.1038/ncomms5115.

Carneiro, S., Villas-Bôas, S.G., Ferreira, E.C., Rocha, I., 2011. Metabolic footprint analysis of recombinant Escherichia coli strains during fed-batch fermentations. Mol.

BioSyst. 7, 899-910. http://dx.doi.org/10.1039/c0mb00143k.

Causey, T.B., Zhou, S., Shanmugam, K.T., Ingram, L.O., 2003. Engineering the metabolism of Escherichia coli W3110 for the conversion of sugar to redox-neutral and oxidized products: homoacetate production. Proc. Natl. Acad. Sci. USA. 100, 825-832. doi: http://dx.doi.org/10.1073/pnas.0337684100.

Chubukov, V., Sauer, U., 2014. Environmental dependence of stationary-phase metabolism in Bacillus subtilis and Escherichia coli. Appl. Environ. Microbiol. 80, 2901-2909. http://dx.doi.org/10.1128/AEM.00061-14.

Cserjan-Puschmann, M., Kramer, W., Duerrschmid, E., Striedner, G., Bayer, K., 1999. Metabolic approaches for the optimisation of recombinant fermentation processes. Appl. Microbiol. Biotechnol. 53, 43-50. http://dx.doi.org/10.1007/s002530051612.

Dedhia, N., Richins, R., Mesina, A., Chen, W., 1997. Improvement in recombinant protein production in ppGpp-deficient Escherichia coli. Biotechnol. Bioeng. 53, 379-386. http://dx.doi.org/10.1002/(SICI)1097-0290(19970220)53:4<379::AID-BIT4>3.0.CO;2-K.

Durfee, T., Hansen, A.M., Zhi, H., Blattner, F.R., Jin, D.J., 2008. Transcription profiling of the stringent response in Escherichia coli. J. Bacteriol. 190, 1084-1096. http://dx.doi.org/10.1128/JB.01092-07.

Filutowicz, M., McEachern, M.J., Helinski, D.R., 1986. Positive and negative roles of an initiator protein at an origin of replication. Proc. Natl. Acad. Sci. USA. 83, 9645-9649. doi: http://dx.doi.org/10.1073/pnas.83.24.9645.

Flores, S., Gosset, G., Flores, N., De Graaf, A.A., Bolívar, F., 2002. Analysis of carbon metabolism in Escherichia coli strains with an inactive phosphotransferase system by ^{13}C labeling and NMR spectroscopy. Metab. Eng. 4, 124-137. http://dx.doi.org/10.1006/mben.2001.0209.

Franzen, J.S., Binkley, S.B., 1961. Comparison of the acid-soluble nucleotides in Escherichia coli at different growth rates. J. Biol. Chem. 236, 515-519.

Gentry, D.R., Cashel, M., 1996. Mutational analysis of the Escherichia coli spoT gene identifies distinct but overlapping regions involved in ppGpp synthesis and degradation. Mol. Microbiol. 19, 1373-1384. http://dx.doi.org/10.1111/j.1365-2958.1996.tb02480.x.

Gentry, D.R., Hernandez, V.J., Nguyen, L.H., Jensen, D.B., Cashel, M., 1993. Synthesis of the stationary-phase sigma factor σ(s) is positively regulated by ppGpp. J. Bacteriol. 175, 7982-7989.

Gibson, D.G., 2011. Enzymatic assembly of overlapping DNA fragments. Methods En-

zym. 498, 349-361. http://dx.doi.org/10.1016/B978-0-12-385120-8.00015-2.

Harcum, S.W., Bentley, W.E., 1999. Heat-shock and stringent responses have overlapping protease activity in Escherichia coli. Appl. Biochem. Biotechnol. 80, 23-37. http://dx.doi.org/10.1385/ABAB:80:1:23.

Hardiman, T., Lemuth, K., Keller, M.A., Reuss, M., Siemann-Herzberg, M., 2007. Topology of the global regulatory network of carbon limitation in Escherichia coli. J. Biotechnol. 132, 359-374. http://dx.doi.org/10.1016/j.jbiotec.2007.08.029.

Haseltine, W.A., Block, R., 1973. Synthesis of guanosine tetra- and pentaphosphate requires the presence of a codon-specific, uncharged transfer ribonucleic acid in the acceptor site of ribosomes. Proc. Natl. Acad. Sci. USA 70, 1564-1568.

Herring, C.D., Glasner, J.D., Blattner, F.R., 2003. Gene replacement without selection: regulated suppression of amber mutations in Escherichia coli. Gene 311, 153-163. http://dx.doi.org/10.1016/S0378-1119(03)00585-7.

Hua, Q., Yang, C., Oshima, T., Mori, H., Shimizu, K., 2004. Analysis of gene expression in Escherichia coli in response to changes of growth-limiting nutrient in chemostat cultures. Appl. Environ. Microbiol. 70, 2354-2366. http://dx.doi.org/10.1128/AEM.70.4.2354.

Imaizumi, A., Kojima, H., Matsui, K., 2006. The effect of intracellular ppGpp levels on glutamate and lysine overproduction in Escherichia coli. J. Biotechnol. 125, 328-337. http://dx.doi.org/10.1016/j.jbiotec.2006.03.015.

Johansson, J., Balsalobre, C., Wang, S.Y., Urbonaviciene, J., Jin, D.J., Sondén, B., Uhlin, B.E., 2000. Nucleoid proteins stimulate stringently controlled bacterial promoters: a link between the cAMP-CRP and the (p)ppGpp regulons in Escherichia coli. Cell 102, 475-485. http://dx.doi.org/10.1016/S0092-8674(00)00052-0.

Koebmann, B.J., Westerhoff, H.V., Snoep, J.L., Nilsson, D., Jensen, P.R., 2002. The glycolytic flux in Escherichia coli is controlled by the demand for ATP. J. Bacteriol. 184, 3909-3916. http://dx.doi.org/10.1128/JB.184.14.3909-3916.2002.

Kumar, R., Shimizu, K., 2010. Metabolic regulation of Escherichia coli and its gdhA, glnL, gltB, D mutants under different carbon and nitrogen limitations in the continuous culture. Microb.Cell Fact., 9. http://dx.doi.org/10.1186/1475-2859-9-8.

Lemuth, K., Hardiman, T., Winter, S., Pfeiffer, D., Keller, M.A., Lange, S., Reuss, M., Schmid, R.D., Siemann-Herzberg, M., 2008. Global transcription and metabolic flux analysis of Escherichia coli in glucose-limited fed-batch cultivations. Appl. Environ. Microbiol. 74, 7002-7015. http://dx.doi.org/10.1128/AEM.01327-08.

Löffler, M., Simen, J.D., Jäger, G., Schäferhoff, K., Freund, A., Takors, R., 2016. En-

gineering E. coli for large-scale production - strategies considering ATP expenses and transcriptional responses. Metab. Eng. 38, 73-85.

Martínez-García, E., de Lorenzo, V., 2012. Transposon-based and plasmid-based genetic tools for editing genomes of gram-negative bacteria. Methods Mol. Biol. 813, 267-283. http://dx.doi.org/10.1007/978-1-61779-412-4_16.

Martínez-García, E., de Lorenzo, V., 2011. Engineering multiple genomic deletions in Gram-negative bacteria: analysis of the multi-resistant antibiotic profile of Pseudomonas putida KT2440. Environ. Microbiol. 13, 2702-2716. http://dx.doi.org/10.1111/j.1462-2920.2011.02538.x.

Michalowski, A., Siemann-Herzberg, M., Takors, R., 2016. Bacterial strain and method for high throughput of sugar in the microbial conversion into biosynthetic products. Eur. Union Pat., EP 16000936.1-1401.

Mittenhuber, G., 2001. Comparative genomics and evolution of genes encoding bacterial (p)ppGpp synthetases / hydrolases (the Rel, RelA and SpoT proteins). J. Mol. Microbiol. Biotechnol. 3, 585-600.

Nielsen, J., Villadsen, J., Lidén, G., 2003. Bioreaction Engineering Principles 2nd ed.. Kluwer Academic/Plenum Publishers, New York. http://dx.doi.org/10.1007/978-1-4615-0767-3.

Sajish, M., Tiwari, D., Rananaware, D., Nandicoori, V.K., Prakash, B., 2007. A charge reversal differentiates (p)ppGpp synthesis by monofunctional and bifunctional Rel proteins. J. Biol. Chem. 282, 34977-34983. http://dx.doi.org/10.1074/jbc.M704828200.

Sambrook, J., Russell, D.W., 2001. Molecular Cloning: A Laboratory Manual 3rd ed.. Cold Spring Harbour Laboratory Press, New York.

Sauer, U., Lasko, D.R., Fiaux, J., Hochuli, M., Glaser, R., Szyperski, T., Wüthrich, K., Bailey, J.E., 1999. Metabolic flux ratio analysis of genetic and environmental modulations of Escherichia coli central carbon metabolism. J. Bacteriol. 181, 6679-6688, (doi: PMC94132).

Schuhmacher, T., Löffler, M., Hurler, T., Takors, R., 2014. Phosphate limited fed-batch processes: impact on carbon usage and energy metabolism in Escherichia coli. J. Biotechnol. 190, 96-104. http://dx.doi.org/10.1016/j.jbiotec.2014.04.025.

Takors, R., 2012. Scale-up of microbial processes: impacts, tools and open questions. J. Biotechnol. 160, 3-9. http://dx.doi.org/10.1016/j.jbiotec.2011.12.010.

Taymaz-Nikerel, H., Borujeni, A.E., Verheijen, P.J.T., Heijnen, J.J., van Gulik, W.M., 2010. Genome-derived minimal metabolic models for Escherichia coli MG1655 with estimated in vivo respiratory ATP stoichiometry. Biotechnol. Bioeng. 107, 369-381.

http://dx.doi.org/10.1002/bit.22802.

Tedin, K., Norel, F., 2001. Comparison of ΔrelA strains of Escherichia coli and Salmonella enterica serovar typhimurium suggests a role for ppGpp in attenuation regulation of branched-chain amino acid biosynthesis. J. Bacteriol. 183, 6184-6196. http://dx.doi.org/10.1128/JB.183.21.6184-6196.2001.

Tran, K.T., Maeda, T., Wood, T.K., 2014. Metabolic engineering of Escherichia coli to enhance hydrogen production from glycerol. Appl. Microbiol. Biotechnol. 98, 4757-4770. http://dx.doi.org/10.1007/s00253-014-5600-3.

Traxler, M.F., Summers, S.M., Nguyen, H.T., Zacharia, V.M., Hightower, G.A., Smith, J.T., Conway, T., 2008. The global, ppGpp-mediated stringent response to amino acid starvation in Escherichia coli. Mol. Microbiol. 68, 1128-1148. http://dx.doi.org/10.1111/j.1365-2958.2008.06229.x.

UniProt Consortium, 2015. UniProt: a hub for protein information. Nucleic Acids Res. 43, D204-D212. http://dx.doi.org/10.1093/nar/gku989.

Xiao, H., Kalman, M., Ikehara, K., Zemel, S., Glaser, G., Cashel, M., 1991. Residual guanosine 3',5'-bispyrophosphate synthetic activity of relA null mutants can be eliminated by spoT null mutations. J. Biol. Chem. 266, 5980-5990.

Zhu, Y., Eiteman, M.A., Altman, R., Altman, E., 2008. High glycolytic flux improves pyruvate production by a metabolically engineered Escherichia coli strain. Appl. Environ. Microbiol. 74, 6649-6655. http://dx.doi.org/10.1128/AEM.01610-08.